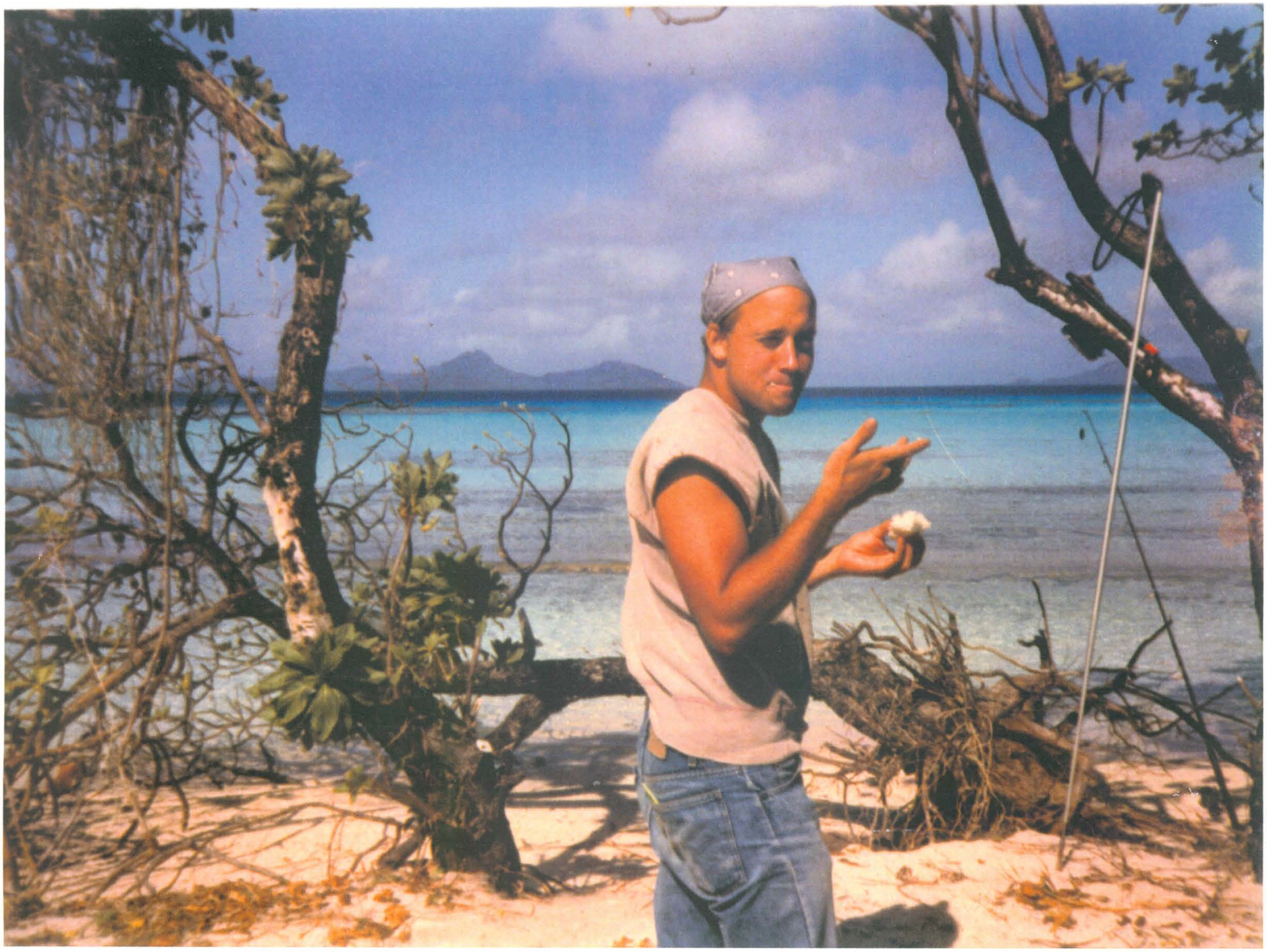

DISTRIBUTION OF PERMEABILITY PATTERNS - UPPER SAN ANDRES FORMATION OUTCROP, GUADALUPE MOUNTAINS, NEW MEXICO

APPROVED:

Supervisor: John M. Sharp, Jr.

John M. Sharp, Jr.

Larry W. Lake

L. W. Lake

Charles Kerans

Charles Kerans

DISTRIBUTION OF PERMEABILITY PATTERNS - UPPER SAN ANDRES FORMATION OUTCROP, GUADALUPE MOUNTAINS, NEW MEXICO

by

MALCOLM ALEXANDER FERRIS, B. S.

THESIS

Presented to the Faculty of the Graduate School of

The University of Texas at Austin

in Partial Fulfillment

of the Requirements

for the Degree of

MASTER OF ARTS

THE UNIVERSITY OF TEXAS AT AUSTIN

May, 1993

ACKNOWLEDGMENTS

WORD... This thesis was written on Macintosh computers using MicrosoftWord software (5.0). My greatest thanks go to the members of my advising committee: Dr. J. M. Sharp, Dr. L.W. Lake, and Dr. C. Kerans, whose combined support has helped make this thesis possible. I also wish to thank the members of the Reservoir Characterization Research Lab who contributed their time to the collection of data: M. Barton, A. Czebiniack, M. Holtz, H.S. Nance, Dr. R. Senger, and R. Single. Additional credit and thanks to (Dr., in progress) B. Fitchen for editing the geologic interpretations. And thanks again to all for staying with me.

The most profound appreciation for the opportunity to pursue this degree goes to my parents, J. Burkam and Eileen, without whose support nothing would have been possible. Love you always.

Word again to everyone who shared the years with me: John^2, Keg, Leo, Bob, Becky, Dave, Rob^2, Carla, Rich, Edna, Tim, and all professors and staff members of the UT-DoGS and BEG with whom I have relied upon for technical support. And the last word to the little people: Dub, W.K., Whamo, Dorie, Tesnus, Otto, Dwim, Dante, Idaho, Carl, and Milt.

DISTRIBUTION OF PERMEABILITY PATTERNS - UPPER SAN ANDRES FORMATION OUTCROP, GUADALUPE MOUNTAINS, NEW MEXICO.

Abstract: Permeability patterns in the subsurface are primary controls on fluid flow. Predictable patterns of permeability can be applied to secondary oil recovery or modeling of solute transport. Conventional field data from well tests are insufficient for accurate modeling of the subsurface environment. The use of analog models from outcrop data with emphasis on analog textures and facies can provide needed insights. Permeability was measured on a 2613 ft. long and 20 - 25 ft. thick outcrop of a single mudstone-bounded carbonate parasequence in a transgressive shelf margin. The four genetic facies were: 1) a mud-dominated deep-water flooded shelf; 2) a coarsening upward, mud-supported ooid and peloid wackestone/packstone shallow shelf; 3) an ooid and peloid grain-supported bar crest; and 4) an ooid and peloid grain-supported, coarsening-upward bar flank. Data were collected in the field with a mini-permeameter and on core plugs from the outcrop. Sampling was performed at 769 locations along 31 vertical transects and in two small-scale grid patterns. Separation distances varied from 325 ft. between the widest spaced vertical transects, down to 1 in. separation within the smallest scale grid.

Horizontal variogram analysis for range values indicate a scale dependency based on the sample separation and related variogram step distance, h. Horizontal variogram ranges were 253 ft. (77.8 m) and 748 ft. (230 m) for h of 100 ft. (30.7 m); 22 ft. (6.7 m) for h of 10 ft. (3.1 m); 4 ft. (1.3 m), for h of 1 ft. (0.3 m); and 8 in. (0.2 m) for h of 1 in. (0.03 m). These all exhibited a proportionately high nugget-to-sill ratio of poorly developed spherical variogram models. Development of vertical variograms indicate vertical variability within the parasequence. In populations which represented increasingly less of the whole parasequence thickness, an h of 1 ft. provided vertical ranges of 13 ft., 10.2 ft. and 4 ft. (a nested set), and 2.1 ft. In the 1 in. grid, an h of 1 in. provided a vertical variogram of range 4.2 in. Nugget-to-sill ratios were all moderate with exhibited poorly developed spherical variogram models. A preliminary model based upon the data in a single parasequence can be applied as a grainstone sequence with randomly distributed permeabilities that is bounded above and below by a confining mud dominated layer which may or may not be continuous.

TABLE OF CONTENTS

LIST OF FIGURES

LIST OF TABLES

CHAPTER 1
INTRODUCTION

Characterization of permeability variation is a fundamental science of the petroleum engineer and the hydrogeologist in order to understand the movements of fluids in the subsurface. In most subsurface environments, the accurate description of permeability distributions is limited by the inaccessibility of the subsurface environment for the required detail of sampling. For this reason, the use of geologically analogous outcrop sampling has been suggested to determine whether the permeability values measured on outcrop exhibit a characterizable pattern that can be applied to fluid flow models. The concepts of statistical evaluation of analogous geologic settings are being widely developed in the field of hydrocarbon reservoir engineering, but the same principles are applicable in hydrogeology for the modeling of environmental contamination, though this later use is less well developed.

This study differs from previous published work in outcrop modeling in that the data are concentrated within genetically-related bed sets bounded by flooding surfaces. This geologic description fits the definition of a single parasequence within cyclically stacked carbonate deposits (Van Wagoner and others, 1988). Selection of the study site was based on attributes of a proven geologic analog between the outcrop and the subsurface of a known productive oil-field, and for an extensive exposure of outcrop accessible for sampling.

Throughout this study, the scale of sample collection has been a most important consideration. To address the unknown scales at which permeability variation within the outcrop may exist, this study was implemented through a series of sampling schemes at various scales. The main consideration for determining the largest scale of permeability sampling used in the investigation was that the results could be used to enhance oil field production and recovery efficiency. This required that the scale of the sampling was comparable with intra- and inter-well spacing of oil fields (i.e., tens to thousands of feet or meters).

1.1 PROJECT OUTLINE

To present the data and findings of this study this thesis is organized as follows:

1) introduce the project through the discussion of its goals and references to previous studies (Chapter 1),
2) provide the general geologic setting of the pore textures observed in the rock fabrics of the study site (Chapter 2),
3) present the theoretical statistics as applied to the data set (Chapter 3),
4) elucidate the methods of data sample collection with reference to the geology of the study area (Chapter 4),
5) analyze the results of the study using geostatistical tools and geologic observations of the stratigraphic and petrologic relationships (Chapter 5), and
6) discussion of results (Chapter 6).

1.2 OVERVIEW

1.2.1 THEORY

As a study of spatial variations in permeability within a depositional unit, this project required an extensive sampling program that would create data sets of spatially-distributed permeability values for statistical interpretation. Because the investigation targeted the ability to determine reservoir-scale heterogeneities, the study site needed to be large enough for outcrop exposures to match the size of typical hydrocarbon reservoirs. In order to apply the results of this study's to actual systems, it was necessary that the study site be proximal to oil fields producing from the same or an otherwise similar formation. Outcrops of the San Andres Limestone on the Algerita Escarpment of the Guadalupe Mountains in Otero County of southwestern New Mexico (Fig. 1) were studied previously by Hinrichs and others (1986) and Kittridge (1988), and the choice of that location for another study was most logical.

This study follows geostatistic techniques first developed by Krige (1943) for estimation of economic ore reserves. These principles were furthered in the fields of geostatistics and stochastic modeling by Matheron (1963), David (1977), and Journel and Huijbregts (1978). More recently, advances have been made that go beyond the early applications of geostatistic theory in ore reserve estimation. These advances have been mainly in the applications of stochastic principles and conditional simulation models to petroleum reservoir and ground water systems (Amhed and de Marsily, 1987; Behrens and Hewett, 1990; Dagan, 1985; Delhomme, 1978 and 1979; Fogg, 1986; Gelhar, 1986; Sudicky and others, 1986; and Weber, 1982).

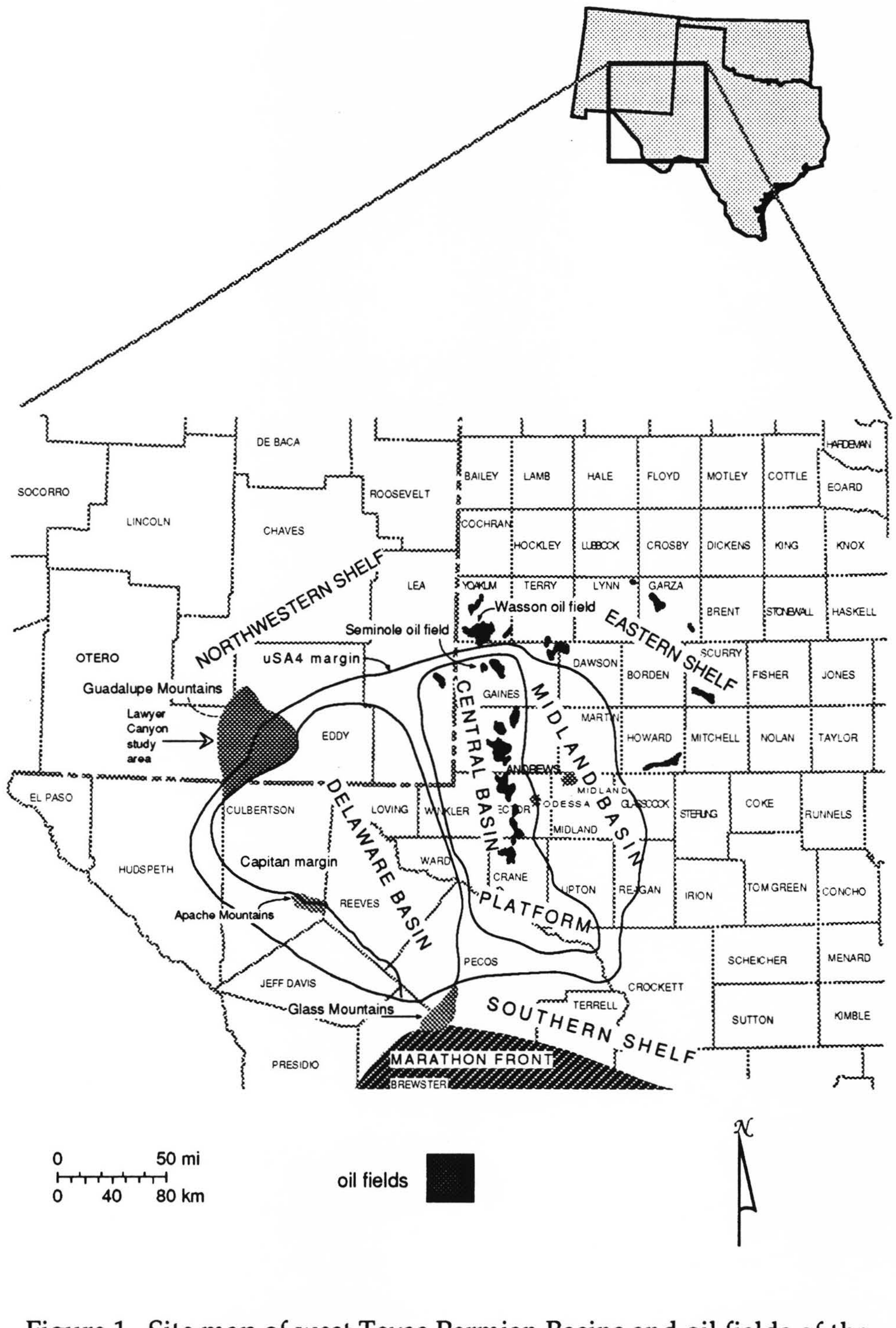

Figure 1. Site map of west Texas Permian Basins and oil fields of the San Andres formation. Adapted from Kerans and others, 1991.

1.2.2 THE MECHANICAL FIELD PERMEAMETER

Measurement of permeability values in the field was made possible with a mechanical field permeameter (hereafter referred to as MFP, photo shown in Fig. 2). The particular instrument used in this study was developed within the University of Texas at Austin, Petroleum Engineering Department by D. Goggin, from a prototype design published by Eijpe and Weber (1971), founded on principles of permeability measurement described by Dykstra and Parsons (1950), and extended by Chandler and others (1989b) and Goggin (1988). Permeability values were calculated through a mass-balance application of Darcy's Law (Goggin, 1988; reprinted in Appendix E), using a flow rotameter and pressure gage recordings to estimate the rate at which a known gas was injected at the rock surface. Previous applications of the MFP on outcrop of the San Andres formation by Kittridge (1988) and on outcrop of the Page Sandstone, northern Arizona, by Chandler (1986) and by Goggin (1988) have proven the accuracy and viability of the MFP in outcrop permeability descriptions. A more precise electronic field mini-permeameter was developed by the Department of Geological Sciences (Fu and others, 1992) after the data collection of this study was completed.

In addition to the MFP derived permeability values, core plug samples were collected from the outcrop. Core plugs were collected on outcrop in selected locations to provide petrographic data through thin section, porosity, and permeability analyses. The spatial distribution of the core plugs sampling was intended to both expand and validate MFP derived permeability data.

Figure 2. Mechanical Field Permeameter (MFP) used for field collection of permeability data. MFP components: A - High pressure nitrogen gas source. B - Three (3) rotameter stands to hold interchangeable flow tubes. C - Test quality pressure gage and back-up units. D - Flexible tubing with silicon probe-tip and on/off valve.

1.2.3 STATISTICAL ANALYSIS

Data were analyzed through the comparison of variances between permeability values based on their spatial relationships. This was accomplished through a FORTRAN demonstration program published by David (1977) that computed semivariance as a function of a vector, h. Values of the semivariance, $\gamma(\mathrm{h})$, were calculated for horizontal and vertical search directions. Represented graphically as experimental variogram plots, $\gamma(\mathrm{h})$ versus distance, these were interpreted for the statistical parameters of range (horizontal or vertical distances defined by the vector, h) and characteristic variance, or sill value.

Range, sill, and other characteristics of the permeability distribution were interpreted from the experimental variograms. These results were compared for direction and relative distance (i.e., the distance value of vector h) between permeability values in catagorized, scale-based sample sets of the permeability data. Comparison of the experimental variogram parameters between the sample sets provided insight as to the statistical nature of the distribution was identifiable from the and estimations for permeability values at distances from known values provided were predictable as a function of the observed statistical parameters. These characteristics of permeability distributions are useful for representing permeability structure of carbonate units in fluid flow simulations.

1.3 Previous Studies

1.3.1 Permeability Distributions in Carbonate Rock Formations

Previous studies have been conducted by Hinrichs and others (1986) and Kittridge (1988) to determine the distribution of permeability measured on the San Andres formation outcrop on the Algerita escarpment of the Guadalupe Mountains. These investigators used permeability and porosity data, supplemented by petrographic data from thin section descriptions, to compare the observed textural characteristics of the rock with the measured permeability. Permeability values were the principal variable for analyses. Other information was interpreted to reinforce correlation between the permeability of the rock and textural characteristics.

These preliminary studies addressed two basic questions. The first question concerned the validity of the assumption that discrete zones of high or low flow exist within a geologic unit. The second question was how these findings might be incorporated into reservoir models that would predict permeability distribution patterns in the subsurface based upon limited information. In both of the early studies, the range of distances and the patterns of sampling were designed to incorporate multiple and varied textures for the identification of permeability correlations within the formation. These were intended to provide accurate parameters for reservoir models. The accuracy of these models depends on the initial assumptions used in the data collection that produces the parameters.

Hinrichs and others (1986) used core plug sample data taken from eight individual porous beds at sample separation distances of 100, 10, and 1 ft or less. The permeability and porosity values were then compared to subsurface data available from the San Andres formation in Wasson field, located to the Northeast in Texas (see Fig. 1). Statistical data of the permeability values were compared for individual bed and for the different lateral sampling distances. Visual representation of the permeability patterns was obtained by contouring the data between individual beds, showing tortuous and discontinuous zones of high permeability within a background of relatively lower permeability.

Kittridge (1988) sampled within a discrete area of the San Andres formation that extended across the boundary of the middle and upper sequences of the formation (sequences as interpreted by Sarg and Lehmann, 1986, and Kerans and others, 1991, and discussed below in Chapter II, Geology). His sampling consisted of closely spaced points within evenly spaced grids and vertical transects of variable separation distances. Kittridge tried to evaluate outcrop distribution patterns and the comparability of outcrop and subsurface data given analogous geologic characteristics. The raw data collected for the study were confounded by an error in the preparation of the weathered surface through his use of a mechanical grinder. Computer contouring showed the permeability heterogeneities to extend down to scales as small as one-half inch, and results of semivariance analysis detected statistical correlation at ranges that were dependent of the distances between sample points.

The statistical work presented in these previous studies on the San Andres formation were able to show two general conclusions. First, the distribution patterns of permeability values were heterogeneous within packages of genetic facies. Second, there exist isolated high permeability zones within an overall low permeability rock matrix. However, these preliminary studies were inconclusive in defining tractable statistical relationships to indicate a predictable trend in the permeability expectations based upon semivariance between known permeability values.

1.3.2 PERMEABILITY DISTRIBUTIONS FOR OTHER LITHOLOGIES

The application of geostatistical analysis should be restricted to geologic sections similar to those where the study was conducted. However, the methodology incorporated in geostatistical analysis is not restricted to any particular rock type, or particular variable (e.g., permeability).

Other researchers have investigated reservoirs and aquifers for permeability patterns in sandstones (Chandler and others, 1989; Fu and others, 1992; Goggin, 1988; Goggin and others, 1988a; and Weber, 1982), unconsolidated deposits (Sudicky and others, 1985, and Beard and Weyl, 1973), and welded ash flow tuffs (Fuller, 1990, Fuller and Sharp, in press; and Sharp and others, in press). The emphases of these studies revolve about the ability of data to determine patterns of permeabilities for use in modeling applications. Of the above, some have used analogous outcrop data to set the model controls (e.g. Chandler, 1986; Chandler and others, 1989; Goggin, 1988; and Weber, 1982), while others have relied upon dense sampling strategies using cores and well tests for their permeability data base (Sudicky and others, 1985) or the inference of geologic process controls such as fracturing and surface weathering on permeability and porosity development (Fu and others, 1992; Fuller, 1990; Fuller and Sharp, 1992; and Sharp and others, in press).

CHAPTER 2
GEOLOGY

The geologic descriptions that follow are compiled from King (1942 and 1948), Skinner (1946), Hayes (1964), Todd and Silver (1969), Sarg and Lehmann (1986), and Kerans and others (1991). Terminology for the facies textures follows that developed for application to carbonate rock systems by Choquette and Pray (1970; Fig. 3). Stratigraphic placement and description of the San Andres formation rely upon the work of Sarg and Lehmann (1986), augmented by Kerans and others (1991) for descriptions in the more immediate area of the Algerita Escarpment. Terminology used in the description of sequence-stratigraphic relationships follows Van Wagoner and others (1988) for carbonate depositional systems and specific application of terms to the local facies geology follows the interpretations of Kerans and others (1991) in their mapping of the Algerita Escarpment.

2.1 STUDY SITE SELECTION

The selection of the San Andres Formation for an outcrop reservoir analog study was based upon the history of the formation as a prolific oil producer in west Texas (Galloway and others, 1983), the accessibility of extensive outcrop exposure on the Algerita Escarpment of the Guadalupe Mountains in southwestern New Mexico, and the proximity of the outcrop to two producing San Andres Formation reservoirs (in Texas, the Seminole Field in Gaines Co., and the Wasson Field in Yoakum/Gaines Co.).The positive results reported by Hinrichs and others (1986) and

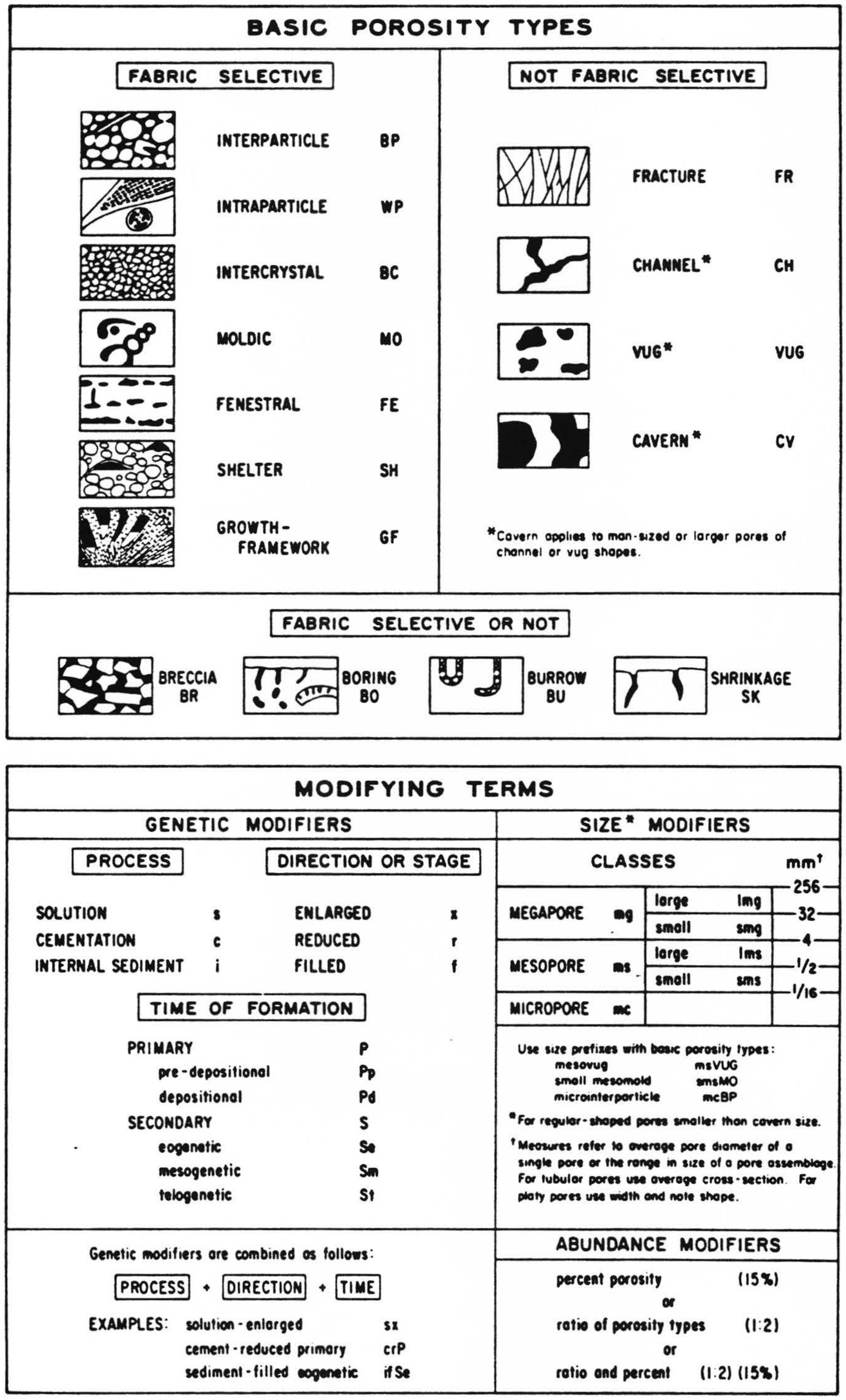

Figure 3. Classification and nomenclature of pore types and pore systems in carbonate rocks as used in this study (from Choquette and Pray, 1970).

Kittridge (1988) further justified locating the study site in the San Andres outcrop of the Algerita Escarpment. In particular, Kittridge's (1988) comparison of the San Andres Formation outcrop at Lawyer Canyon to the subsurface unit at Wasson Field obviated the choice for the same general study area.

San Andres reservoirs are within shallow-water platform top and upper slope carbonates with laterally extensive facies distributions and generally low (30%) recovery efficiencies (Galloway and others, 1983). Well spacing in the Wasson and Seminole fields is one well per 10- or 20-acres, in standard 5-spot or 9-spot pattern, providing inter-well distances of 660 to 1320 feet. To be able to characterize lateral variability of permeabilities at such distances, the outcrop selected needed to be undisrupted laterally for at least 2,000 feet. The Lawyer Canyon area easily satisfies this requirement, because lateral exposures of continuous outcrop are double the inter-well distances of the oil-fields.

Finalizing the decision of site selection was the criterion that this study would characterize a single cycle of genetically related beds. In the previous investigations of Hinrichs and others (1986) and Kittridge (1988), the goals were to sample at a large scale and thereby include many different rock textures. For this study, the area was confined to a single cycle of genetically related and flood-bounded bed sets, the single parasequence of Van Wagoner and others (1988). This limits the number of different facies involved in the analyses of permeability distributions and allows a significant number of measurements to be collected at various lateral separation distances within each depositional facies of the parasequence.

2.2 REGIONAL STRUCTURAL AND STRATIGRAPHIC FRAMEWORK

Early structural descriptions of the Guadalupe Mountains were provided by King (1942, 1948) and Hayes (1964). They identified the mountains as the desiccated remnants of a Tertiary age uplift that tilts gently to the northeast (Fig. 4). The uplift is bounded by north-northwest striking normal faults to the west (the Algerita Escarpment in the north section of the mountains) and to the east by a monoclinal fold superimposed over late Paleozoic thrust faults (the Huapache monocline). To the southeast, the boundary is represented by the intersecting northeast striking reef front composed of the resistant Capitan Limestone. West of the Guadalupe uplift, Big Dog and Little Dog Canyons form a graben area that separates the Brokeoff Mountains, a collapsed plateau, from the Guadalupe Mountain uplift (King, 1948). The north-northeast striking line of normal faults continues south of the Guadalupe Mountains where it forms the western boundary of the Delaware Mountains.

The San Andres Formation was originally named by Lee (1909) for outcrops in the San Andres Mountains of south-central New Mexico. The San Andres is acknowledged to be part of a wide spread Permian (Leonardian/Guadalupian) aged platform composed of stacked upward-coarsening carbonate cycles rimming the margins of the Delaware and Midland Basins in southeastern New Mexico and west Texas (King, 1942 and 1948). In the area of the Algerita Escarpment, the San Andres rests between unconformable contacts at the top of the Yeso and at the bottom of the Grayburg (Sarg and Lehmann, 1986, and Kerans and others, 1991). In this area, the San Andres Formation is predominantly dolomitic, the principle diagenetic alteration

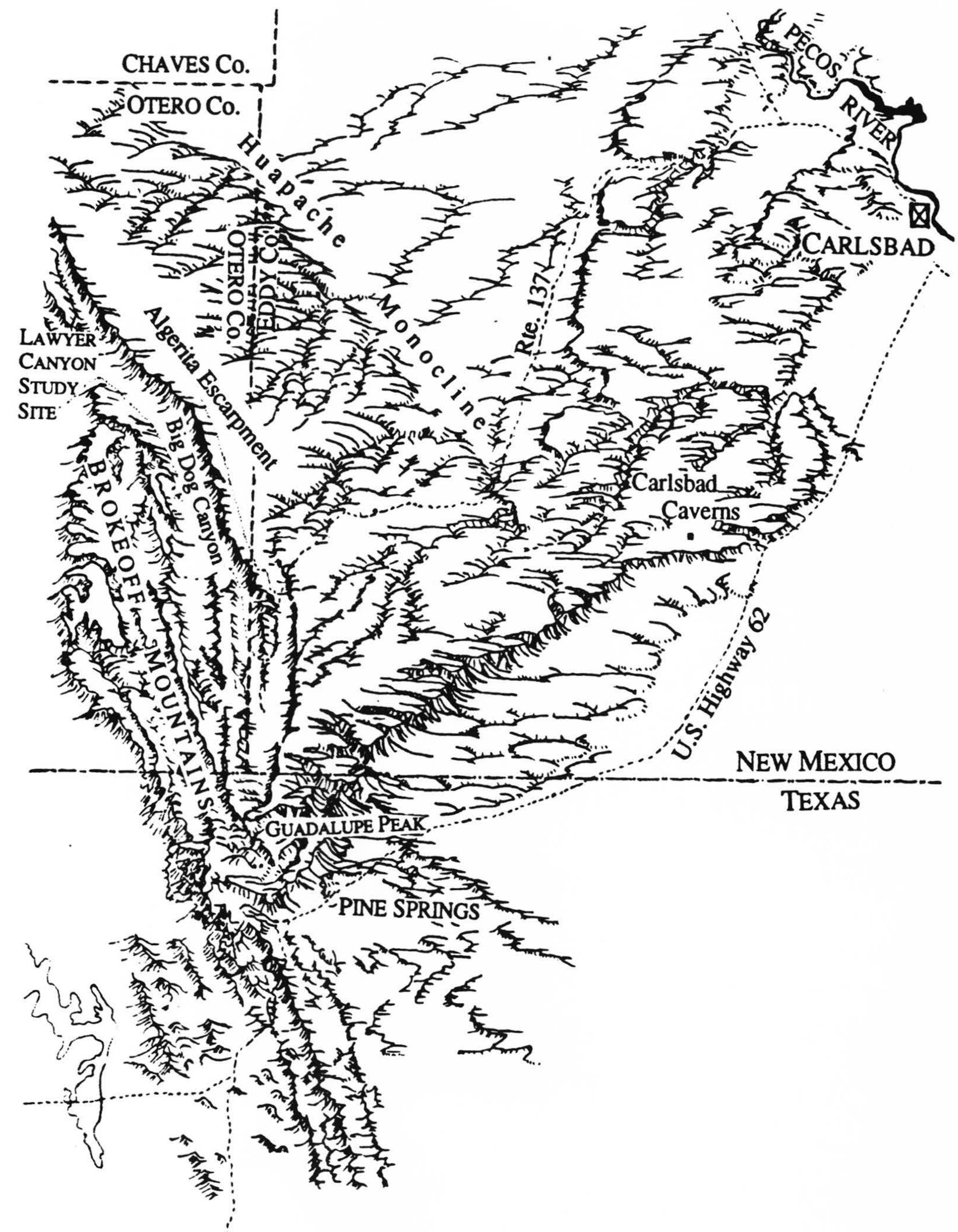

Figure 4. Guadalupe Mountains and location of Lawyer Canyon on the Algerita Escarpment, Otero Co., New Mexico. Shown are the major structural features in relation to the study site (after King, 1942).

dated to have occurred in late Guadalupian time, with infiltration of hypersaline waters percolating down from overlying tidal flats (Leary, 1984; Todd and Silver, 1969).

2.3 Local Geology

Development of a sequence-stratigraphic model for the San Andres in the region of the Guadalupe Mountains was first presented by Sarg and Lehmann (1986) and recently refined by Kerans and others (1991; Figs. 5-7). This model divides the San Andres into two major third-order sequences, the combined lower and middle lithologic units (lmSA) and an upper unit (uSA). The lower-middle San Andres third-order sequence (lmSA) is composed of a lower open marine transgressive bank unit overlain by a middle prograding restricted ramp system. The sequence boundary between lmSA and uSA is a conformable boundary that is well exposed in Lawyer Canyon. The upper third-order sequence (uSA) is further divided into four fourth-order sequences (uSA1-4) by Kerans and others (1991) based on interpretations of detailed stratigraphic maps completed along the Algerita Escarpment. Each fourth-order sequence is a progradational, generally offlapping package of parasequence sets composed of ramp crest, restricted outer ramp, and inner ramp facies tracts.

Fourth-order sequence boundaries are identified from karst surfaces or tidal flat complexes located in the top parasequence of the previous sequence. The top of

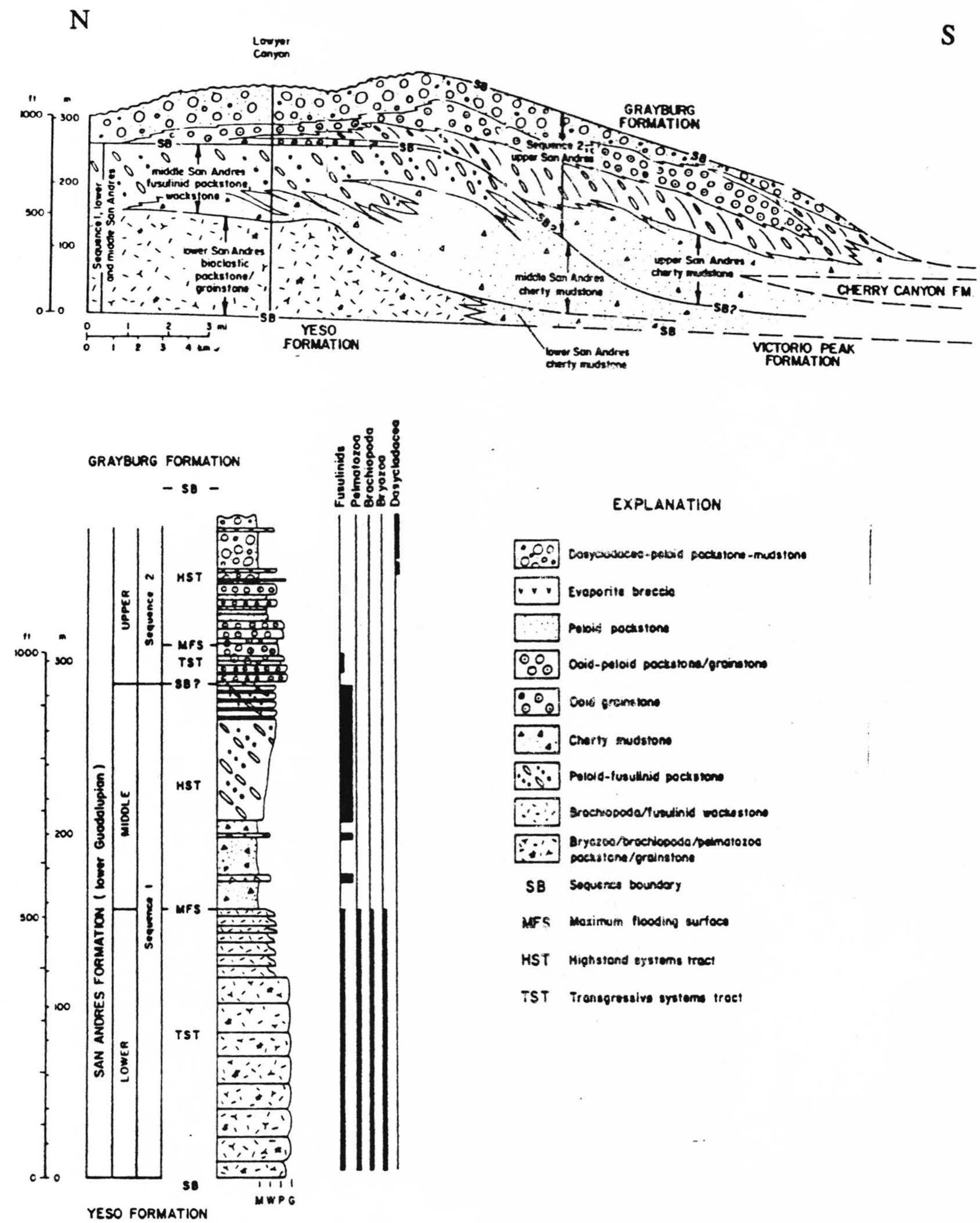

Figure 5. Simplified geologic cross-section of San Andres formation based on compiled information from outcrop data along the Algerita Escarpment (top). Sequence stratigraphic interpretation of major (third order) sequences (from Kerans and others, 1990).

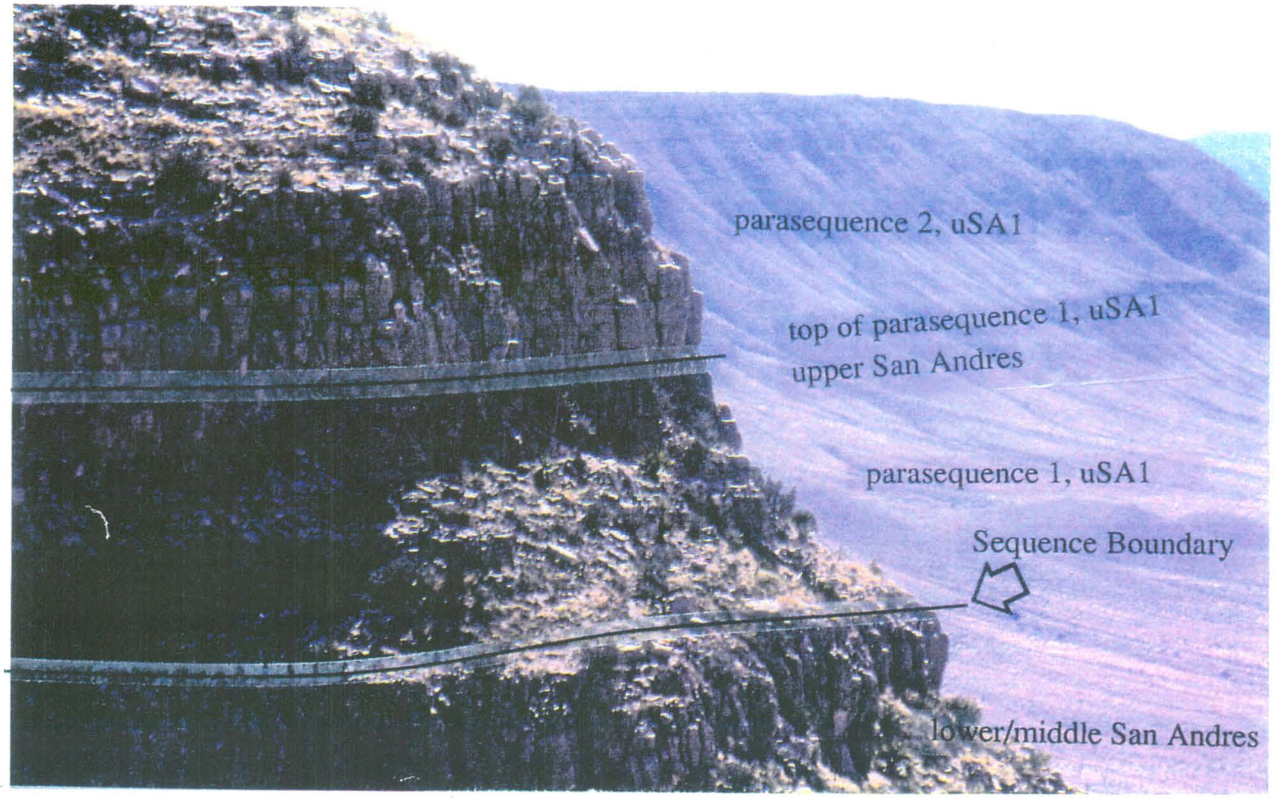

Figure 6. Sequence boundary (lmSA/uSA) exposure at Lawyer Canyon, Algerita Escarpment. View is from north-side of canyon looking south at transects A17 and A18.

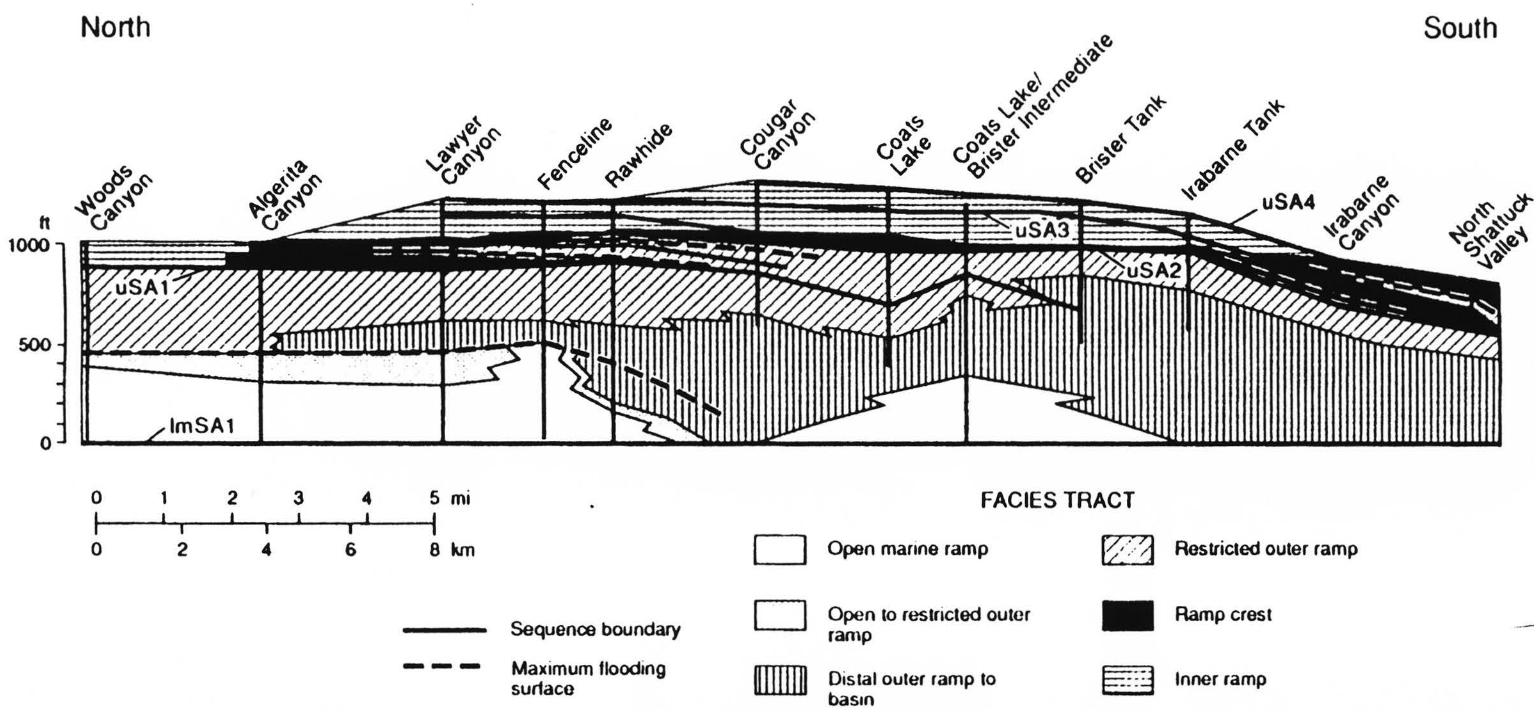

Figure 7. Fourth-order sequences of San Andres formation outcrop, Algerita Escarpment, Guadalupe Mountains. From Kerans and others (1991).

uSA1 is a karsted bar-top surface exhibiting characteristics of subaerial exposure and subsequent onlap of uSA2 burrowed mud facies. Exposure of uSA2 is predominant 1.5 miles (approximately 2 kilometers) down-dip from Lawyer Canyon. At the top of uSA2, the sequence boundary of uSA2/3 is demarked by a karst surface. Between the uSA3 and uSA4 the sequence boundary is interpreted from a tidal flat complex at the top of uSA3. The top of uSA4 is set at a variably developed karst surface that is also the upper sequence boundary between the San Andres and Grayburg formations.

2.4 Geologic Descriptions Of Study Area

Exposure of uSA1 in the Lawyer Canyon area (Fig. 8) varies from 140-190 ft thick and it is composed of nine identified parasequences, of which the basal parasequence is the study area for this investigation. Here, the third-order sequence boundary (lmSA/uSA1-SB) exists at the base of a thick, light-white colored mudstone bed that overlies darker, fusulinid-rich packstones. This mudstone is interpreted as the flooded surface in the basal parasequence of uSA1, representing a minor downward shift in relative sea-level (30 - 50 feet) and a lateral shift of several miles in facies tracts (Kerans and others, 1991).

As the general case among the parasequences of uSA1, the basal parasequence is a shallowing-upward cycle (after James, 1979; Fig. 9) composed of dolomitic, upward-coarsening mudstone to grainstone beds. A cross-section of sixteen (16) measured sections (Fig. 10), provided by C. Kerans, shows this basal parasequence to be composed of four genetically related deep-to-shallow water facies: (1) deeper-water, flooded shelf mudstone; (2) shallow shelf mud-supported, ooid and peloid

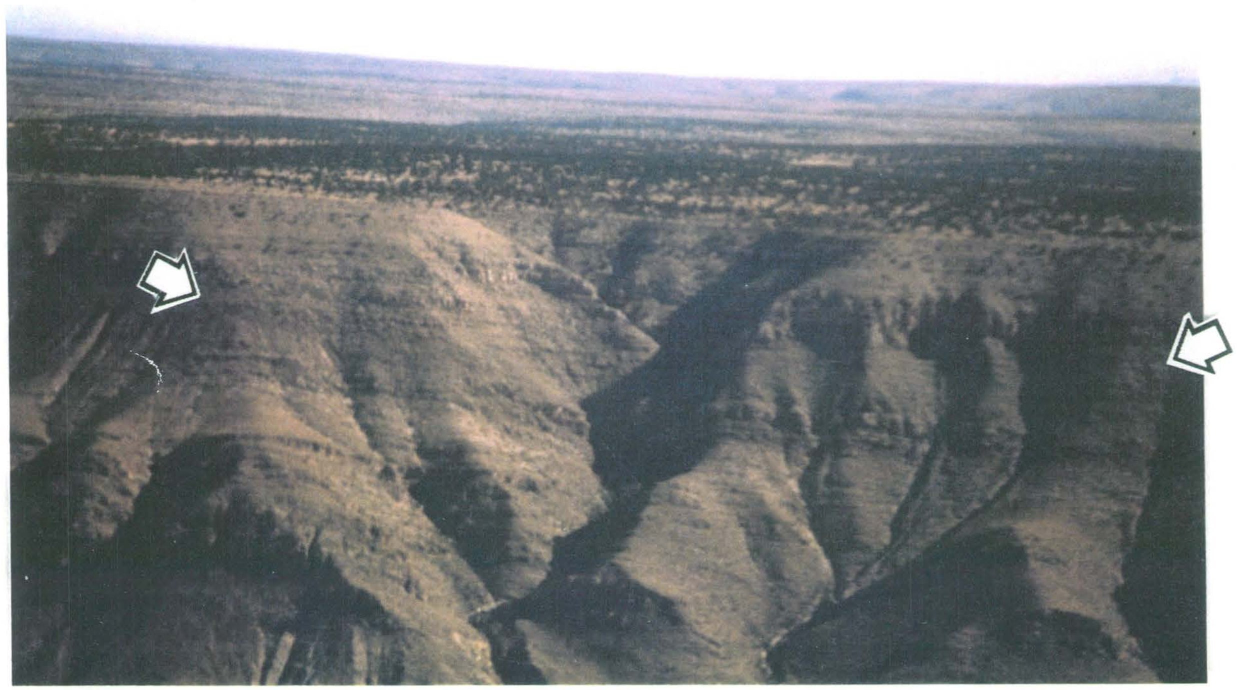

Figure 8. Aerial photograph of Lawyer Canyon taken from over Dog Canyon facing east-northeast. Arrows point to lmSA/uSA sequence boundary at approximated lateral boundaries of the study area.

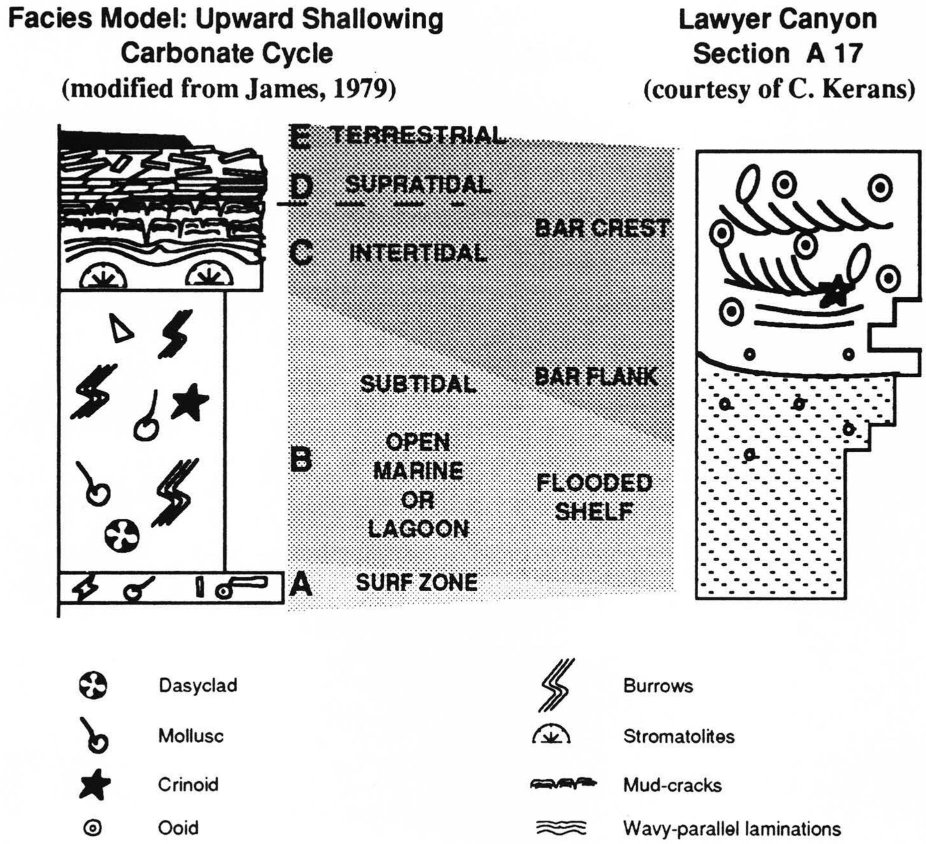

Figure 9. Generic model for shallowing-upward carbonate deposition with comparison to a measured section used in this study. A) Lithoclast-rich lime conglomerate or sand (this facies not present in uSA1 basal parasequence). B) Fossiliferous limestone (present as mud-dominated flooded shelf in uSA1 basal parasequence). C) Stromatolitic, mud-cracked cryptalgal limestone or dolomite (present but with few mud-cracks evident in uSA1 basal parasequence). D) Well laminated dolomite or limestone, flat-pebble breccia (present in uSA1 basal parasequence as tabular or troughed-cross bedded dolomite, no breccia). E) Shale or calcrete, this unit often missing (not present in uSA1 basal parasequence).

Figure 10. Symbols.

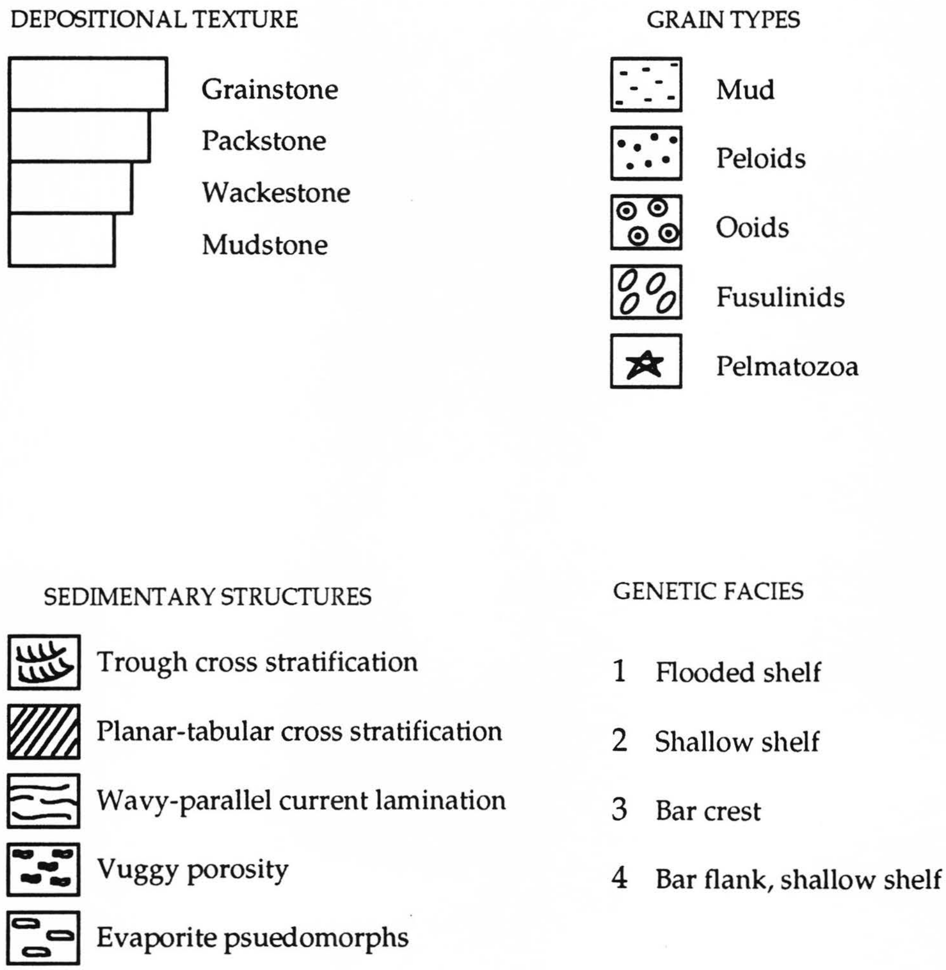

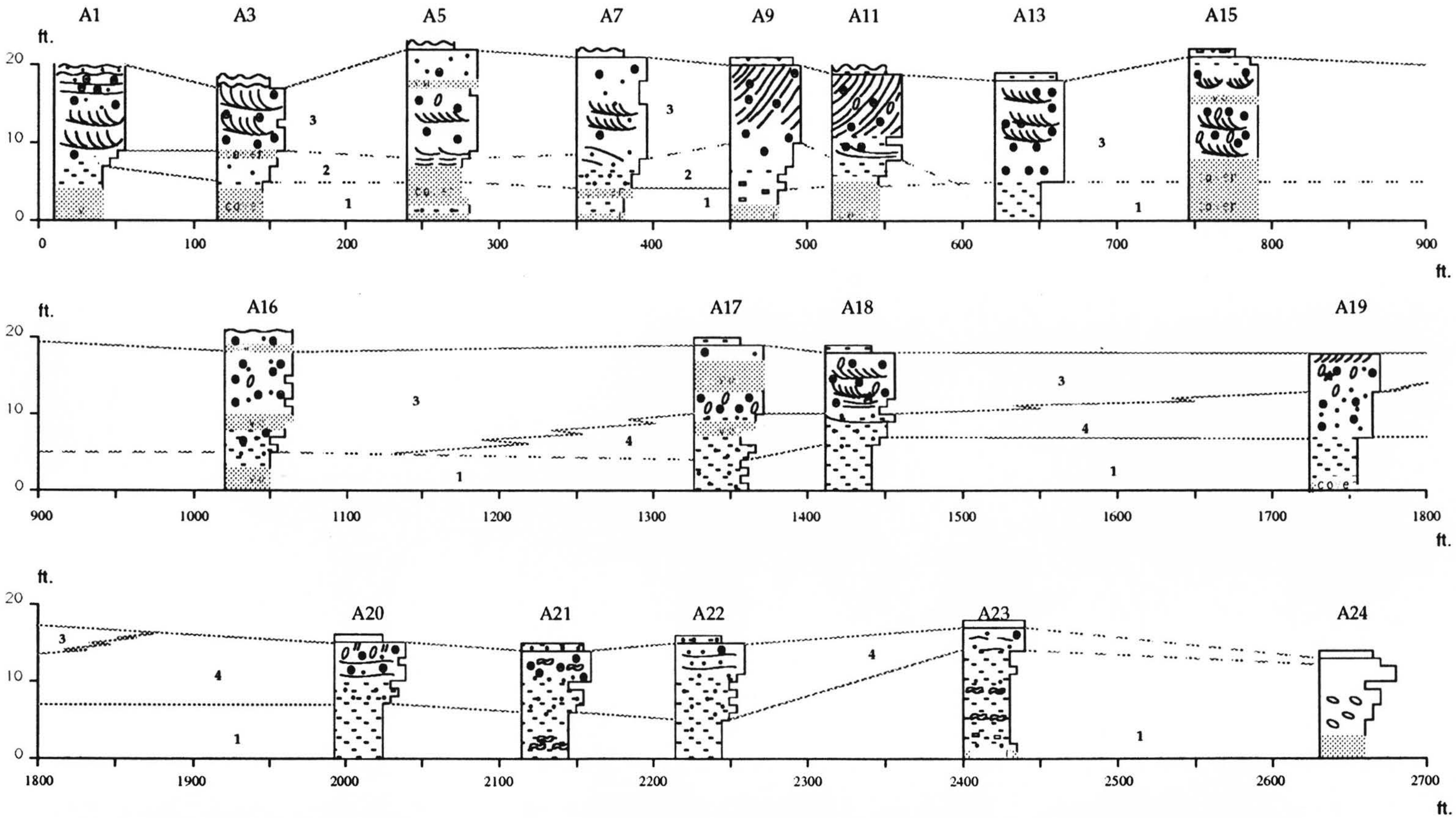

Figure 10. Original sixteen (16) measured geologic sections mapped in parasequence 1, Upper San Andres formation, in Lawyer Canyon study site, as mapped by Kerans and Nance (1989, unpublished). Depositional texture, grain types and sedimentary structures shown with interpretations of genetic facies lateral continuity (see explanation on opposite page).

wackestone/packstone; (3) ooid and peloid grainstone bar crest deposits; and (4) shallow shelf, bar flank coarsening upward ooid and peloid wackestone to grainstone.

Facies #1 is a low-energy, flooded shelf, sheet-like deposit that thickens southward. This facies is the marker bed that is continuous throughout the study area. Within the study area, the bed thickens from approximately five (5) feet in the north (sections A3 to A13) to 13 feet in the south (section A24). Internally, the facies is characteristically massive and lacking in preserved laminations. This may be indicative of bioturbation or diagenetic alteration of the carbonate mudstone fabric that resulted in a recrystallization of lime mud to dolomite microspar (5 to 10 μm diameter; Fig. 11A). The exposed rock fabric is repeatedly interrupted by fractures at microscopic and larger scales, of which many at the smaller scales are filled by calcite and dolomite cements.

Facies #2 is a laterally discontinuous, low-energy draped shallow shelf deposit that overlies the mudstone bed (facies #1). Facies #2 coarsens gradationally upward from mudstone to wackestone. Thicknesses vary from 2 ft (section A1) to 5 ft (section A9) and the facies is assumed to pinch out between sections A11 and A13. Facies #2 contains wavy, parallel laminations interspersed with more massive intervals that show signs of bioturbation. Dolomite microspar replacement of carbonate mud and peloids overprints the original texture. Intercrystalline porosity is observed in thin section (Fig. 11B) as the dominant pore type. As in facies #1, calcite cement infilled fractures are also present in facies #2.

Facies #3 consists of a high-energy, shallow shelf ooid-rich grainstone and has been interpreted as a bar crest deposit. This facies caps the lower mud-rich facies

Figure 11. Thin sections from Lawyer Canyon core plug samples (uSA1 first parasequence) showing the variable textures found within each of the four identified generic facies. All scales are 1.3 mm = 100 μ (magnification 40x).

(A - top left) Flooded shelf facies (#1), mudstone texture: carbonate mudstone replaced dolomite microspars (>30 μ diameter), fractures and vugs have been infilled by later calcite cement. Core plug location: A9 - 2 ft. from base of parasequence; $\phi = 9.50$; k = 13.51 md.

(B - top right) Shallow shelf facies (#2), mudstone/wackestone texture: remnant peloids (arrows) in mudstone replaced by dolomite microspars, fractures have been infilled by later calcite cement. Core plug location: A9 - 7 ft. from base of parasequence; $\phi = 8.50$; k = 0.71 md.

(C - bottom left) Bar crest facies (#3), grainstone texture: grains replaced by dolomite microspars, later dissolution and cementation (dolomite/calcite) has disrupted the grain fabric and filled intergranular pore spaces. Core plug location: A5 - 13 ft. from base of parasequence; $\phi = 15.60$; k = 13.67 md.

(D - bottom right) Bar flank facies (#4), grainstone texture: micritic-dolomite crystalization has replaced the grain-dominant fabric with relatively large crystals, later dissolution and compaction has disrupted the original intergranular porosity. Core plug location: A18 - 15 ft. from base of parasequence; $\phi = 19.60$;
k = 333.0 md.

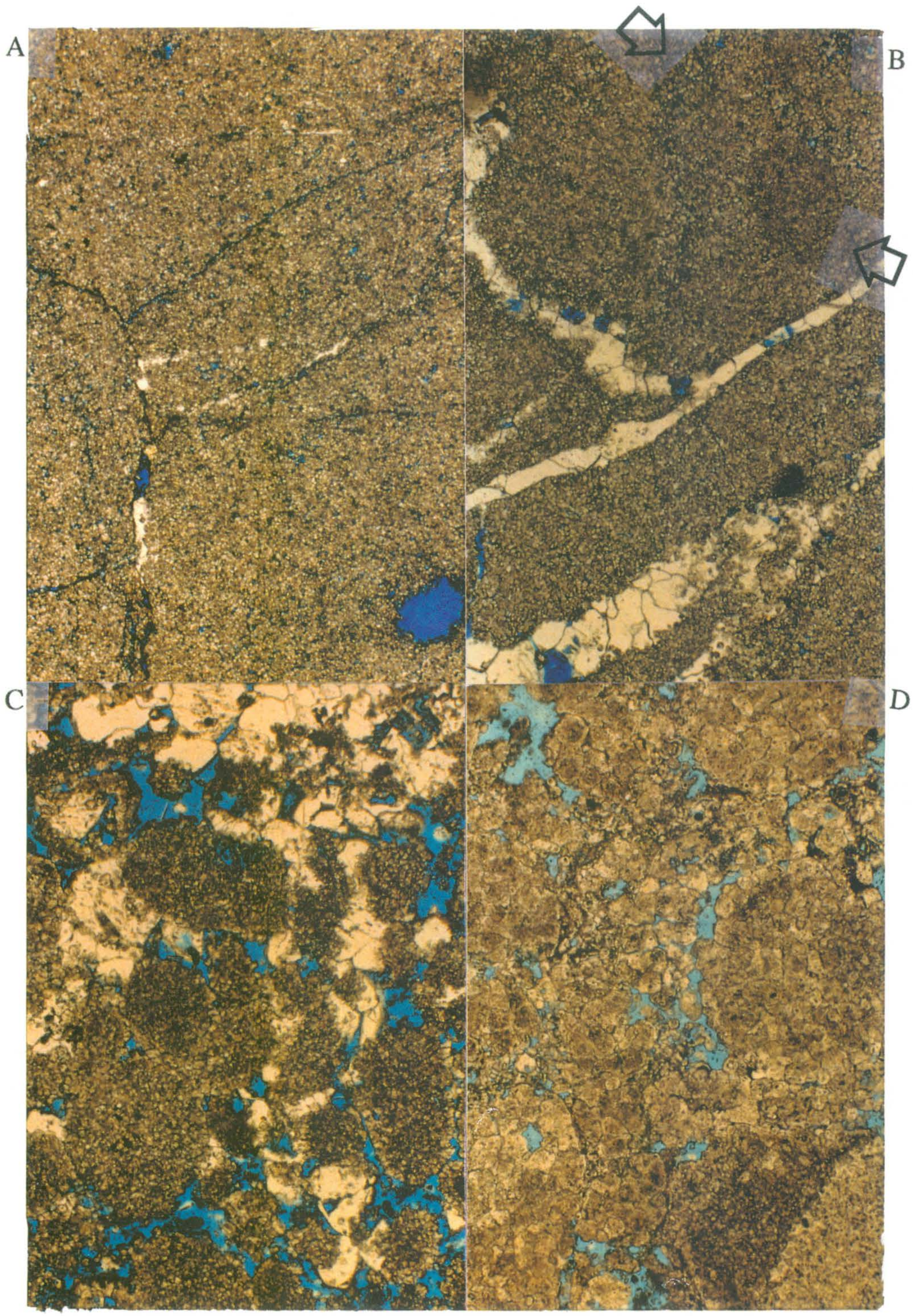
A
B
C
D

#2 in the northern end of the study area and is observed to pinch-out to the south (between sections A19 and A20) after varying thicknesses of 6 ft (section A3) to 15 ft (section A15). Trough cross stratification and planar-tabular stratification patterns are observed within facies #3, indicating reworking of the sediments by wave and tidal currents. The fabric is largely replaced by dolomitic microspar (less than 30 microns; Fig. 11C). Interparticle porosity is retained in thin section, though later dissolution and cementation by calcite and dolomite disrupts the grain-dominated fabric and infills some interparticle and fracture pore space.

Facies #4 is a shallow water, moderate energy shallow shelf facies, composed of packstone and wackestone textures. It is transitional between facies #2 and #3 and is interpreted as a bar-flank deposit. Thicknesses range from 9 feet (section A22) to a near pinch-out of 1 feet at the southern-most transect of the study area (section A24). The transition from mud- to grain-dominated texture is gradational through this facies. Facies #4 is typified by an upward increase in grain size. The southern (basinward) deposits show intermittently preserved wavy to parallel lamination. Replacement of the mud and grain fabric by dolomite microspar (10 to 30 μm diameter) caused an increase in intercrystalline porosity in the mud-supported fabric but did not significantly change the interparticle porosity (Fig. 11D).

2.5 OUTCROP WEATHERING

Alteration of the rock matrix with the weathering of the outcrop was an important concern in the set-up of the outcrop-reservoir analog study. Differences in porosity and permeability values for Lawyer Canyon outcrop and proximal subsurface reservoir samples were observed by Hinrichs and others (1986), Kittridge (1988) and Kerans and others (1991). These differences correlated with the presence of anhydrite and gypsum in the subsurface which are missing from the outcrop. Weathering of the sulfates from the outcrop increased porosity and permeability measurements of those rocks, but the overall change in values was assumed to represent a relative shift in values and not a change in the relative distribution of values in the rock matrix.

Surface weathering of the outcrop was assumed to be moderate, although examination of outcrop hand-samples revealed a dark-colored weathering rind between from 1/32- to 1/8-inch in thickness. Kittridge (1988) recognized the significance of removing this rind to expose the unaltered rock matrix for measuring permeability with the MFP device, however, the method he employed was later determined to be destructive and inappropriate for the study. For this study, the method of removing the weathered rind from the rock surface was determined prior to sampling and is presented in Chapter 4, Section 3 (Permeability Sampling Patterns). As explained in that section, the technique was chosen for the completeness of rind removal and relative lack of damage to the newly exposed rock fabric.

The most distinctive feature of the Lawyer Canyon study area is the pervasive fracturing on the outcrop. Fractures were observed to occur along bedding contacts as well as numerous other planes unassociated with depositional structure. Fractures range from the microscopic to the macroscopic scale (Fig. 12). Cored wells drilled through the San Andres formation in a location 1,000 feet behind the Escarpment front (Kerans and others, 1991; Fig. 13) provided evidence of similar fracturing extending into the raised plateau. This fracturing of the formation was not a shared

Figure 12. Outcrop fractures of macroscopic scale. Shown here, the MFP probe-tip is applied to a prepared, unfractured location for a permeability measurement. This photograph is representative of the facies #1 (mudstone) outcrop.

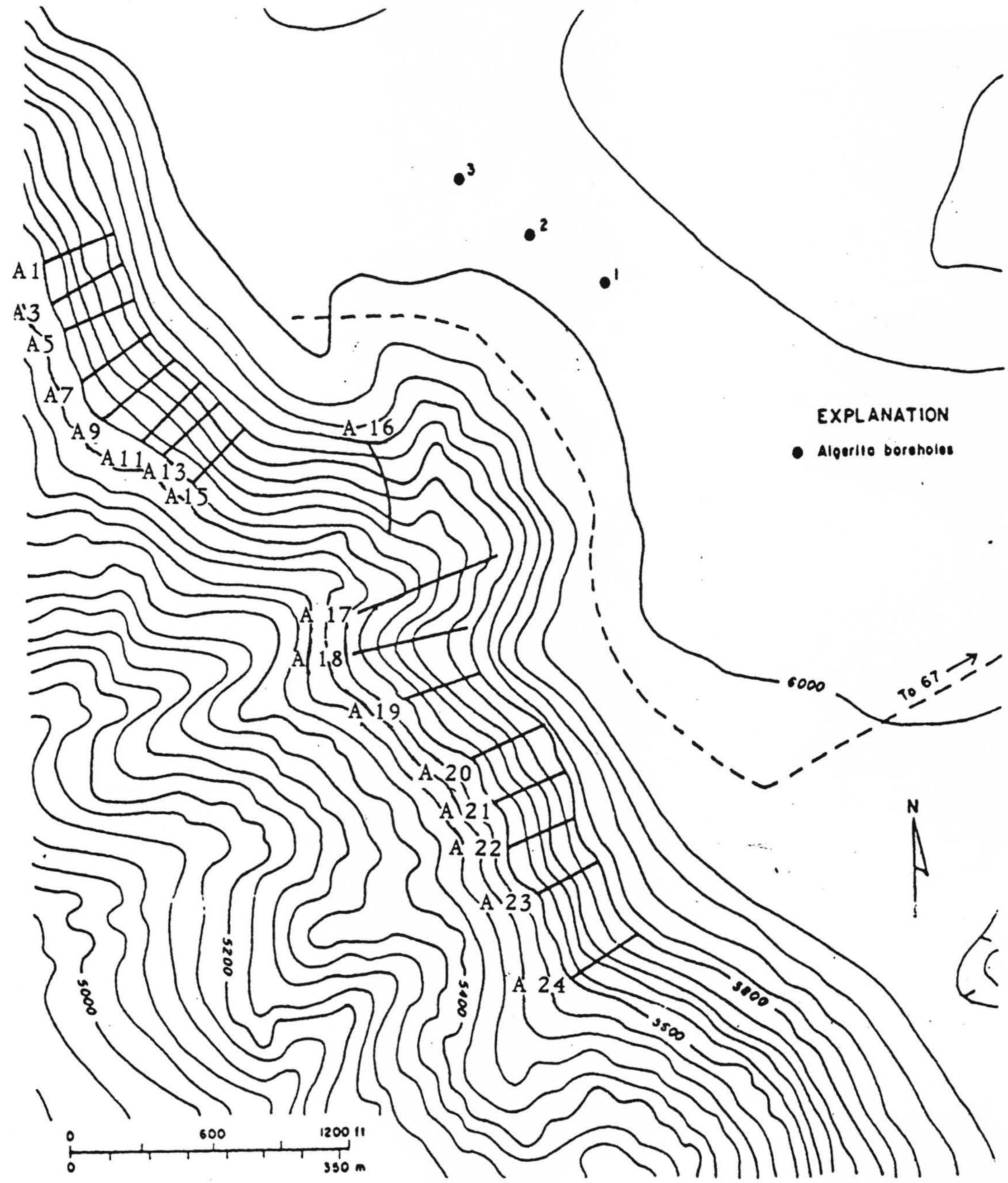

Figure 13. Topographic map of Lawyer Canyon study area showing core recovery well locations in relation to detailed measured sections in uSA1 (from Kerans and others, 1991).

feature in the subsurface rocks of the compared reservoirs (Kittridge, 1988; Hinrichs and others, 1986; and Kerans and others, 1991). The fracturing of the outcrop was attributed to the Tertiary faulting and uplift.

Another influence on outcrop permeability and porosity was a surficial calcareous tufa, observed as a white precipitate deposited on the rock surface and within fractures. Leaching of the rock matrix by dissolution of carbonate minerals and the precipitation of calcite on the rock surface has a dual effect on the rock permeability. Initial dissolution of the solids opened the pores and/or fractures in the rock, while subsequent precipitation of tufa reduces the pore connectivity on the rock surface. Thin sections from selected core plugs confirmed the presence of calcite infilled fractures in the near surface of the rock (Fig. 14 A and B).

In conclusion, the effect of weathering on the distribution of permeabilities beneath the weathered rind was assumed minimal. On the basis of on these assumptions, the relative distribution of permeability and porosity on outcrop was comparable with the subsurface data. The MFP device precluded sampling the permeability of macroscopic fractures; smaller fractures were usually associated with gas-leakage around the probe-tip. These were easily observable indicators of the presence of fractures and such samples were avoided in the data collection.

2.6 CONCEPTS OF PERMEABILITY AND POROSITY FOR THE CARBONATE ROCKS IN THIS STUDY

In order to characterize permeability, it is important to define permeability as a quantitative variable based on the pertinent physical aspects of the specific rock type

Figure 14. Thin section photomicrographs of calcite infilling fractures and interparticle pore spaces in rock matrix at the surface of the outcrop. Scales are 1.3 mm = 100μ (magnification 40x)

(A - top) Calcite infilled fracture in dolomitized wackestone, flooded shelf facies. Core plug location: A23 - 6 ft. above base of the parasequence; ϕ = 5.60, k = 0.13 md.

(B - bottom) Calcite infilled pore space in dolomitized grainstone, bar flank facies. Core plug location: A9 - 9 ft. above base of the parasequence; magnificaion 40x, 1.3 mm = 100μ; ϕ = 7.80, k = 5.27 md.

A

B

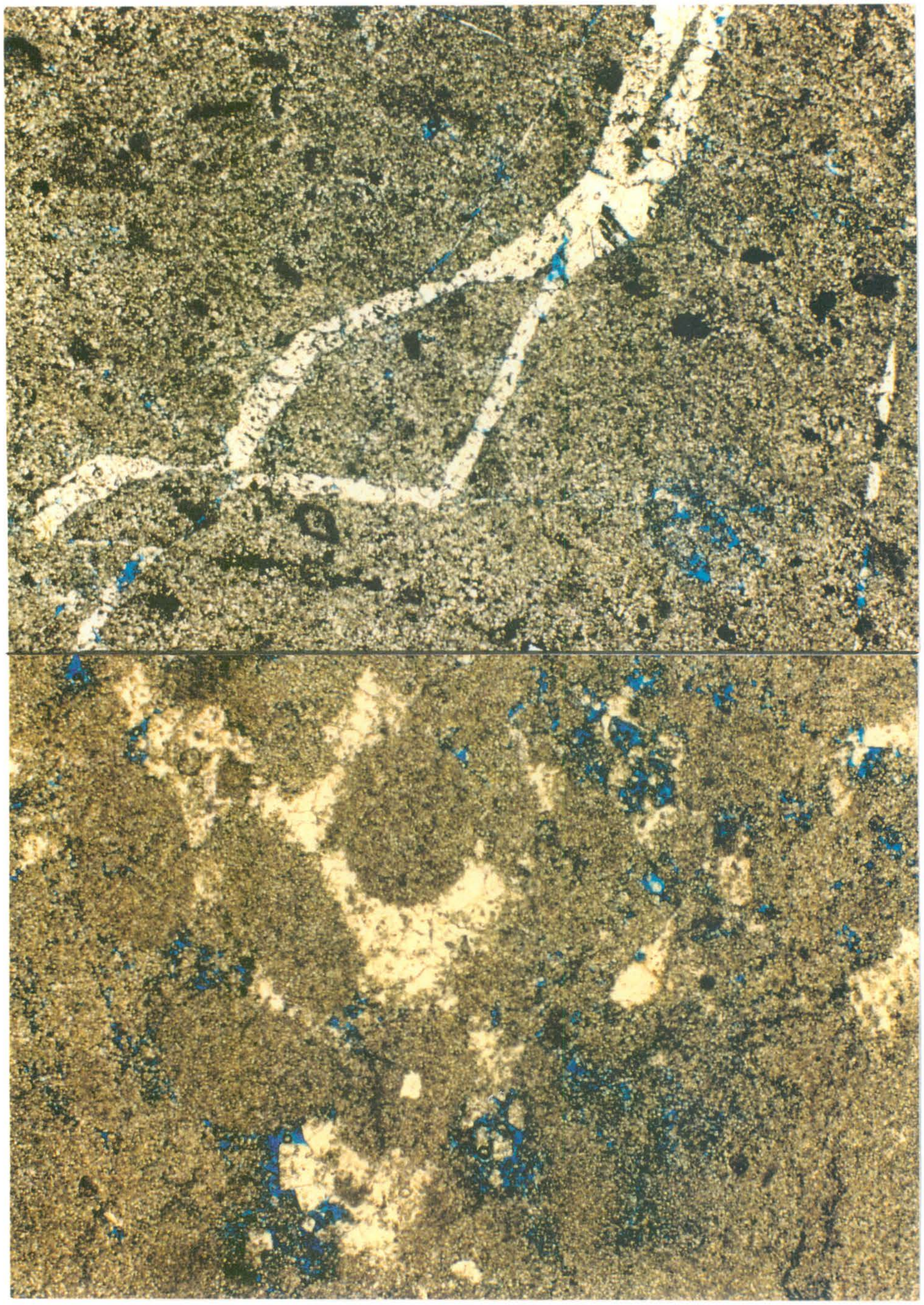

targeted for measurement. This requires a description of the rock's physical texture and the formulation of a conceptual model that describes the permeability within the rock in question.

Permeability is a measure of the ease with which a porous medium transmits a fluid. Aside from fluid properties and fluid-rock interaction, the differences in pore connectivity are critical in determining relative permeability. The physical differences are important for the identification of a volume that is representative of a permeability value. Ideally, the representative volume of a porous medium is that which encapsulates the average ratio of pore to solid spaces in the material. Therefore, the ideal scale of a sample to characterize the medium should be the scale for which the void space and solid connections are equally represented.

A model of pore-texture relationships in rocks (Meinzer, 1942, his figure XA-1) illustrates the variability of geometries possible for various lithologies. As a composite of capillary tubes and variable pore textures, Meinzer's model also illustrates the variability of size-scales encountered in determining the ability of a porous medium to transmit a fluid (i.e., permeability). Pore spaces have been shown to extend from small-scale micropores within individual grains to large-scale fractures in crystalline rocks and karstic solution cavities in carbonate rocks.

In carbonate rocks, the size of the connecting pores spaces in the rock matrix covers a wide spectrum of sizes from the microscopic to the macroscopic (Choquette and Pray, 1970; see also Fig. 3 above). Assumptions stated above consider only those porous connections in the rock fabric that were measurable by the MFP. Consequently, the smallest intraparticle micropores and most larger-scale (micro- to macroscopic) fractures were excluded since these were not directly measurable by the

MFP. To correct for this limitation, core plug porosity and permeability data were incorporated in this study, though most fracture permeability remained outside of the measurement capability of the core plugs. However, as stated above, fracture permeability was not germane to the scope of the project, especially so since the fractures were assumed to result from outcrop weathering.

Variability of pore sizes within core plug samples collected from the outcrop was illustrated in thin section photomicrographs (see also Fig. 11 A-D above). It was from the examination of pore space configurations, at the microscopic scale, that facies classifications were defined for use in this study (Kerans and others, 1991). The petrographic analysis separated the permeability data into subsets of related rock type for further statistical analysis.

CHAPTER 3
GEOSTATISTICS

The purpose of this section is to state the nomenclature and methods for the statistical analyses upon which the conclusions are based. This study applies statistical theory to the geologically-defined permeability data to investigate the influences of textures and depositional environment on permeability values. The nomenclature used in this study has been compiled from the works of David (1977), Davis (1973), Hewett and Behrens (1990), Isaaks and Srivastava (1989), Journel and Huijbregts (1978), and Mandelbrot (1984).

3.1 DEFINITION OF PERMEABILITY AS A REGIONALIZED VARIABLE

Basic to geostatistical theory is the concept of the regionalized variable (Journel and Huijbregts, 1978). This term for the theoretical behavior of a measurable natural phenomenon is defined as the value of a measurement that is found to vary systematically over space and yet exhibits a randomness that is superficially unpredictable. Permeability values measured from the outcrop satisfy this definition since they are associated with a measurement point location and, in a heterogeneous and anisotropic rock, are observed to vary in a seemingly unpredictable fashion between locations.

An initial assumption is made that each measurement of permeability represents an occurrence of the value $z(x)$ for the location x. For a particular location on a rock the permeability value is an unknown until measured. This is because naturally occurring rocks are heterogeneous to some degree, the location at which a permeability value occurs is variable and for any one location the permeability can be assumed to vary within some upper and lower limits. For this study, it was possible to determine that the variance observed in permeability would be constrained (i.e., the range of values would be noncontinuous) by the nature of the rock matrix and by the limits of detection for the measuring apparatus.

From the above conditions, the collected permeability data are definable as a set of random variables, $Z(x_i)$. By definition {Krige (1943); Matheron (1960); David (1977); and Journel and Huijbregts (1978)}, the random variable $Z(x_i)$ represents a set of random occurrences for the permeability variable $z(x)$, which are known to vary within a continuous or a noncontinuous range as the coordinate location x_i varies within the study area. In these terms, each permeability measurement, $z(x_i)$, is a true realization of the expected value for the random variable $Z(x_i)$ at a location x_i.

3.2 General Statistical Analysis

The primary statistics of a sample are the arithmetic mean ($\overline{x}$), variance (σ^2) and standard deviation (σ). These numerical representations of distribution within the sample are used to describe the data and compare one sample (or presumed subsets of a single sample) to another. The assumption of a Gaussian distribution for the sample data is fundamental to the development of the geostatistical theory.

3.2.1 Sample Statistics

The arithmetic mean $\overline{x}$ of a sample is the sum of measured values $\Sigma\, z(x_i)$

divided by the number n of measurements in the sample or:

$$\bar{x} = \frac{\Sigma\, z(x_i)}{n} \tag{1}$$

The sample variance (s^2) of a sample is the sum of the squared differences from the mean and represents a measure of the distribution of values about the mean:

$$s^2 = \frac{1}{n-1}\Sigma\left(z(x_i) - \bar{x}\right)^2 . \tag{2}$$

The sample standard deviation (s) provides another description of the data distribution and is simply the positive square root of the variance (s^2), or:

$$s = \sqrt{s^2} = \sqrt{\frac{1}{n-1}\Sigma\left(z(x_i) - \bar{x}\right)^2} . \tag{3}$$

Equations 1 through 3 are parameters that characterize the sample to which they are applied.

A frequency histogram allows for visual display of a sample's statistical analysis. This simple graphic provides an observation of the distributions in the sample. The mean ($\bar{x}$) of the sample provides a numerical mark from which the variance (s^2) and standard deviation (s) measure the distribution of the data about that mean.

The symmetry of the histogram is described by the coefficient of skewness, which is calculated as:

$$\gamma = \frac{\Sigma\left(z(x_i) - \bar{x}\right)^3}{n(s^3)} \tag{4}$$

Skewness is the second-order moment of the variance and the symmetry of the sample distribution is indicated by the sign of the coefficient. A positive γ means that the sample possesses a long tail of values to the right (above the mean) and a negative γ indicates a sample in which there is a long tail of values to the left (below the mean).

Another statistical measurement of the shape of the distribution is provided by the coefficient of variation, C_V, defined as the ratio of the sample standard deviation to the mean:

$$C_V = \frac{s}{\bar{x}} \tag{5}$$

This is commonly applied to sample data sets in which the data values and the γ are positive. A coefficient of variation greater than one indicates erratically high values within the sample.

3.2.2 Normal and Lognormal Distributions

A common distribution about the mean is the normal distribution. A normally distributed data set is commonly referred to as bell-shaped. Variance and standard deviation both indicate the spread of values about the mean. For many geologic and natural phenomena the data are found normally distributed when the data is transformed to $\log_{10}$ values. This is referred to as a lognormal distribution. In this case, we utilize the geometric mean ($\bar{Y}$), where:

$$\bar{Y} = \sqrt[n]{\Pi z(x)_i}\,, \tag{6}$$

in which $\Pi z(x)_i$ are the products of the n measurements of the occurrence $z(x_i)$ (permeability). For this study, it is required that the data exhibit a normal distribution with a minimal amount of skewness. Other distributions of data are not valid for the assumptions of the geostatistical theories that follow and, while not discussed here, these are explained in detail for geologic applications in the works of David (1977), Davis (1973), Isaaks and Srivastava (1989), and Journel and Huijbregts (1978).

The above sequence of parameters leads toward the formulation of a mathematical expression for the expected measured values of permeability within a geologically-related sample area. The expression of expected occurrences depends upon the assumptions of the spatial behavior of the regionalized variable. This "spatial behavior" is the vectoral relationship of the function $m(x)$ between the data points in the defined study area. In geostatistics, this spatial behavior is defined as the moment (the variance between values separated by a vector of length increment h) and the stationarity (the variance in Euclidean space) of the permeability.

3.2.3 MOMENT AND STATIONARITY

The moment of the variable takes on two definitions. The theory of the first-order moment states that the expectation of a random variable, $E\{Z(x)\}$, is the function $m(x)$, or:

$$E\{Z(x)\} = m(x). \tag{7}$$

The second-order moment is developed from the assumption for the random variable that stated that the distribution of values is finite and within finite limits of variance. This is often called the "a priori" variance of z(x) which is expressed as:

$$\mathrm{Var}\{Z(x)\} = E\{[Z(x) - m(x)]^2\}. \tag{8}$$

For two points, x_1 and x_2, the assumption of variance applies as a function of the random variable, where:

$$C(x_1, x_2) = E\{[Z(x_1) - m(x_1)]\,[Z(x_2) - m(x_2)]\}. \tag{9}$$

Equation 8 solves for covariance as calculated between the points x_1 and x_2. Finally, given the increment between the two points, the variance between the points is the semivariogram function $\gamma(x_1, x_2)$, expressed as:

$$\gamma(x_1, x_2) = \frac{1}{2}\,\mathrm{Var}\{Z(x_1) - Z(x_2)\}. \tag{10}$$

The introduction of a vector dimension $\mathbf{h}$, representing the separation between x_1 and x_2, leads to the theory of stationarity in the random variable $Z(x)$. Stationarity assumes that the mean and variance are true functions and are the same throughout the field of interest. This assumption is the groundwork for the "intrinsic hypothesis", which has the following properties (Journel and Huijbregts, 1978):

1) the mathematical expectation is, $E\{Z(x)\} = m(x)$, for all x;

2) and, the vector $\mathbf{h}$ increment $[Z(x) - Z(x+\mathbf{h})]$ is finite and variable for the set of all x and $x+\mathbf{h}$.

where $\mathbf{h}$ represents the direction and distance of separation between data points. Given the intrinsic hypothesis, the set of data pairs separated by the vector $\mathbf{h}$ are different realizations $z(x)$ and $z(x+\mathbf{h})$ of the set $Z(x_i)$. In a purely homogeneous medium, the expected relationship between individual realizations of the random variable is constant regardless of the vector $\mathbf{h}$. By comparison, in a heterogeneous medium, the relationship between two points is dependent solely on the vector $\mathbf{h}$. The variogram function between the points x and $x+\mathbf{h}$ is:

$$2\gamma(x, x+\mathbf{h}) = E\{[Z(x) - Z(x+\mathbf{h})]^2\}. \tag{11}$$

This last equation is the equation from which a variogram is created.

3.2.4 The Variogram

3.2.4.1 General theory

As explained above, the variance (or the standard deviation) of a sample describes the distribution of the regionalized variable. To find the variation from point to point in the 2-D realization of the data set it is necessary to use a different statistical tool, the variogram function, $2\gamma\{x, x+h\}$. By computing the squares of differences between the known data points $z(x_i)$ and $Z(x_i+h)$, it is possible to create subsets of the data related by h, the multiples of h, and the radial dimension ascribed to the vector h. The semivariance $\gamma(h)$ is one-half the sum of the squared differences of the set of realizations $z(x_i)$ for the vector quantity h, or:

$$\gamma(h) = \frac{1}{2n(h)} \sum_{i=1}^{n(h)} \{z(x_i) - z(x_i+h)\}^2. \tag{12}$$

By plotting the semivariance $\gamma(h)$ against the average separation distance of the data pairs that fit the description of the subset, it is possible to visualize the data set in the form of a graph.

In addition to the distance component of the vector h, there are additional prerequisites for inclusion to the subsets of data for the computation of the variogram function. These requirements are the direction and window which serve to constrain the data within the subset such that the resultant values of semivariance describe defined vectoral quantities as are desired by the application to the geological context. The direction is the compass direction or rotational orientation to which the length quantity of h is to be defined for the subset. The window is the latitude or margin of spatial distortion to either side of the directional vector of length h at which the data pairs can be located for inclusion into the subset. Variations of the direction and window allow for the isolation of anisotropic trends in the distribution of the realizations $z(x_i)$.

The graph of the semivariance $\gamma(h)$ versus separation distance h is the standard means of presenting and interpreting the variogram function $2\gamma(x, h)$. This graph has various expected shapes and associated terminology for the characteristics of these shapes. The primary of these is the spherical variogram (Fig. 15a). In theory of these shapes. The primary of these is the spherical variogram (Fig. 15a). In theory a regionalized random variable is given expectations $E\{Z(x_i)\}$ which are related by the function of the second order moment $m(x_i)$ to have values approaching the set of realizations $z(x_i)$ as the separation distance decreases (i.e., $E\{Z(x_i+h)\}\ z(x_i)$ as $h \rightarrow 0$). Conversely, as the separation distance h increases, the expectation for the regionalized random variable $E\{Z(x_i+h)\}$ becomes less correlatable to the realization $z(x_i)$. Finally, at some separation distance the correlation of the values will be undeterministically random (as white noise).

The separation distance and the nondeterministic randomness of the variogram function $2\gamma(x,h)$ are characteristic for the sample of realizations $z(x_i)$. These characteristic parameters are termed the range and sill of the variogram function $2\gamma(x,h)$ for the vector h. In the graphic presentation of the spherical variogram, the sill and range are interpreted at the inflection of semivariance, ideally, this increases from near $\gamma(h) = 0$ to a plateau of characteristic variance. The sill, or $C_{(i)}$, is the characteristic variance limit at which $\gamma(h)$ is (ideally) unchanging or (more practically) non-deterministic and characterized by a scatter of $\gamma(h)$ values below and or above the sill $C_{(i)}$. The range is the separation distance at which the relationship between $z(x_i)$ and $Z(x_i+h)$ becomes random, which is the zone of influence for the expectations of the regionalized random variable $E\{Z(x_i)\}$ based upon the vector h.

The nugget effect is a perturbation of the spherical variogram (Fig. 15b) which is named from the observed disruption in the continuity of the rate at which $\gamma(h)$ increases at small separation distances. This is created by the sampling of a regional variable that exists as nuggets (e.g., gold) or as concentrated veinlets within the parent material. The immediate occurrence of a characteristic variance ($C_{(0)}$) at the

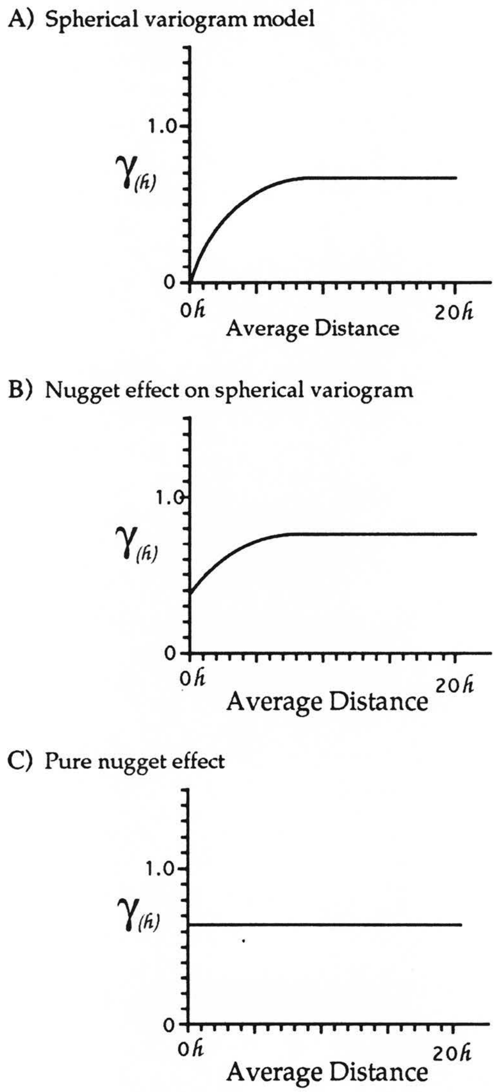

Figure 15. Models of the standard variogram configurations.
A) Spherical model, covariance approaches zero as $h \to 0$.
B) Nugget effect in a spherical variogram, immediate variance between values at the smallest distances.
C) Pure nugget, all values vary about a characteristic sill.

smallest intervals ($h \rightarrow 0$) is the measure of the low-scale variability as expressed by the regionalized variable.

An extreme condition of the nugget affected variogram is one in which the variogram is described as "all nugget". Such a variogram (e.g., Fig. 15c) indicates unfiltered randomness, or a white-noise signal, in the regionalized variable at the separation distances tested for in the data set. In this case, the observed phenomenon is either effected by another unaccounted for variable, hence the appellation of white-noise, or it otherwise falls outside of the definition for a regionalized variable. Another explanation may lie in the separation distance h used in the calculation of semivariance. For should the continuity exist at smaller separation distances than tested for in the sample collection, then the range will not be perceived in the computation of the variogram function $2\gamma(x,h)$.

Permutations of the above variogram types are the developments of nested sets and that of the "hole effect" or saddles at distances beyond the range (Fogg, 1986). The concept of a nested set (Fig. 16a) incorporates the theory that a characteristic correlation ($C_{(i)}$) may exist for the regionalized random variable $Z(x_i)$ at more than one range. Given the assumption that the length h will detect such layered correlation, the variogram function $2\gamma(x,h)$ will increase as h increases until the lowest order of characteristic variance is reached, at which the sill $C_{(1)}$ and range$_{(1)}$ are interpreted; then the values of $\gamma(h)$ will again be seen to increase as h increases until the next order of characteristic variance is reached at $C_{(2)}$ and range$_{(2)}$. The nugget value is effectively the characteristic variance of $2\gamma(x,h)$ at $h = 0$ (i.e., $C_{(0)}$) and constitutes a first order nested set.

Development of a saddle in the values of $\gamma(h)$ after the interpreted range (Fig.

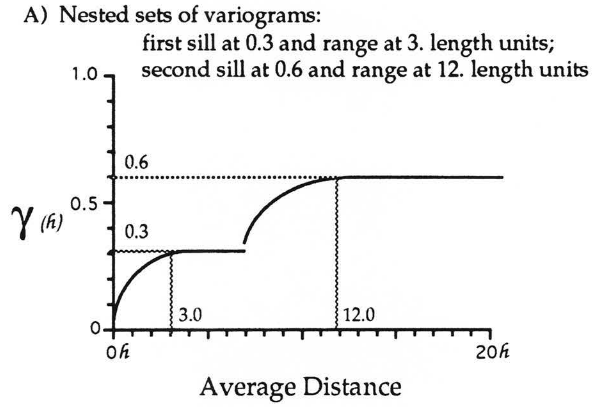

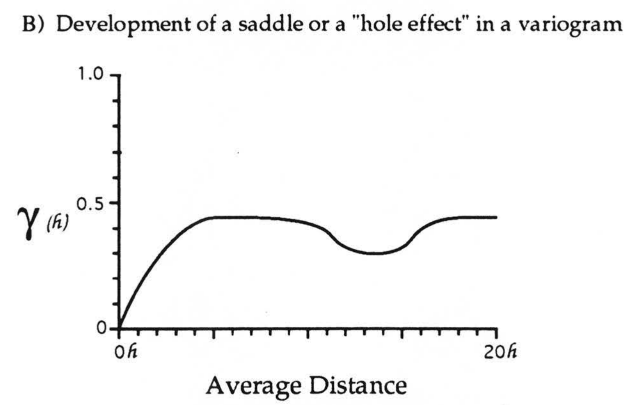

Figure 16. Variations of variogram models considered in this study.
A) Nested variogram sets indicating multiple correlation ranges (3.0 and 12.0) with characteristic variances for each range.
B) Saddle or "hole effect' of increased covariance after an initial sill has been reached (Fogg, 1983).

16b) is seen as the lowering of variance at the multiples of h after the characteristic variance has been reached. The ideal saddle is one in which $\gamma(h)$ is seen to decrease and increase back to the original sill value and does not increase to a new plateau that may be interpreted as a nested variogram characteristic. The saddle or hole effect is an indication of recurrent correlation distances based on the characteristic length h.

3.2.4.2 The power-law variogram

For a more advanced analysis of the permeability distributions, an intrinsic test function of the Euclidean geometries is suggested by Mandelbrot (1983) for self-similar regionalized variables. The form of the intrinsic test function is given as:

$$h_S(\rho) = \gamma(D)\rho^D \tag{13}$$

where $h_S(\rho)$, the intrinsic test function is the fractal measure of S when S is the set of very small discs (in two-dimensions) or balls (in three-dimensions) which approximate an area (two-dimensions) or a volume (three-dimensions), $h(\rho)$ is a function of the radii ρ of the shapes in the set of S. And the expression $\gamma(D)\rho^D$ is the D-dimensional function for the standard shape of radius ρ, such that $\gamma(D)$ is the function of the contents of the shape with radius ρ (and related to, but not to be confused with, the use of $\gamma(h)$ in semivariance). The D-dimension is the Hausdorff-Besicovitch dimension (Mandelbrot, 1983) of S and, if S is self-similar, then the similar dimension is equal to D. In this form and applied to a 2-dimensional shape defined by a self-similar regionalized variable, the intrinsic test function is a power-law relationship of the characteristic length ρ and the fractal dimension D.

From the above function for a test of the fractal dimension D, the application to the variogram was suggested by Hewett and Behrens (1990) for variograms that exhibit a characteristic increase in sill and range which corresponded to an increase in the separation distance h. For that case, the power-law variogram model was developed by the superposition of variograms of different h. The mathematical expression for the power-law relationship for the variogram was proposed by Hewett and Behrens (1990) to be:

$$\gamma(h) = \gamma_0 h^{2H} \tag{14}$$

where: $\gamma(h)$ is the mean-square variation of the regionalized variable as a function of h; γ_0 is the characteristic variance scale at a reference-unit of the separation distance h; and H is the fractal codimension equal to the difference between the Euclidean dimension E in which the distribution is described and the fractal dimension of the distribution D, or simply stated $E-D$ (Hewett and Behrens, 1990).

In log-transform, the power-law variogram function becomes the equation of a straight line:

$$\log(\gamma_{(h)}) = \log(\gamma_0) + 2H \log(h). \tag{15}$$

This power-law relationship provides $2H$ as the slope of the best-fit line through the superpositioned points of the combined variograms, $\log(\gamma_0)$ as the value of the characteristic variance value at the reference $h=1$ ($\log_{10}(1)=0$), and $\log(\gamma_{(h)})$ as the function of the set of mean-square variation in the realizations $z(x_i)$ and $z(x_i+h)$ that tends to 0 with h. The relationship follows the theory of power-law relationships forwarded by Hewett and Behrens (1990) for identification of fractal relationships in reservoir heterogeneities and the above discourse on the intrinsic test function of Mandelbrot (1984) in studies of the fractal dimension of natural systems.

The relationship between the intrinsic test function and the power-law variogram function rests in the dimensional quality of the fractal dimension D and the fractal codimension H (defined by D), the characteristic length properties of both ρ and h, and the functions $h_S(\rho)$ and $\gamma(h)$ which define sets of shapes in the Euclidean dimension based upon the characteristic lengths ρ and h, respectively. For the fractal codimension H the values have been found to generally vary between 0.7 and 0.9 for measurements of topographic features such as coastlines (Hewett and Behrens, 1990).

CHAPTER 4
METHODS OF PERMEABILITY MEASUREMENT

Permeability data were collected with the Mechanical Field Permeameter (MFP) and augmented by permeabilities estimated from core plug measured permeability. Permeabilities were calculated from steady-state flow and pressure values as recorded from flow tubes and dial gages, respectively, on the device. The particular MFP apparatus used in this study was constructed and calibrated by D. Goggin, for The University of Texas at Austin Petroleum Engineering Dept., through adaptation of published designs for air flow permeameters (Dykstra and Parsons, 1950; Eijpe and Weber, 1971).

4.1 MFP SAMPLE POINT PREPARATION

The reason for using a mobile permeameter such as the Mechanical Field Permeameter was to create a "robust" sample of spatially distributed permeability realizations $z(x_i)$. A robust sample was one for which data were well founded upon the principles required for analysis. Application of the term "robust" in this context was defined as: 1) in definition, the measured variable (i.e., permeability) is conformed to by the measurement method, 2) the value of the variable was statistically representative of the location, and 3) creation of a sample that was sufficient for analytical review based on the statistical theory.

As stated above, sampling with the MFP device required preparation of the rock surface. The study by Kittridge (1988) was complicated by the practice of preparing the outcrop surface with a mechanical grinder. The impact of rock fines generation by the destruction of the outcrop surface was considered by Kittridge to be most significant for samples where the rock is in the lower range of permeability. This lower range of permeability, as defined by Kittridge, coincided with the lower range of detection for the mini-field permeameter. Therefore, another surface preparation method was required. Several surface preparation methods were tested: the mechanical grinder, a water saw, and a hammer and chisel. Prepared samples were viewed by scanning electron microscope (S.E.M.) for pore throat disruption effects of three possible surface preparation techniques. This analysis indicated that the surface exposed by breaking the rock (Fig. 17a) was less disrupted than the surfaces created by either the saw-cut method (Fig. 17b) or the mechanical grinding of the surface (Fig. 17c).

Figure 18 shows the typical markings on the outcrop after preparation with the hammer and chisel. Noticeable in the photograph are the outlines of powdered rock around the sample point. This exemplifies the problems encountered when applying laboratory results in the field. Obviously the hammer and chisel did not create a perfectly clean sample surface at the edge of the sample point. Therefore, sampling was conducted with the MFP nozzle-tip positioned inside of the chisel marks for each measurement.

The inability to obtain data on an evenly spaced small scale grid was an unfortunate side effect of the surface preparation method on the outcrop using a hammer and chisel. With the mechanical grinder Kittridge (1988) was able to expose a continuous area of the outcrop for sampling down to one-half of an inch in an

Figure 17. Scanning electron micrographs of rock surfaces subjected to three means of removing the weathered rind to expose the pristine rock matrix.

(A - top) Broken rock surface exposing undisturbed dolomite crystals at lower left (arrow).

(B - middle) Cut with a water saw, the end of a core plug retains curvaceous grain surface and pore throat with few white rock fines in view (arrow).

(C - bottom) Mechanically ground rock surface is heavily littered with fine white rock particles, especially in the low areas of the pore throats, also flat ground surfaces are partially smeared (arrow) in the direction of grinder rotation.

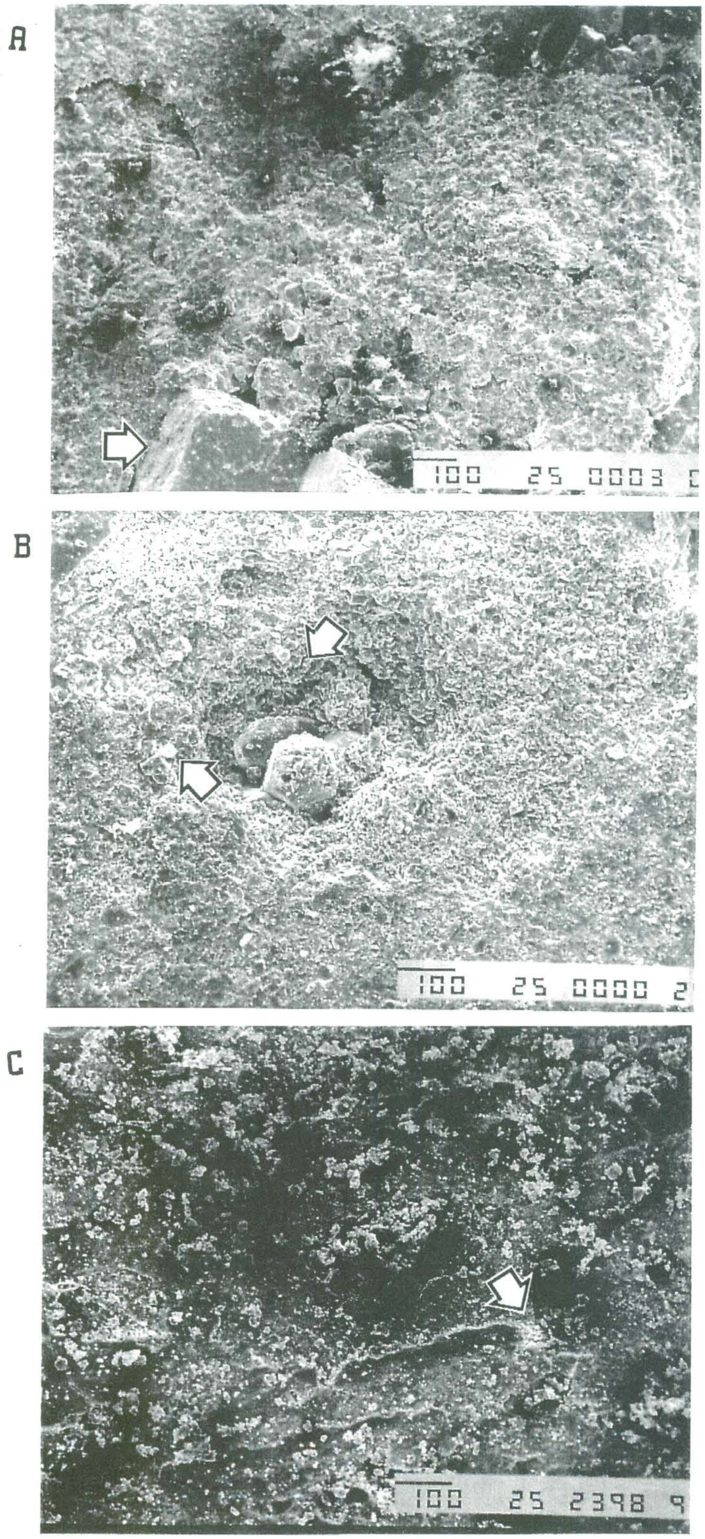
A
100 25 0003 0
B
100 25 0000 2
C
100 25 2398 9

Figure 18. Typical outcropmarking created by hammer and chisel (approximate scale 1:1.8)

evenly spaced grid. Sampling in an evenly spaced grid has obvious advantages for equitable statistical analysis of the permeability in the vertical and horizontal, as well as at intervening angles if sufficient data is obtained. Because this was not feasible, the smallest scale of outcrop data collection was limited to straight-line sampling at one inch intervals along transects which connected further spaced sample points.

Another significant problem in the field sampling program was the difficulty of maintaining a proper seal between the rock surface and the MFP's nozzle-tip. Fractures, large vuggy pore spaces, irregularities from large or cemented clumps of grains, and the chisel markings all combined in the difficulty of chipping away the weathered rind and exposing a large and flat unweathered surface.

Initially, MFP measurements were performed once or twice at each sample point within a newly chipped area. However, it was known that small scale heterogeneities did not guarantee a spatially representative realization of permeability $z(x_i)$ for a single sample point; therefore, a new sampling scheme was suggested which reflected the representative permeability at the sample location. This new sampling design was suggested coincidentally by D. Goggin and G. Fogg (personal communications, 1989) so as to make the most use of statistical interpretation of an average value for the sample point.

Through the improved data collection method, multiple measurements were made in a single prepared "patch" (Fig. 19). Ideally, this "patch" was a chiseled-off square of one and one-quarter inch sides, and measurements were made in a five spot pattern to provide maximum separation distances inside the sample location. For the purpose of this study, the assumption was made that averaged values of the permeabilities measured in each "patch" were more accurately representative of

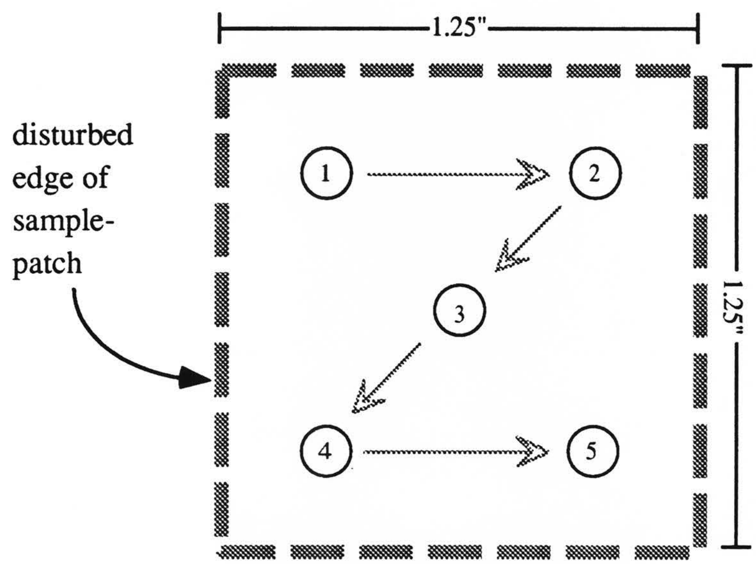

Figure 19. Typical MFP sampling of a hammer and chisel prepared "patch" showing the order and relative positions of the individual measurement sites.

permeability values at a sample location.

4.2 Core Plug Permeability Measurements

The collected core plugs were sent for contracted analysis as part of the related projects conducted by the Bureau of Economic Geology Reservoir Characterization Research Laboratory. After collection from the outcrop with a portable drill, each plug sample was trimmed at both ends. The whole cylinders were sent for analysis while the trimmed ends were used to make thin section slides by the Core Research Center (CRC) division of the BEG. The data of permeability and porosity values were received for only those core plug samples which conformed to the requirements of length and regularity of shape as required for the Hassler sleeve method. This meant that not all of the collected core plugs were measured for permeability and porosity values. However, all of the sampled locations were available for microscopic review in thin section.

4.3 Permeability Sampling Patterns

The permeability and porosity data were collected in four distinctly scaled grids with each smaller scale grid existing within the larger scale grid(s). The largest scale grid is herein referred to as GRID A. This incorporates the measured geologic sections provided by Kerans and others (1991) and covers nearly one-half mile of the first parasequence in outcrop on the Algerita Escarpment. Because the initial permeability measurements in GRID A indicated a region of high permeability values at the center of the grid, a second scale of investigation (GRID B) was prepared as vertical transects intended to follow the trend of the high permeability values. The third and the fourth grids (GRIDs C and D) followed in turn as the investigation delved into increasingly smaller scale.

For individual referencing, all of the sample points have been assigned "x"- and "y"-coordinates based upon a combination of aerial photographs (for large distances) and real ground measurements (for small distances). In this manner, the sample points have been assigned a distance from an arbitrarily positioned "zero" coordinate to the north of the study site and measured vertically from the base of the first parasequence.

GRID A was the most laterally extensive in area and included all of the genetic facies described in Chapter 2 (Geology). The sample pattern of GRID A included the sixteen measured geologic sections described above and was augmented by infilling vertical transects (Fig. 20) in the northern section of the study area. The average separation distance between transects on the north-side of the canyon (transects A1 - A16) was less than that of the south-side of the canyon (transects A17 - A23). This was the unfortunate result of the loss of exposed outcrop in the south by talus from the overlying parasequences. However, the few vertical transects on the south-side of the canyon allowed for a laterally extensive view of the permeability values.

GRID B (Fig. 21) was located between the transects A15 and A16 of GRID A. This was the direct result of the preliminary permeability measurements in the study site which at the time had included the transects referred here as B1, B2, B3, B4, B5, B12, B13, and B14. The addition of six (6) more closely spaced transects in between B5 and B12 were intended to detail a high permeability zone where the

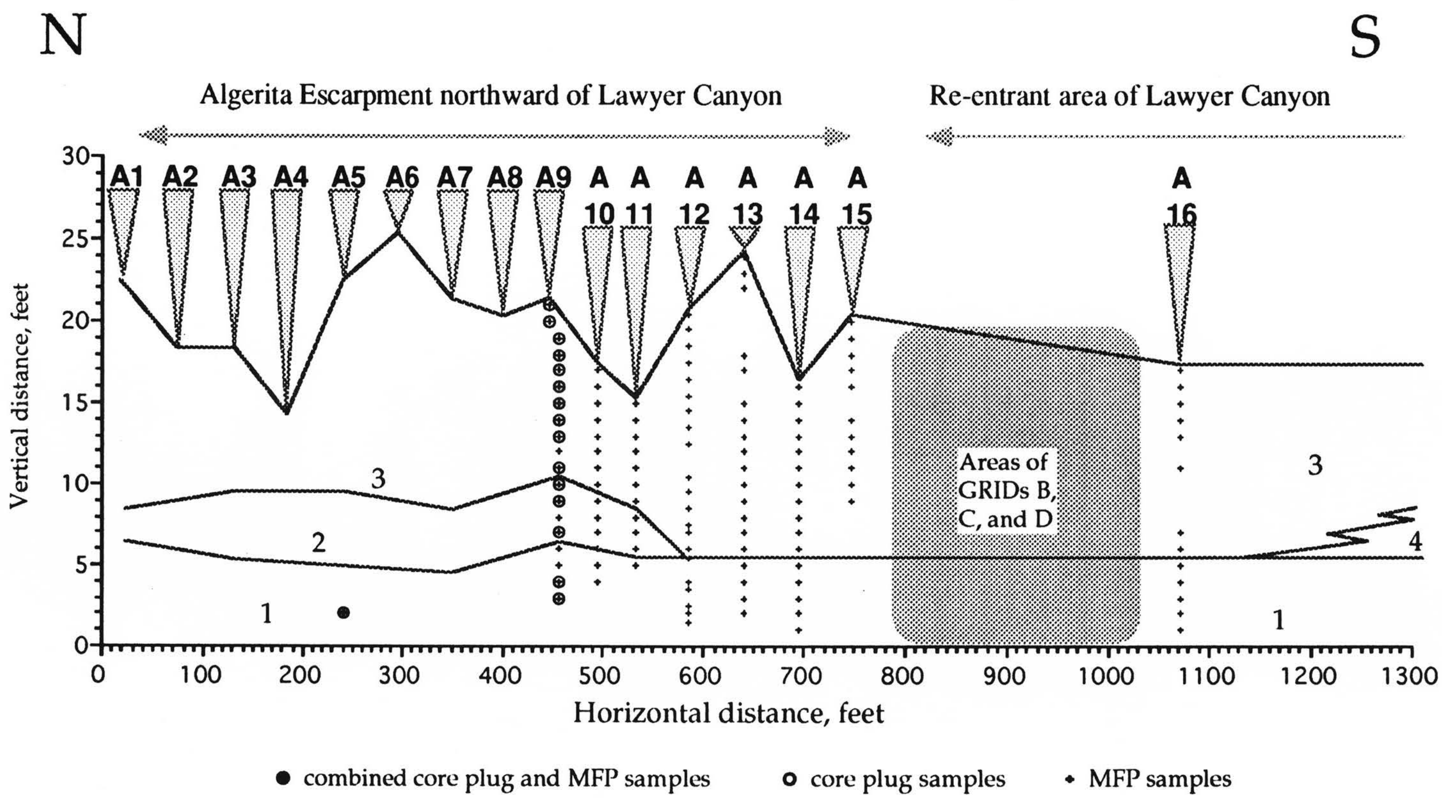

Figure 20a. First of two figures that show the sample point locations used in the GRIDA data set. Shown are the relative positions of the points and transects sampled with the MFP and/or core plugs. Perspective is facing east from Big Dog Canyon toward the Algerita Escarpment. Also shown are the identified genetic facies #1 through #4 (see Fig. 10).

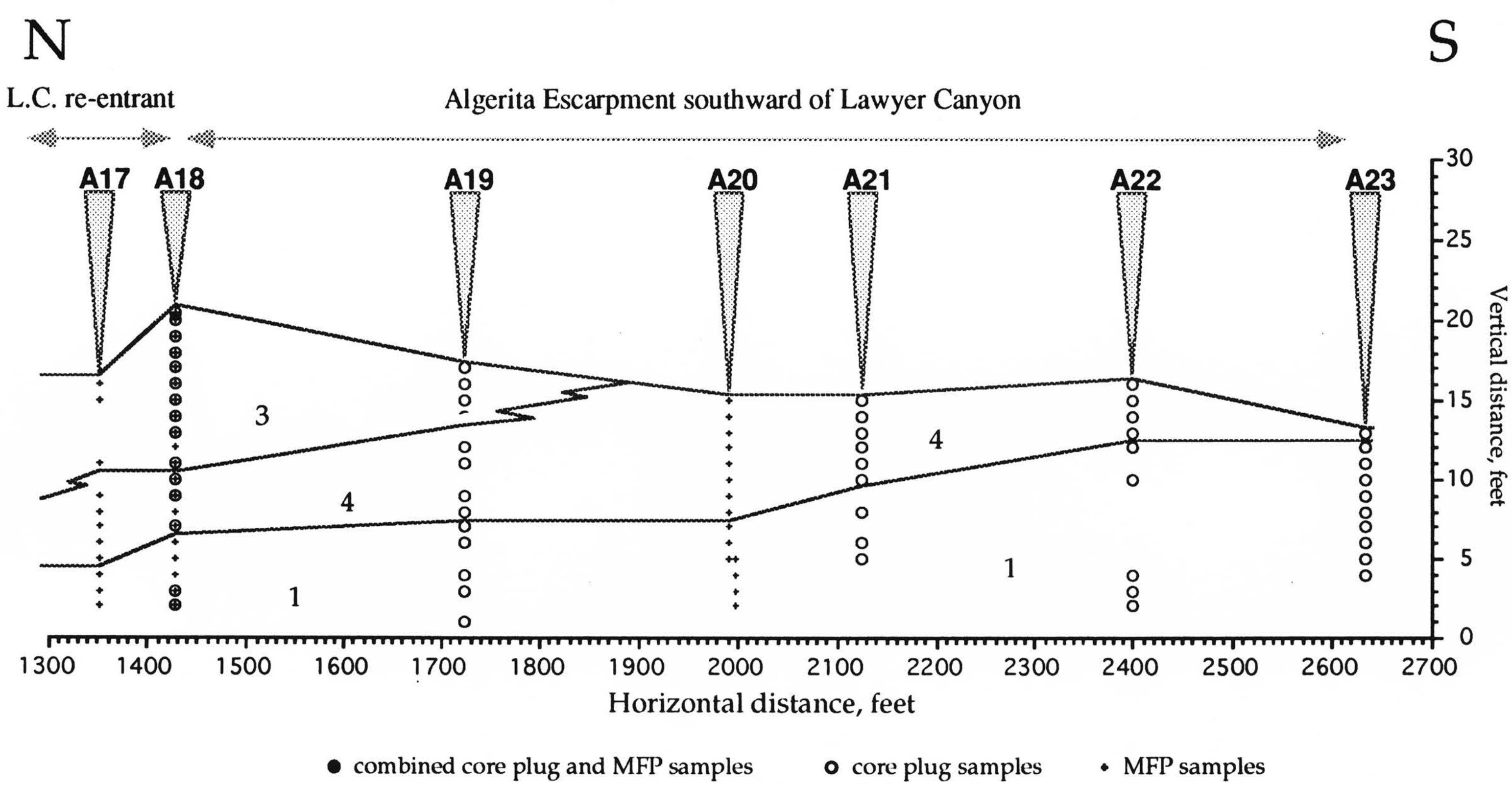

Figure 20b. Second of two figures that show the sample point locations used in the GRIDA data set. Shown are the relative positions of the points and the transects sampled with MFP and core plugs on the south side of Lawyer Canyon. Also shown are the boundaries of the genetic facies #1 through #4 (see Fig. 10).

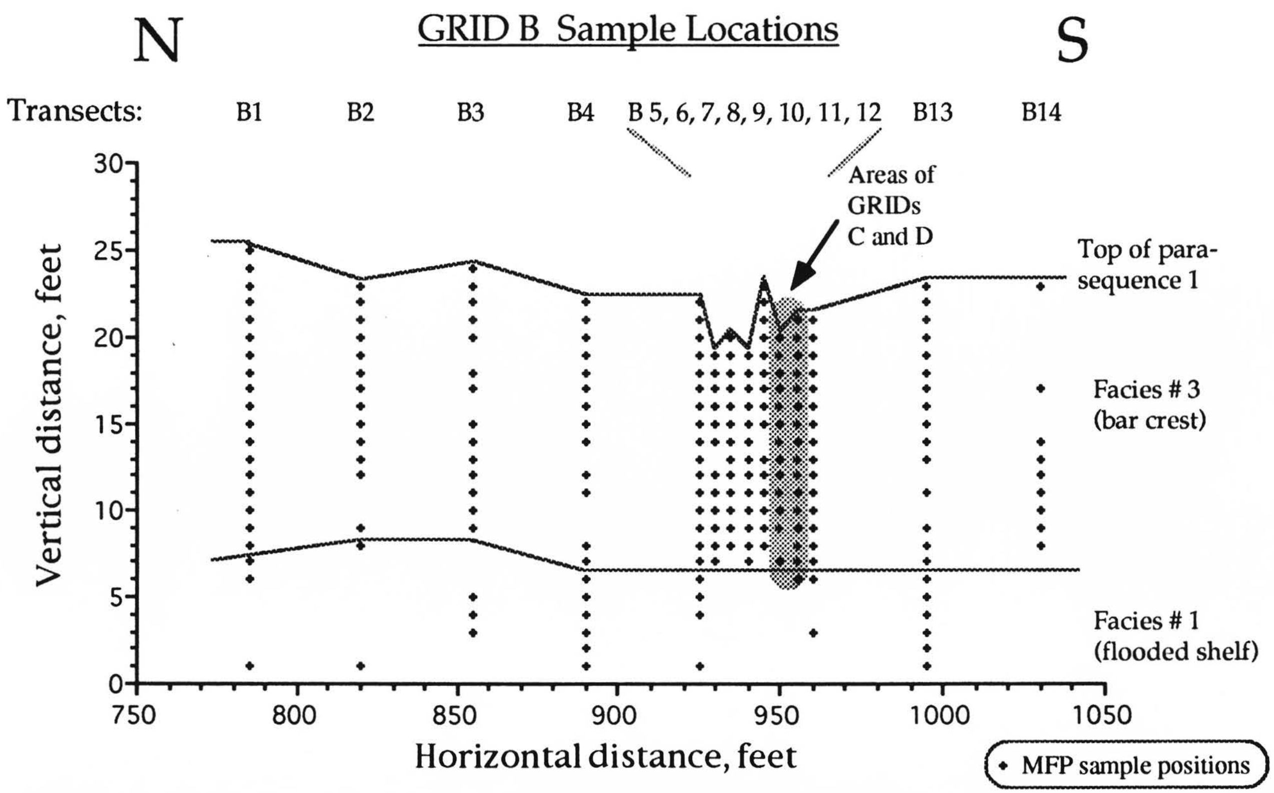

Figure 21. Sample point locations of GRIDB data set. The vertical and horizontal distances correlate with the coordinates used in GRIDA. The facies boundary positions have been extrapolated from the geologic sections of Kerans and others (1990).

outcrop was well exposed and accessible. The average separation distance of the transects in GRID B actually existed in two lengths: the original eight (8) transects at thirty-five (35) ft. intervals, and the additional six (6) transects at five (5) ft. intervals. Included within the sampled boundaries of GRID B were rocks of the facies #1 and #3, though it should be noted that facies #1 was available in only a few of the transects and in poor quality for sampling of the permeability.

GRID C (Fig. 22) was planned as a regular one-foot square grid overlapping transects B10 and B11 of GRID B. Similar to GRID B, this grid pattern was designed to identify the small scale continuity of a high permeability zone that was observed to continue through GRID B from GRID A. The positions of the sample points were of too small a scale to be corrected for in the aerial photographs used to locate positions in GRIDs A and B, therefore the horizontal coordinate positions of GRID C are relative to themselves and not to the coordinates of GRID A. The position of GRID C was in an area of broad exposure on the outcrop which allowed for the construction of a regularly spaced grid, but the location was also one were the entire vertical section of facies #1 was covered. Therefore, the permeability data set of GRID C includes only permeability values taken from the outcrop in the facies #3.

GRID D (Fig. 23) followed the progression to smaller scales to a separation distance of one inch between measurements. Even more so than in GRID C, the small scale (one inch) separation between sample points precluded the use of aerial photographs to correlate positions in the coordinate system as in GRIDs A and B. The surface preparation of sample points in GRID D was too destructive for an equally spaced small scale grid. Since the entire sampling area of GRID D was within that of GRID C, then it follows that the permeability values are representative of facies #3.

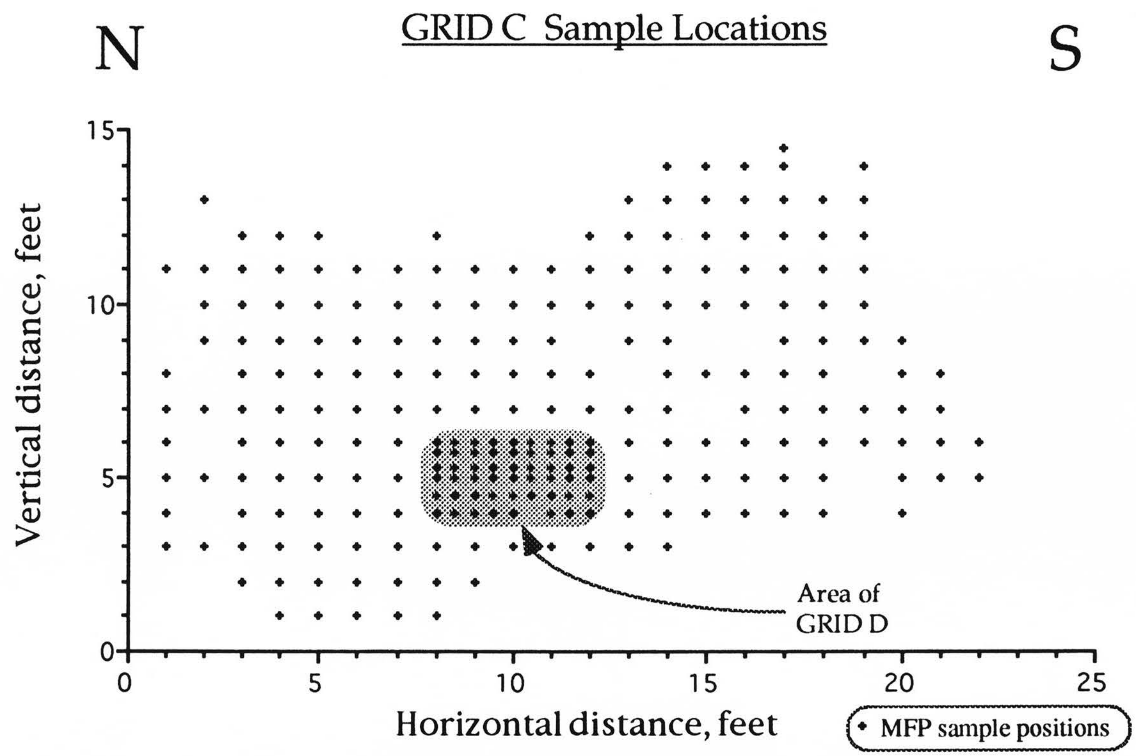

Figure 22. Sample point locations of GRIDC data set. The vertical and horizontal distances do not correlate with the coordinates used in GRIDA. The position of the grids within the bar crest grain-dominated genetic facies #3 (as seen in Figure 20).

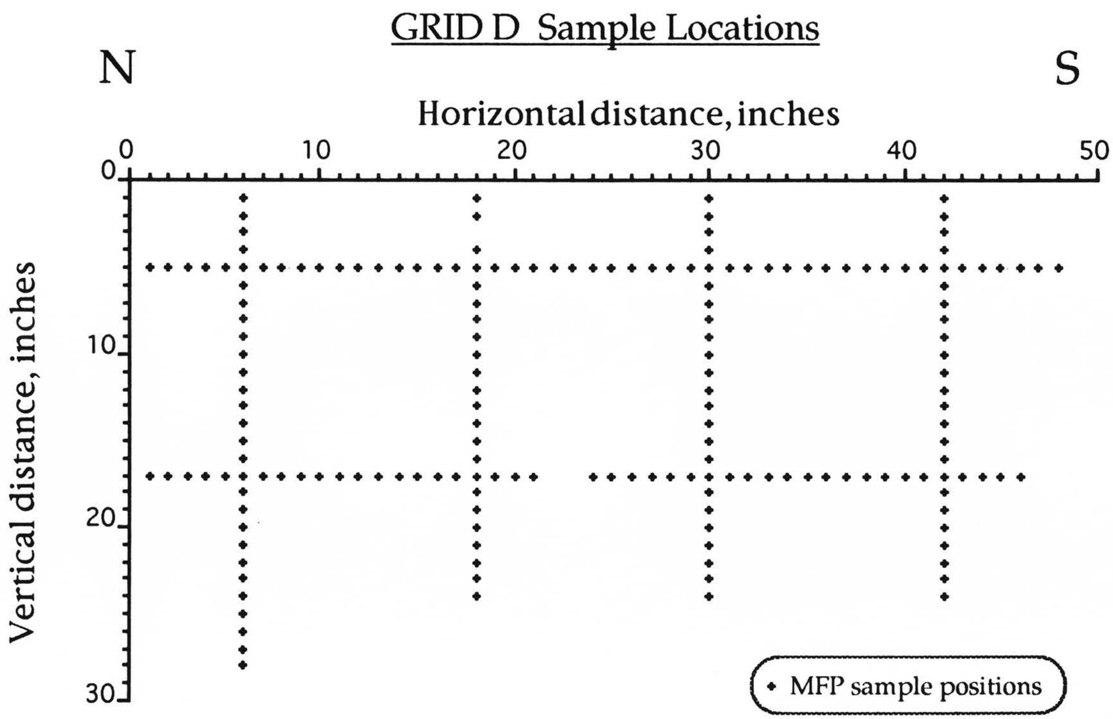

Figure 23. Sample point locations of GRID D data set. The vertical and horizontal distances do not correlate with the coordinates used in GRID A. The entire grid is located completely within the grain-dominated bar-crest facies #3.

CHAPTER 5
DATA AND RESULTS

Permeability data collected from the outcrop were analyzed using various methods in order to illustrate, support, and further define the results of statistical correlation based on the previously identified samples of grids and facies. Contour maps of the digitally posted data were created for each of the grid samples to illustrate whether identifiable continuities existed within the samples. Histograms and probability plots provided graphic evidence that the permeability data were lognormally distributed. The coefficients of variation (C_v) were calculated for each sample data set and compared to determine whether the sample data sets were representative of the same sample. Semivariance values ($\gamma(h)$) were calculated for both vertical and horizontal search directions with step (lag) distances conforming to the scales in the various samples. Experimental variograms of semivariance ($\gamma(h)$) vs. average separation distance were interpreted for range and sill estimates of covariance within the permeability data. Horizontal variograms were overlaid on logarithmic axes to solve for $2H$, the fractal codimension, in the power-law equation (see Eqn. 13). The value of the fractal codimension was anticipated to determine the validity of a hypothesis concerning the scale dependent correlation of permeability distribution.

5.1 PERMEABILITY AND POROSITY DATA

The permeability data analyzed in this study are representative of two measurement techniques, the MFP surface permeability method and the Hassler-sleeve method for core plugs. Previous studies by Goggin (1988) and Kittridge (1988) demonstrated the accuracy of the MFP derived permeability data when compared with the more conventional Hassler-sleeve permeability data from core plugs. Because the two methods are comparable, incorporating the permeability data derived from the core plugs augments the data derived from the MFP, most significantly for the low permeability range (less than 1 md).

5.1.1 MFP DATA

Appendix A contains all of the MFP permeability measurements which were used in this study. MFP measurements which recorded no observable gas flow (below detection limit, or bdl) were included. The bdl measurements were assumed to be non-zero, low-permeability measurements (less than 1 md). However, the assignment of definitive values for those measurements would have been statistically unsound, hence the bdl measurements were dropped from the samples for the statistical analyses. As stated above, this limitation of the MFP device was anticipated and partially compensated by the inclusion of core plug permeability data.

5.1.2 CORE PLUG DATA

Core plug sampling extended over a wide area compared to the MFP sampling. This wide spread sampling provided porosity and textural data for the various rock fabrics, as well as providing additional permeability data. Core-plug permeability measurements were most valuable where MFP data was not collected or where permeability values were below detection range for the MFP (i.e., in the mudstone of the flooded shelf and shallow shelf facies) in order to provide more robust data.

Figure 24 shows the locations of the core plugs in vertical transects where they were collected. By themselves, the core plug permeability data are too widely dispersed to be analyzed through variograms for the goals of this investigation. Core plug collection destroyed the rock surface and sampling was unreproducible for a precise position. In this respect, the collection of core plug permeability values was not conducive to the generation of a robust sample of data, but combined with the MFP permeability data made the entire sample of permeability data more robust.

Appendix B contains the permeability and porosity data from core plugs in the first parasequence. In the core plug collection, there were cases where more than one core plug was collected from the same coordinate location on the outcrop. The data in Appendix B shows the low variability among these dual samples. The low variance was an advantage of the core plug data collection which was not shared by the MFP data collection. The advantage of the core-plug permeabilities low variance at closely spaced sample points allowed the assumption to be made that the core-plug values were less influenced by small scale heterogeneities, and therefore more representative of the average permeability for a sample point.

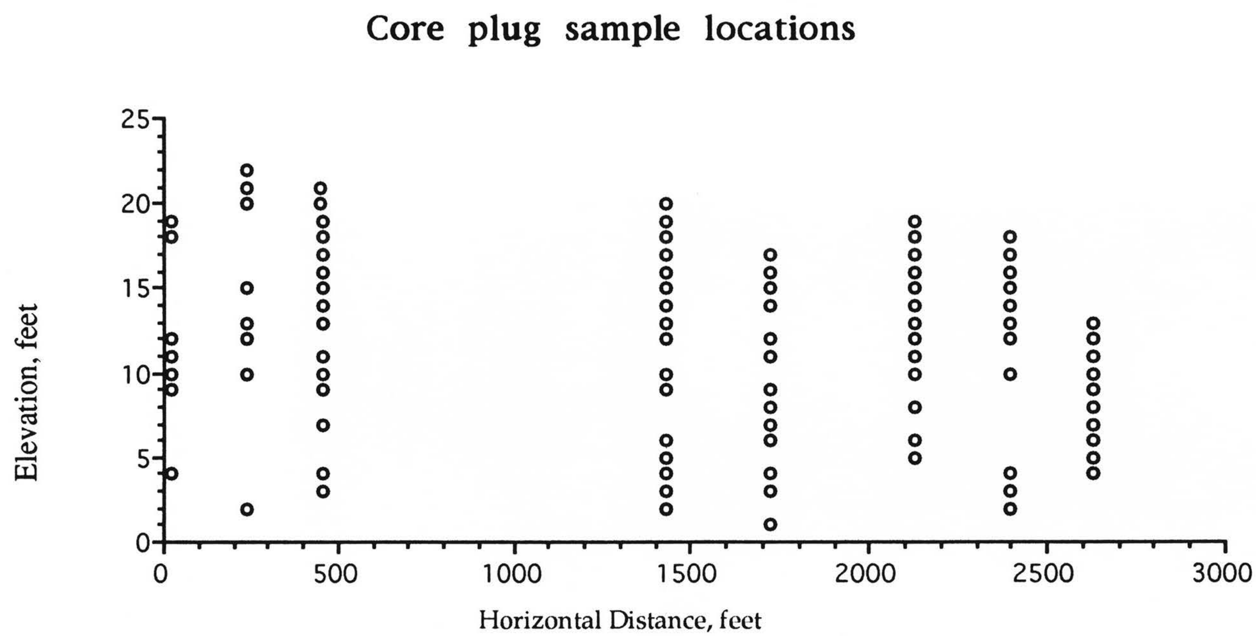

Figure 24. Location of core plugs in the first parasequence study site, Lawyer Canyon. Distances conform to those of GRID A locations, as shown in Figure 20.

5.2 Statistical Analyses of Sample Data

The variogram function $2\gamma(x,h)$ is based on the premise that the regionalized variable (i.e., permeability) displays a normal or lognormal distribution about the mean of the sample. In the previous studies of permeability distributions on the San Andres formation outcrop of the Guadalupe Mountains (Kittridge, 1988; and Hinrichs and others, 1986), permeabilities were found to approximate a lognormal distribution. The data for this study was also found to exhibit lognormal distributions. In the following section, the data for each of the previously identified sample sets (GRIDs A - D and genetic facies #1 - #4) were each analyzed for the parameters of a lognormal distribution and then presented with results from the interpretations of experimental variograms.

The experimental variograms presented in this section were calculated for horizontal (0°) and vertical (90°) search directions, with step increments (h) based on the (ideal) average distance between transects (GRIDs A, B, and D) or the spacing in a regular grid pattern (GRID C). Additional experimental variograms were created for other step increments for analysis and comparison of the sample data.

5.2.1 GRID A

The largest sampled grid in area and in number of measurements, GRID A is the only sample set to include data from all four of the identified genetic facies. A contour map of the log-transformed GRID A permeability values was created (Plate 1) for a contour interval of 0.25 log units. The most notable relationship between rock fabric and permeability is the bottom-to-top correlation of increasing permeability with the coarsening of the grain fabric (see measured sections presented above in Fig. 21). This illustrates permeability variation between facies #1 (generally low permeabilities) and the overlying facies (generally higher permeabilities). No other obvious facies and permeability relationships have been deduced from the contour map of GRID A.

Also from the contour map of GRID A data, permeability heterogeneities are interpreted for vertical and horizontal directions. Permeability varies over two orders of magnitude between sample points one foot apart along the individual vertical transects of the GRID A sample data. Transects A1, A3, A10, and A16 are noted for such vertical permeability variability between consecutive one-foot spaced sample points. These fluctuations suggest that vertical heterogeneities exist on, at least, the one foot scale.

Horizontally continuous permeability relationships are only observed in the relationship of the average low values of facies #1 and the average high values in the overlying facies (#2 - #4). The relatively wide horizontal separation distances (35 feet to 350 feet) between vertical transects provide neither proof of dramatic changes in permeabilities nor proof for horizontal continuity of permeabilities across the transects. In the most densely sampled area, the northern half of GRID A (transects A1 - A15), the complexity values suggests that horizontal permeability heterogeneities exist at smaller scales than that of the GRID A sampled pattern.

Statistics for the GRID A log-transformed data (Fig. 25) indicate a deviation from lognormality in the low permeabilities range. In a frequency histogram, the tail of low permeabilities below 1 md is characterized by the negative coefficient of skewness (-0.739). In the same low permeability range, the plot of log-transformed GRID A data on probability paper produces an observable deviation from the ideal

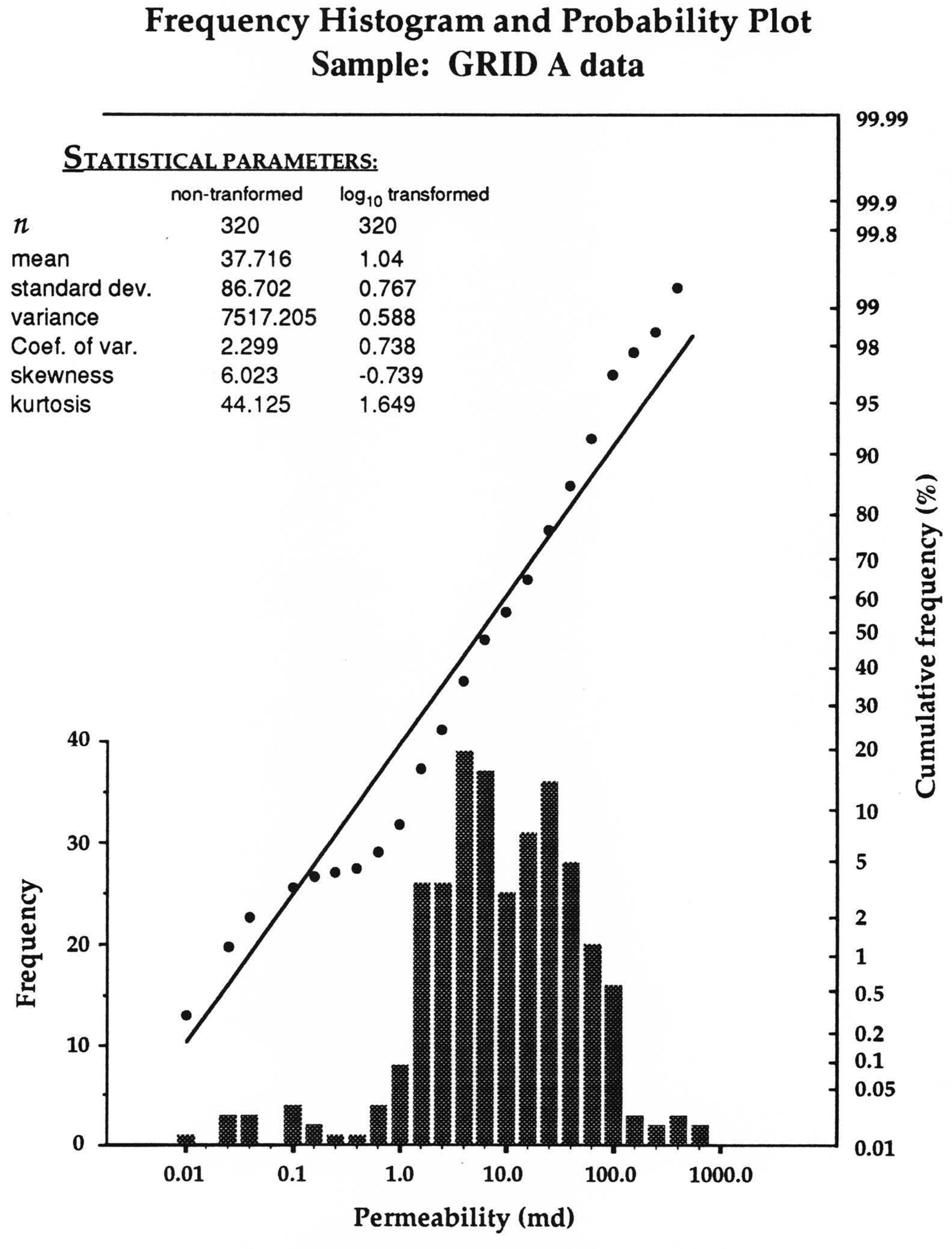

Figure 25. Frequency histogram and probability plot graphs for GRID A sample data. Data shown to exhibit lognormal distribution with exeption in the low permeability range (i.e., <1.0 md), corresponding to bdl range for MFP. The negative and relatively high coefficient of skewness corresponds to this observed deviation from lognormality.

straight-line pattern for lognormal distribution. The offset between the straight-line relationships <0.1 and >1.0 md on this probability plot indicates a possible bimodal distribution for the data sample. However, mean and standard deviation values of the log-transformed data (1.04 or 10.959 md and 0.588 or 3.87 md, respectively) conform to a lognormally distributed sample (i.e., the standard deviation was less than the mean).

Removal of the core-plug derived permeabilities from the sample data results in a better fit to a lognormal distribution. For the restricted sample data, the deviation from lognormality in the low permeability range (<1 md) is not present in the probability plot (Fig. 26), and the mean (1.137 or 13.713 md) is greater than the standard deviation (0.767 or md). The most significant change in the data statistics is the change in the coefficient of skewness from negative to positive and closer to zero.

Alternatively, statistics for the non-transformed GRID A data do not conform to the model for a normal distribution. The data statistics for mean (37.716 md), standard deviation (86.702 md), variance (7517.205), and skewness (6.023) are not indicative of a normal distribution. In frequency histogram and cumulative probability plot (Fig. 27) presentation the non-normal distribution is plainly observed.

Horizontal semivariance calculations made on the GRID A data (Fig. 28) provides the most significant variogram interpretations for h = 100 feet. This experimental horizontal variogram is interpreted as two sets of nested spherical variograms. Interpretation for a nested variogram model indicates an initial nugget value ($C_{(0)}$) between 0.23 and 0.13 for the average separation distance of 75 feet, followed by values for sills of 0.305 ($C_{(1)}$) and 0.497 ($C_{(2)}$), for ranges of 253.5 feet ($r_{(1)}$) and 748.3 feet ($r_{(2)}$). Beyond the second range value ($r_{(2)}$), the calculated

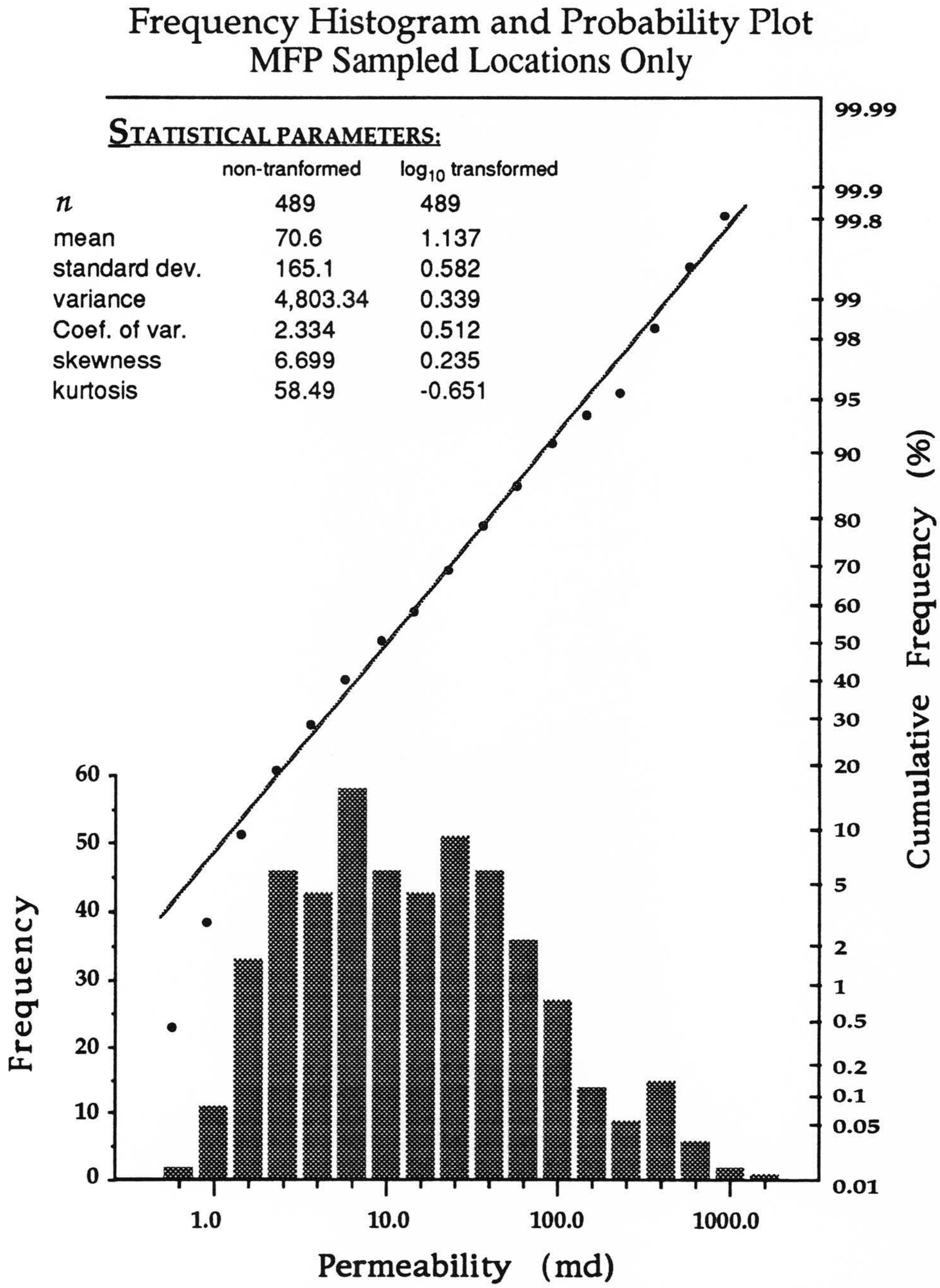

Figure 26. Frequency histogram and probability plot graphs of a restricted sample populaation of the log-transformed GRID A data, only the MFP permeabilities. Removal of the core plug permeability data produced a slight down-turn in the low-permeability end of the cumulative probability plot, an increase in the mean, and a shift to positive value for the coefficient of skewness.

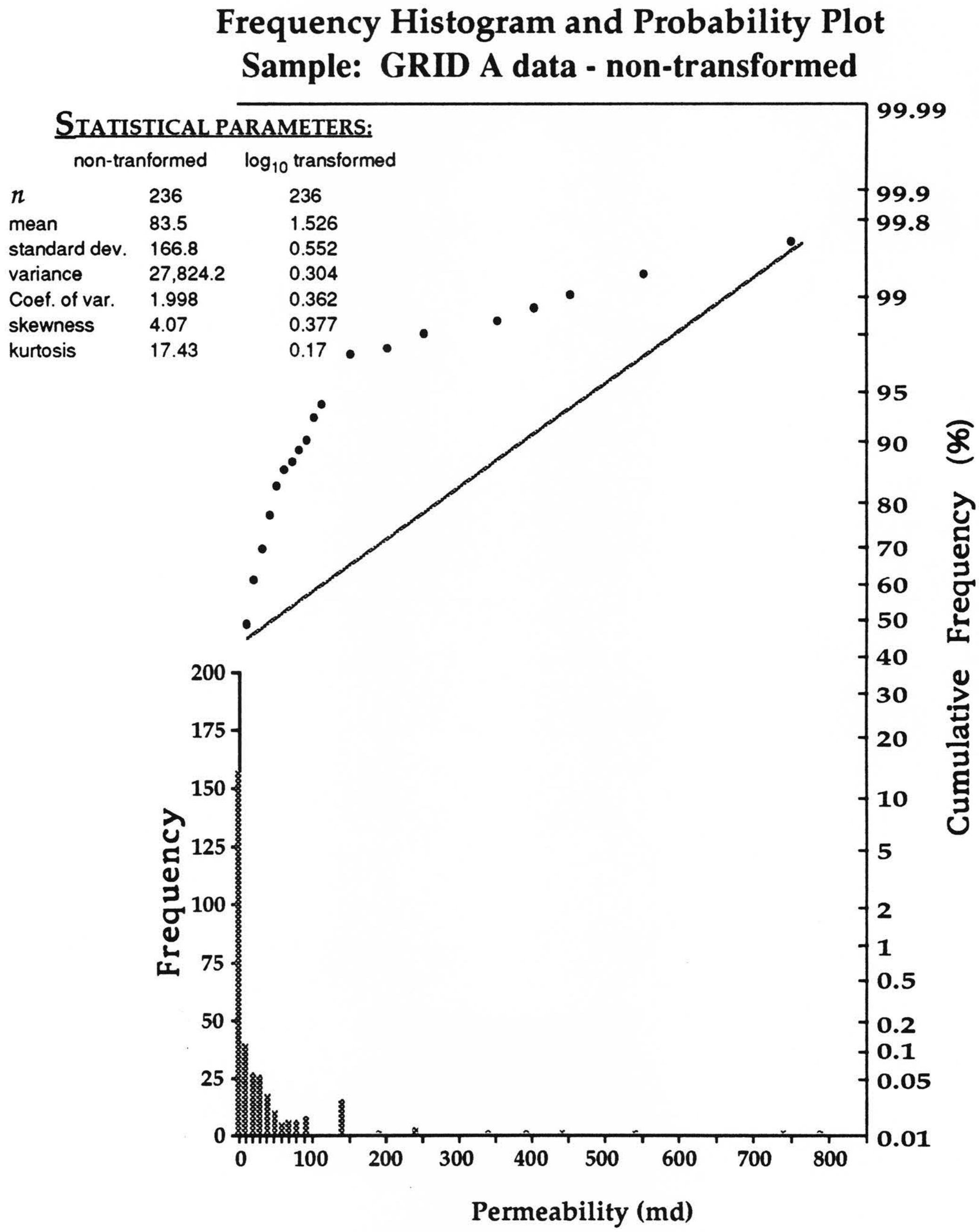

Figure 27. Frequency histogram and probability plot graphs of nontransformed GRID A data. The data do not exhibit a normal distribution in either the shape of the histogram nor the curve of the cumulative frequencies plotted on probability axes.

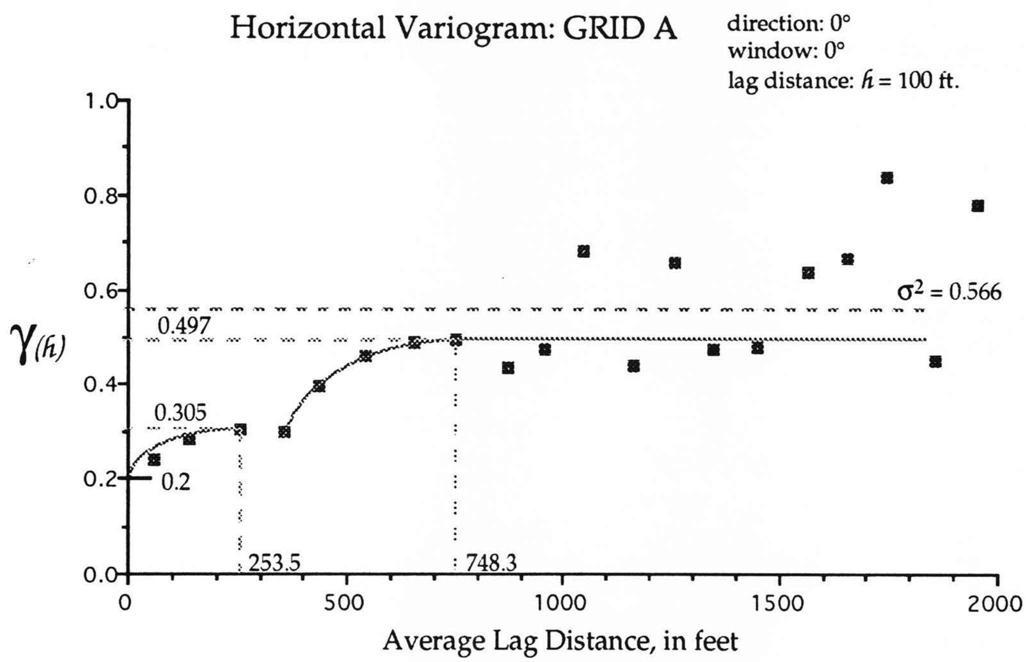

Figure 28. Horizontal variogram of GRID A data, $\hbar = 100$ feet. The variogram has been interpreted for nested variograms with an initial nugget.
Nugget ($C_{(0)}$) = 0.2 ; range($r_{(1)}$) = 253.5 ft.; sill ($C_{(1)}$) = 0.305; range($r_{(2)}$) = 748.3 ft.; sill ($C_{(2)}$) = 0.497; sample population variance ($\sigma^2 =$ 0.566).

Legend

■ $n \geq 30$, statistically significant

□ $n < 30$, not statistically significant semivariance values are scattered about both the estimated sill ($C_{(2)}$) and the data statistic of variance ($\sigma^2 = 0.588$).

The experimental vertical variogram for h = 1 foot (Fig. 29) provides a distinct linear relationship for semivariance and average separation distances. This is followed by a precipitous drop in semivariance values beyond the average separation distance of 13 feet. This drop in semivariance coincides with a decrease in the number of data pairs used in calculating semivariance; from a peak of 268 at 1 foot, to 57 at 13 feet, 41 at 14 feet, and 30 or less for average distances of 15 feet and greater. The initial linear relationship exhibits a possible nugget value (0.162) based on a well fit line (R^2 = 0.986). Beyond the average separation distance of 13 feet, calculated semivariance values decrease in a nearly linear fashion, hence, neither sill nor range values were estimated.

5.2.2 GRID B

The contoured posting of the GRID B sample permeability data (Fig. 30) exhibit similar distribution characteristics as GRID A. The pattern of the contour lines is complex in the areas of densest sampling (transects B5 - B12), indicating heterogeneous permeability distributions at the smallest scale of the grid. Also as noted in the GRID A sample data, permeability values generally increased in value from the bottom to the top of the vertical transects.

In contrast to the contour map of GRID A sample data, continuous high permeability streaks are observed in GRID B. In GRID A, the high permeability occurs as isolated zones against a background of average low permeability, whereas transects B2 - B5 and B9 - B12 are connected by tongues of high permeabilities.

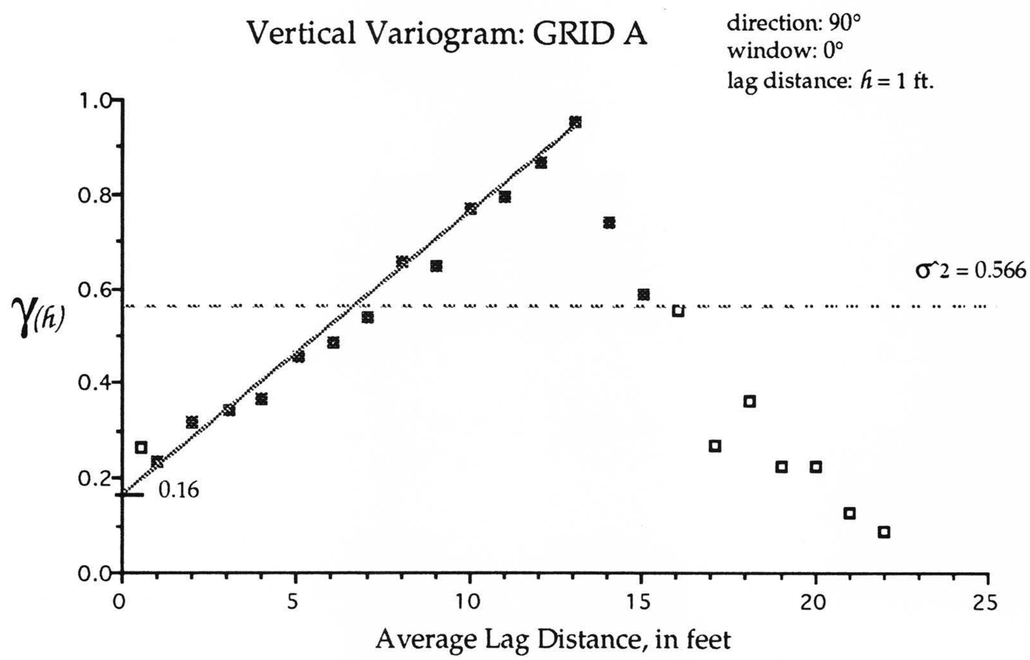

Figure 29. Vertical variogram of GRID A data, h = 1 foot. The variogram has been interpreted for a single nugget affected variogram. The sill plateau was poorly developed, therefore range and sill values were approximated. Nugget ($C_{(0)}$) = 0.16; range($r_{(1)}$) = 13.0 ft.; sill ($C_{(1)}$) = 0.95; sample population variance (σ^2) = 0.566 .

Legend

- $n \geq 30$, statistically significant
- $n < 30$, not statistically significant

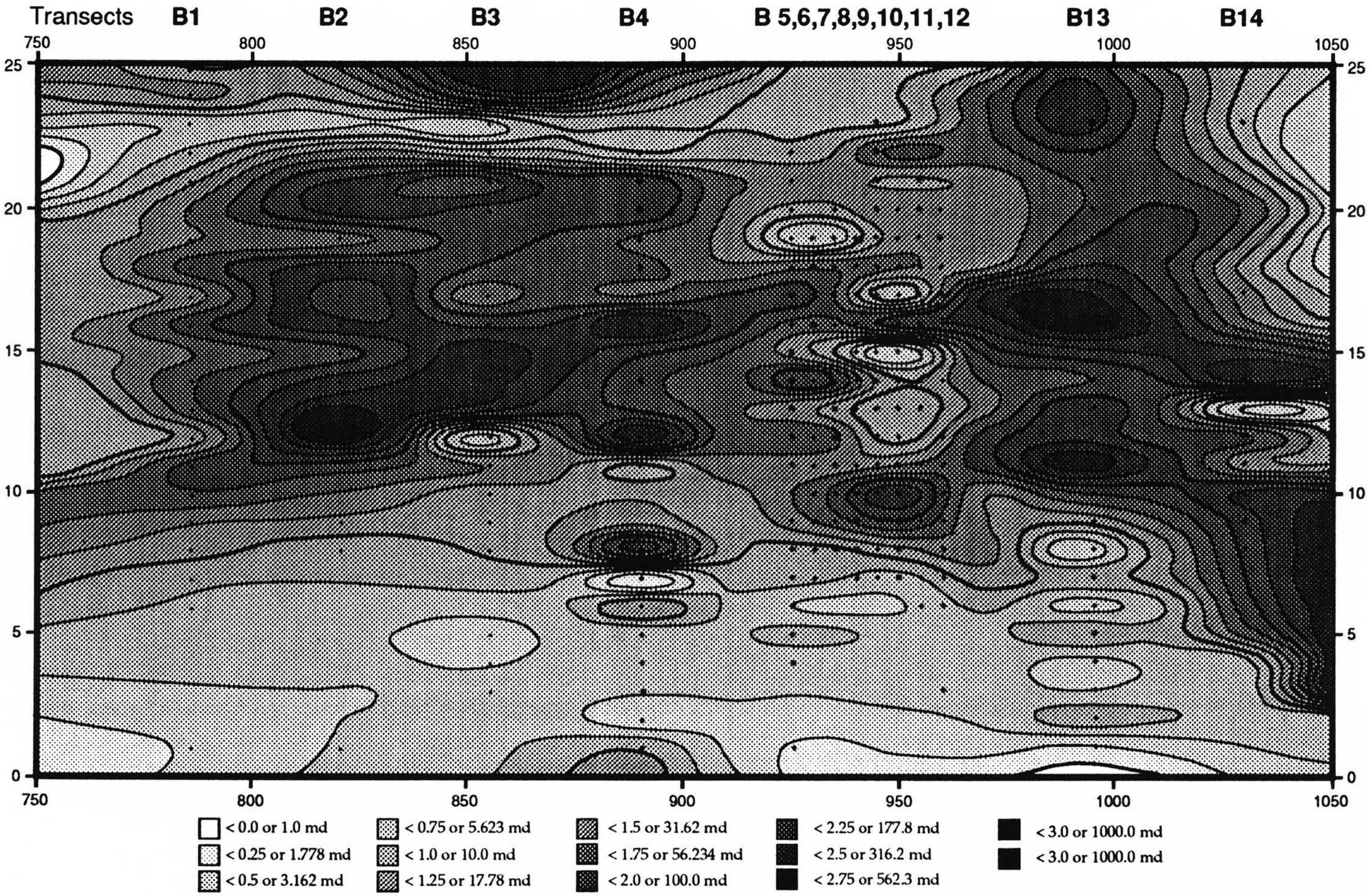

Figure 30. Contoured map of permeability measurements collected on outcrop; GRID B sample population. Vertical and horizontal heterogeneities were observed to occur in areas of high density sampling. Also of note was the upper left region (transects B1 to B5, above 12 foot elevation) where high permeabilities exist in a continuous pattern.

However, these tongues are not continuous through the densely sampled area of transects B6 - B9, where horizontal and vertical heterogeneities are observed at smaller scales (<10 feet).

Statistically, the GRID B sample data fit a lognormal distribution. As shown on frequency histogram and cumulative probability plots (Fig. 31), the log-transforms of the sample data conform to the respective bell-shape and straight-line models for a lognormally distributed sample. Statistics calculated for the sample data also conform to those of a lognormal distribution. The coefficient of skewness (0.279) is closer (absolutely) to zero than that for the GRID A sample data. Additionally, the geometric mean (Y = 1.434 or 27.14 md), standard deviation (σ = 0.748 or 3.63), and variance (σ^2 = 0.560 or 3.631) values follow the general precepts that for a lognormally distributed sample the mean should be greater than the standard deviation.

The experimental horizontal variogram is poorly developed for a h of 10 feet (Fig. 32) because of a high nugget value, a weakly defined slope, a low nugget-to-sill ratio, and possible hole effects in the sill. The initial slope of the variogram starts at 0.378 and is based on only three calculated points. The estimated sill (0.570) closely approximates the sample data's variance (0.560). The shape of the sill punctuates the possible "hole effects" which follow immediately (at the step increments of $4h$ and $7h$-to-$9h$) and are nearly as low as the nugget value (0.378). In addition, the high nugget provides a low nugget-to-sill ratio (1.482), an indication of non-correlative data at the smallest scale in the sample. Beyond the step increment for $11h$ (110 feet), the wide scatter in calculated semivariance is coincidental with the decrease in the number of data pairs at those distances.

Frequency Histogram and Probability Plot
Sample: GRID B data

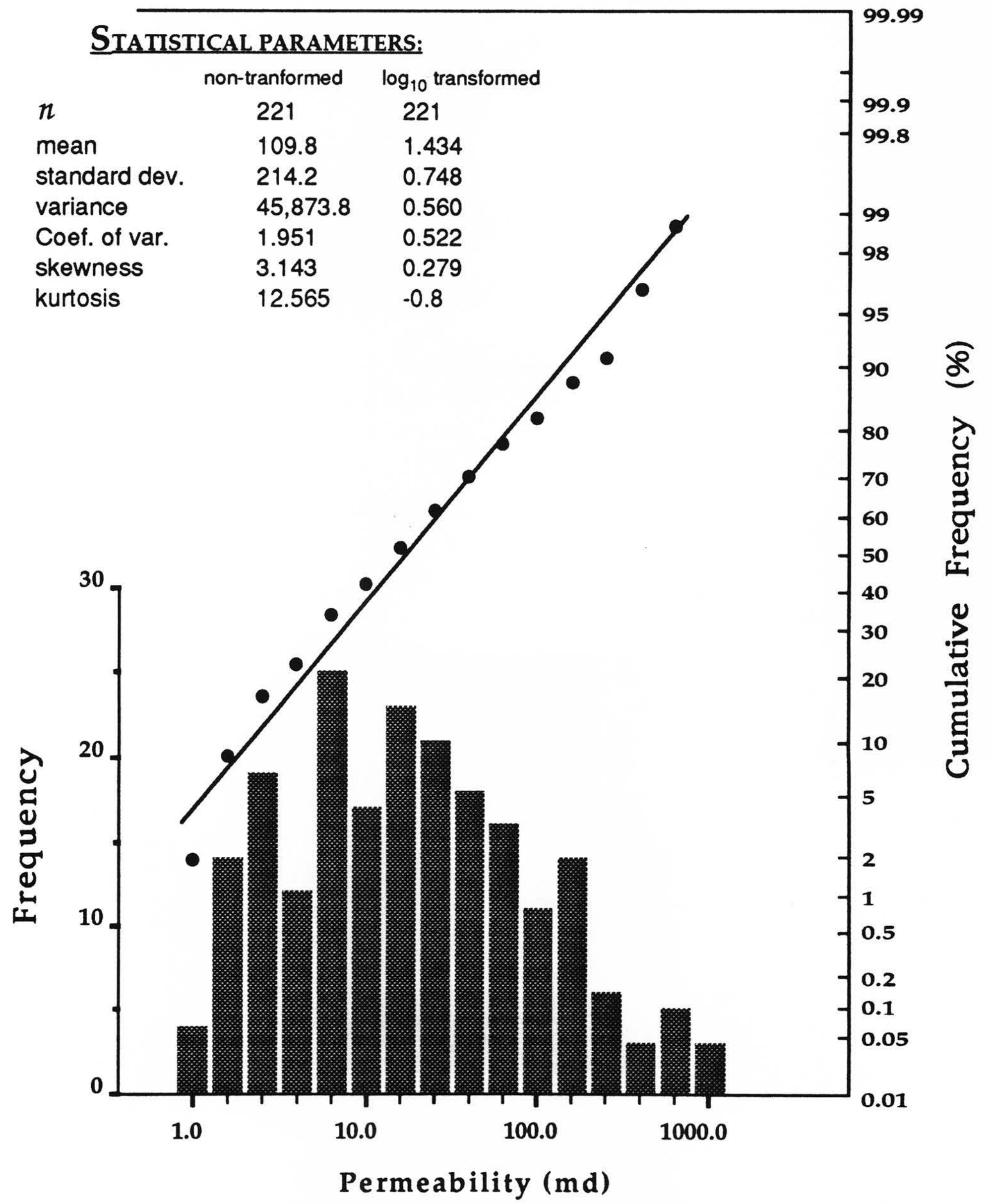

Figure 31. Frequency histogram and probaility plot graphs of the GRID B sample data. The data exhibits lognormal distribution with a slight deviation. The positive and moderately high coefficient of skewness conforms to the tail of high permeability values (i.e., >200 md) in the frequency histogram.

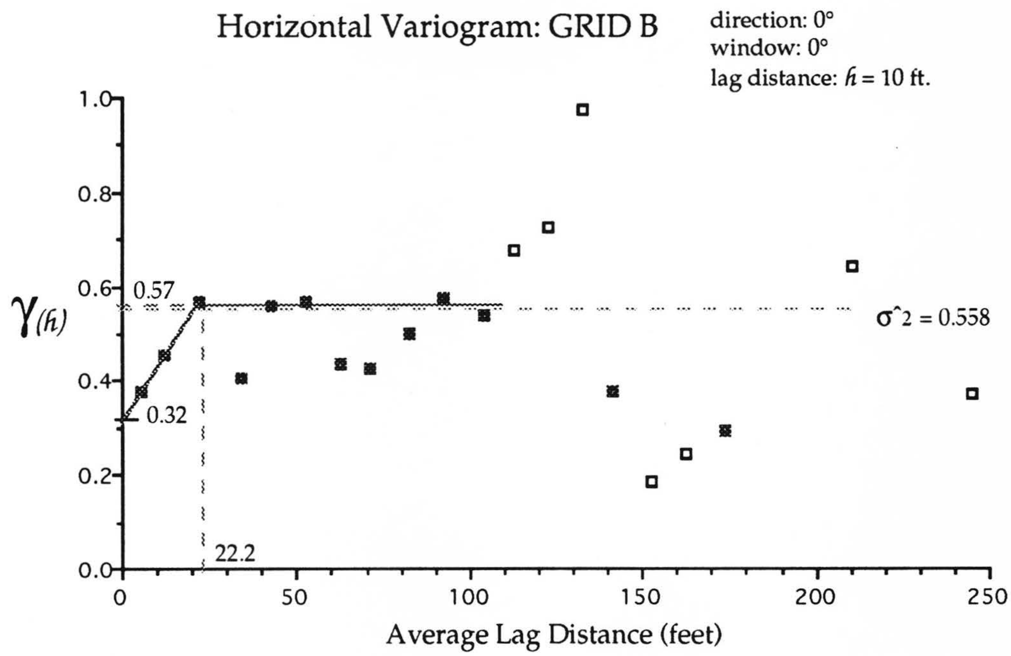

Figure 32. Horizontal variogram of GRID B data, $\hbar = 10$ feet. This variogram was interpreted for a single nugget effected variogram.
Nugget ($C_{(0)}$) = 0.32; range($r_{(1)}$) = 22.2 ft.; sill($C_{(1)}$) = 0.57; sample population variance (σ^2) = 0.558 .

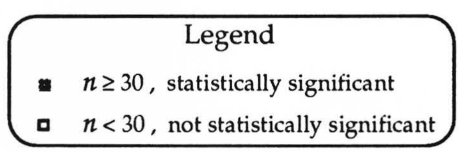

As in the above horizontal variogram, the initial slope and sill of the experimental vertical variogam is a poor match to the spherical variogram model (Fig. 33). The initial $\gamma(h)$ value is high (0.313) and is followed by a slope of three $\gamma(h)$ values. After this initial short range (4 feet) and sill (0.44), another four points form a second slope from which second values for range and sill are estimated (10 feet and 0.71, respectively). This variation of the spherical variogram model indicates a correlation of permeability values in the GRID B sample data at two scales with individual characteristic variances.

5.2.3 GRID C

Located within the densest sampled area of GRID B, GRID C represents an attempt to determine the continuity of the high permeability zones at a smaller scale. Separation distances of the data in GRID C are an equal one foot distance in the vertical and the horizontal, except for a central patch of one-half and one-third foot separations. The contoured pattern (Fig. 34) exhibits both horizontal and vertical heterogeneities. A near continuous horizontal streak of high permeabilities is extends across the upper middle section of GRID C, and correlates the nearly continuous high permeability streak observed in GRID B.

The probability plot of GRID C data (Fig. 35) indicates the most definitively lognormal distribution of all the other sample data, although there is a slight deviation at the high permeability values. The frequency histogram also indicates a lognormal distribution because of the very symmetrical bell shape to the histogram, this correlates with the sample's low coefficient of skewness (0.377). Mean and standard deviation values of the log-transformed sample data (33.60 md and 3.565 md,

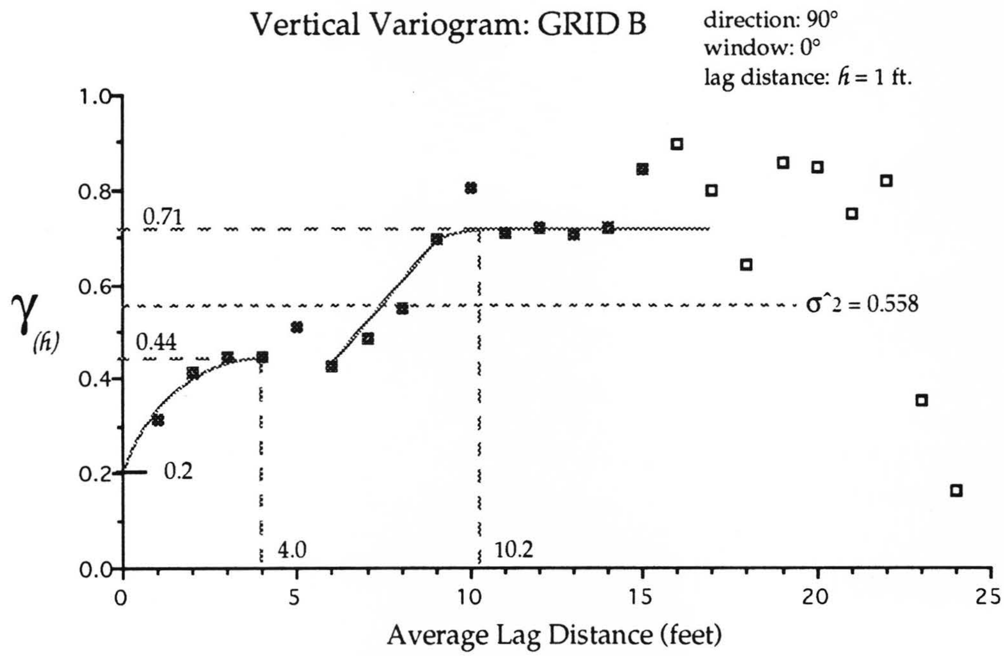

Figure 33. Vertical variogram of GRID B data, $\hbar = 1$ foot. Nested sets of two variograms with an initial nugget effect are interpreted for this example. Nugget ($C_{(0)}$) = 0.2; range($r_{(1)}$) = 4.0 ft.; sill ($C_{(1)}$) = 0.44; range($r_{(2)}$) = 10.2 ft.; sill($C_{(2)}$) = 0.71; population variance (σ^2) = 0.558 .

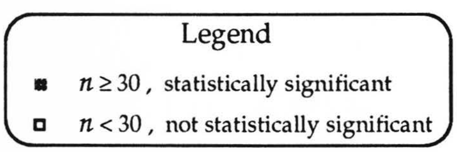

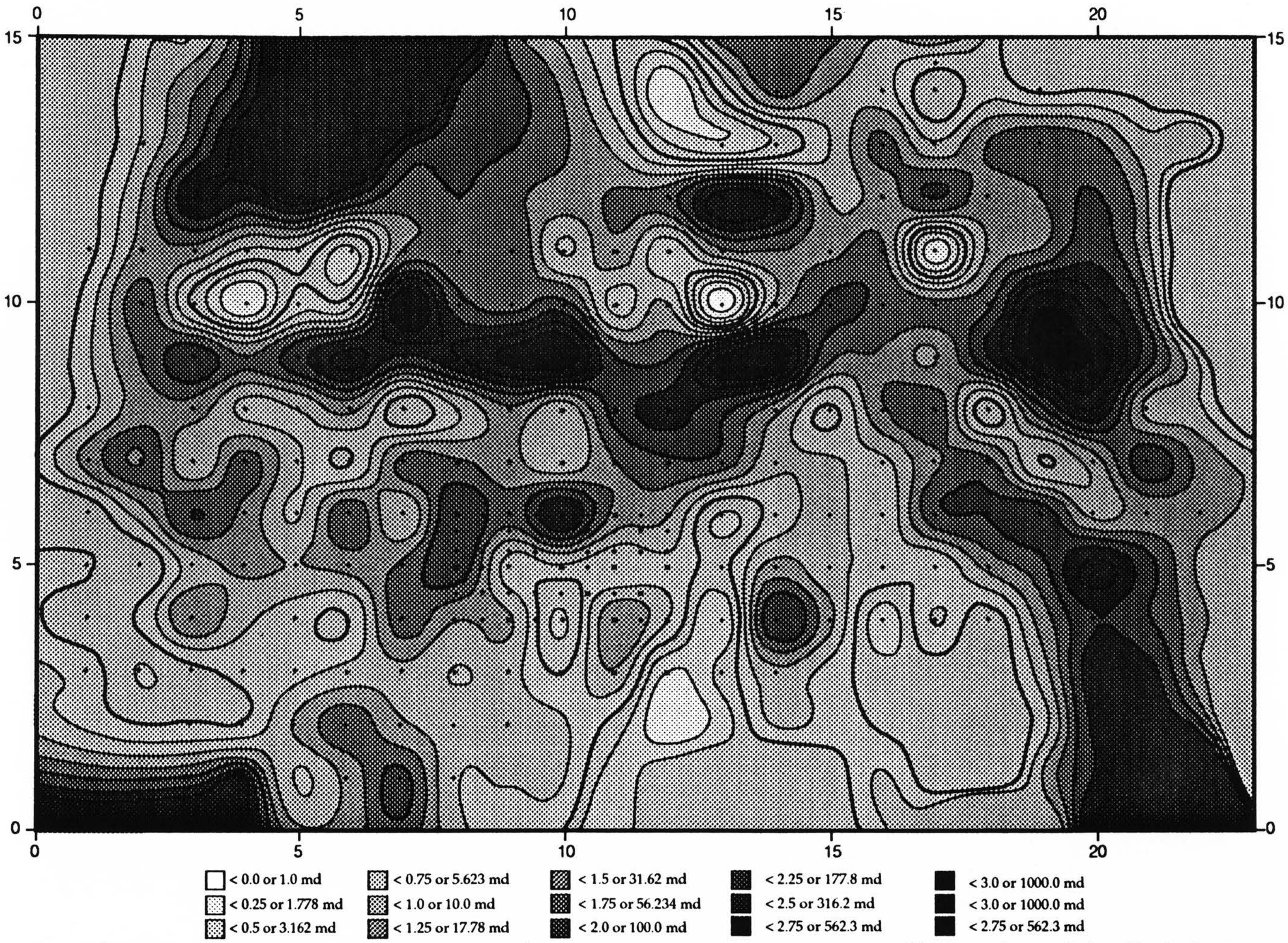

Figure 34. Contoured map of log-transformed permeability measurements collected on outcrop; GRID C sample population. Vertical and horizontal heterogeneities are observed to show a modest continuity of high permeability strreaks, most notably at the 9 foot elevation.

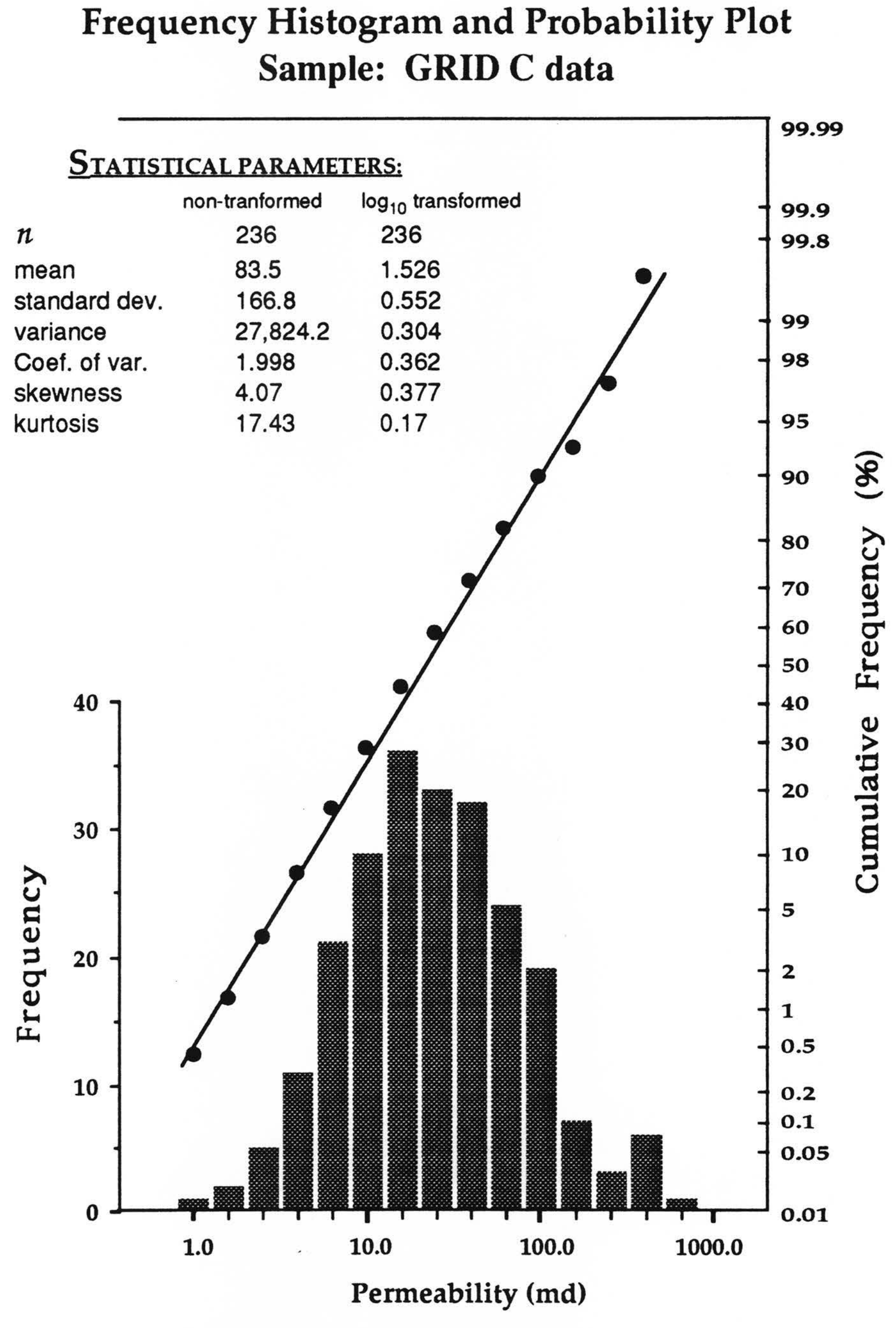

Figure 35. Frequency histogram and probability plot graphs of GRID C data. The data exhibit lognormal distribution in both the shape of the histogram and the close fit of the cumulative frequency to the straight line.

respectively) follows the general convention for a lognormal distribution because the mean is greater than the standard deviation.

GRID C is the only sample set in which the vertical and horizontal correlations are directly comparable in scale, but the grid is limited in extent as a result. The choice of h =1 ft. used in the calculation of the variogram was made simple since the realizations of the permeability $z(x_i)$ were regularly spaced and thus fulfills the variogram theory better than the other sample sets (GRIDs A, B, or D). The results are moderately developed variograms, which are limited primarily by the number of data points in the GRID C sample data.

Parameters from the horizontal experimental variogram (Fig. 36) are estimated for a high nugget on a moderately developed slope and a sill with a moderate saddle of $\gamma(h)$ values. The nugget (0.15) is extrapolated from the five $\gamma(h)$ values on the slope. The sill (0.27) is lower than the calculated variance of the sample data and it exhibits a saddle of increased correlation after the initial range (4 feet). Beyond the 14h step increment, the scatter of $\gamma(h)$ values is coincidental with the decrease in the number of data pairs at those distances.

The vertical experimental variogram (Fig. 37) calculated for the sample data is interpreted for a spherical variogram with nugget. The nugget (0.1) is one-half to one-third the value of the sill (0.34) and the slope is represented by only three $\gamma(h)$ points. The sill plateau is moderately flat and is near to the variance of the sample data (0.321). The total multiple of step increments for the vertical search direction are limited to 11h due to the shape of the sample area and the thickness of the parasequence.

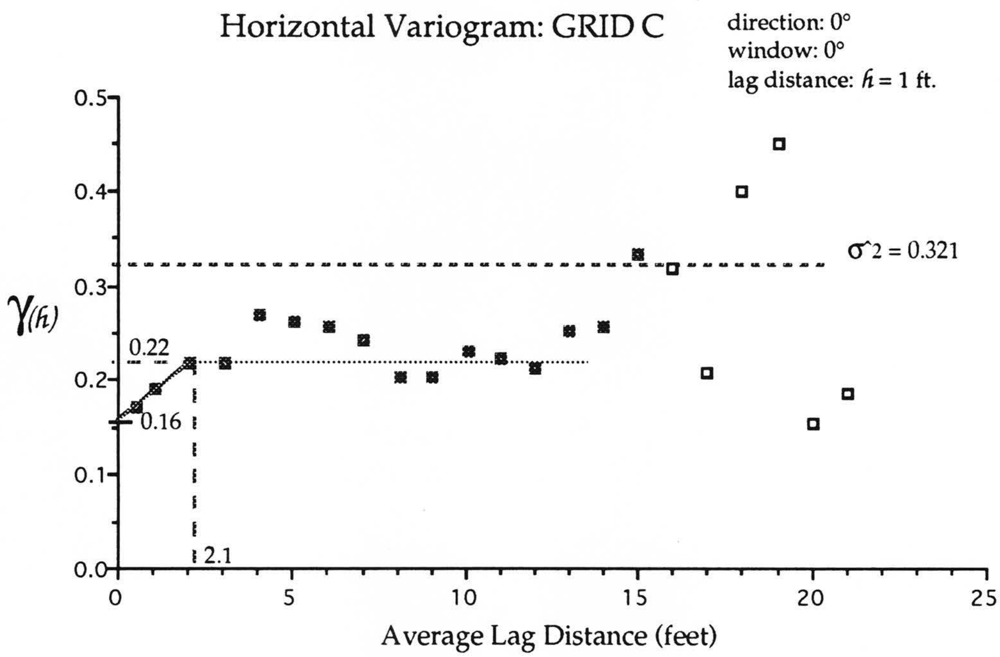

Figure 36. Horizontal variogram of GRID C data, $h = 1$ foot. The variogram has been interpreted for a single nugget affected spherical variogram with a minor component of high variance scatter at the intermediate distances. Nugget ($C_{(0)}$) = 0.16; range($r_{(1)}$) = 2.1 ft.; sill($C_{(1)}$) = 0.22; sample population variance (σ^2) = 0.321 .

Legend	
■	$n \geq 30$, statistically significant
□	$n < 30$, not statistically significant

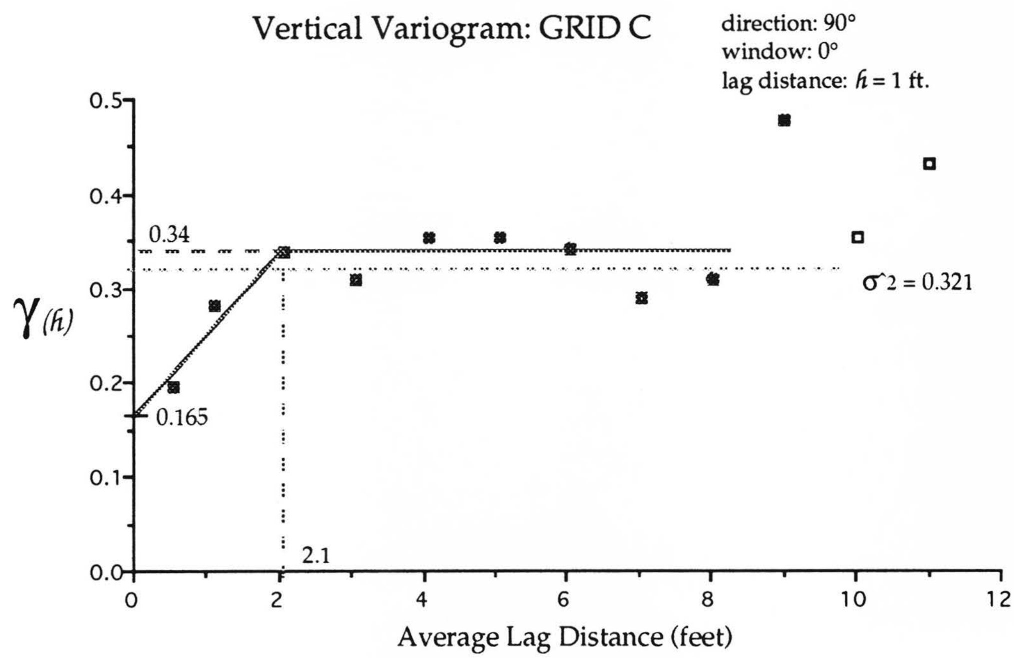

Figure 37. Vertical variogram of GRID C data, $\hbar = 1$ foot. The variogram has been interpreted for a single nugget affected spherical variogram. Nugget ($C_{(0)}$) = 0.165 , range$_{(1)}$ = 2.1 ft., sill$_{(1)}$ = 0.34; sample population variance (σ^2) = 0.321 .

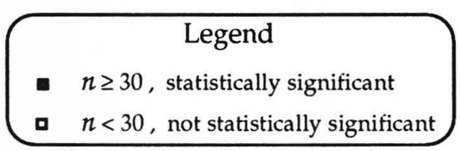

5.2.4 GRID D

As stated above, GRID D is located at the center of GRID C, entirely in the wackestone/packstone fabric of the transition zone between the mud-dominated facies #1 and the grain-dominated facies #3 (see Fig. 22, p. 64). Due to the site preparation method and the small-scale of the investigation, the data are not composed of averaged MFP measurements for each location, but rather the direct representation of a single measurement. In that respect, the site is unique among the scale-based sample data sets. The combination of the singular MFP measurements and the location of the grid, resulted in a relatively high number of points for which no data are available due to the detection limit of the MFP device. Unrecovered data are noted for 15 of the 196 sampled locations (7.65%). The lack of these assumed low permeability data is perceived as a sampling bias which affects the sample statistics in the manner of elevating the mean and decreasing the variance.

The GRID D sample data are contoured on Figure 38, they exhibit a dominant matrix of low average permeability surrounding localized zones of high and low permeabilities. The heterogeneity of permeabilities in the vertical and horizontal transact lines are not conducive to the contouring algorithm, this was observed in the high and low permeabilities which followed the grid pattern as viewed against the background averaged permeability as drawn by the CPS-1 program.

Frequency histogram and probability plot presentations of the log transformed sample data (Fig. 39) indicates that the distribution is weighted to the low end of the permeability range. The histogram shape is nearly flat for the 0.6 md to 100 md range, exhibiting two modes and a short tail of high values. The cumulative frequencies plotted on a probability graph vary slightly from a straight-line. These

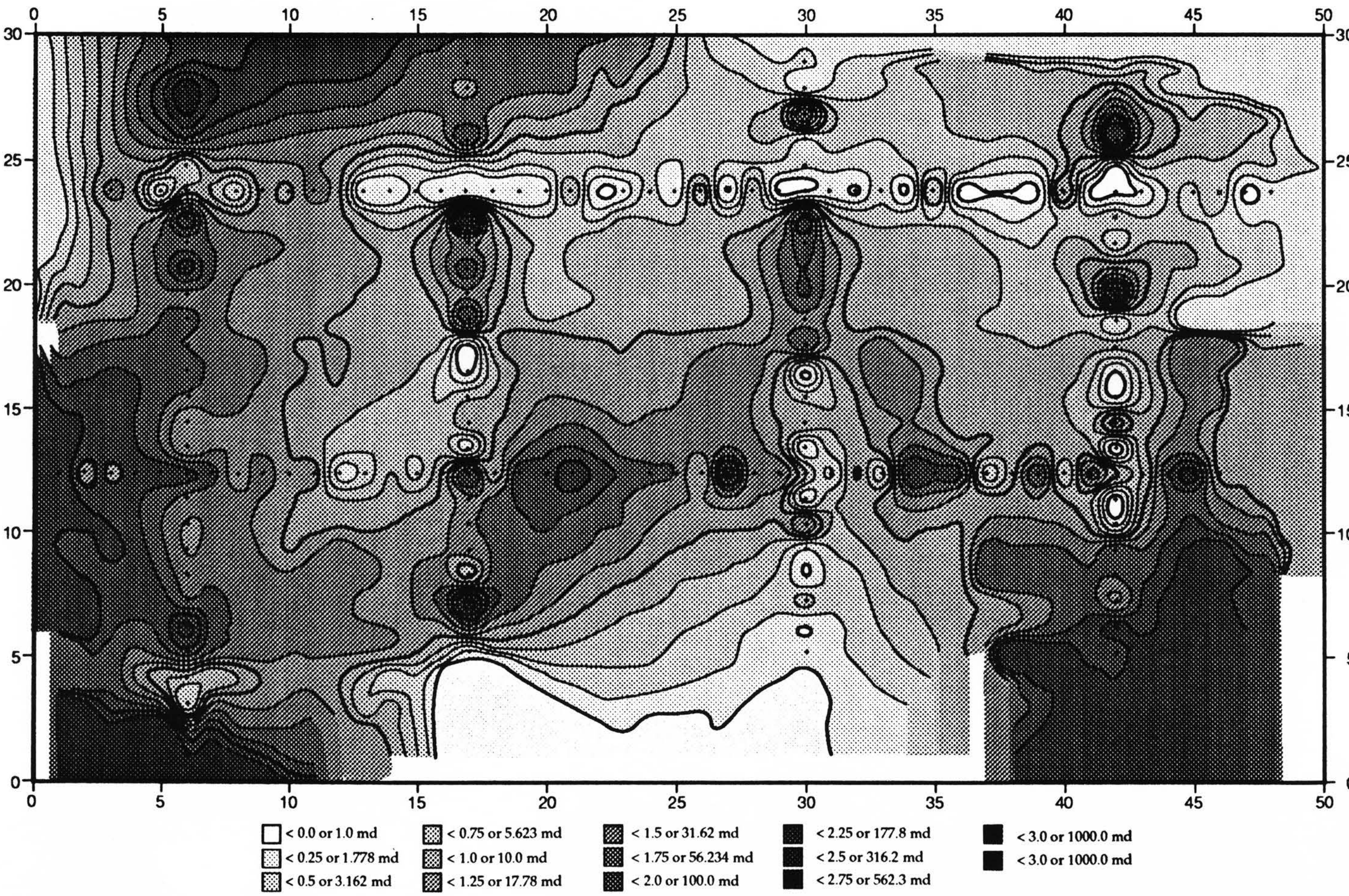

Figure 38. Contoured map of log-transformed permeability measurements collected on outcrop; GRID D sample population. Vertical and horizontal heterogeneities are observed and are especially noticable about the sample points. The complexity of the heterogeneities created difficulties in the ability of the computer software to contour the data, this resulted in uncontoured areas, unconnected contours, and other contouring mistakes in the figure.

Frequency Histogram and Probability Plot
Sample: GRID D data

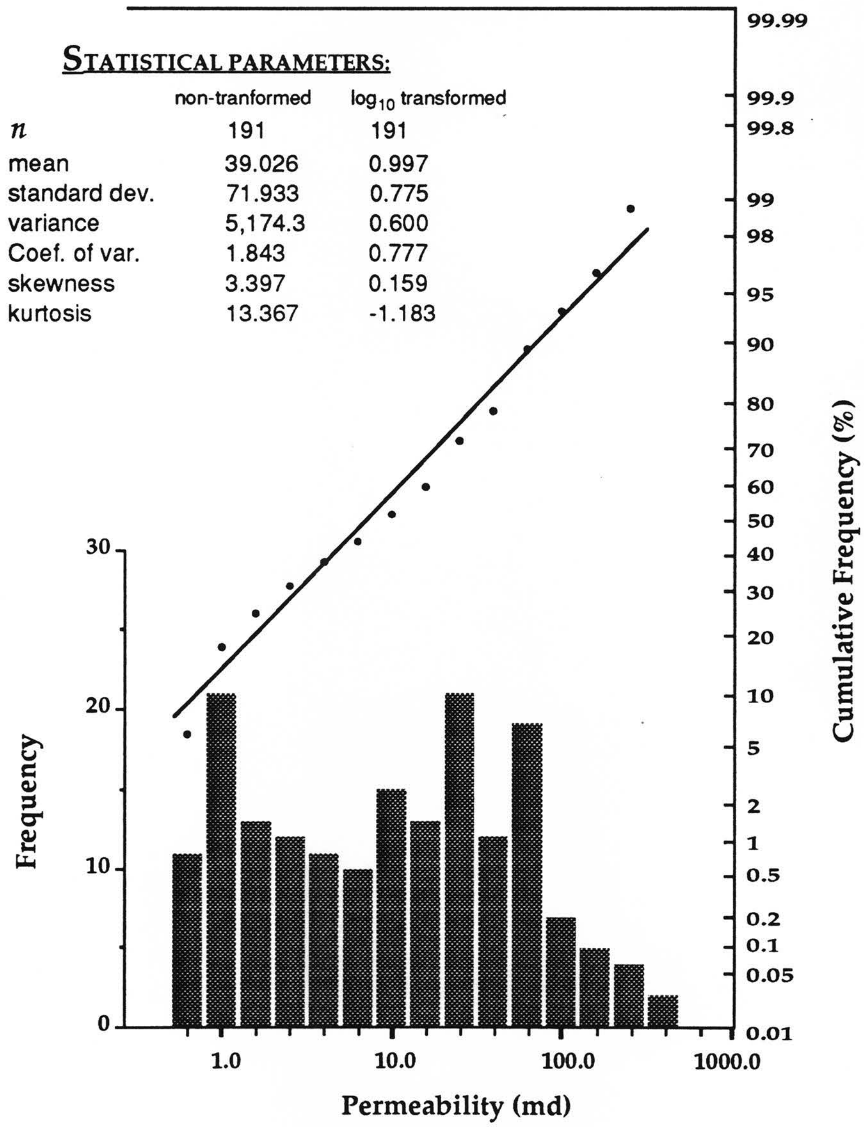

Figure 39. Frequency histogram and probabiilty plot graphs of GRID D data. The data exhibit a lognormal distribution with a slight deviation in the low permeability range (i.e., <1.0 md). This is seen as the presence of two modes in the histogram and the sinoidal curve of the cumulative frequncies in the probability scale graph.

observations of non-characteristic lognormality are not significant to the assessment of a Gaussian distribution for the sample data.

Statistics of the sample data confirms a lognormal distribution, while the statistics of the non-transformed data were not representative of a normal distribution. For the log-transformed data, the geometric mean (12.089 md) is greater than the standard deviation (5.598 md), and the skew is very low and positive (0.051). These indicate that the log-transformed data are well-behaved about the mean. In contrast, statistics of the non-transformed data follow a similar non-Gaussian model as observed in the other non-transformed sample data sets.

Experimental horizontal and vertical variograms (Fig. 40 and Fig. 41, respectively) of the sample data were analyzed for the step interval (h) of 1 inch. The experimental horizontal variogram (psi = 0°) displays the characteristics of a well developed spherical model, with a relatively low nugget (0.256) based on a range of 7 inches and a sill (0.378) which is significantly less than the sample variance (0.559). The experimental vertical variogram is relatively poorly developed, exhibiting a slope based on the initial two semivariance values which is followed by an increasingly scattered sill. The overall shape of the vertical variogram differs from an all-nugget variogram model by the initial semivariance value calculated for a lag increment of 1 inch. The nugget indicated by the vertical variogram is 0.35, only slightly lower than the sample variance value of 0.559, which itself is very close to the estimated sill value (0.54).

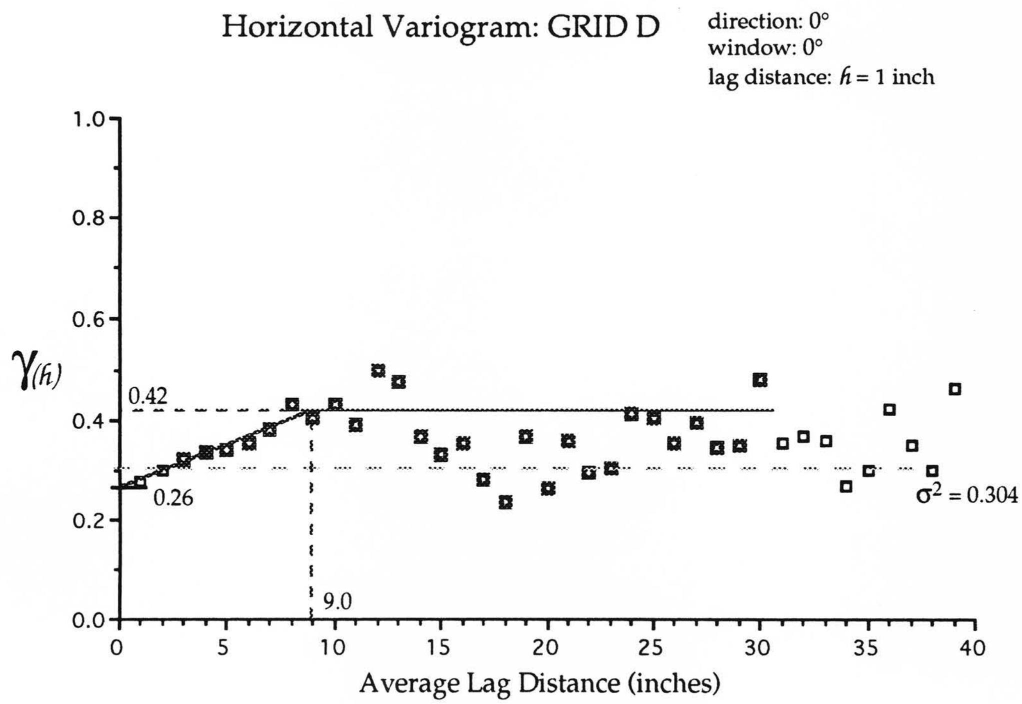

Figure 40. Horizontal variogram of GRID D data, h = 1 inch. A singe nugget affected variogram is interpreted for this example. The variance is highly vaiable at the intermediate distances indicative of undeveloped nested sets or "hole effects" in the statistics.

Nugget ($C_{(0)}$) = 0.26; range($r_{(1)}$) = 9.0 in.; sill($C_{(1)}$) = 0.42; sample population variance (σ^2) = 0.304 .

Legend

- $n \geq 30$, statistically significant
- $n < 30$, not statistically significant

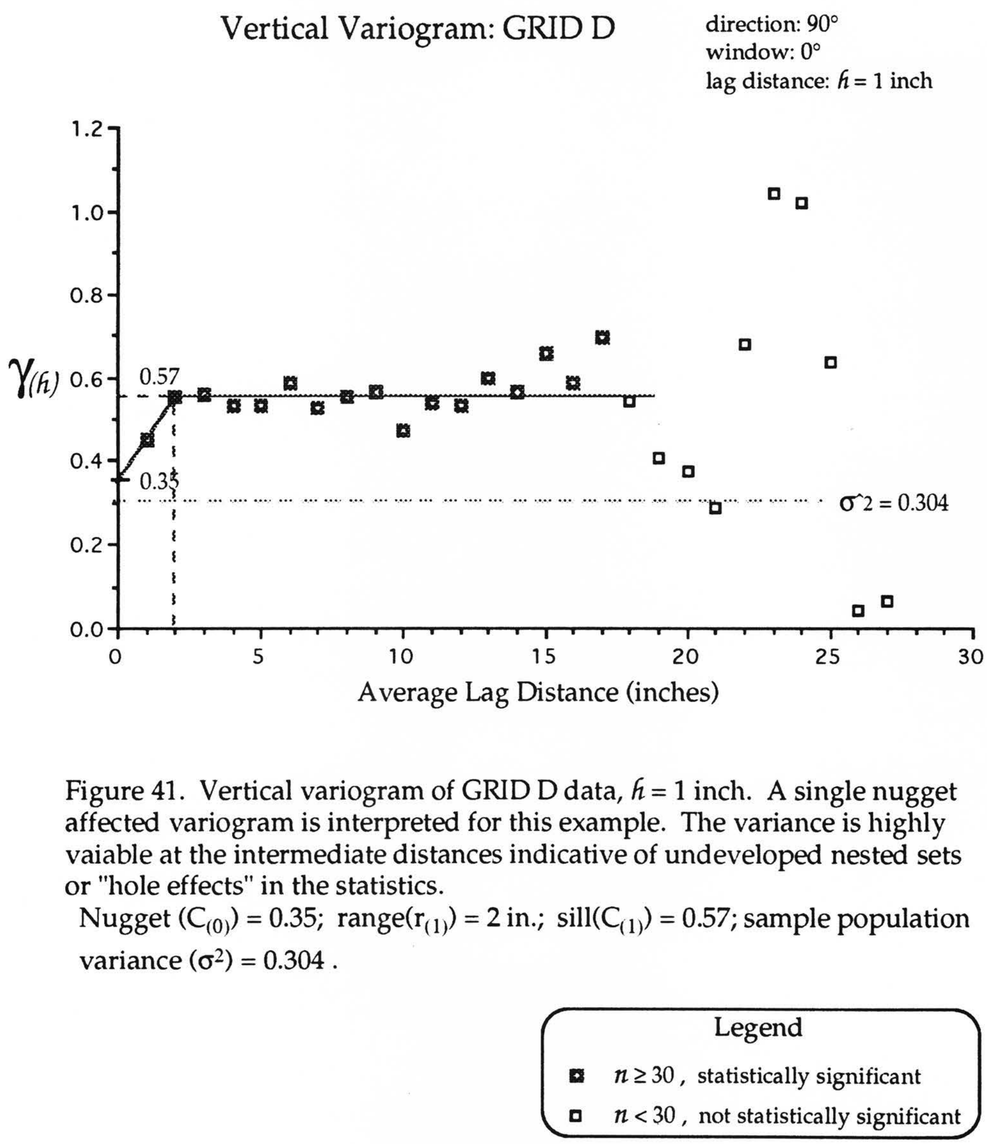

Figure 41. Vertical variogram of GRID D data, $\hbar = 1$ inch. A single nugget affected variogram is interpreted for this example. The variance is highly vaiable at the intermediate distances indicative of undeveloped nested sets or "hole effects" in the statistics.

Nugget ($C_{(0)}$) = 0.35; range($r_{(1)}$) = 2 in.; sill($C_{(1)}$) = 0.57; sample population variance (σ^2) = 0.304 .

5.3 DISTRIBUTIONS OF DATA IN THE GENETIC FACIES

The permeability data associated with specific genetic facies were also analyzed for lognormal distribution and sample statistics. Contour patterns for these sample data sets are presented in the above sections, where the relationships to the other facies are described. The following graphical and statistical analyses provide further information as to the distributions of permeability in descretized areas, based on the description of the rock fabric.

Facies #1, described above as a mud-dominated flooded shelf matrix, is represented by 91 permeability measurements which include much of the core plug data also used in the GRID A sample data. The normal and geometric means of this sample data (5.652 and 2.312 md, respectively) conform to the expectation for low permeability in a mud matrix.

Statistics of the log-transformed facies #1 sample data and the graphic representations of histogram and probability plot (Fig. 42) are not indicative of a sample which is well-fit to a lognormal sample. Evidence for a lognormal distribution to the sample data is not observed in the values for mean (0.364 or 2.312 md), variance (0.564), and standard deviation (0.751 or 5.636 md), because the geometric mean is not greater than the standard deviation. The long tail of low permeabilities observed in the histogram reflects a relatively high negative skew (-1.255). The probability plot of cumulative percent frequencies deviates from the straight-line model for a lognormal sample in the low permeability range, this is similar to the deviation observed for GRID A sample data which also incorporates core plug permeability data.

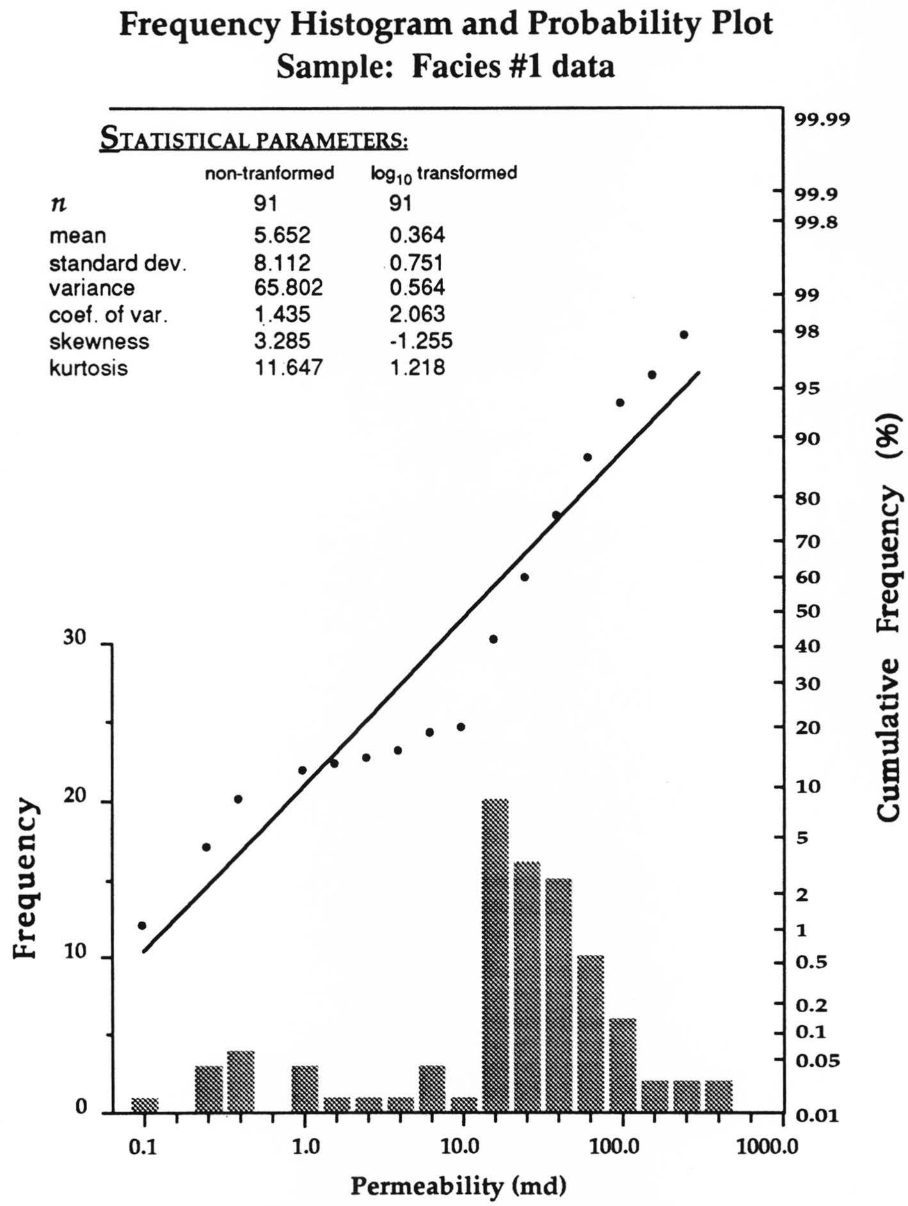

Figure 42. Frequency histogram and probability plot graphs for facies #1 data. The cumulative frequencies plotted on probability axes deviate from that of a lognormally distributed sample population. High values for the coefficient of skewness and coefficient of variation confirm the nonconformance of the facies #1 sample data to the lognormal population attributes shared by the above GRID sample data populations. As noted for the GRID A sample data, two populations are indicated for this sample.

Facies #2 is represented by 29 permeability measurements, a statistically non-significant sample. The limited extent of the facies in the northern section of the parasequence hindered sampling. Regardless of this limitation and its implication on the meaningfulness of the statistics, the sample data fit the general conditions of mean and standard deviation for a lognormal distribution.

Statistics and graphic representations (Fig. 43) of the facies #2 sample data are indicative of a relatively low permeability facies with permeabilities evenly distributed within a narrow range of values. The geometric mean (7.874 md), standard deviation (3.155 md), and variance (0.249) values are well-fit to the model of lognormal distribution. The straight-line relationship of the probability plot is based on a relatively few data points and the even-ness of the distribution was evident in the histogram and the low coefficient of skewness (0.074).

The majority of the collected data were from facies #3. It has a grain-dominated fabric, high porosity, and was therefore expected to be characterized by (relatively high) lognormally distributed permeability values. Comparison of the non-transformed and log-transformed data was made for the mean (85.851 md and 24.1 md respectively) and standard deviation (174.545 md and 4.508 md, respectively) values, these results also support the assumption of lognormality in the distribution. Frequency histogram and probability plot analyses also indicate a lognormal distribution (Fig. 44). The bell shape of the histogram and straight-line relationship of the cumulative frequencies are well-fit to the lognormal model. This is emphasized by the low coefficient of skewness (0.117), and by the broadest range of values for any facies identified in this study.

Frequency Histogram and Probability Plot
Sample: Facies #2 data

STATISTICAL PARAMETERS:

	non-tranformed	$\log_{10}$ transformed
n	29	29
mean	14.17	0.896
standard dev.	15.181	0.499
variance	230.453	0.249
coef. of var.	1.071	0.557
skewness	1.218	0.074
kurtosis	0.166	-1.07

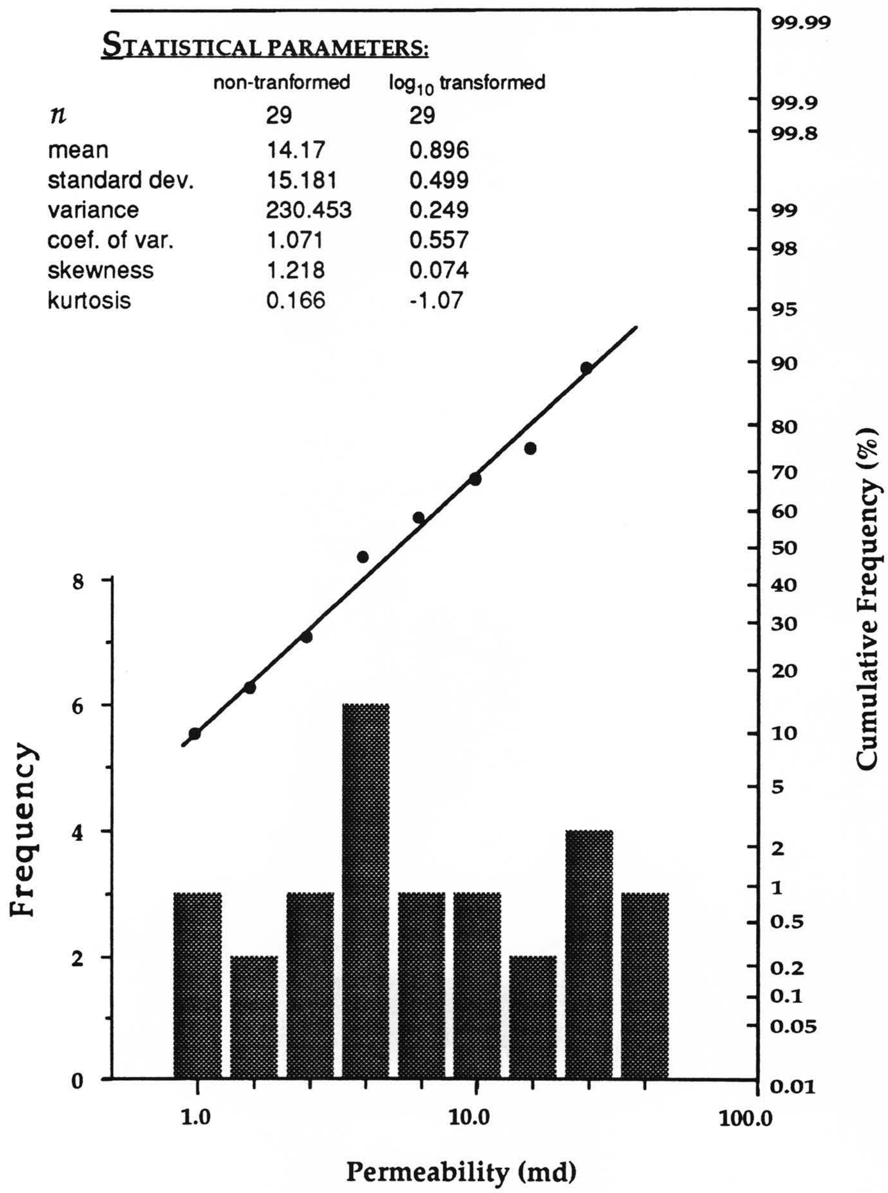

Figure 43. Frequency histogram and probability plot graphs for facies #2 data. The data exhibit attributes of a lognormal distribution in cumulative frequency plot, but the low coefficient of skewness and low relief over short range in histogram were difficult to interpret due to the small size of the sample population (29).

Frequency Histogram and Probability Plot
Sample: Facies #3 data

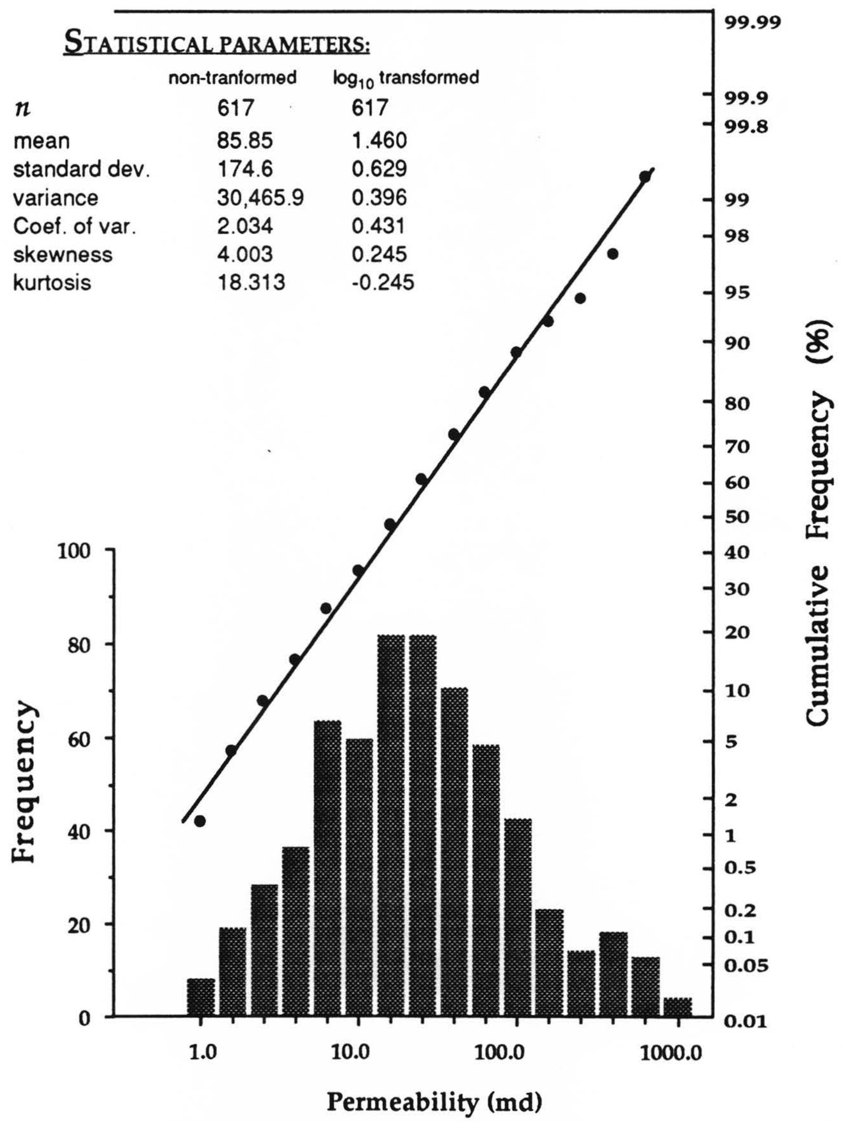

Figure 44. Frequency hstogram and probability plot graphs for Facies #3 data. The data exhibits lognormal distribution in both the shape of the histogram and the close fit of the cumulative frequency to a straight-line.

The shallow shelf, mud supported wackestone facies (#4) of the southern end of the parasequence is poorly fit to the lognormal model of distribution. The sample data for the facies include some or all of the core plug data of transects A19, A20, A22, A23, and A24. In the probability plot and frequency histogram (Fig. 45), a deviation from the lognormal distribution is observed in the below detection limit (bdl) range of the MFP device. This deviation is also observed in the relatively high negative value of the coefficient of skewness (-0.431). The statistics of the log-transformed sample data supports the graphical observations, since the mean (10.955 md) is greater than the standard deviation (5.689 md).

5.4 Comparison of Sample Permeability Data Sets

Determination of whether the four scale-based data sets and the facies-defined data sets were representative of a single total population of permeability data was necessary in order to fulfill the above mentioned assumptions for the behavior of permeability as a regionalized variable. These assumptions were that the permeabilities measured in the parasequence, uSA1, were randomized occurrences of a natural phenomenon and were sample statistics of a total population which was characterizable as a function ($m[x]$) with a single mean value and a Gaussian distribution (i.e., lognormal). The method for comparing the sample data sets and determining whether these were representative of a single population was the calculation of the coefficients of variation (C_V) and an ANOVA (one-sided test) comparisons for each sample data set.

Frequency Histogram and Probability Plot
Sample: Facies #4 data

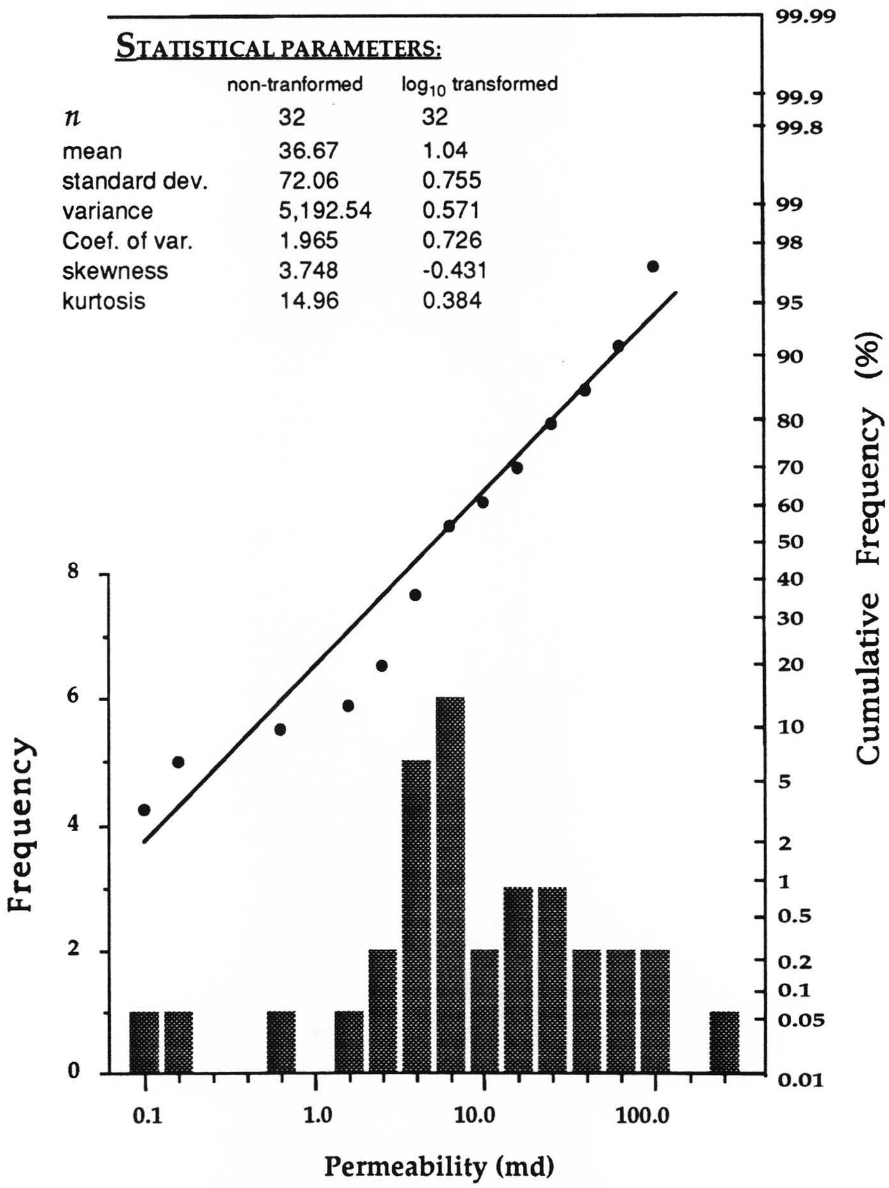

Figure 45. Frequency histogram and probability plot graphs for facies #4 data. Data shown to exhibit deviations from lognormality in the low permeability range (i.e., <1.0 md) which corresponds to the negative and moderately high coefficient of skewness. Values below 1.0 md represent core plug permeability data, other data for facies #4 comprised of mixed MFP and core plug permeability data.

The coefficients of variation compared the sample statistics as the ratio of the mean to the variance for each sample data set (Table 1). This method of characterizing the shapes of the distributions provides a simple comparison between the sample data sets. For all sample data sets, both scale-based and facies defined, the coefficient of variation values calculated for statistics of the log-transformed data falls within a closer range than the CV values of the non-transformed data.

The C_V values for statistics of log-transformed data are closely related and describable in two groups with one outlier. GRIDs A, D, and facies #4 (values between 0.517 and 0.565) comprise one group, and GRIDs B, C, and facies #2 and #3 (values between 0.199 and 0.391) comprise another group. The CV calculated for the facies #1 statistics is the greatest outlier of the sample data sets, possibly indicative of the high ratio of core plug permeability data associated with that sample data. Though slightly dissimilar, these CV values do not disprove the hypothesis that the above data sets represent related samples of a larger population.

Determination of the relationship between the samples of the GRIDs permeability data in the terms of whether the sample data represent a larger population, in this case the population of permeability data for the entire parasequence, was deemed necessary in order to substantiate further discussion in which the variogram parameters of the samples were to be grouped and analyzed. The means for this comparison is through the statistical method of analysis of variance (ANOVA).

The null hypothesis (H_0) tested was whether the comparison of the sample means are significant at a 5% level, and this test was conducted through a one-way (regressive) analysis for a 5% level of significance. The ANOVA test was analyzed

TABLE 1a

STATISTICS OF UNTRANSFORMED DATA

	Number in Sample	Mean (md)	Geometric Mean (md)	Standard Deviation (md)	Variance	Coefficient of Variation	Minimum	Maximum	Coefficient of Skewness
GRID A	320	37.716	10.959	86.702	7,517.2	199.311	0.01	827.0	6.023
GRID B	221	109.8	27.14	214.2	45,873.8	417.794	1.215	1388.5	3.301
GRID C	236	83.5	33.60	166.8	27,824.2	333.224	1.284	1066.55	4.07
GRID D	176	42.4	12.089	74.0	5,476.1	129.153	0.786	460.31	3.24
FACIES #1	91	5.652	2.31	8.112	65.802	11.642	0.01	46.285	3.285
FACIES #2	29	14.166	7.874	15.181	230.453	16.268	1.047	52.891	1.218
FACIES #3	617	85.851	28.872	174.545	30,465.928	354.87	1.215	1,388.461	4.003
FACIES #4	32	36.672	10.955	72.059	5,192.54	141.594	0.15	382.613	3.748

TABLE 1b

STATISTICS OF LOG-TRANSFORMED DATA

	Number in Sample	Mean (md)	Geometric Mean (md)	Standard Deviation (md)	Variance	Coefficient of Variation	Minimum	Maximum	Coefficient of Skewness
GRID A	320	1.04	-	0.767	0.588	0.565	-2.0	2.917	-0.739
GRID B	221	1.434	-	0.748	0.560	0.391	0.084	3.143	0.279
GRID C	236	1.526	-	0.552	0.304	0.199	0.109	3.028	0.377
GRID D	176	1.082	-	0.748	0.559	0.517	-0.105	2.663	0.051
FACIES #1	91	0.364	-	0.751	0.564	1.55	-2.0	1.665	-1.255
FACIES #2	29	0.896	-	0.499	0.249	0.278	0.02	1.723	0.074
FACIES #3	617	1.46	-	0.629	0.396	0.271	0.084	3.143	0.245
FACIES #4	32	1.04	-	0.755	0.571	0.549	-0.824	2.583	-0.431

for the least significant difference (LSD) given the proven significance of the F-test, as proscribed by Fisher (1935) and referenced by Snedecor (1980). This type of the ANOVA test is commonly referred to as the protected least significant difference method (PLSD). Since the lognormality of sample data was of interest, the comparisons were conducted on the permeability data in the log-transform state.

Results from the ANOVA test (Table 2) substantiate the continued analysis of the sample GRIDs with nearly a 5% level of confidence. The F-test results are found to be significant for comparisons between samples and within samples. Comparisons of the samples are found to be significant to the 5% level for all sample GRIDs except for that between GRIDs B and D. These sample grids are found to have a difference between means which is less than the $t_{0.05}$ value for four samples at 173 degrees of freedom. This result indicates that there is greater than a 5% probability of error in the assumption that sample GRIDs B and D shared the same population mean. Continued analysis of the sample GRIDs is not precluded by this result, however, the following power-law variogram results are strengthened by the exclusion of both the B and D sample GRIDs.

5.5 POWER-LAW VARIOGRAMS

The power-law variograms were created from the combined horizontal variograms of all four sample data sets plotted on a log-transformed axis of average distance. Originally, the scales of each sampled grid were established, in part, to represent the pattern of permeability distribution for different orders of magnitude. The GRID A sample data represented the permeability distribution in hundreds of

TABLE 2
ONE FACTOR ANOVA COMPARISONS

(Calculations and table configuration modified from Statview 512+ v1.0, 1986)

ANOVA TABLE

Source:	df:	Sum of Squares:	Mean Square (s^2):	F-test:	P
Between Subjects	173	224.192	1.296	6.846	0.0001
Within subjects	522	98.817	0.189		
treatments	3	74.984	24.995	544.289	0.0001
residual	519	23.833	0.046		
Total	695	323.009			

Note: first 174 measurements from sorted (ascending) sample GRID data incorporated in comparisons.

Pooled Mean Squares (s_w^2) = $\dfrac{\Sigma x^2}{df_w}$

Standard Error of the Difference Between Two Means ($s_{\bar{D}}$) = $\left(\sqrt{\dfrac{2s_w^2}{n}}\right)$

STATISTICS OF SELECTED SAMPLE GRID DATA

Selected Sample:	Count:	Mean:	Standard Deviation:	Standard Error:
GRID A	174	0.492	0.581	0.044
GRID B	174	1.072	0.509	0.039
GRID C	174	1.404	0.548	0.042
GRID D	174	1.064	0.733	0.056

Standard Error = $\left(\sqrt{\dfrac{2s^2}{n}}\right)$

COMPARISON OF SAMPLE GRID DATA

Comparison:	Mean Difference:	Protected Least Significant Difference:	Scheffe F-test:
GRID A vs. GRID B	- 0.581	0.045*	212.916*
GRID A vs. GRID C	- 0.913	0.045*	525.902*
GRID A vs. GRID D	- 0.573	0.045*	207.333*
GRID B vs. GRID C	- 0.332	0.045*	69.571*
GRID B vs. GRID D	7.663E-3	0.045	0.037
GRID C vs. GRID D	0.34	0.045*	72.82*

* Significant at the 5% level of confidence.

Protected Least Significant Difference = ($s_{\bar{D}}$) * ($t_{0.05}$), for total n = 696 and total df = 695.

Sheffe's F-test: the comparison L (= λ_1\o(x, ‾)$_1$ + λ_2\o(x, ‾)$_2$ + ... + λ_n\o(x, ‾)$_n$) is significant at the 5% level if $|L| / s_L > \sqrt{(a - 1)F_{0.05}}$, where: a is the number of samples and s_L is the mean squares of the samples which are being compared.

feet, the GRID B sample data represented the distribution in tens of feet, GRID C data represented distribution in individual feet, and the GRID D data represented distribution in inches (approximately tenths of feet). Combinations of experimental horizontal variograms were made for step increments representing each scale of sample data and analyzed for possible correlation.

The four horizontal variograms presented above were posted on log-axes and the powerlog parameters were estimated using fitted lines through the data. Calculations of the slope, y-intercept and the coefficient of correlation for the fitted line were compared for various configurations of the $\gamma(h)$ values. Comparisons of the parameters for selected data sets were intended to find the most statistically significant results which could be applied to the powerlog equation (Eqn. 13) and provide a value for the fractal codimension (H). The combined $\gamma(h)$ values of all four sample grids (Fig. 46) were determined to represent an uncorrelated scatter by fitted lines calculated for the data. The slope of the best fit line was low (0.067) and a low coefficient of correlation ($R^2 = 0.228$) confirmed the unacceptability of the statistical relationship for these $\gamma(h)$ values.

Removal of selected semivariance data resulted in increasingly better fit lines and steeper positive slopes. The $\gamma(h)$ values based on less than 30 data pairs from the data were removed and the remaining data (Fig. 47) produced a fitted line with a slightly higher coefficient of correlation (0.288) and a similar slope (0.068). For the data collected at separation intervals 1 foot and greater (i.e., GRIDs A, B and C; Fig. 48), the fitted lines were better correlated ($R^2 = 0.617$) and were defined by a higher positive slope ($m = 0.143$). Similarly, the removal of another variogram set stated above as poorly matching the spherical model (i.e., the GRID B sample data)

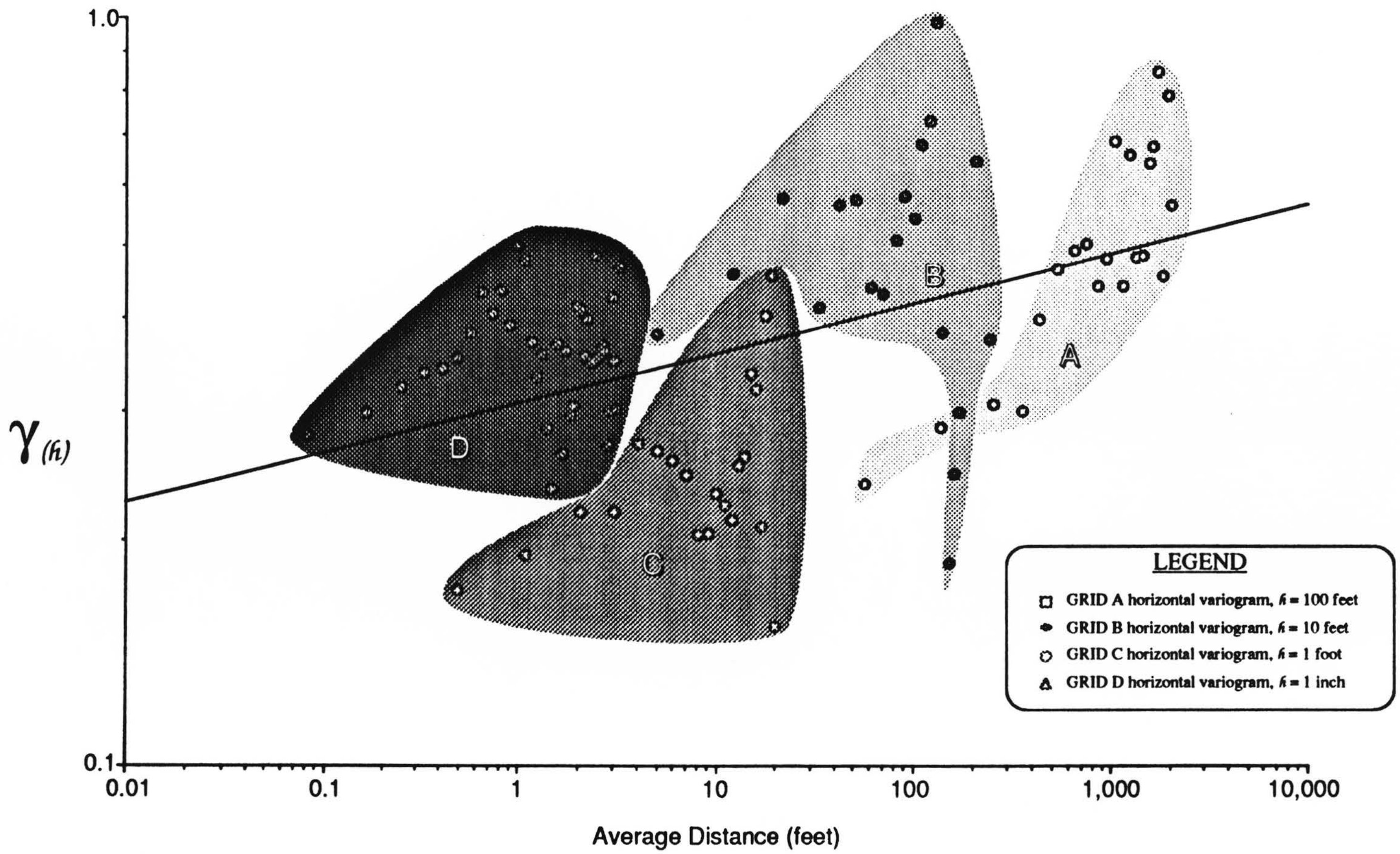

Figure 46. Variogram postings from GRIDs A, B, C, and D sample data calculations for semivariance [γ(h)], plotted on log-axes. Best fit line through variogram data: y = -0.515 + 6.65e-2x (R^2 = 0.228).

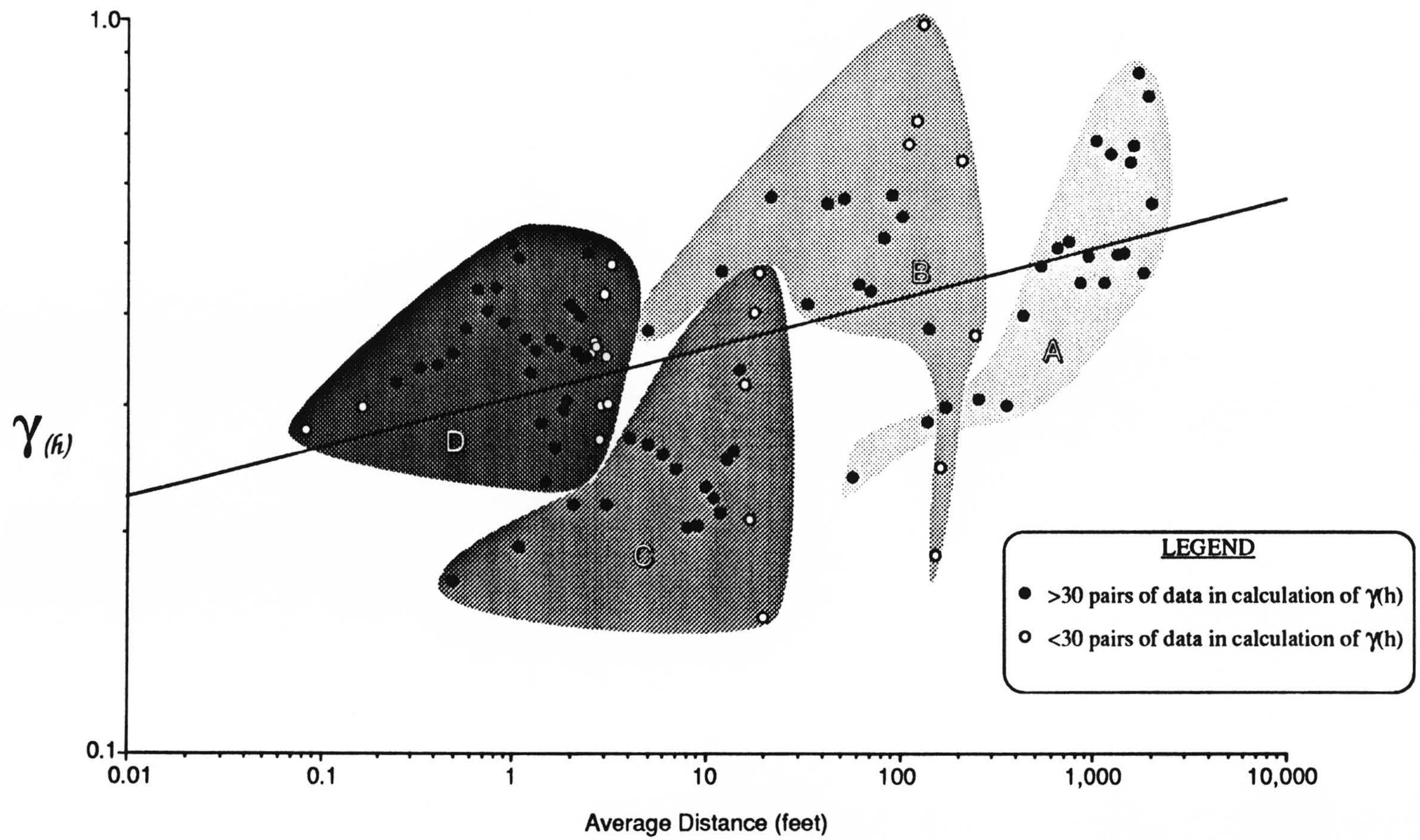

Figure 47. Variogram postings from GRIDs A, B, C, and D sample data indicating the significant calculations for semivariance [γ(h)], plotted on log-axes. Best fit line through variogram data: y = -0.516 + 6.76e-2x (R^2 = 0.288).

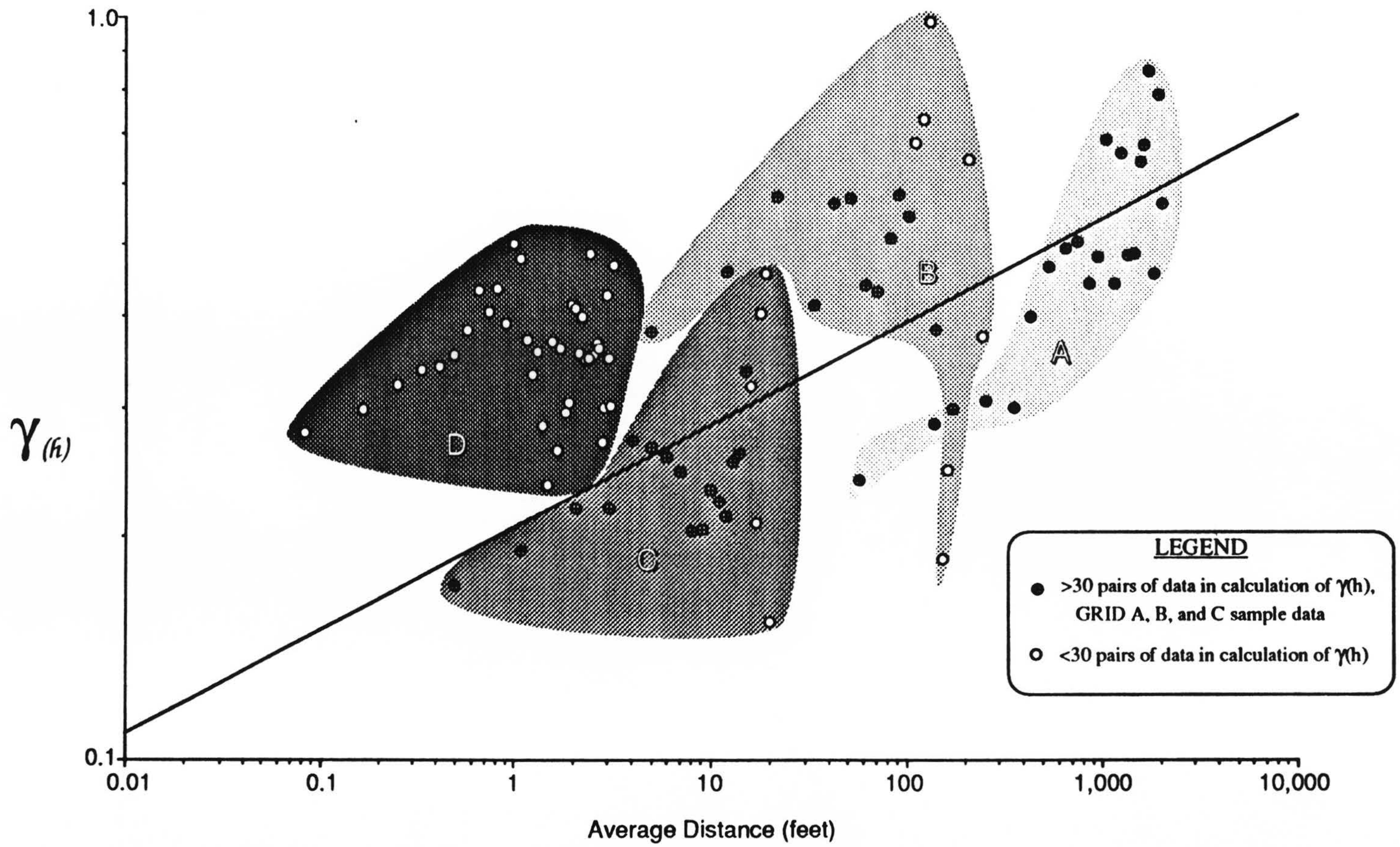

Figure 48. Variogram postings of the significant semivariance [γ(h)] calcualtions (γ(h); $n \geq 30$ data pairs) from GRIDs A, B, and C samples and plotted on log-axes. Best fit line through variogram data: $y = -0.688 + 0.138x$ ($R^2 = 0.602$).

produced powerlog variograms (Fig. 49) with a steeper slope (m = 0.155) and highest R^2 value (0.824).

Parameters of the powerlog variogram which displayed the most statistical confidence were analyzed for the fit the powerlaw theoretical model. The slope of superimposed experimental variograms on log-transformed axes described the fractal codimension (2H) in Eqn. 14 [$\log(\gamma(h)) = \log(\gamma_0) + 2H(\log(h))$]. The fitted line through the log-transforms of the horizontal variograms for GRIDs A and C, with $\gamma(h)$ values based on greater than 30 data pairs ($R^2 = 0.824$), provided a slope of 0.155 which corresponds to the fractal codimension (2H) parameter of Eqn. 14. This value transforms to a (horizontal) fractal codimension (H) of 0.0775, which falls an order of magnitude below the stated range of 0.7 - 0.9 for typical fractal codimension values of natural phenomena, as suggested by both Hewett and Berhens (1990) and Mandelbrot (1983).

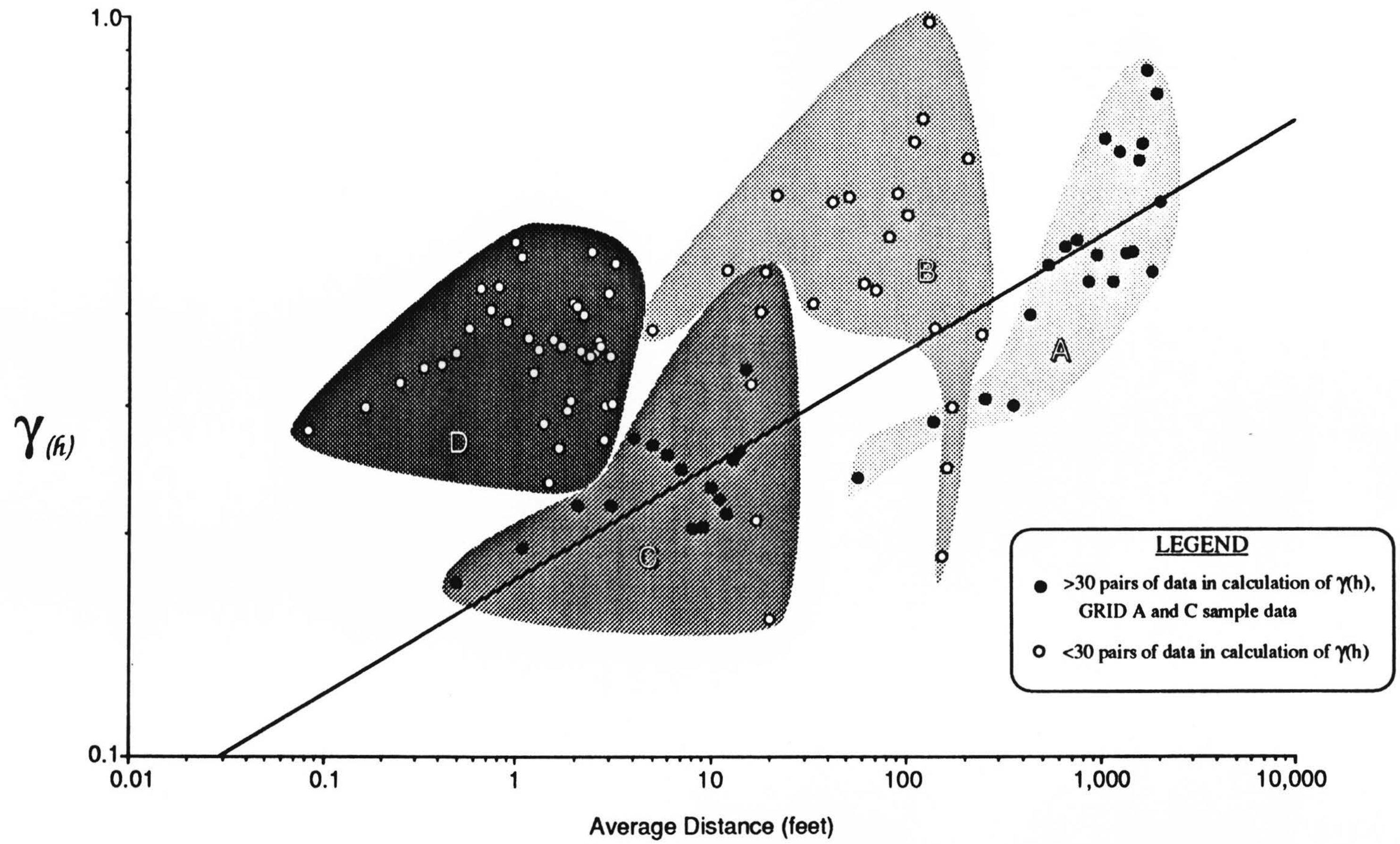

Figure 49. Variogram postings of the significant semivariance [γ(h)] calcualtions (γ(h); $n \geq 30$ data pairs) from only GRIDs A and C samples and plotted on log-axes. Best fit line through variogram data: $y = -0.761 + 0.155x$ ($R^2 = 0.824$).

CHAPTER 6
DISCUSSION AND CONCLUSIONS

Permeability data collected from the outcrop of the first parasequence in the upper San Andres formation's first third-order sequence (uSA1), at Lawyer Canyon on the Algerita Escarpment in the Guadalupe Mountains of New Mexico, were analyzed for identifiable patterns of distribution. The purpose for this type of study was to statistically characterize permeability patterns as an aid in understanding the expectations of permeability occurrences in analogous subsurface environments. The parameters of statistical characterizations covered in these analyses were those of the spatial covariance based on the value and the relative location of permeability measurements. Spatial covariance relationships were analyzed from variograms and determined to exhibit scale-dependent attributes. As a test for the existence of fractal sets in the data, the variograms were analyzed for adherence to power-law theory.

6.1 DISCUSSION

6.1.1 TWO-DIMENSIONAL VISUALIZATION OF THE SAMPLE DATA

The sample populations of scale-based permeability data (GRIDs A, B, C, and D) were initially analyzed as the posting and contouring of the data in sample populations. Contouring of the data was intended to show whether the permeability values exhibited continuity between data points at the separation distances of the transects in the grid. The contoured postings exhibited a tortuous pattern of localized high permeabilities in a background of low average permeabilities.

Horizontal heterogeneities were observed at each scale of the grids, and vertical heterogeneities were observed at the one foot scale in all transects and grid patterns. In the vertical transects (GRIDs A and B) and the regular spaced pattern of GRID C, vertical and horizontal variation of values was noted to range across two orders of magnitude between measurements taken one foot apart. At the inch scale of GRID D, the vertical and horizontal variations of values was also noted to range over two orders of magnitude. These variations were similar to those noted in the previous studies of Kittridge (1988) and Hinrichs and others (1986).

At the largest scale, GRID A (see Plate #1) was divided horizontally into two regions, one of low permeabilities (<10 md) which was overlain by a region of higher permeabilities (10 - 100 md). This pattern coincided with the area of facies #1 (mud-dominated fabric) which underlaid the other three identified facies (mud-supported grain to grain-dominated fabrics). Since the model for a shallowing-upward depositional parasequence predicted a bed of mud-dominated fabric at the base of each cycle, the assumption of low flow boundaries controlling fluid movement was validated in the observed contouring of the sample data.

Some horizontally and vertically continuous high permeability (>100 md) streaks were noted in the larger scaled (GRIDs A and B) contour postings. In GRID A, two high permeability zones were observed between transects A18-A20. The pattern of GRID B data was more akin to irregular tongues of high permeabilities which extended both horizontally and vertically. These large scale continuities (376 to 35 feet horizontally, and 5 feet vertically) were based on few data points and were disrupted irregularly.

The contour patterns of GRIDs B, C, and D indicated that continuity at the large scale was not carried through to the smaller scales. The location of the smaller-scale sample populations inside the area of the larger-scale sample populations provided the opportunity for visual comparisons of permeability pattern continuities. The primary target for these comparisons were the zones of high permeability first identified in the sampling of the parasequence, in particular at the center of the study area. This was observed between the sample populations as the horizontal scale of sampling decreased, the zones of high permeability that were identified at the larger scales were disrupted in the contoured patterns of data for the smaller-scale patterns.

6.1.2 Lognormal Distributions in the Sample Data

The statistical theory of the regionalized variable requires that the natural phenomenon exhibit a Gaussian distribution (normal or lognormal). In view of the heterogeneity observed in the contour patterns, this step of data analysis was a most serious consideration. To prove normality in the populations, the sample populations of permeability data were analyzed through statistical and graphical methods. Analyzed in the above results were the relationships for normal and log-transformed values of mean-to-standard deviation comparisons, coefficients of variation (mean divided by variance), and coefficients of skewness. Also, graphical presentations were constructed to view the distribution of each sample population. The sample data statistics and observed distributions were compared to the theoretical expectations for Gaussian distributions. From this analysis, the permeability data collected for this study were found to be lognormally or nearly lognormally distributed for each of the sample populations.

The description of GRID A permeability data indicated some deviation from lognormality for the low-end of the permeability range (<10 md). This was seen in the frequency histogram and probability plot graphics and in the statistics of the sample data. The data in that range was comprised of mostly core plug measurements, stated above as measurements representative of a larger sample of the rock matrix than that of the MFP device and providing data for permeabilities as low as 0.01 md. The MFP's detection limit was stated as <1 md (Goggin, 1988), but the nature of the rock which exhibited low permeabilities (i.e., mud-dominated) was heavily fractured and rarely provided a smooth and expansive prepared surface for accurate MFP-sampling. Therefore, a sampling bias was determined as the cause for the data distribution abnormalities which were observed in the low range of permeability data.

The sampling bias was the result of the inclusion of core plug permeability measurements with the MFP data. The core plugs were collected preferentially within the parasequence where low permeabilities (<10 md) were anticipated. Sampling bias resulted since the core plug data were fewer numerically than the MFP data, yet these values were concentrated in the low end of the total range of permeabilities. The deviation noted in the probability plot was, therefore, the rise in relative cumulative percentages represented by core plug permeabilities in the range where the population of MFP permeabilities were underrepresented due to the detection limit of the apparatus.

Since the facies #1 and #4 sample data were the only other sample population which included core plug measurements, the presence of similar deviations from lognormality follows the above discussion for GRID A. Again, the distributions of the sample data deviated in the range of core plug permeabilities. This deviation reflected the bias of collecting core plugs preferentially in the areas where low permeability values were anticipated, and these areas were predominantly those of the mud-dominated facies #1 and #4.

The deviation from lognormality observed in the probability plot for facies #4 data was less pronounced than that for facies #1 or for GRID A. This due in part to the fact that core plug permeabilities comprised 8 of the 9 transects of that sample data, and in part to the relatively few data points from which the sample population was derived. Both facies #1 and GRID A sample data included significantly less core-plug than MFP data, so that the numerical superiority of the MFP data over the core plug data effectively smoothed-out any potential deviation from a lognormal distribution.

6.1.3 VARIOGRAM PARAMETERS AND SCALE DEPENDENCY

Confirmation of lognormal distributions in the sample data sets validated the further statistical analyses of permeability as a regionalized variable. These further analyses included the estimation of variogram parameters from the semivariance calculations. The variogram parameters of sill, range, and nugget are the results needed to "Krige" permeability values between known permeability values for characterization models of analogous reservoirs. The determination that both the permeability sample data were representative of a regionalized variable, and were describable as a Gaussian distribution, were crucial to the theory of the variogram.

The semivariance calculations for the GRIDs A, B, C, and D indicated the best development of nugget effected spherical variogram models for the lag increments of 100, 10, 1 feet, and 1 inch, respectively. These values of lag increments represented the orders of magnitude which were of interest to the study, the characterization of permeability patterns and distributions for intra-well distances (<2,000 feet).

The parameters interpreted from the experimental variograms were presented above for each sample GRID and facies sample data set. Each experimental variogram was interpreted for sill, range, and nugget values based on a spherical variogram model. These parameters (Table 3) were compared for each scale of the lag interval (h) used in the calculation of semivariance ($\gamma(h)$). The sill and range values represented the characteristic variance in which permeability values could be expected.

These variogram parameters provided insight to the existence of a scale-dependent relationship between permeability and distance. At each of the sampling scales represented by the GRID data, sill and ranges were interpreted from nugget-effected spherical variograms which possessed moderately well developed initial slopes based on 3 to 8 semivariance values. The initial semivariance, or nugget values, for these variograms were also closely related, varying by only 0.1 for GRIDs A, C, and D, and by 0.2 for GRID B. These similarities and the scale-dependency for the values of the variogram parameters indicated the possible

TABLE 3

VARIOGRAM RESULTS FOR GRID SAMPLES

Sample	Horizontal ($\theta = 0°$)	Vertical ($\theta = 90°$)
GRID A		
nugget ($C_{(0)}$)	0.2	0.16
range ($r_{(1)}$)	253.5 feet	13.0 feet
sill ($C_{(1)}$)	0.305	0.95
range ($r_{(2)}$)	748.3 feet	N.A.
sill ($C_{(2)}$)	0.497	N.A.
GRID B		
nugget ($C_{(0)}$)	0.32	0.2
range ($r_{(1)}$)	22.2 feet	4.0 feet
sill ($C_{(1)}$)	0.57	0.44
range ($r_{(2)}$)	N.A.	10.2 feet
sill ($C_{(2)}$)	N.A.	0.71
GRID C		
nugget ($C_{(0)}$)	0.16	0.165
range ($r_{(1)}$)	2.1 feet	2.1 feet
sill ($C_{(1)}$)	0.22	0.34
GRID D		
nugget ($C_{(0)}$)	0.26	0.35
range ($r_{(1)}$)	9.0 inches	2.0 inches
sill ($C_{(1)}$)	0.42	0.57

existence of fractal relationships for permeability based on the separation distance between known values.

Application of the power-law theory to estimate the fractal codimension was introduced to extend the usefulness of information gained in the experimental variograms. Results from variograms representing different horizontal separation distances indicated that variogram parameters were interpretable for scales from one foot to one hundred feet. In particular, the sample GRIDs A and C were compared on logarithmic axes and were found to be described by a best fit line with a slope of 0.15454x. This was applied to the power-law equation (13) as the value for 2H, resulting in a fractal codimension (H = 0.07727) an order of magnitude lower than the range proposed by Hewett and Berhens (1990) for natural phenomena.

6.2 CONCLUSIONS

Based upon the statistical analyses of the variograms and power-law variograms this investigation has determined certain aspects of the permeability distribution and anisotropy for a single shallowing upward carbonate parasequence.

1) The pattern of permeability observed on the outcrop was characterizable as vertically and horizontally heterogeneous high (>100 md) and low (<10 md) zones distributed within a matrix of average (moderately low, <100 md) permeability values.

2) The observed heterogeneity of the permeability patterns were found to exist at all linear scales covered in this study, from inches to hundreds of feet.
3) The analysis of horizontal and vertical search direction variograms supported the visual observations of the existence of continuous heterogeneity across the range of scales.
4) The distribution of permeability within genetically defined depositional facies was found to reflect the range and mean permeabilities based on the fabric textures of the facies.
5) The application of power-law theory to the variogram data based on linear scale samples produced a result for the fractal codimension which was an order of magnitude below the range proposed by other researchers (Mandelbrot, 1983, and Hewett and Berhens, 1990) for natural phenomena.

6.3 RECOMMENDATIONS

From these conclusions, the recommendations for further study are a based upon the success of this study and an urge to promote interest in the determination of the fundamental controls on permeability. This study shows that it is reasonable to accept the conclusions of anisotropy and the scale dependence of the permeability distributions, at least, for this particular shallowing-upward parasequence in the upper San Andres formation outcrop of the Guadalupe Mountains. These conclusions should be tested in other parasequences of this outcrop. This will provide both additional evidence of the distributional characteristics in shallowing-upward parasequences and a comparison of the effects of the different depositional histories for the other parasequences.

For other investigations into the distribution of permeabilities on outcrop, it is suggested that the sampling pattern follow the guidelines adhered to in the start of this study. Most importantly, the sampling pattern should be specifically targeted to a well defined geologic interval (i.e., one which is as homogeneous in depositional environment as possible). Sampling should be equally spaced both horizontally and vertically for all scales of the investigation to reduce variogram range bias which may have contributed to the development of the nested variogram sets in the GRID A data.

The heightened degree of heterogeneity at the small (inch spaced) scale of investigation in this study is an indication that more information is required for determination of the controls of permeabilities at dimensions of less than a square foot. Heterogeneities within the generally high permeable bar crest facies indicate that values do vary widely within the space of an inch, creating low permeability baffles and high permeability conduits. Small scale continuity and prevalence of the occurrence within a formation can be most significant in determining the capacity of a reservoir to retain trapped fluids.

Small scale heterogeneities are the most difficult area of study for the characterization of permeability. The problem is one of diminishing returns on the quantity of work needed to collect the measurements. Preparation and measurement of the permeability data are equally time consuming for large and small scaled sample sets. The small scale investigation is tied to a very localized site of specific geologic conditions, while the large scale investigation produces analyses which may be applied to a more general condition or sets of conditions. Also, the small scale investigation is perhaps most influenced by the "noise" of anisotropy in all three (3) dimensions than a broad profile of large scaled data.

In closing, the suggestions for further study are summed as the following.

1) Apply similar sampling and analyses of this study to other parasequences of shallowing-upward carbonate deposition.
2) Retain a rigorous adherence to equal spacing between sample points at all scales of the investigation, while the scale of the investigation is controlled by outcrop and geologic changes in texture and structure.
3) Investigate the small scale patterns of permeability more completely for all rock fabrics in the study site, especially for three-dimensional anisotropy effects on permeability distributions.

REFERENCES

Amhed, S. and de Marsily, G., 1987, Comparison of geostatistical methods for estimating transmissivity using data on transmissivity and specific capacity: Water Resources Research, v. 23, no. 9 (Sept.), p. 171-1737.

Bear, J., 1972, Dynamics of fluids in porous media: Dover Publications, Inc., New York, 764 p. Reprint, 1988: originally published: New York: American Elsevier Pub. Co., 1972.

Beard, D. C. and Weyl, P. K., 1973, Influence of texture on porosity and permeability of unconsolidated sand: Am. Assoc. of Petrol. Geol. Bulletin, v. 57 , p. 349-369.

Bodner, D. P., 1985, Heat variation caused by groundwater flow in growth faults of the south Texas Gulf Coast basin: University of Texas at Austin, Masters thesis, December, 188 p., 1 plate.

Boyd, D. W., 1958, Permian Sedimentary Facies, Central Guadalupe Mountains, New Mexico: Bulletin 49, State Bureau of Mines and Mineral Resources, New Mexico Institute of Mining and Technology, Socorro, New Mexico, 100 p., 2 plates.

Brown, S. R., 1987, A note on the description of surface roughness using fractal dimension: Geophysical Research Letters, v. 14, no. 11, p. 1095-1098.

Chandler, M. A., 1986, Depositional Controls on Permeability in an Eolian Sandstone Sequence, Page Sandstone, Northern Arizona: The University of Texas at Austin, M.A. thesis (December),131 p.

Chandler, M. A., Goggin, D. J. and Lake, L. W. 1989b, Field measurement of permeability using a minipermeameter: Journ. of Sed. Petrology, Research Methods.

Chandler, M. A., Kocurek, G., Goggin, D.J. and Lake, L.W., 1989a, Effects of stratigraphic heterogeneity on permeability in eolian sandstone sequence, Page Sandstone, northern Arizona: Amer. Assoc. of Petrol. Geol. Bulletin, v. 73 , no. 5 (May), p. 658-668.

Choquette, P. W. and Pray, L. C., 1970, Geologic nomenclature and classification of porosity in sedimentary carbonates: Am. Assoc. of Petroleum Geologists Bulletin, v.54, no. 2 (February), p. 207-250.

Dagan, G. 1985, Stochastic modeling of groundwater flow by unconditional and conditional probabilities: The inverse problem: Water Resources Research, v. 21, no. 1 (January), p. 65-72.

Dagan, G., 1986, Statistical theory of groundwater flow and transport: pore to laboratory, laboratory to formation, and formation to regional scale: Water Resources Research, v. 22, no. 9 (August), p. 120S-134S.

Dake, L. P., 1978, Fundamentals of Reservoir Engineering: (Developments in Petroleum Science, 8): Elsevier Science Publishing Co. Inc., Amsterdam., 432 p.

David, M., 1977, Geostatistical Ore Reserve Estimation: Elsevier Scientific Publishing Co., New York.

Davis, J. C., 1986, Statistical and Data Analysis in Geology: John Wiley and Sons, New York, 2nd ed., 646 p.

Delhomme, J. P., 1978, Kriging in the hydrosciences: Advances in Water Resources, v. 1 no. 5, p. 251-266.

Delhomme, J. P., 1979, Spatial variability and uncertainty in groundwater flow parameters: A geostatistical approach: Water Resources Research, v. 15 no. 2 (April), p. 269-180.

Dykstra, H., and Parsons, R. L., 1950, The prediction of oil recovery by water flood: *in* Secondary recovery in the USA, 2nd ed.; Am. Petroleum Inst., p. 160-174.

Eijpe, R. and Weber, K. J., 1971, Mini-permeameters for consolidated rock and unconsolidated sand: Am. Assoc. Petroleum Geologists Bulletin, v. 55, no. 2, p. 307-309.

Feinerman, E., Dagan, G. and Bresler, E., 1986, Statistical inference of spatial random functions: Water Resources Research, v. 22, no. 6 (June), p. 935-942.

Fogg, G. E., 1986, Stochastic Analysis of Aquifer Interconnections, with a Test Case in the Wilcox Group, East Texas: Ph.D. dissertation, Univ. of Texas at Austin, Texas.

Fu, L., Milliken, K. L., and Sharp, J. M., Jr., 1992, Permeability variations in liesegang-banded Breathitt Sandstone (Pennsylvanian) - diagenetic controls: Geol. Soc. America Abs. with Programs (Ann. Mtg.), v. 24, p. 254.

Fuller, Carla Mathern, 1990, Fracture and permeability analysis of the Santana Tuff, Trans-Pecos Texas: M.A. Thesis, Dept. of Geological Sciences, Univ. of Texas at Austin.

Fuller, C. M. and Sharp, J. M., 1992, Permeability and fracture patterns in extrusive volcanic rocks: Implications from the welded Santana Tuff, Trans-Pecos Texas: Geological Society of America Bulletin, v. 104 (November), p. 1485-1496.

Gelhar, L. W., 1986, Stochastic subsurface hydrology from theory to applications: Water Resources Research, v. 22, no. 9 (August), p. 135S-145S.

Goggin, D. J., 1988, Geologically-sensible modeling of the spatial distribution of permeability in eolian deposits: Page Sandstone (Jurassic), northern Arizona: Ph.D. dissertation, University of Texas at Austin, Texas, 417 p.

Goggin, D. J., Chandler, M. A., Kocurek, G.A. and Lake, L.W., 1988(a), Patterns of permeability in eolian deposits: Page Sandstone (Jurassic), northern Arizona: SPE Formation Evaluation (June), p. 297-306.

Goggin, D. J., Thrasher, R. and Lake, L. W., 1988(b), A theoretical and experimental analysis of mini-permeameter response Including Gas-Slippage and High-Velocity Flow Effects: In-Situ, v. 12, nos. 1&2, p. 79-116.

Hewett, T. A. and Behrens, R. A., 1990, Conditional Simulation of Reservoir Heterogeneity With Fractals: SPE Formation Evaluation (September), p. 217-225.

Hild, G. P., 1986, The Relationship of San Andres Facies to the Distribution of Porosity and Permeability - Garza Field, Garza County, Texas: Permian Basin/Soc. Econ. Paleon. and Mineralogists, Publication 86-26, p. 17-20.

James, Noel P., 1979, Shallowing upward sequences in carbonates: *in* Facies Models, ed. Roger G. Walker, Geological Assoc. of Canada, p.

Journel, A. G. and Huijbregts, C., 1978, Mining Geostatistics: Academic Press, London.

Kerans, C., Lucia, F. J., Senger, R. K., Fogg, G. E., Nance, H. S., Kasap, E., and Hovorka, S. D., 1991, Characterization of reservoir heterogeneity in carbonate-ramp systems, San Andres/Grayburg, Permian Basin: Reservoir Characterization Research Laboratory, Final Report, Bureau of Economic Geology, University of Texas at Austin, Texas, 245 p., 2 plates.

King, P., 1942, Permian of west Texas and southeastern New Mexico: A.A.P.G. Publication, p 229.

Kittridge, M. G., 1988, Analysis of Aerial Permeability Variations, San Andres Formation (Guadalupian): Algerita Escarpment, Otero County, New Mexico: M.S. Thesis, Dept. of Petroleum Engineering, U. of Texas at Austin, 361 p.

Kittridge, M. G., Lake, L. W., Lucia, F. J., and Fogg, G. E., 1990, Outcrop/Subsurface Comparisons of Heterogeneity in the San Andres Formation: SPE Formation Evaluation (September), p. 233-240.

Mandelbrot, B. B., 1983, The Fractal Geometry of Nature: W.H. Freeman & Co., New York City

Matheron, G. and de Marsily, G., 1980, Is transport in porous media always diffusive? A Counterexample: Water Resources Research, v. 16, no. 5 (October), p. 901-917.

Matheron, G., 1963, Principles of Geostatistics: Economic Geology, v. 58, p. 1246-1266.

Meinzer, O. E., 1942, Hydrology: Physics of the Earth - IX, Dover Publications, Inc., New York.

Press, Wm. H., Flannery, B. P., Teukolsky, S. A., and Vetterling, Wm. T., 1986, Numerical Recipes: the art of scientific computing: Cambridge University Press, Cambridge.

Radian Corporation, 1989, CPS-1 user's guide.

Sarg, J. F. and Lehmann, P. J., 1986, Facies and Stratigraphy of Lower-Upper San Andres Shelf Crest and Outer Shelf and Lower Grayburg Inner Shelf: *Proc.*, San Andres/Grayburg Formations, Guadalupe Mountains, New Mexico and Texas: Soc. Economic Paleontologists and Mineralogists, Permian Basin Section Pub. No. 86-25, p. 9-36.

Scheidegger,, 1974, The Physics of Flow Through Porous Media: Univ of Toronto Press, 3rd edition, 353 p.

Sharp, J. M., Jr., Fuller, C. M., and Smyth, R., 1993, Permeability-porosity variations and fracture patterns in tuffs: in Hydrogeology of Hard Rocks, Proceedings of the 24th Congress, International Association of Hydrologists, Oslo, June 1993, in press.

Snedecor, G.W. and Cochran, W.G., 1980, Statistical Methods, The Iowa State University Press, Ames, Iowa, 7th edition, 507 p.

Sudicky, E. A., Gillham, R. W. and Frind, E. O., 1985, Experimental investigation of solute transport in stratified porous media 1. The nonreactive case: Water Resources Research, v. 21, no. 7 (July), p. 1035-1041.

Sudicky, E.A., 1986, A natural gradient experiment on solute transport in a sand aquifer: spatial variability of the hydraulic conductivity and its role in the dispersion process: Water Resources Research, v. 22, no. 13 (December), p. 2069-2083.

Van Wagoner, J.C., Posamentier, H.W., Mitchum, R.M., Vail, P.R., Sarg, J.F., Loutit, T.S., and Hardenbol, J., 1988, An overview of the fundamentals of sequence stratigraphy and key definitions: *in* Sea-Level Changes - An Integrated Approach, SEPM Special Publication, No. 42, pp. 40-45.

Weber, K. J., 1982, Influence of common sedimentary structures on fluid flow in reservoir models: Journal of Petroleum Technology, v. 34, no. 3 (March), p. 665-672.

Weber, K. J., 1986, How Heterogeneity Affects Oil Recovery: *in* Reservoir Characterization; Lake, L. W. and Carroll, H. B., Jr. (eds.): April 29 - May 1, 1985, Dallas, Texas, U.S. Acad. Press, Orlando, FL., p.487-544.

APPENDICES

APPENDIX A

MFP MEASURED PERMEABILITY DATA

GRID A DATA

Coordinates (feet) X	Y	Tube number	Percent of flow	Pressure (psi)	Permeability (md)
20	18	5	10	12.5	20.39082
20	18	5	12	12.5	26.00821
20	18	5	11	12.5	23.18361
20	19	4	11	12.45	48.20317
20	19	5	40	12.3	85.75803
20	19	5	12	12.5	26.00821
20	19	5	17	12.5	40.61234
20	20	4	11	12.5	48.05441
20	20	5	75	12.3	141.92081
20	20	5	20	12.5	49.63115
20	20	5	17	12.5	40.61234
20	21	4	1	13	3.16213
20	21	5	15	12.4	34.90329
20	21	7	65	12.2	11.88119
20	21	7	22	12.7	2.42937
20	22	4	0	13.3	0
20	22	7	70	12.6	12.1958
20	22	7	80	12.3	14.83543
20	22	7	85	12.3	15.67978
20	22	7	70	12.6	12.1958
25	4	4	0	13.35	0
25	4	7	0	12.8	0
25	5	4	1	13.05	3.15259
25	5	4	26	12.1	138.56409
25	5	7	64	12.6	11.46423
25	5	5	16	12.5	37.63218
25	5	5	17	12.5	40.61234
25	6	4	1	13	3.16213
25	6	7	50	12.6	8.38048
25	6	7	24	12.7	2.71002
25	7	4	1	13.1	3.14311
25	7	7	16	12.8	1.61614
25	7	5	65	12.3	125.04013
25	7	7	16	12.8	1.61614
25	8	4	10	12.85	41.41633
25	8	4	1	12.7	3.22091
25	8	5	9	12.6	18.05258
25	8	5	50	12.4	99.20332
25	9	4	10	13	41.06246
25	9	5	60	12.3	117.37685
25	9	5	35	12.4	77.45811
25	9	5	85	12.4	157.53995
25	9	5	20	12.4	49.97361
25	10	4	28	12.1	149.79184
25	10	5	11	12.6	23.04125
25	10	5	35	12.4	77.45811
25	10	5	16	12.6	37.38681
25	10	5	16	12.5	37.63218
25	11	4	32	12.1	173.53099
25	11	5	9	12.6	18.05258
25	11	5	25	12.4	59.83427
25	11	5	16	12.5	37.63218
25	11	5	17	12.4	40.88382
25	12	4	14	12.5	65.62891
25	12	5	12	12.6	25.84533
25	12	5	10	12.4	20.51441
25	12	5	12	12.5	26.00821
25	12	5	25	12.6	59.01941
25	12	5	10	12.4	20.51441
25	12	5	14	12.4	31.95506
25	13	4	52	12	273.16299

Coordinates (feet) X	Y	Tube number	Percent of flow	Pressure (psi)	Permeability (md)
25	13	4	17	13	80.96838
25	13	5	30	12.4	69.88026
25	13	5	95	12.2	182.39359
25	13	5	60	12.4	116.55519
25	13	5	60	12.4	116.55519
25	14	7	26	12.7	2.99331
25	14	4	45	12.3	216.26797
25	14	4	40	12.3	198.42722
25	14	4	14	12.4	59.89384
25	14	4	10	12.4	38.60483
25	14	4	12	12.3	49.49736
25	15	7	20	12.5	2.18698
25	15	7	12	12.8	1.11387
25	15	7	34	12.7	4.43144
25	16	4	28	12.1	149.79184
25	16	5	85	12.3	158.61641
25	16	5	30	12.3	70.36008
25	16	5	50	12.4	99.20332
25	16	5	40	12.4	85.19501
25	17	4	0	13	0
25	17	5	35	12.4	77.45811
25	17	5	85	12.3	158.61641
25	17	5	30	12.4	69.88026
25	18	4	1	12.6	3.24111
75	1	4	1	13.3	3.10591
75	1	5	7	12.8	13.52416
75	1	7	0	13.1	0
75	1	7	12	13.1	1.08933
75	1	5	15	12.7	34.23092
75	12	4	10	12.55	42.14788
75	12	5	5	12.8	9.32142
75	12	7	50	12.4	8.47898
75	12	5	6	12.9	11.33893
75	12	5	30	12.6	68.94514
75	12	5	15	12.8	34.01368
75	12	5	25	12.7	58.6216
75	13	4	0	13.2	0
75	13	7	0	13.2	0
75	13	5	6	12.9	11.33893
75	13	5	14	12.8	31.16
75	13	5	9	12.9	17.73627
75	14	4	23	12.1	121.99863
75	14	4	25	12.2	132.04112
75	14	5	14	12.7	31.35711
75	14	5	60	12.5	115.74745
75	14	5	95	12.5	178.43701
75	15	4	0	13	0
75	15	5	16	12.6	37.38681
75	15	5	25	12.4	59.83427
75	15	7	50	13	8.19211
75	15	7	42	13	6.14964
75	16	4	0	13.2	0
75	16	5	6	12.9	11.33893
75	16	7	28	13	3.21279
75	16	7	32	13	3.91961
75	17	4	0	13.3	0
75	17	5	20	12.5	49.63115
75	17	5	30	12.5	69.40867
75	17	5	80	12.5	149.18785
75	18	4	5	12.7	19.42876
75	18	5	12	12.7	25.68499

Coordinates (feet) X	Y	Tube number	Percent of flow	Pressure (psi)	Permeability (md)
75	18	5	15	12.8	34.01368
75	18	5	17	12.6	40.34498
76.5	14	5	30	12.6	68.94514
76.5	14	5	7	12.8	13.52416
76.5	14	5	50	12.6	97.87176
132	5	4	0	13.6	0
132	5	7	0	13.1	0
132	5	7	0	13.1	0
132	6	4	1	13.35	3.09678
132	6	7	45	12.9	6.9501
132	6	5	10	12.4	20.51441
132	6	7	18	13	1.84431
132	6	7	75	12.9	13.12992
132	7	4	1	13.3	3.10591
132	7	5	14	11.9	33.04047
132	7	5	10	12.8	20.03105
132	7	5	4	12.8	7.27828
132	7	7	50	12.5	8.42936
132	7	7	75	12.8	13.20905
132	8	4	1	13.35	3.09678
132	8	4	10	13	41.06246
132	8	5	17	12.6	40.34498
132	8	5	12	12.6	25.84533
132	8	5	30	12.6	68.94514
132	10	4	0	13.4	0
132	10	7	0	13.3	0
132	10	7	32	13	3.91961
132	10	7	10	13.2	0.84638
132	10	7	24	13	2.65149
132	11	4	0	13.2	0
132	11	7	10	13.2	0.84638
132	11	5	70	12.5	131.08252
132	12	4	0	13.55	0
132	12	7	12	13.1	1.08933
132	12	7	24	13.1	2.63259
132	12	7	24	13.1	2.63259
132	13	4	0.5	13.6	1.37635
132	13	4	0.5	13.55	1.38033
132	13	7	70	12.9	11.98163
132	13	5	8	12.2	16.24823
132	13	4	35	12.4	170.65923
132	13	4	30	12.5	142.61304
132	13	4	24	12.5	112.24384
132	13	4	35	12.5	169.4614
132	14	4	0	12.85	0
132	14	5	9	12.2	18.49709
132	14	7	75	12.3	13.62312
132	14	7	65	12.9	11.37599
132	14	7	50	13	8.19211
132	14	7	34	13	4.34639
132	14	7	46	13	7.16433
132	15	4	10	12.7	41.77805
132	15	7	75	12.8	13.20905
132	15	5	10	12.7	20.14918
132	15	5	14	12.7	31.35711
132	16	4	0	13.3	0
132	16	7	12	13.1	1.08933
132	16	7	15	13.1	1.45495
132	16	7	32	13	3.91961
132	17	4	0	13.2	0
132	17	7	32	13	3.91961

Coordinates (feet) X	Y	Tube number	Percent of flow	Pressure (psi)	Permeability (md)
132	17	7	32	13	3.91961
132	17	5	6	12.9	11.33893
132	17	5	6	12.8	11.40575
132	18	4	0	13.3	0
132	18	4	40	12.4	196.94371
132	18	4	35	12.5	169.4614
132	18	5	10	12.8	20.03105
185	5	4	20	12.1	105.4657
185	5	5	11	12.2	23.62414
185	5	5	17	12.1	41.72412
185	6	4	0.5	12.5	1.47126
185	6	7	65	11.8	12.19581
185	6	7	53	12.3	9.32195
185	12	4	0.5	13.05	1.42185
185	12	7	33	12.4	4.29896
185	12	5	15	11.5	37.12889
185	12	6	40	12.3	14.94192
185	12	6	19	12.4	4.23537
185	13	4	5.5	12.4	21.98209
185	13	6	14	12.4	2.62084
185	13	7	22	12.4	2.48681
185	13	7	80	12.2	14.93193
185	13	6	42	11.7	16.62049
185	13	6	42	12.1	16.18019
185	14	4	6.5	12.6	26.10039
185	14	5	20	11.4	53.70881
185	14	5	6	12.3	11.75538
185	14	5	10	12.2	20.76732
240	2	4	0	14	0
240	2	7	17	12.4	1.80132
240	2	7	19	12.5	2.05273
240	8	4	0	14.1	0
240	8	7	21	12.3	2.36467
240	8	7	70	12.2	12.49695
240	9	4	0	13.85	0
240	9	6	17	12.3	3.60786
240	9	6	24	12.2	6.58049
240	10	4	10.5	12.45	45.29262
240	10	6	17	12.3	3.60786
240	10	7	15	12.5	1.52449
240	11	4	0.5	12.95	1.43053
240	11	6	34	12.2	11.74968
240	11	5	25	11.3	64.82305
240	12	4	14	12.2	66.98052
240	12	5	40	12	87.50269
240	12	5	13	12.1	29.62923
240	13	4	8.5	12.35	35.61609
240	13	5	18	12.1	44.81544
240	13	5	18	12.1	44.81544
240	14	4	13.5	12.15	64.17744
240	14	5	18	12.1	44.81544
240	14	5	10	12.2	20.76732
240	15	4	35.5	12.1	195.33777
240	15	5	20	12.1	51.03306
240	15	5	16	12.1	38.65316
240	16	4	0	12.6	0
240	16	5	16	12.1	38.65316
240	16	5	6	12.3	11.75538
240	17	4	0	12.7	0
240	17	5	10	12.2	20.76732
240	17	5	8	12.2	16.24823

Coordinates (feet) X	Y	Tube number	Percent of flow	Pressure (psi)	Permeability (md)	Coordinates (feet) X	Y	Tube number	Percent of flow	Pressure (psi)	Permeability (md)
240	19	4	0.5	12.4	1.48071	350	10	7	12	12.3	1.15752
240	19	5	8	12.2	16.24823	350	10	7	34	12.3	4.55119
240	19	5	6	12.3	11.75538	350	11	4	0	12.9	0
240	20	4	0.5	12.9	1.43492	350	11	7	40	12.2	5.94665
240	20	5	50	12	101.98283	350	11	7	50	12.3	8.52938
240	20	5	13	12.1	29.62923	350	12	4	0	12.4	0
240	21	4	0.5	12.6	1.46197	350	12	6	56	12.1	23.4479
240	21	5	35	12	79.58904	350	12	6	14	12.2	2.66277
240	21	5	45	12	94.72251	350	13	4	20	12	106.21929
240	22	4	6.5	12.5	26.25987	350	13	5	25	12.1	61.10664
240	22	5	9	12.2	18.49709	350	13	5	22	12.1	55.04947
240	22	7	42	11.9	6.59605	350	14	4	31	11.65	172.97401
240	22	5	20	12.2	50.67445	350	14	5	10	12.2	20.76732
295	8	4	1	12.1	3.34694	350	14	5	13	12.2	29.43386
295	8	5	12	12.2	26.51251	350	15	4	32	11.65	179.26221
295	8	5	25	12.1	61.10664	350	15	5	12	12.2	26.51251
295	9	4	0	12.9	0	350	15	5	16	12.2	38.39179
295	9	7	0	12.2	0	350	16	4	0	13	0
295	9	7	14	12.5	1.39497	350	16	5	6	12.3	11.75538
295	9	7	16	12.4	1.66853	350	16	5	7	12.3	13.93721
295	12	4	0	12.8	0	350	17	4	26	11.75	142.2851
295	12	7	30	12.3	3.66556	350	17	5	12	12.2	26.51251
295	12	7	36	12.3	4.9998	350	17	5	52	12.1	104.82548
295	19	4	0	12.95	0	350	18	4	0	12.9	0
295	19	7	18	12.4	1.93505	350	18	7	16	12.3	1.68219
295	19	6	24	12.2	6.58049	350	18	6	30	12.2	9.6011
295	20	4	0	12.6	0	350	19	4	0	12.9	0
295	20	7	12	12.5	1.13962	350	19	6	12	12.4	1.997
295	20	7	22	12.4	2.48681	350	19	5	19	12.1	47.9204
295	21	4	10.5	12.1	46.28325	350	20	4	12	12.05	55.48689
295	21	4	0	12.5	0	350	20	4	14	12.05	67.68066
295	21	7	45	12.3	7.20781	350	20	5	6	12.3	11.75538
295	21	7	32	12.3	4.10632	350	20	5	5	12.3	9.60868
295	22	4	0	12.45	0	350	21	4	1	12.3	3.3036
295	22	7	34	12.3	4.55119	350	21	7	25	12.2	2.95881
295	22	7	34	12.4	4.52053	350	21	7	40	12.2	5.94665
295	23	4	0	12.9	0	400	5	4	0	13.3	0
295	23	6	48	12.2	19.21783	400	5	7	26	12.3	3.08125
295	23	5	20	12.2	50.67445	400	5	7	14	12.3	1.41741
295	24	4	8.5	12.35	35.61609	400	6	4	1	12.1	3.34694
295	24	5	10	12.3	20.6399	400	6	7	38	12.2	5.48856
295	24	5	10	12.3	20.6399	400	6	7	30	12.2	3.69123
295	25	4	0.5	12.6	1.46197	400	7	4	9	12.05	38.65216
295	25	5	18	12.2	44.50697	400	7	7	20	12.2	2.24227
295	25	5	6	12.4	11.6833	400	7	7	12	12.2	1.1667
350	5	4	0	12.7	0	400	8	4	1	12.15	3.33597
350	5	5	6	12.3	11.75538	400	8	7	90	12.1	16.75062
350	5	7	20	12.3	2.22352	400	8	7	16	12.2	1.69608
350	6	4	1	12.8	3.20102	400	13	4	19	12.6	95.55928
350	6	7	12	12.4	1.1485	400	13	4	53	11.7	284.06229
350	6	7	14	12.3	1.41741	400	13	6	40	12.2	15.03679
350	7	4	0	12.7	0	400	13	6	60	12.1	25.48675
350	7	7	16	12.2	1.69608	400	14	4	13	12.05	61.56932
350	7	7	14	12.4	1.4061	400	14	6	18	12.3	3.93538
350	8	4	1	12.65	3.23097	400	14	6	18	12.3	3.93538
350	8	7	50	12.2	8.58055	400	15	4	0	13	0
350	8	7	20	12.3	2.22352	400	15	7	18	12.3	1.95108
350	9	4	0	12.8	0	400	15	7	20	12.2	2.24227
350	9	7	30	12.3	3.66556	400	16	4	0	12.6	0
350	9	7	80	12.2	14.93193	400	16	7	30	12.2	3.69123
350	10	4	0	12.7	0	400	16	7	56	12.2	10.18542

Coordinates (feet) X	Y	Tube number	Percent of flow	Pressure (psi)	Permeability (md)	Coordinates (feet) X	Y	Tube number	Percent of flow	Pressure (psi)	Permeability (md)
400	17	4	0	12.7	0	455	17	4	11	12.45	48.20317
400	17	6	65	12.2	27.0576	455	17	4	50	12.1	263.18417
400	17	6	48	12.2	19.21783	455	17	5	20	11.4	53.70881
400	18	4	0	12.8	0	455	17	5	20	12.4	49.97361
400	18	6	16	12.3	3.28289	455	18	4	17	12.1	86.03898
400	18	6	16	12.3	3.28289	455	18	5	10	12.3	20.6399
400	19	4	9	12.1	38.53181	455	18	5	10	12.3	20.6399
400	19	5	20	12.1	51.03306	455	19	4	0	12.7	0
400	19	5	12	12.2	26.51251	455	19	5	6	12.4	11.6833
400	20	5	18	12.1	44.81544	455	19	6	37	11.7	13.82954
400	20	5	20	12.1	51.03306	495	4	4	0	13.6	0
444	15	4	1	12.85	3.19119	495	4	7	24	12.6	2.73016
447	20	4	19	12.65	95.23891	495	4	7	20	12.4	2.2051
447	20	6	20	12.4	4.56562	495	5	4	0	13.35	0
447	20	6	40	12.3	14.94192	495	5	5	20	11.5	53.30783
447	21	4	23	12.05	122.44761	495	5	6	20	12.4	4.56562
447	21	6	18	12.4	3.90731	495	6	4	0	13.75	0
447	21	6	80	12.3	32.67113	495	6	6	38	12.3	13.84536
455	3	4	1	13	3.16213	495	6	6	26	12.2	7.57605
455	3	7	34	12.2	4.58233	495	6	6	56	12	23.61542
455	3	7	38	12.2	5.48856	495	6	6	80	12.2	32.89445
455	4	4	0	13.1	0	495	7	4	17.5	13.5	81.3607
455	4	7	30	12.2	3.69123	495	7	6	58	12.1	24.46537
455	4	7	20	12.3	2.22352	495	7	7	26	12.1	3.12742
455	5	4	18	12	93.08128	495	8	4	0	13.7	0
455	5	7	40	12.2	5.94665	495	8	7	60	12.4	11.12121
455	5	7	75	12.2	13.70983	495	8	7	38	12.4	5.41579
455	6	4	1	12.8	3.20102	495	9	4	0	13.6	0
455	6	7	24	12.3	2.7926	495	9	7	30	12.4	3.6403
455	6	7	24	12.3	2.7926	495	9	7	14	12.6	1.38402
455	7	4	1	12.95	3.17174	495	10	4	1	13.35	3.09678
455	7	7	20	12.3	2.22352	495	10	4	0	13.9	0
455	7	7	65	12.2	11.88119	495	10	7	40	12.4	5.86836
455	8	4	0	13	0	495	10	7	70	12.3	12.41992
455	8	7	34	12.4	4.52053	495	11	4	0	13.8	0
455	8	7	24	12.3	2.7926	495	11	7	32	12.3	4.10632
455	9	4	11	12.1	49.2764	495	11	7	23	12.5	2.60864
455	9	7	15	12.3	1.54924	495	12	4	0.5	13.3	1.40071
455	9	7	54	12.4	9.52817	495	12	7	14	12.5	1.39497
455	10	4	7	12.1	29.21009	495	12	6	28	11.7	8.87637
455	10	7	73	12.1	13.30767	495	12	6	30	12.4	9.47847
455	10	7	25	12.3	2.93661	495	13	4	28.5	12.8	145.33603
455	11	4	1	12.95	3.17174	495	13	5	50	11.2	108.06399
455	11	6	56	12.2	23.28307	495	13	5	60	12.2	118.21263
455	11	6	52	12.4	20.9793	495	14	4	0	13.6	0
455	12	4	0.5	12.45	1.47597	495	14	5	10	12.1	20.89675
455	12	6	40	12.4	14.84851	495	14	7	22	12.2	2.52672
455	12	5	13	12.4	29.05254	495	15	4	27	12.5	140.01833
455	13	4	27	12	145.22768	495	15	5	19	11.6	49.66793
455	13	5	35	12.4	77.45811	495	15	5	75	12.2	142.89215
455	13	5	75	12	144.89281	495	16	4	0	13.6	0
455	14	4	22	12.1	116.49016	495	16	6	12	12.6	1.96349
455	14	4	0	12.3	0	495	16	6	36	12.2	12.83757
455	14	5	40	12.1	86.91157	495	17	4	0	13.6	0
455	14	5	55	12.1	110.15192	495	17	7	22	12.4	2.48681
455	15	5	10	12.3	20.6399	495	17	7	60	12.5	11.04943
455	15	5	95	12	185.11929	532	5	7	34	12.5	4.49037
455	16	4	0.5	12.7	1.45281	532	5	7	42	12.5	6.34309
455	16	5	10	12.3	20.6399	532	6	7	46	12.5	7.37968
455	16	5	12	12.3	26.34174	532	6	7	75	12.4	13.53775
455	17	4	44	12.1	238.84694	532	7	5	8	12.5	15.95287

Coordinates (feet) X	Y	Tube number	Percent of flow	Pressure (psi)	Permeability (md)
532	7	5	16	12.4	37.8814
532	8	4	0.5	13.7	1.36845
532	8	7	10	12.5	0.89017
532	8	7	10	12.6	0.88361
532	9	4	19	12.7	94.921
532	9	4	0.5	13.4	1.39247
532	9	7	70	12.5	12.26937
532	9	7	40	12.5	5.83014
532	10	4	0.5	13.4	1.39247
532	10	7	26	12.6	3.01477
532	10	7	20	12.6	2.16916
532	11	4	0	13.5	0
532	11	7	18	12.5	1.9193
532	11	7	24	12.6	2.73016
532	12	4	0	13.5	0
532	12	7	20	12.6	2.16916
532	12	7	70	12.5	12.26937
532	12	7	16	12.6	1.6419
532	12	7	24	12.5	2.75064
532	13	4	0	13.6	0
532	13	7	20	12.6	2.16916
532	13	7	70	12.5	12.26937
532	14	4	22	13.1	108.63085
532	14	4	14.5	13.55	64.10949
532	14	7	75	12.5	13.45369
532	14	5	15	12.5	34.67563
532	15	4	0	13.7	0
532	15	5	6	12.6	11.54243
532	15	7	22	12.6	2.4482
585	4	4	20	13	99.17632
585	4	7	28	12.6	3.30176
585	5	4	1	13.55	3.0609
585	5	7	16	12.6	1.6419
585	5	7	12	12.6	1.1309
585	6	4	0	13.8	0
585	6	7	18	12.6	1.9038
585	6	7	75	12.5	13.45369
585	7	7	14	12.6	1.38402
585	7	7	11	12.8	0.99153
585	8	4	0	13.35	0
585	8	7	11	12.8	0.99153
585	9	4	0.5	13.2	1.40908
585	9	7	26	12.6	3.01477
585	10	4	0	13.6	0
585	10	7	12	12.7	1.12231
585	10	7	14	12.7	1.37325
585	11	4	0	13.6	0
585	11	7	40	12.7	5.75547
585	11	7	22	12.7	2.42937
585	12	4	15	13.2	68.35593
585	12	4	10	13.1	40.83073
585	12	6	90	12.5	34.54901
585	12	5	18	11.7	46.09963
585	12	5	12	12.7	25.68499
585	13	4	0	13.7	0
585	13	7	14	12.7	1.37325
585	14	4	0	13.5	0
585	14	7	80	12.6	14.55478
585	15	4	19	12.9	93.67313
585	15	4	8	13.25	31.60037
585	15	7	75	12.6	13.3709
585	15	6	14	12.7	2.5605
585	16	4	0.5	13.75	1.36455
585	16	6	30	12.6	9.35963
585	16	6	50	12.6	19.72215
585	17	4	10	13.1	40.83073
585	17	6	48	12.6	18.70176
585	17	6	12	12.8	1.93108
585	18	4	0	13.6	0
585	18	4	0.5	13.5	1.38435
585	18	6	57	12.6	23.14093
585	18	6	14	12.7	2.5605
585	19	4	0	13.8	0
585	19	6	10	12.8	1.33909
585	19	6	14	12.8	2.54104
585	20	4	1	13.4	3.08771
585	20	5	45	11.4	98.82943
585	20	7	20	12.8	2.13441
585	21	4	0	13.7	0
585	21	7	17	12.8	1.7444
585	21	7	65	12.7	11.51486
585	22	4	0	13.8	0
585	22	7	80	12.6	14.55478
585	22	7	10	12.9	0.86455
585	23	4	0	13.6	0
585	23	7	38	12.7	5.31086
585	24	4	0	13.5	0
585	24	7	26	12.8	2.97219
585	24	7	36	12.8	4.8381
640	2	4	0	13.7	0
640	2	6	20	12.8	4.44357
640	2	6	18	12.8	3.79944
640	3	4	9	12.2	38.29402
640	3	6	18	12.8	3.79944
640	3	6	16	12.8	3.16469
640	4	4	0	13	0
640	4	6	30	12.7	9.30158
640	4	6	17	12.8	3.4808
640	5	4	10	12.45	42.39913
640	5	4	0	13.45	0
640	5	6	22	12.7	5.41319
640	5	6	18	12.8	3.79944
640	6	4	0	13.3	0
640	6	6	18	12.8	3.79944
640	6	6	18	12.8	3.79944
640	7	4	0	13.1	0
640	7	6	30	12.7	9.30158
640	7	6	14	12.8	2.54104
640	8	4	8	12.45	33.10484
640	8	6	60	12.6	24.6209
640	8	6	90	12.6	34.31661
640	9	4	0	13.2	0
640	9	6	60	12.6	24.6209
640	9	6	63	12.6	25.63717
640	10	4	10	12.6	42.02369
640	10	5	20	12.6	49.29386
640	10	5	14	12.7	31.35711
640	11	4	23	12.25	120.67171
640	11	5	35	12.5	76.94772
640	11	5	19	12.6	46.30301
640	12	4	6	12.8	23.612
640	12	6	16	12.9	3.14216

Coordinates (feet) X	Y	Tube number	Percent of flow	Pressure (psi)	Permeability (md)
640	12	6	17	12.8	3.4808
640	13	4	0	13.35	0
640	13	6	30	12.8	9.2444
640	13	6	20	12.7	4.47337
640	14	4	0	13.2	0
640	14	6	22	12.8	5.37798
640	14	6	28	12.8	8.26106
640	15	4	0.5	12.9	1.43492
640	15	6	26	12.8	7.28814
640	15	6	28	12.9	8.2102
640	16	4	0	13.5	0
640	17	4	0	13.4	0
640	17	6	56	12.7	22.49738
640	17	6	15	12.9	2.83051
640	18	4	0	13.4	0
640	18	6	10	12.9	1.3266
640	18	6	28	12.9	8.2102
640	21	4	0.5	12.5	1.47126
640	22	4	0	12.85	0
640	23	4	1	12.65	3.23097
695	1	4	0	13.4	0
695	1	7	10	12.9	0.86455
695	1	7	11	12.9	0.98426
695	2	4	0	13.4	0
695	2	7	52	12.8	8.79103
695	2	7	20	13	2.10077
695	3	4	0	13.4	0
695	3	7	34	12.9	4.3743
695	3	7	32	12.9	3.94506
695	4	4	0.5	12.75	1.44829
695	4	7	42	12.9	6.18717
695	4	6	24	12.8	6.32671
695	5	4	1	12.9	3.18143
695	5	6	30	12.8	9.2444
695	5	6	16	13	3.11999
695	6	4	1	12.75	3.21093
695	6	6	42	12.8	15.4734
695	6	6	28	13	8.16009
695	7	4	1	12.8	3.20102
695	7	6	46	12.8	17.45696
695	7	6	22	12.9	5.3433
695	8	4	1	12.3	3.3036
695	8	6	24	12.8	6.32671
695	8	6	22	12.9	5.3433
695	9	4	52	122.3	46.52975
695	9	5	10	12.7	20.14918
695	9	5	22	12.6	53.16828
695	10	4	12	12.5	53.88377
695	10	4	17	12.3	84.84309
695	10	5	40	12.3	85.75803
695	10	5	20	12.6	49.29386
695	11	4	6	12.8	23.612
695	11	5	6	12.9	11.33893
695	11	5	14	12.7	31.35711
695	12	4	1	12.9	3.18143
695	12	5	6	12.9	11.33893
695	12	5	14	12.7	31.35711
695	13	4	16	12.6	77.05556
695	13	5	40	12.4	85.19501
695	13	5	45	12.3	92.81168
695	14	4	6	13.2	23.06425

Coordinates (feet) X	Y	Tube number	Percent of flow	Pressure (psi)	Permeability (md)
695	14	4	16	12.4	78.11102
695	14	5	8	12.8	15.67056
695	14	5	12	12.7	25.68499
695	15	4	10	12.55	42.14788
695	15	5	25	12.3	60.25157
695	15	5	16	12.5	37.63218
695	16	4	1	12.9	3.18143
695	16	6	77	12.4	31.24226
695	16	6	20	12.7	4.47337
705	1	7	16	12.6	1.6419
705	1	7	20	12.6	2.16916
705	6	7	18	12.5	1.9193
705	6	7	50	12.4	8.47898
705	7	7	28	12.5	3.3249
705	7	7	75	12.3	13.62312
705	8	7	70	12.4	12.34406
705	9	7	80	12.4	14.74043
705	9	7	22	12.5	2.46734
705	10	5	13	12.3	29.24166
705	10	5	18	12.2	44.50697
705	11	5	45	12.7	90.39119
705	11	5	20	12.8	48.63429
705	12	6	28	13.1	8.11073
705	12	6	45	13	16.7457
705	13	5	14	12.9	30.96591
705	13	5	35	12.8	75.46611
705	14	5	17	12.9	39.56662
705	14	5	10	13	19.79992
705	15	5	5	13	9.21245
705	15	5	9	13	17.63389
705	16	5	20	12.9	48.31179
705	16	5	16	12.9	36.67286
705	17	5	14	12.9	30.96591
705	17	5	6	13.2	11.14425
705	18	5	35	12.8	75.46611
705	18	5	20	12.9	48.31179
705	19	5	10	13	19.79992
705	19	5	10	13	19.79992
705	20	6	22	13.2	5.24238
705	20	6	26	13.1	7.15385
705	21	6	24	13.1	6.20837
705	21	6	32	13	10.1526
705	22	6	18	13.2	3.69811
705	22	6	29	13	8.64511
705	23	6	16	13.2	3.07667
705	23	6	16	13.2	3.07667
705	24	6	14	13.3	2.44825
705	24	6	52	12.9	20.28252
705	25	6	38	13	13.26472
705	25	6	18	13.3	3.67373
747	9	4	1	12.5	3.26161
747	9	7	12	12.3	1.15752
747	9	7	85	12.2	15.78327
747	10	4	6	12.5	24.04461
747	10	4	13	12.05	61.56932
747	10	5	18	11.3	47.47121
747	10	5	25	12.1	61.10664
747	11	4	4	12.2	15.65755
747	11	5	18	12.2	44.50697
747	11	5	13	12.2	29.43386
747	12	4	0	12.6	0

Coordinates (feet) X	Y	Tube number	Percent of flow	Pressure (psi)	Permeability (md)
747	12	6	14	12.4	2.62084
747	12	6	20	12.3	4.59736
747	13	4	0	12.6	0
747	13	6	13	12.4	2.30698
747	13	6	16	12.3	3.28289
747	14	4	0	12.6	0
747	14	6	16	12.4	3.25848
747	14	6	18	12.4	3.90731
747	17	4	15.5	12	77.20576
747	17	6	40	12.2	15.03679
747	17	6	30	12.3	9.53931
747	18	4	1	12.3	3.3036
747	18	6	65	12.2	27.0576
747	18	6	30	12.3	9.53931
747	19	4	15	12	74.09592
747	19	5	55	12.1	110.15192
747	19	5	18	12.2	44.50697
747	20	4	28	12.35	147.09598
747	20	6	24	12.3	6.53651
747	20	6	30	12.3	9.53931
795	1	4	0	14.2	0
795	6	4	0.5	11.9	1.53027
795	7	4	0.5	11.6	1.56203
795	8	4	0.5	12.4	1.48071
795	9	4	1	12.7	3.22091
795	9	4	11	12.1	49.2764
795	10	4	18	12.05	92.75114
795	11	4	14	12.1	67.44541
795	11	4	29.5	11.55	165.0934
795	12	4	0.5	12.4	1.48071
795	13	4	11.5	12.1	52.28471
795	13	4	11	12.1	49.2764
795	14	4	20	12.1	105.4657
795	15	4	11	11.7	50.57642
795	16	4	35	11.7	197.93155
795	17	4	0	12.6	0
795	17	4	0.5	12.5	1.47126
795	18	4	22	12.1	116.49016
795	19	4	9	12.1	38.53181
795	20	4	19.5	11.8	104.40034
795	21	4	0	12.5	0
795	21	4	8	12.15	33.72299
795	22	4	0.5	12.4	1.48071
795	23	4	0	12.9	0
795	24	4	10	11.7	44.41413
795	25	4	0	12.6	0
820	1	4	0	12.05	0
820	1	6	14	13.3	2.44825
820	1	6	20	13	4.38534
820	8	4	0	12.7	0
820	8	6	26	13	7.19794
820	8	6	20	13	4.38534
820	9	4	6	12.3	24.34412
820	9	4	0	12.9	0
820	9	6	18	13	3.74799
820	9	6	46	12.9	17.34512
820	12	3	79.5	10.65	1496.94092
820	12	2	29	11.85	1385.48145
820	12	3	80	11.4	1282.96033
820	13	3	68	11.2	1185.70605
820	13	3	47	11.1	802.26135

Coordinates (feet) X	Y	Tube number	Percent of flow	Pressure (psi)	Permeability (md)
820	13	3	30	12.3	415.65112
820	13	3	75	11.5	1178.25732
820	14	4	89	11.3	468.57709
820	14	3	8	12.1	126.32437
820	14	3	26	12.4	397.89029
820	14	3	20	12.6	281.4758
820	14	5	70	12.6	130.20815
820	14	3	25	12.4	348.16125
820	15	4	11	11.6	50.91467
820	15	5	18	12.8	42.75167
820	15	5	20	12.8	48.63429
820	16	3	26	12.3	400.80194
820	16	5	95	12.6	177.15273
820	16	3	50	12.3	709.49554
820	17	3	68	10.85	1221.91064
820	17	3	60	12	872.11896
820	17	5	19	12	48.25895
820	18	3	26.5	12.4	404.95871
820	18	3	30	11.3	495.48572
820	18	3	30	12.3	415.65112
820	19	4	1	12.1	3.34694
820	19	4	9.5	12.1	40.91207
820	19	7	50	13	8.19211
820	19	7	80	13	14.19993
820	20	3	51.5	10.9	902.52008
820	20	3	10	12.7	142.41273
820	20	3	20	12.5	283.34833
820	21	3	52	10.9	910.99133
820	21	3	20	12.5	283.34833
820	21	3	5	12.7	65.09188
820	22	4	15	12.1	73.57364
820	22	5	20	12.8	48.63429
820	22	5	14	12.8	31.16
820	23	4	0.5	12.7	1.45281
820	23	7	26	13.1	2.9108
855	3	4	0	13.3	0
855	3	7	20	13.3	2.05229
855	3	7	42	13	6.14964
855	4	4	0	13.3	0
855	4	7	22	13.1	2.35701
855	4	7	32	13.1	3.89455
855	5	4	0	13.3	0
855	5	7	22	13.1	2.35701
855	5	7	20	13.2	2.0682
855	9	4	0	13.25	0
855	9	5	5	13	9.21245
855	9	5	10	12.9	19.91464
855	10	4	0	13.25	0
855	10	5	5	13	9.21245
855	10	5	8	12.9	15.57919
855	11	4	1	13.2	3.12438
855	11	5	20	12.8	48.63429
855	11	5	8	13	15.48914
855	12	4	0	13.2	0
855	12	7	23	13.2	2.47646
855	13	3	32	11.3	526.02893
855	13	3	10	12.6	143.19189
855	13	3	15	12.5	211.86848
855	14	3	26	11.25	434.36099
855	14	3	50	12.2	714.75079
855	14	3	20	12.5	283.34833

Coordinates (feet) X	Y	Tube number	Percent of flow	Pressure (psi)	Permeability (md)
855	15	3	38	11.1	630.61163
855	15	3	40	12.3	548.12238
855	15	3	25	12.5	345.75021
855	17	4	8	12.2	33.6179
855	17	5	20	12.8	48.63429
855	17	5	10	12.9	19.91464
855	18	4	21	12.1	110.97361
855	18	4	19	12.1	98.90776
855	18	4	21	11.9	112.5854
855	18	5	70	12.7	129.35123
855	18	5	8	13	15.48914
855	20	4	9	12.7	37.15991
855	20	5	8	13	15.48914
855	20	3	20	12.5	283.34833
855	20	3	20	12.6	281.4758
855	21	3	80	11.4	1414.84241
855	21	2	27.5	10.7	1425.61816
855	21	2	16	11	752.91541
855	21	3	5	12.9	64.29708
855	21	5	16	12	38.91882
855	21	5	13	12.9	28.1508
855	22	4	0	13	0
855	22	5	8	13	15.48914
855	22	5	12	12.9	25.37159
855	23	4	0	13	0
855	23	7	26	13.2	2.89096
855	23	7	22	13.1	2.35701
855	24	5	25	12	61.5447
855	24	3	20	12.5	283.34833
890	1	4	1	12.7	3.22091
890	1	7	54	12.8	9.29978
890	1	7	80	12.7	14.46407
890	2	4	0	12.8	0
890	2	7	16	12.9	1.60358
890	2	7	26	12.9	2.95141
890	3	4	0	13	0
890	3	7	38	12.9	5.24356
890	3	7	15	13	1.46608
890	4	4	0	12.75	0
890	4	7	31	12.9	3.73192
890	4	7	46	12.8	7.24854
890	5	4	0	12.45	0
890	5	7	24	13	2.65149
890	5	7	34	12.9	4.3743
890	6	4	9	12.6	37.37971
890	6	7	46	12.8	7.24854
890	6	7	38	12.9	5.24356
890	7	4	0	12.9	0
890	7	7	11	13.2	0.96312
890	7	7	15	13	1.46608
890	8	4	80	12.1	395.46112
890	8	5	40	11.8	88.71529
890	8	5	55	12.6	106.37453
890	11	4	0	13.2	0
890	11	5	6	12.8	11.40575
890	11	5	4	12.9	7.23514
890	12	3	56	10.7	997.33179
890	12	3	25	12.4	348.16125
890	12	7	48	12.9	7.72059
890	14	4	18.5	11.4	100.67909
890	14	5	16	12.7	37.14521

Coordinates (feet) X	Y	Tube number	Percent of flow	Pressure (psi)	Permeability (md)
890	14	5	30	12.7	68.48952
890	15	4	37	11.4	215.80817
890	15	4	25.5	11.4	143.2951
890	15	5	50	12.6	97.87176
890	15	7	20	13	2.10077
890	16	3	40	12	617.96869
890	16	3	41	12	636.01526
890	16	3	35	12.2	484.52576
890	16	3	35	12.3	481.09653
890	17	4	12	12.1	55.30344
890	17	5	8	12.8	15.67056
890	17	5	50	12.6	97.87176
890	18	4	16	12.1	79.7632
890	18	5	60	12.6	114.95346
890	18	5	5	12.8	9.32142
890	19	4	11	12.1	49.2764
890	19	5	12	12.8	25.52709
890	19	5	35	12.6	76.44574
890	20	4	28.5	11.5	159.76903
890	20	3	15	12.5	211.86848
890	20	3	10	12.5	143.98293
890	21	4	34	11.35	196.50688
890	21	3	15	12.4	213.32048
890	21	3	5	12.6	65.49924
890	22	4	0	12.3	0
890	22	7	46	12.9	7.20612
890	22	7	75	12.9	13.12992
995	1	4	0	12.2	0
995	1	7	20	13.5	2.24548
995	1	7	12	13.7	1.15222
995	2	4	0	12.9	0
995	2	7	26	13.5	3.15578
995	2	7	80	13.5	15.49109
995	3	4	0	13	0
995	3	7	30	13.5	3.77737
995	3	7	18	13.5	1.96997
995	4	4	0	12.1	0
995	4	7	18	13.6	1.95479
995	4	7	25	13.5	3.00208
995	5	4	0	12.75	0
995	5	5	4	13.5	7.82933
995	5	5	6	13.5	12.30156
995	6	4	0	12.5	0
995	6	7	18	13.5	1.96997
995	6	7	20	13.6	2.22801
995	7	4	0	12.95	0
995	7	7	70	13.5	13.00378
995	7	7	26	13.6	3.13412
995	8	4	0	12.8	0
995	8	7	12	13.7	1.15222
995	8	7	14	13.7	1.40985
995	9	4	0	12.65	0
995	9	7	95	13.1	18.43862
995	9	7	34	13.6	4.6756
995	11	3	40	12.6	590.78021
995	12	4	0	13.3	0
995	13	4	39	12.85	204.72464
995	13	5	20	12.6	55.77725
995	13	3	20	13	309.77655
995	14	4	38	12.1	210.64638
995	14	5	18	12.5	49.32502

Coordinates (feet) X	Y	Tube number	Percent of flow	Pressure (psi)	Permeability (md)	Coordinates (feet) X	Y	Tube number	Percent of flow	Pressure (psi)	Permeability (md)
995	14	5	55	13.2	115.56769	1072	3	5	6	13	12.67433
995	15	4	43	12.8	222.3629	1072	4	5	7	13	15.04043
995	15	5	30	13.3	74.40796	1072	4	7	16	13.1	1.75207
995	15	3	25	13	377.6506	1072	5	7	49	13	8.90524
995	15	3	45	12.7	688.60876	1072	5	7	24	13.1	2.93336
995	16	2	35	10.15	1973.60095	1072	6	7	60	13	12.03466
995	16	3	40	12.7	602.02814	1072	6	5	16	12.3	43.13987
995	16	2	35	10.3	2002.02441	1072	7	4	32	12.7	170.9274
995	16	2	35	10	2057.24487	1072	7	4	12	13	53.60254
995	17	3	52	11.45	868.91846	1072	11	5	80	12.9	163.87489
995	17	3	55	11.45	918.65424	1072	11	5	10	13	22.3156
995	17	3	25	12.7	385.68903	1072	13	7	60	13	12.03466
995	17	3	70	11.5	1228.73474	1072	13	5	14	13	34.70987
995	18	3	15	12.85	228.36462	1072	14	5	13	13	31.56111
995	18	5	45	12.1	106.59996	1072	14	7	24	13	2.95526
995	18	3	30	12.2	474.23239	1072	15	7	14	13	1.48718
995	18	3	20	12.9	311.86816	1072	15	7	24	13.1	2.93336
995	19	4	0	13.25	0	1072	16	7	24	13	2.95526
995	19	5	50	12.9	95.94406	1072	16	7	60	13	12.03466
995	19	7	75	13.5	14.24274	1072	17	5	25	12.8	65.88681
995	19	7	16	13.6	1.68538	1072	17	5	12	13	28.4429
995	20	4	0	13.6	0	1352	2	7	20	12.9	2.35635
995	20	7	20	13.5	2.24548	1352	2	7	24	13	2.95526
995	20	5	50	12.2	113.98105	1352	2	7	26	13	3.2692
995	20	5	8	13	17.43933	1352	3	7	20	12.9	2.35635
995	21	4	20	12.1	105.4657	1352	3	7	22	13	2.64444
995	21	5	30	13	75.91518	1352	4	7	38	12.8	5.91249
995	21	5	10	13	22.3156	1352	4	7	54	12.9	10.38716
995	22	4	30	12.1	161.35692	1352	5	7	26	12.8	3.31711
995	22	5	50	13	107.80484	1352	5	7	28	12.9	3.61128
995	22	5	45	13	100.20515	1352	6	7	30	13	3.90541
995	23	3	28	11.6	452.98135	1352	6	7	70	12.8	13.56162
995	23	3	20	12.9	311.86816	1352	7	5	10	12.9	22.45181
995	23	3	10	12.9	158.85789	1352	7	5	12	12.8	28.80966
995	23	4	30	12.7	158.89728	1352	8	5	14	12.8	35.1678
995	23	4	65	12.5	323.25208	1352	8	7	42	12.9	6.93711
1030	8	4	43	12.05	235.75957	1352	8	7	44	12.9	7.50973
1030	8	4	16	12.8	78.06532	1352	9	5	18	12.8	48.31111
1030	8	5	30	12.9	76.4345	1352	9	5	25	12.8	65.88681
1030	8	5	30	12.9	76.4345	1352	10	5	40	12.7	94.48206
1030	9	4	17	12.15	85.736	1352	10	5	60	12.7	129.29102
1030	9	5	80	13	162.77887	1352	11	4	80	12.5	393.78891
1030	9	5	80	12.7	166.11916	1352	11	4	50	12.6	259.87387
1030	10	4	53	12.1	274.87778	1352	15	4	18	12.8	90.46283
1030	10	5	75	12.8	154.92863	1352	15	4	18	12.8	90.46283
1030	10	5	60	12.8	128.3727	1352	15	5	25	12.8	65.88681
1030	11	4	15	12.8	70.14718	1352	15	5	30	12.8	76.96252
1030	11	7	16	13.1	1.75207	1352	16	4	35	12.6	190.42363
1030	11	7	26	13.1	3.24581	1352	16	4	20	12.7	103.88091
1030	12	4	23	12.9	118.34447	1352	16	5	27	12.8	70.28721
1030	12	4	50	12.7	257.86774	1352	16	5	40	12.8	93.85275
1030	13	7	26	13	3.2692	1428	2	7	26	13.1	3.24581
1030	13	7	24	13.1	2.93336	1428	2	7	24	13	2.95526
1030	14	3	27	11.8	430.99127	1428	3	7	24	13.1	2.93336
1030	17	4	6	12.5	24.04461	1428	3	7	26	13	3.2692
1030	23	4	2	12.4	7.15697	1428	4	7	30	13	3.90541
1072	1	7	14	13	1.48718	1428	4	7	24	13	2.95526
1072	1	7	20	13	2.33712	1428	5	7	25	13	3.11186
1072	2	7	22	13	2.64444	1428	5	7	24	13	2.95526
1072	2	7	16	13.1	1.75207	1428	6	7	50	13	9.19641
1072	3	7	95	12.9	18.68715	1428	6	7	80	13	15.98151

Coordinates (feet) X	Y	Tube number	Percent of flow	Pressure (psi)	Permeability (md)
1428	6	7	85	12.9	16.99404
1428	7	7	34	13	4.86141
1428	7	7	32	13	4.38104
1428	8	7	26	13	3.2692
1428	8	7	22	13	2.64444
1428	9	5	15	12.9	38.1546
1428	9	5	6	13	12.67433
1428	10	4	60	12.5	301.53488
1428	10	4	55	12.6	279.3038
1428	11	5	19	12.8	51.65022
1428	11	5	10	13	22.3156
1428	12	7	32	13	4.38104
1428	12	7	30	13	3.90541
1428	13	5	14	12.9	34.93704
1428	13	5	16	12.9	41.4055
1428	14	5	25	12.9	65.42874
1428	14	5	40	12.8	93.85275
1428	15	4	80	12.5	393.78891
1428	15	3	70	11.9	1189.32947
1428	15	3	45	12.1	721.51263
1428	16	4	10	12.9	42.38251
1428	16	3	50	12.1	814.75427
1428	16	3	50	12.2	808.34149
1428	17	4	10	12.9	42.38251
1428	17	5	20	12.8	54.99789
1428	17	5	40	12.8	93.85275
1428	18	4	50	12.6	259.87387
1428	18	4	45	12.5	241.75627
1428	19	4	10	12.8	42.63029
1428	19	5	16	12.8	41.68337
1428	19	5	45	12.5	103.64897
1428	20	5	16	12.7	41.96557
1428	20	5	10	12.9	22.45181
1428	20	5	80	12.5	168.4399
1428	20.5	7	38	12.9	5.87335
1990	5	6	14	13	2.78856
1990	5	6	14	13	2.78856
1990	6	6	24	12.8	7.09632
1990	6	6	38	12.9	15.01815
1990	7	6	22	13	5.94576
1990	7	6	19	13	4.54531
1990	8	6	30	12.9	10.32311
1990	8	6	30	12.9	10.32311
1990	9	6	14	13	2.78856
1990	9	6	30	13	10.25767
1990	10	6	14	13	2.78856
1990	10	6	16	13	3.48168
1990	11	6	12	13	2.11169
1990	11	6	18	13	4.18793
1990	12	6	30	13	10.25767
1990	12	6	80	12.9	35.44609
1990	13	6	20	13	4.90526
1990	13	6	50	12.9	21.78988
1990	14	6	30	13	10.25767
1990	14	6	16	13	3.48168
1990	15	6	18	13	4.18793
1990	15	6	38	13	14.92442
1998	2	6	12	13	2.11169
1998	2	6	26	13	8.07499
1998	3	6	14	13	2.78856
1998	3	6	14	13.1	2.7671

Coordinates (feet) X	Y	Tube number	Percent of flow	Pressure (psi)	Permeability (md)
1998	4	6	18	13	4.18793
1998	4	6	16	13	3.48168
1998	5	6	75	12.8	33.43349
1998	5	6	14	13	2.78856

MFP MEASURED PERMEABILITY DATA

GRID B DATA

Coordinates (feet) X	Y	Tube number	Percent of flow	Pressure (psi)	Permeability (md)	Coordinates (feet) X	Y	Tube number	Percent of flow	Pressure (psi)	Permeability (md)
925	1	4	0	12.2	0	930	7	7	60	12.8	10.84064
925	1	7	16	13	1.59121	930	7	7	20	12.9	2.11745
925	1	7	16	13	1.59121	930	8	7	20	13.1	2.08435
925	4	4	0	13	0	930	8	7	80	12.8	14.3747
925	4	7	28	12.9	3.23452	930	9	5	25	12.1	61.10664
925	4	7	32	12.8	3.9709	930	9	7	26	12.9	2.95141
925	5	4	0	12.6	0	930	10	5	20	12.1	51.03306
925	5	7	26	13	2.93094	930	10	5	16	12.7	37.14521
925	5	7	70	12.8	12.05196	930	11	5	10	12.8	20.03105
925	6	4	0	12.25	0	930	11	5	12	12.8	25.52709
925	6	7	20	12.9	2.11745	930	12	5	20	12.7	48.96161
925	6	7	24	12.9	2.67069	930	12	5	25	12.7	58.6216
925	7	4	6	111.55	5.6123	930	14	7	24	12.9	2.67069
925	7	7	85	12.8	15.18568	930	14	5	50	11.9	102.70292
925	7	7	50	12.8	8.2849	930	14	3	25	12.4	348.16125
925	8	4	1	11.7	3.43793	930	15	5	18	12.6	43.31935
925	8	7	60	12.9	10.77315	930	15	7	24	12.7	2.71002
925	8	7	22	12.9	2.39261	930	15	7	40	12.9	5.68306
925	9	4	0	12.2	0	930	16	7	20	13.1	2.08435
925	9	7	20	13	2.10077	930	16	5	40	12.1	86.91157
925	9	7	18	13	1.84431	930	17	5	14	12.7	31.35711
925	10	4	0	11	0	930	17	5	95	12.5	178.43701
925	10	7	42	12.9	6.18717	930	18	5	25	12.6	59.01941
925	10	7	65	12.8	11.4449	930	18	5	18	12.7	43.03344
925	11	4	9	12.05	38.65216	930	19	7	20	12.9	2.11745
925	11	5	30	12.6	68.94514	930	19	7	34	12.9	4.3743
925	11	5	9	12.7	17.94558	935	8	7	36	12.8	4.8381
925	12	4	9	12.05	38.65216	935	8	7	26	13.1	2.9108
925	12	5	8	12.8	15.67056	935	9	7	40	12.8	5.71899
925	12	5	14	12.7	31.35711	935	9	7	40	12.8	5.71899
925	13	4	0	12.4	0	935	10	5	45	12.5	91.58425
925	13	5	10	12.8	20.03105	935	10	5	40	12.6	84.09503
925	13	7	30	12.9	3.51983	935	11	5	4	12.8	7.27828
925	13	7	30	13	3.49684	935	11	7	50	12.9	8.23817
925	14	4	0	12.1	0	935	12	7	14	13.1	1.3319
925	14	5	6	12.9	11.33893	935	12	7	26	12.9	2.95141
925	14	5	9	12.8	17.84016	935	13	7	34	12.8	4.40265
925	15	4	0	12.05	0	935	13	7	24	12.9	2.67069
925	15	5	7	12.9	13.44519	935	13	5	75	12.6	139.11258
925	15	5	9	12.8	17.84016	935	14	5	19	12.7	45.99385
925	16	4	38	11.3	224.21811	935	14	5	25	12.8	58.23
925	16	3	15	12.5	211.86848	935	15	5	12	12.8	25.52709
925	16	3	15	12.4	213.32048	935	15	5	6	12.9	11.33893
925	17	3	27	11.1	455.57227	935	16	5	45	12.7	90.39119
925	17	3	45	12.1	636.65942	935	16	5	60	12.6	114.95346
925	17	3	40	12.2	552.17194	935	16	5	16	12.7	37.14521
925	18	4	0	12.25	0	935	17	5	18	12.7	43.03344
925	18	7	18	13	1.84431	935	17	5	50	12.6	97.87176
925	18	7	36	12.9	4.80723	935	18	3	50	12.1	720.09772
925	19	4	0	12.7	0	935	18	3	40	12.3	548.12238
925	19	7	50	12.9	8.23817	935	19	3	20	12.5	283.34833
925	19	7	46	12.9	7.20612	935	19	3	15	12.5	211.86848
925	20	4	0	12.35	0	935	20	5	16	12.1	38.65316
925	20	7	48	12.9	7.72059	935	20	5	16	12.7	37.14521
925	20	7	26	13	2.93094	940	7	7	32	12.8	3.9709
925	21	4	14.5	12.45	68.82347	940	7	7	20	12.7	2.15164
925	21	5	10	12.8	20.03105	940	8	7	26	12.7	2.99331
925	21	5	25	12.7	58.6216	940	9	7	42	12.7	6.26394
925	22	4	0	12.9	0	940	9	7	75	12.8	13.20905
925	22	5	8	12.8	15.67056	940	10	5	10	12.4	20.51441
925	22	7	32	12.4	4.07837	940	10	5	20	12.8	48.63429

Coordinates (feet) X	Y	Tube number	Percent of flow	Pressure (psi)	Permeability (md)
940	11	5	7	12.4	13.85207
940	11	5	12	12.7	25.68499
940	12	5	10	12.9	19.91464
940	12	7	38	12.7	5.31086
940	13	7	50	13	8.19211
940	13	5	12	12.4	26.17366
940	14	7	50	12.8	8.2849
940	14	5	18	12.1	44.81544
940	15	5	55	12.6	106.37453
940	15	5	8	12.9	15.57919
940	16	3	15	12.5	211.86848
940	16	3	25	12.5	345.75021
940	16	3	40	12.4	544.13092
940	17	3	45	12.3	627.13043
940	17	3	35	12.3	481.09653
940	18	5	30	12.7	68.48952
940	18	5	40	12.6	84.09503
940	19	5	95	12.6	177.15273
940	19	3	20	11.9	295.2366
940	19	3	15	12.6	210.44266
945	8	7	14	12.9	1.35224
945	8	7	15	12.9	1.47738
945	9	5	18	12.7	43.03344
945	9	7	32	12.8	3.9709
945	10	7	28	12.9	3.23452
945	10	7	22	12.9	2.39261
945	11	5	10	12.2	20.76732
945	11	5	9	12.8	17.84016
945	12	5	10	12.8	20.03105
945	12	5	14	12.8	31.16
945	13	5	15	12.7	34.23092
945	15	5	6	12.7	11.47357
945	15	5	18	12.7	43.03344
945	16	7	14	13	1.34199
945	16	7	90	12.7	16.10237
945	16	5	9	12.4	18.27146
945	17	7	14	13	1.34199
945	17	7	18	12.9	1.85882
945	18	3	40	12.4	544.13092
945	18	3	35	12.6	471.12378
945	19	7	85	12.5	15.47758
945	19	7	50	12.9	8.23817
945	20	7	22	13	2.37467
945	20	7	35	13	4.56117
945	21	7	60	12.9	10.77315
945	21	5	23	12.4	55.87463
945	22	5	70	12.8	128.51094
945	22	5	18	12.9	42.47397
945	23	7	60	13	10.70666
945	23	7	40	13	5.64767
950	7	7	12	13.2	1.08141
950	7	7	60	13	10.70666
950	7	7	20	13	2.10077
950	9	5	50	12.8	96.57752
950	9	5	50	12.9	95.94406
950	10	3	15	12.7	209.04298
950	10	3	20	12.6	281.4758
950	11	5	12	12.9	25.37159
950	11	5	15	12.9	33.79973
950	12	5	6	12.9	11.33893
950	12	7	32	12.7	3.99714

Coordinates (feet) X	Y	Tube number	Percent of flow	Pressure (psi)	Permeability (md)
950	13	7	30	13	3.49684
950	13	7	50	12.9	8.23817
950	14	7	42	12.9	6.18717
950	14	7	80	12.9	14.28668
950	15	7	16	13.1	1.57904
950	15	7	24	13.1	2.63259
950	16	5	45	12.8	89.80678
950	16	5	95	12.7	175.88554
950	17	5	80	12.7	147.22572
950	17	5	9	13	17.63389
950	17	7	24	12.9	2.67069
950	18	5	10	12.9	19.91464
950	18	5	20	12.9	48.31179
950	19	5	10	12.9	19.91464
950	19	5	12	12.9	25.37159
950	20	5	12	12.9	25.37159
950	20	5	16	12.9	36.67286
955	6	7	30	12.6	3.59097
955	6	7	14	13	1.34199
955	7	7	90	13	15.79988
955	7	7	20	13	2.10077
955	8	3	15	12.4	213.32048
955	8	3	10	12.8	141.64447
955	9	5	16	12.3	38.13457
955	9	5	6	13	11.27309
955	9	7	26	13	2.93094
955	10	7	50	13	8.19211
955	10	7	70	13	11.91233
955	11	5	65	12.7	121.64696
955	11	5	16	12.7	37.14521
955	12	5	8	13	15.48914
955	12	3	15	11.8	222.58832
955	13	5	6	13	11.27309
955	13	5	20	12.9	48.31179
955	14	3	50	12.4	704.32928
955	14	3	10	12.8	141.64447
955	14	3	15	12.7	209.04298
955	15	5	10	13	19.79992
955	15	3	20	12.7	279.63232
955	15	3	25	12.6	343.37546
955	16	3	75	11.8	1151.01819
955	16	3	70	11.9	1051.84558
955	17	3	25	12.6	343.37546
955	17	5	20	13	47.99402
955	18	7	18	13.2	1.81598
955	18	7	40	13.1	5.6128
955	19	5	9	12.6	18.05258
955	20	7	15	13.2	1.444
955	20	7	17	13.2	1.69108
955	21	7	50	13.1	8.14672
960	2	4	0	12.1	0
960	3	4	0	12.1	0
960	3	7	32	13.2	4.32297
960	3	7	28	13.2	3.5366
960	4	4	0	13	0
960	6	4	0	12.6	0
960	6	7	60	13.1	11.95741
960	6	7	40	13.2	6.24604
960	7	4	10	11.65	44.55736
960	7	5	14	13	34.70987
960	7	5	8	13.2	17.23059

Coordinates (feet) X	Y	Tube number	Percent of flow	Pressure (psi)	Permeability (md)
960	8	4	13	11.55	63.75771
960	8	5	11	13.1	25.20485
960	8	5	20	13	54.2414
960	9	4	1	12.1	3.34694
960	9	5	8	13.2	17.23059
960	9	5	18	13	47.66008
960	10	4	0	12.7	0
960	10	7	12	13.3	1.18658
960	10	7	95	13.2	18.31713
960	11	4	18	11.5	96.55164
960	11	5	16	13	41.13183
960	11	5	12	13	28.4429
960	11	5	14	13.1	34.48618
960	12	4	16.5	11.6	85.95828
960	12	5	18	13	47.66008
960	12	5	20	13	54.2414
960	13	4	0	12.5	0
960	13	7	30	13.3	3.82743
960	13	7	50	13.1	9.14275
960	14	4	0	12.5	0
960	14	7	16	13.3	1.72475
960	14	7	95	13.1	18.43862
960	15	4	8	12.1	33.82893
960	15	5	10	13.1	22.18136
960	15	5	6	13.2	12.52197
960	16	4	56	11.3	306.54303
960	16	5	50	13	107.80484
960	16	5	14	13.1	34.48618
960	17	4	55	11.5	297.15814
960	17	3	70	12.2	1161.54382
960	17	3	60	12.3	963.70856
960	17	3	50	12.5	789.79401
960	18	4	0	12.65	0
960	18	5	4	13.3	7.92311
960	18	7	24	13.4	2.86969
960	19	4	0	13	0
960	19	7	34	13.3	4.76642
960	19	7	48	13.3	8.46383
960	20	4	0	12.05	0
960	20	7	60	13.3	11.80636
960	20	5	12	13.2	28.0871
960	21	4	0	12.8	0
960	21	5	8	13.2	17.23059
960	21	5	5	13.3	10.16177
960	21	7	56	13.3	10.69076

Coordinates (feet) X	Y	Tube number	Percent of flow	Pressure (psi)	Permeability (md)

MFP MEASURED PERMEABILITY DATA

GRID C DATA

Coordinates (feet) X	Y	Tube number	Percent of flow	Pressure (psi)	Permeability (md)
4	1	4	25	13.80	118.37946
1	3	6	78	14.3	30.82139
1	3	6	27	14.5	7.68589
1	3	6	13	14.7	2.10768
1	4	6	36	14.4	12.35153
1	4	6	10	14.8	1.214
1	5	6	30	14.7	9.06123
1	5	6	36	14.5	12.28386
1	6	6	19	14.4	4.05371
1	6	6	31	14.3	9.78411
1	7	5	18	14.2	43.01988
1	7	5	14	14.2	31.44975
1	7	5	18	14.2	43.01988
1	8	6	32	14.6	10.13708
1	8	6	29	14.6	8.61896
1	8	5	12	14.4	25.51987
1	11	7	33	14.6	4.08552
1	11	7	65	14	11.68507
1	11	7	53	14.15	9.16992
2	3	6	36	14.4	12.35153
2	3	6	12	14.7	1.80795
2	3	6	14	14.7	2.41166
2	5	6	15	14.7	2.71937
2	5	6	25	14.3	6.79418
2	5	6	29	14.6	8.61896
2	7	4	63	13.8	279.09311
2	7	6	14	14.7	2.41166
2	7	5	13	14.2	28.61105
2	9	5	75	14.1	139.03484
2	9	5	28	14.5	63.36814
2	9	6	28	14.5	8.17498
2	9	6	90	14.3	33.82864
2	10	5	5	14.5	9.26854
2	10	5	29	13.4	69.92488
2	10	5	84	13.15	163.26059
2	10	5	17.5	14.1	41.81478
2	11	5	18	13.3	45.52971
2	11	5	32	13.3	75.65646
2	11	5	14	13.9	31.99793
2	11	5	5	14.6	9.21926
2	13	7	73	13.5	13.40982
2	13	5	9	14	18.28347
2	13	5	14	13.9	31.99793
2	13	5	12	14.3	25.66291
2	13	7	53	14	9.24588
3	2	6	56	14	22.71001
3	2	6	22	14.6	5.25686
3	2	6	18	14.7	3.66136
3	3	6	18	14.7	3.66136
3	3	6	21	14.8	4.73496
3	3	6	14	14.7	2.41166
3	3	6	35	14.5	11.75793
3	3	6	52	14.4	20.2358
3	4	5	43	14.1	88.3517
3	4	6	39	14.4	13.949
3	5	5	17	14.3	39.86481
3	5	6	27	14.6	7.64297
3	5	6	53	14.4	20.71476
3	6	5	12	14.2	25.80797
3	6	5	94	13.9	175.40359
3	7	5	18	14.1	43.28392

Coordinates (feet) X	Y	Tube number	Percent of flow	Pressure (psi)	Permeability (md)
3	7	6	18	14.7	3.66136
3	7	6	31	14.4	9.7296
3	8	6	46	14.5	17.24739
3	8	5	30	14.1	68.96229
3	9	4	50	13.9	230.37314
3	9	4	14	14.2	59.03829
3	10	7	42	14.6	6.12338
3	10	7	17	15	1.60933
3	10	5	12	14	26.10426
3	10	7	18	15	1.72762
3	11	5	15	13.55	35.67588
3	11	5	15	13.9	34.92345
3	11	5	19.5	14.6	46.26831
3	11	5	30	14.15	68.75516
3	12	4	66	12.9	309.77936
3	12	4	70	12.9	326.49924
3	12	4	46	13	230.24782
3	12	4	82	12.8	384.09769
3	12	4	61	12.5	297.84933
4	1	4	35	13.8	170.74991
4	2	6	52	14.3	20.35943
4	2	6	14	14.7	2.41166
4	2	6	30	14.5	9.16131
4	3	6	47	14.4	17.83014
4	3	6	41	14.4	14.95921
4	3	6	14	14.7	2.41166
4	4	6	0	14.7	0
4	4	6	0	14.7	0
4	5	5	43	14.2	87.81989
4	5	6	17	14.3	3.42992
4	5	6	40	14.4	14.4849
4	6	6	40	14.3	14.56501
4	6	5	55	14	106.86218
4	6	5	11	14.2	23.04357
4	7	5	25	14.1	58.92549
4	7	5	37	14.1	79.66366
4	8	5	9	14.4	17.89009
4	8	6	37	14.5	12.81172
4	9	4	14	14.1	59.38125
4	9	4	13	14.2	53.82322
4	10	7	0	15.2	0
4	10	7	20	14.5	2.03747
4	10	7	21	14.3	2.20814
4	10	7	18	14.6	1.77654
4	10	7	19	14.6	1.89932
4	10	7	20	14.6	2.02289
4	11	7	40	14	5.8058
4	11	5	22	13.6	54.77392
4	11	5	4	14.6	7.18725
4	11	7	49	14.6	7.95941
4	11	7	34	14.8	4.25104
4	12	5	22	14.3	52.40255
4	12	5	33	13.9	74.4088
4	12	4	55	12.9	265.93839
4	12	4	99	13.8	431.10098
5	1	6	27	14	7.90945
5	1	5	17	14	40.59379
5	1	6	0	14.8	0
5	1	6	20	14.4	4.38018
5	2	6	20	14.7	4.30255
5	2	6	22	14.6	5.25686

Coordinates (feet) X	Y	Tube number	Percent of flow	Pressure (psi)	Permeability (md)
5	2	5	75	14.1	139.03484
5	2	6	38	14.4	13.41474
5	2	6	18	14.7	3.66136
5	3	6	14	14.6	2.428
5	3	4	10	14.3	38.28164
5	3	6	17	14.7	3.34451
5	4	6	32	14.5	10.19286
5	4	6	41	14.4	14.95921
5	5	5	11	14.4	22.7906
5	5	5	17	14.3	39.86481
5	6	6	35	14.3	11.88851
5	6	6	66	14.2	26.3913
5	6	6	36	14.3	12.4201
5	7	6	15	14.7	2.71937
5	7	6	15	14.7	2.71937
5	7	5	23	14.1	55.00317
5	8	6	11	14.7	1.51315
5	8	5	15	14.3	34.10745
5	9	6	21	14.7	4.76249
5	9	4	65	13.8	286.88351
5	10	7	0	15.5	0
5	10	7	73	14.05	12.99437
5	10	7	0	15	0
5	10	7	0	15.6	0
5	11	7	100	14.2	17.44787
5	11	5	12	13.8	26.40914
5	11	5	6	14.4	11.41503
5	11	5	6	14.6	11.29392
5	11	7	100	14.6	17.03071
5	11	7	75	14.5	13.12708
5	12	4	81	12.8	379.55893
5	12	4	82	12.8	384.09769
5	12	4	95	13.8	413.46509
5	12	3	41	13	590.17383
5	12	3	36	13.25	509.16653
5	12	3	32	13.2	456.36145
5	12	3	40	13.5	553.99286
6	1	5	22	14	53.38999
6	1	6	48	14.2	18.53486
6	2	4	36	14.1	172.38707
6	2	6	42	14.6	15.26294
6	2	5	24	14.2	56.60739
6	3	5	14	14.3	31.26878
6	3	6	70	14.4	27.39489
6	3	6	23	14.6	5.7272
6	4	6	49	14.5	18.68381
6	4	6	10	14.7	1.22421
6	5	6	56	14.4	22.15839
6	5	5	16	14.3	36.97886
6	5	5	23	14.2	54.66257
6	6	5	70	13.8	132.55441
6	6	5	17	14.1	40.34761
6	7	6	27	14.5	7.68589
6	7	6	35	14.4	11.82279
6	8	6	45	14.4	16.86849
6	8	5	24	14.1	56.95913
6	9	4	78	13.8	340.70715
6	9	4	94	13.7	411.87009
6	10	7	58	14.6	10.17276
6	10	7	60	14.6	10.66533
6	10	7	100	14.2	17.44787

Coordinates (feet) X	Y	Tube number	Percent of flow	Pressure (psi)	Permeability (md)
6	10	5	5	14.6	9.21926
6	10	5	12	14.2	25.80797
6	11	7	0	15.5	0
6	11	7	22	14.9	2.25591
6	11	7	47	14.6	7.43028
6	11	7	0	15.2	0
7	1	5	49	14	97.05679
7	1	5	29	14.1	66.92559
7	1	4	50	13.8	231.94383
7	1	4	26	14	121.92503
7	1	5	30	14.1	68.96229
7	2	5	19	14.1	46.22881
7	2	6	78	14.2	31.00653
7	2	6	70	14.3	27.56326
7	3	5	25	14.3	58.20575
7	3	5	8	14.5	15.62214
7	3	5	8	14.4	15.7058
7	3	6	56	14.5	22.02525
7	3	6	70	14.3	27.56326
7	4	6	20	14.7	4.30255
7	4	6	12	14.7	1.80795
7	4	5	85	14.1	154.84763
7	4	5	16	14.2	37.19824
7	4	5	95	14.1	175.86617
7	5	5	25	14.2	58.56296
7	5	5	77	14.2	141.69836
7	5	5	25	14.3	58.20575
7	5	5	16	14.3	36.97886
7	5	6	49	14.4	18.79638
7	6	5	4	14.4	7.26502
7	6	5	14	14.2	31.44975
7	7	5	40	14	84.80281
7	7	5	76	14	141.66524
7	7	5	11	14.3	22.91622
7	7	5	8	14.2	15.87646
7	8	6	32	14.5	10.19286
7	8	6	17	14.7	3.34451
7	9	4	50	13.9	230.37314
7	9	4	19	14.1	86.8748
7	10	3	74	13.9	1069.82178
7	10	3	72	12.8	1118.90308
7	10	3	48	13.05	704.37183
7	10	3	74	13.8	1077.12817
7	11	7	39	14.3	5.4811
7	11	7	84	14.55	14.84364
7	11	5	5	14.5	9.26854
7	11	5	80	13.1	157.62277
7	11	5	56	13.3	113.60707
8	1	6	78	14	31.38468
8	1	6	27	14.5	7.68589
8	2	6	30	14.4	9.21236
8	2	6	32	14.2	10.36475
8	2	5	23	14.3	54.32683
8	2	4	8	14.3	29.86552
8	3	6	53	14.4	20.71476
8	3	5	16	14.3	36.97886
8	3	6	35	14.5	11.75793
8	3	6	21	14.6	4.79039
8	3	6	37	14.4	12.88221
8	4	6	43	14.4	15.91147
8	4	6	0	14.7	0

Coordinates (feet) X	Y	Tube number	Percent of flow	Pressure (psi)	Permeability (md)
8	4	5	38	14.1	81.20724
8	4	5	9	14.4	17.89009
8	4	5	9	14.5	17.79496
8	4.5	6	14	14.7	2.41166
8	4.5	6	23	14.7	5.69452
8	5	4	58	14	256.79202
8	5	5	22	14.4	52.08254
8	5.3	6	43	14.5	15.8213
8	5.3	6	0	14.7	0
8	5.7	5	11	14.2	23.04357
8	5.7	6	80	14	32.20679
8	6	5	72	14	134.5191
8	6	4	60	13.8	267.47556
8	6	4	10	14.2	38.47933
8	6	4	30	14	142.77911
8	6	4	45	13.9	212.4561
8	6	4	46	13.9	215.99706
8	6	4	50	13.9	230.37314
8	7	6	17	14.7	3.34451
8	7	6	27	14.5	7.68589
8	7	5	17	14.7	38.93579
8	7	4	40	13.9	195.08896
8	8	5	9	14.4	17.89009
8	8	5	9	14.5	17.79496
8	9	4	73	13.8	319.28159
8	9	4	90	13.7	394.47751
8	9	4	42	13.9	201.96835
8	10	5	47	13.2	99.26354
8	10	4	55	14.2	242.97417
8	10	4	31	13.4	153.6181
8	10	5	6	14.1	11.60277
8	11	5	30	13.9	69.80658
8	11	5	26	14.55	59.26918
8	11	5	28	14.6	62.99855
8	11	5	15	14.65	33.42871
8	12	5	85	13.3	163.15703
8	12	5	75	13.9	140.73282
8	12	5	16	14.4	36.76234
8	12	5	33	13.6	75.79417
8	12	5	30	14.8	66.19527
8.5	4	5	12	14.4	25.51987
8.5	4	5	10	14.4	20.09822
8.5	4	5	9	14.4	17.89009
8.5	4.5	6	29	14.6	8.61896
8.5	5	5	9	14.4	17.89009
8.5	5	5	6	14.5	11.35408
8.5	5.3	6	48	14.4	18.31269
8.5	5.7	6	48	14.2	18.53486
8.5	6	5	28	14.1	64.90305
8.5	6	6	70	13.9	28.26133
9	2	4	11	14.2	43.56103
9	2	6	30	14.5	9.16131
9	2	6	53	14.3	20.84125
9	3	6	65	14.4	25.74019
9	3	6	34	14.5	11.23404
9	3	5	12	14.5	25.3788
9	4	5	27	14.6	61.03895
9	4	6	0	14.7	0
9	4	6	28	14.6	8.12959
9	4.5	5	14	14.4	31.09026
9	4.5	5	17	14.3	39.86481

Coordinates (feet) X	Y	Tube number	Percent of flow	Pressure (psi)	Permeability (md)
9	5	5	12	14.5	25.3788
9	5	6	15	14.7	2.71937
9	5.3	6	37	14.5	12.81172
9	5.3	5	16	14.2	37.19824
9	5.7	5	60	14.1	114.77042
9	5.7	6	12	14.6	1.8213
9	6	5	18	14.1	43.28392
9	6	5	49	14	97.05679
9	7	5	25	14.1	58.92549
9	7	6	45	14.4	16.86849
9	8	6	27	14.7	7.60062
9	8	5	45	14.1	91.05173
9	9	3	50	13.5	716.14032
9	9	3	43	13.6	596.92255
9	10	5	59	14.6	109.70744
9	10	5	21	14.15	50.95768
9	10	5	58	13.9	112.7082
9	10	5	20	14.7	47.41297
9	11	5	36	13.25	82.31139
9	11	4	34	13.5	168.91454
9	11	4	20	14.3	91.34606
9	11	4	31	13.3	154.58633
9	11	7	21	14.9	2.11771
9.5	4	6	53	14.4	20.71476
9.5	4	6	58	14.3	23.26721
9.5	4.5	5	52	14.2	100.52548
9.5	5	6	0	14.7	0
9.5	5	6	0	14.7	0
9.5	5.3	5	14	14.4	31.09026
9.5	5.3	5	45	14.2	90.49895
9.5	5.7	6	14	14.6	2.428
9.5	5.7	6	25	14.4	6.75512
9.5	6	6	24	14.4	6.27279
9.5	6	6	54	14.2	21.45533
10	3	6	37	14.5	12.81172
10	3	6	38	14.6	13.26903
10	3	6	17	14.7	3.34451
10	4	6	13	14.7	2.10768
10	4	6	27	14.6	7.64297
10	4	6	23	14.6	5.7272
10	4	6	0	14.7	0
10	4.5	6	53	14.4	20.71476
10	4.5	6	31	14.5	9.67582
10	5	5	13	14.5	28.12937
10	5	6	15	14.6	2.73723
10	5.3	6	0	14.7	0
10	5.7	6	0	14.8	0
10	5.7	6	26	14.3	7.28228
10	6	4	70	13.8	306.49515
10	6	4	72	13.9	312.88675
10	7	5	19	14.1	46.22881
10	7	5	11	14.4	22.7906
10	7	5	18	14.2	43.01988
10	7	6	31	14.4	9.7296
10	7	6	17	14.7	3.34451
10	7	6	13	14.7	2.10768
10	8	6	52	14.4	20.2358
10	8	6	53	14.4	20.71476
10	9	3	78	13.2	1195.53479
10	9	3	59	13.4	852.02008
10	9	3	41	13.5	569.60895

Coordinates (feet) X	Y	Tube number	Percent of flow	Pressure (psi)	Permeability (md)
10	10	5	70	13.4	135.90352
10	10	4	69	14.6	287.01099
10	10	4	30	13.6	146.26187
10	10	4	8	14.95	28.90917
10	10	5	27	14.05	63.08938
10	11	5	6	14.2	11.53936
10	11	7	27	15.1	2.92317
10	11	7	50	14.6	8.22523
10	11	5	14	14	31.80917
10	11	5	14	14.1	31.62304
10.5	4.5	6	31	14.5	9.67582
10.5	4.5	6	48	14.3	18.42301
10.5	5	6	0	14.5	0
10.5	5	6	53	14.1	21.09958
10.5	5.3	6	29	14.5	8.66684
10.5	5.3	6	90	14.3	33.82864
10.5	5.7	6	70	14.2	27.73403
10.5	6	6	23	14.5	5.76033
11	3	6	10	14.7	1.22421
11	3	5	24	14.2	56.60739
11	4	5	30	14.2	68.54958
11	4	5	35	14.3	75.68585
11	4	6	41	14.4	14.95921
11	4.5	6	21	14.6	4.79039
11	4.5	6	13	14.7	2.10768
11	5	6	36	14.5	12.28386
11	5	6	32	14.5	10.19286
11	5.3	6	42	14.4	15.43473
11	5.3	5	23	14.3	54.32683
11	5.7	6	16	14.6	3.04981
11	5.7	6	95	14.1	35.09544
11	6	5	30	14.1	68.96229
11	6	5	13	14.2	28.61105
11	7	5	18	14.2	43.01988
11	7	5	32	14.1	71.99387
11	7	5	20	14.1	49.18431
11	8	4	34	14	163.4238
11	8	4	19	14.1	86.8748
11	9	4	19	13.9	87.93598
11	9	4	27	13.9	127.79872
11	10	7	26	15	2.79934
11	10	5	12	15.1	24.57145
11	10	5	12	15.1	24.57145
11	10	7	48	15.2	7.46443
11	11	5	14	14	31.80917
11	11	5	16.5	14.9	37.10367
11	11	5	14	14.95	30.15008
11	11	5	42	14.5	84.95413
11.5	4	5	57	14.2	108.92232
11.5	4	5	54	14.2	103.86252
11.5	4.5	6	25	14.6	6.6786
11.5	4.5	6	0	14.8	0
11.5	4.5	6	26	14.6	7.15925
11.5	5	6	0	14.8	0
11.5	5	6	0	14.8	0
11.5	5.3	4	38	14.1	182.38959
11.5	5.3	6	16	14.8	3.01132
11.5	5.7	6	10	14.7	1.22421
11.5	5.7	6	30	14.4	9.21236
11.5	6	5	34	14.2	74.60543
12	3	6	12	14.7	1.80795
12	3	6	20	14.8	4.27737
12	4	6	89	14.4	33.40654
12	4	6	18	14.7	3.66136
12	4.5	6	17	14.6	3.36542
12	4.5	6	0	14.8	0
12	5	6	32	14.5	10.19286
12	5	6	53	14.4	20.71476
12	5.3	6	18	14.7	3.66136
12	5.3	6	35	14.5	11.75793
12	5.7	6	45	14.3	16.96744
12	5.7	6	32	14.4	10.2494
12	6	5	16	14	37.64591
12	6	5	13	14.2	28.61105
12	6	6	78	14.2	31.00653
12	7	5	44	14.2	89.15943
12	8	5	34	14.2	74.60543
12	8	4	35	14	168.49156
12	8	4	92	13.8	400.40714
12	10	5	32	13.65	73.99857
12	10	5	9	15	17.3373
12	10	5	14	14.85	30.31599
12	10	7	43	14.95	6.26398
12	11	7	58	14.9	10.00727
12	11	7	84	14.9	14.55776
12	11	7	72	14.8	12.25521
12	11	7	74	15.1	12.49717
12	11	7	0	15.6	0
12	12	5	36	13.7	80.02956
12	12	5	46	13.7	94.72826
12	12	5	58	14.8	106.7776
12	12	5	15	15	32.78024
13	3	6	18	14.6	3.6838
13	3	6	38	14.4	13.41474
13	3	6	15	14.7	2.71937
13	4	6	0	14.7	0
13	4	6	17	14.7	3.34451
13	5	6	29	14.5	8.66684
13	6	6	0	14.8	0
13	6	6	22	14.5	5.28757
13	7	5	65	14.1	122.35767
13	7	5	40	14.2	83.79819
13	7	5	45	14.2	90.49895
13	7	6	21	14.7	4.76249
13	9	4	15	14.1	64.71836
13	9	4	73	13.2	332.88815
13	9	3	65	13.2	964.0874
13	9	3	72	13	1102.80188
13	10	7	13	15	1.14572
13	10	7	15	15	1.37546
13	10	7	15	15.5	1.33076
13	10	7	0	15.7	0
13	11	7	54	14.7	9.14551
13	11	5	37	13.8	81.11116
13	11	5	14.5	14.7	31.94347
13	11	5	30	14.1	68.96229
13	12	4	100	14.6	413.55328
13	12	3	45	14.1	608.08893
13	12	3	21	13.4	306.7265
13	12	3	27	13.4	384.1293
13	12	3	33	14.6	429.53049
13	13	7	37	15.2	4.78674

Coordinates (feet) X	Y	Tube number	Percent of flow	Pressure (psi)	Permeability (md)
13	13	7	0	15.6	0
13	13	7	0	15.6	0
13	13	7	24	15.1	2.50287
14	3	6	14	14.7	2.41166
14	3	4	14	14.2	59.03829
14	3	5	9	14.4	17.89009
14	4	4	45	14.1	209.61497
14	4	4	26	14.2	120.49095
14	5	5	23	14.2	54.66257
14	5	5	12	14.4	25.51987
14	6	6	36	14.4	12.35153
14	7	6	80	14.4	31.45644
14	7	6	34	14.7	11.11233
14	8	6	78	14.4	30.6388
14	8	5	20	14.3	48.57771
14	9	3	72	13.2	1087.16345
14	9	3	64	13.2	946.88605
14	9	3	55	13.3	798.93213
14	10	5	30	13.75	70.45698
14	10	5	19	15	43.79646
14	10	5	11	15.2	21.84399
14	10	7	14	15.1	1.2517
14	11	7	0	15.7	0
14	11	7	0	15.7	0
14	11	7	0	15.7	0
14	12	4	45	14.05	210.31656
14	12	4	59	13.3	273.17563
14	12	4	60	13.6	271.16592
14	12	3	15	13.8	214.62988
14	12	3	17	14.65	230.95575
14	12	3	26	13.2	376.11792
14	12	3	38	14.6	490.3717
14	13	7	0	15.8	0
14	13	7	10	15.5	0.78636
14	13	7	40	14.7	5.57612
14	13	7	73	15.2	12.2182
14	14	7	100	13.9	17.77625
14	14	7	100	14.8	16.83046
14	14	5	55	13.6	109.63103
14	14	5	58	14.65	107.70183
14	14	5	36	13.95	78.82501
15	4	4	16	14.2	69.75662
15	4	6	27	14.5	7.68589
15	5	5	17	14.3	39.86481
15	5	6	11	14.5	1.53704
15	6	5	11	14.4	22.7906
15	6	5	11	14.3	22.91622
15	8	6	33	14.6	10.6538
15	8	6	27	14.7	7.60062
15	10	5	51	14.85	95.08611
15	10	5	61	13.75	118.82617
15	10	5	61	14.7	112.24361
15	10	5	61	14.1	116.26559
15	11	5	5	14.65	9.19486
15	11	5	5	15.4	8.84699
15	11	5	23	15	52.10522
15	11	5	70	14.75	125.38691
15	12	5	16	13.85	37.98973
15	12	5	7	14.6	13.40289
15	12	5	13	15.1	27.22277
15	12	5	19	14.7	44.57534
15	13	7	18	15.2	1.70419
15	13	5	13	14.5	28.12937
15	13	5	13	14.4	28.2877
15	13	5	6	14.7	11.23455
15	14	5	5	15.2	8.93656
15	14	5	5	15.2	8.93656
15	14	5	35	14.3	75.68585
16	4	6	18	14.7	3.66136
16	4	6	21	14.6	4.79039
16	5	6	72	14.3	28.37347
16	5	6	13	14.3	2.16835
16	6	6	20	14.6	4.32807
16	6	6	48	14.3	18.42301
16	7	5	13	14.4	28.2877
16	7	6	16	14.7	3.03043
16	8	5	30	14.1	68.96229
16	8	5	15	14.2	34.30727
16	10	5	35	13.4	79.93432
16	10	5	30	14.6	66.9578
16	10	5	60	14.7	110.78021
16	10	5	55	14.8	101.81981
16	11	5	14	13.7	32.38363
16	11	5	95	14.55	170.7122
16	11	5	17	15	38.26929
16	11	7	50	14.9	8.10202
16	12	5	13	14.6	27.97317
16	12	5	53	13.8	104.79003
16	12	5	6	15.15	10.97651
16	12	5	9.5	15.05	18.35843
16	13	5	21	14.1	51.11692
16	13	5	49	14.6	93.57379
16	13	5	20	15	46.57963
16	13	5	34	14.6	72.89049
16	14	5	11	14.55	22.60534
16	14	5	11	15.05	22.01396
16	14	5	16	15	35.52001
16	14	7	60	14.6	10.66533
17	4	6	21	14.6	4.79039
17	4	6	80	14.1	32.01258
17	5	6	20	14.2	4.43375
17	5	5	9	14.4	17.89009
17	6	5	39	14.1	82.75214
17	7	5	23	14.1	55.00317
17	7	5	20	14.3	48.57771
17	8	5	18	14.3	42.75932
17	8	5	63	14.1	119.28931
17	9	5	11	14.1	23.17267
17	9	5	16	14	37.64591
17	10	5	65	14.6	118.85424
17	10	5	27	14.6	61.03895
17	10	5	10.5	15.1	20.66421
17	10	5	27	14.9	59.98972
17	11	7	42	15.35	5.88241
17	11	7	13	15.6	1.10231
17	11	7	11	15.6	0.88715
17	11	7	15	15.3	1.34827
17	12	5	60	14.6	111.41496
17	12	5	41	14.45	83.89035
17	12	5	31	14.6	68.43378
17	12	5	85	14.4	151.90709
17	13	7	100	14.2	17.44787

Coordinates (feet)		Tube	Percent	Pressure	Permeability
X	Y	number	of flow	(psi)	(md)
17	13	7	85	15.1	14.5508
17	13	7	100	14.7	16.92993
17	13	5	13	15.15	27.1504
17	13	7	0	15.6	0
17	14	7	29	14.7	3.28276
17	14	7	13	15.4	1.11639
17	14	7	88	15.1	15.00357
17	14.5	7	75	14.6	13.0559
17	14.5	7	100	14.8	16.83046
17	14.5	5	18	14.2	43.01988
17	14.5	5	25	14.1	58.92549
18	4	6	19	14.7	3.98076
18	4	6	10	14.7	1.22421
18	4	6	44	14.5	16.2955
18	5	5	20	14.3	48.57771
18	5	5	17	14.2	40.10464
18	5	6	63	14.4	25.0822
18	6	4	77	13.9	334.12921
18	6	4	22	14.1	101.82304
18	6	5	14	14.2	31.44975
18	6	5	13	14.3	28.44827
18	6	5	10	14.3	20.20619
18	7	6	49	14.4	18.79638
18	7	5	58	14.1	111.30952
18	8	6	0	14.8	0
18	8	6	27	14.7	7.60062
18	9	5	95	13.8	179.48062
18	10	5	85	14.4	151.90709
18	10	4	17	13.75	77.27659
18	10	5	6	15	11.0609
18	10	5	60	14.6	111.41496
18	11	5	20	13.75	50.28714
18	11	7	51	14.8	8.38036
18	11	7	16	15.4	1.45254
18	11	5	40	14.7	81.38821
18	12	5	23	14.9	52.40934
18	12	5	35	14.85	73.33477
18	12	5	14	15.1	29.90522
18	12	5	6	15.2	10.94873
18	13	5	73	13.6	139.67435
18	13	5	17	14.7	38.93579
18	13	5	6	15.1	11.00446
18	13	5	16	14.6	36.33767
19	6	5	44	14.2	89.15943
19	6	4	50	14	228.82738
19	6	4	23	14.1	106.55104
19	7	6	26	14.7	7.11933
19	7	6	37	14.5	12.81172
19	9	3	80	13	1249.90112
19	9	3	90	12.6	1463.01782
19	9	3	78	13	1212.91223
19	9	3	40	13.4	557.85632
19	9	3	58	13.2	849.08417
19	10	3	32	14.6	417.33731
19	10	3	83	13.7	1238.05762
19	10	3	30	13.6	418.4104
19	10	3	87	13.5	1321.80249
19	11	5	15	13.5	35.78648
19	11	5	50	14.1	97.8103
19	11	5	37	14.9	76.06485
19	11	5	12.5	15.05	25.96164

Coordinates (feet)		Tube	Percent	Pressure	Permeability
X	Y	number	of flow	(psi)	(md)
19	12	4	32	14.65	147.13173
19	12	5	6	14.8	11.17593
19	12	5	20	14.9	46.85371
19	12	5	8	15.1	15.14206
19	13	5	55	13.5	110.35016
19	13	5	80	13.7	151.62561
19	13	5	53	14.15	102.50753
19	13	5	7.5	15.05	14.13371
19	14	7	15	15.5	1.33076
19	14	7	100	15.3	16.35242
20	4	5	65	14.1	122.35767
20	4	4	84	14	361.23633
20	4	4	14	14.3	58.70035
20	4	6	78	14.4	30.6388
20	4	4	63	14	275.35825
20	5	4	82	14	352.90781
20	5	4	92	13.9	397.72192
20	6	6	70	14.2	27.73403
20	6	5	18	14.2	43.01988
20	6	6	31	14.4	9.7296
20	7	6	14	14.7	2.41166
20	7	5	19	14.3	45.66288
20	8	4	74	13.8	323.55524
20	9	3	50	13.2	731.23206
20	9	3	80	12.8	1268.36951
20	9	3	57	13.2	834.19647
21	5	4	55	14	246.21169
21	5	6	12	14.7	1.80795
21	6	6	78	14.4	30.6388
21	6	5	22	14.2	52.72707
21	7	5	70	14.1	130.18553
21	7	5	80	14	148.76257
21	8	6	27	14.7	7.60062
21	8	6	25	14.7	6.6411
21	8	5	30	14.2	68.54958
22	5	5	14	14.2	31.44975
22	5	5	11	14.4	22.7906
22	6	5	25	14.2	58.56296
22	6	5	11	14.3	22.91622

MFP Measured Permeability Data

Grid D Data

Coordinates (feet) X	Y	Tube number	Percent of flow	Pressure (psi)	Permeability (md)
1	1	5	46	13.7	94.72826
1	2	4	100	13	460.3136
1	3	4	80	14.6	331.30521
1	4	4	19	14.8	83.3567
1	5	7	30	14.3	3.5105
1	6	5	13	14.6	27.97317
1	7	5	75	14.8	133.34912
1	8	5	20	14.6	47.69827
1	9	4	26	14.8	116.47495
1	10	5	13	14.6	27.97317
1	11	5	17	15	38.26929
1	12	5	14	14.6	30.74041
1	13	5	22	14.8	50.84629
1	14	5	13	14.9	27.51698
1	15	5	6	15.2	10.94873
1	16	7	59	15.05	10.16498
1	17	7	23	15.4	2.31964
1	18	5	13	15.1	27.22277
1	19	5	9	15.2	17.16223
1	20	5	9	15.2	17.16223
1	21	5	12	15.1	24.57145
1	22	5	16	15	35.52001
1	23	4	46	14.6	206.29167
1	24	4	18	15	77.17626
1	25	7	38	15.15	5.01221
1	26	7	20	15.5	1.90062
1	27	5	23	14.7	53.03053
1	28	4	44	13.4	216.35658
2	1	4	14	14.95	56.62147
2	1	5	10	14.6	19.88651
2	2	5	29	14.6	64.97195
2	4	4	19	14.75	83.59819
2	5	7	28	15.4	3.01174
2	6	4	35	14.6	162.0399
2	7	4	100	14.6	413.55328
2	8	5	17	14.95	38.37864
2	9	5	35	14.4	75.2459
2	10	5	14	15.1	29.90522
2	11	5	38	14.8	77.97269
2	12	7	11	15.4	0.8981
2	13	7	11	15.55	0.88986
2	14	7	38	15.2	4.99857
2	15	7	53	15.2	8.67837
2	16	7	17	15.4	1.56654
2	17	7	15	15.4	1.33946
2	18	5	13	15.2	27.07851
2	19	5	13	14.8	27.66702
2	20	5	11	15.15	21.90028
2	21	5	5	15.3	8.89149
2	22	4	85	14.3	358.22043
2	23	4	12	14.6	47.60909
2	24	7	16	15.45	1.44777
3	1	7	21	15.4	2.048
3	2	7	13	15.5	1.1093
3	3	5	45	14.4	89.4143
3	4	7	27	15.3	2.88882
3	5	7	20	15.4	1.91346
3	6	7	11	15.55	0.88986
3	7	5	51	13.6	102.67908
3	8	5	36	14.6	75.87769
3	9	5	25	14.7	56.8285

Coordinates (feet) X	Y	Tube number	Percent of flow	Pressure (psi)	Permeability (md)
3	10	5	26	14.7	58.7485
3	11	5	13	14.8	27.66702
3	12	5	21	14.6	49.5731
3	13	7	0	15.6	0
3	14	7	34	15.05	4.19144
3	15	7	58	15.2	9.84809
3	16	7	14	15.5	1.21949
3	17	7	100	14.6	17.03071
3	17	5	12	14.6	25.23966
3	18	7	16	15.4	1.45254
3	19	5	14	14.6	30.74041
3	20	7	19	15.4	1.79705
3	21	7	0	15.6	0
3	22	7	32	15.3	3.72054
3	23	7	12	15.5	1.00029
3	24	7	15	15.4	1.33946
4	1	7	20	15	1.96663
4	2	7	100	15.1	16.53989
4	2	5	7	15.1	13.05975
4	3	5	52	14.8	96.96535
4	4	4	76	14.6	314.97064
4	5	7	12	15.5	1.00029
4	6	7	0	15.6	0
4	7	7	35	15	4.41444
4	8	7	22	15	2.24101
4	9	5	10	14.6	19.88651
4	10	4	44	14.7	198.26831
4	11	7	21	15.2	2.07531
4	12	7	43	15.2	6.18232
4	13	7	0	15.6	0
4	14	7	0	15.6	0
4	15	5	15	15	32.78024
4	15	5	5	15.2	8.93656
4	16	7	10	15.5	0.78636
4	17	7	52	15.2	8.44611
4	18	7	10	15.5	0.78636
4	19	7	17	15.25	1.58231
4	20	5	25	14.9	56.16972
4	21	5	15	15	32.78024
4	22	5	9	15.15	17.20558
4	23	5	70	14.2	129.41978
4	24	5	35	14.75	73.75021
1	5	7	14	15.25	1.23941
2	5	7	40	15.1	5.45423
3	5	5	10	14.5	19.99167
4	5	5	6	15.2	10.94873
5	5	7	16	15.35	1.45734
6	5	7	50	15.1	8.02245
7	5	7	40	15.2	5.42474
8	5	7	23	15.3	2.3343
9	5	7	70	15.1	11.63544
10	5	7	54	15.1	8.95689
11	5	7	100	15.1	16.53989
11	5	5	12.5	15	26.03089
12	5	7	72	15.1	12.06567
13	5	7	0	15.5	0
14	5	7	0	15.5	0
15	5	7	19	15.05	1.84038
16	5	7	10	15.5	0.78636
17	5	7	12	15.5	1.00029
18	5	7	12	15.5	1.00029

Coordinates (feet) X	Y	Tube number	Percent of flow	Pressure (psi)	Permeability (md)
19	5	7	11	15.5	0.89259
20	5	7	14	15.4	1.22738
21	5	7	52	15.1	8.48846
22	5	7	0	15.6	0
23	5	7	14	15.1	1.2517
24	5	7	32	15.1	3.76237
25	5	7	20	15.4	1.91346
25	5	7	22	15.3	2.19751
26	5	7	72	15	12.12806
27	5	7	0	15.5	0
28	5	7	48	15.1	7.50156
29	5	7	11	15.5	0.89259
30	5	7	12	15.5	1.00029
31	5	7	15	15.5	1.33076
32	5	7	0	15.6	0
33	5	7	25	15.4	2.59441
34	5	7	0	25.6	0
35	5	7	100	14.5	17.13288
36	5	7	11	15.5	0.89259
37	5	7	0	15.6	0
38	5	7	0	15.6	0
39	5	7	0	15.6	0
40	5	7	100	15.05	16.58752
41	5	7	0	15.6	0
42	5	7	11	15.5	0.89259
43	5	7	13	15.4	1.11639
44	5	7	30	15.4	3.29308
45	5	7	27	15.2	2.90588
46	5	6	22	15.3	5.05303
47	5	7	11	15.5	0.89259
48	5	7	15	15.4	1.33946
1	17	4	60	14.6	253.73215
2	17	4	13	14.6	52.62635
2	17	5	15	14.7	33.33427
3	17	5	60	14.75	110.46707
4	17	5	36	14.55	76.09573
5	17	5	39	14.8	79.44823
6	17	5	30	14.8	66.19527
7	17	5	17	14.95	38.37864
8	17	5	7	15.2	12.99366
9	17	5	12.5	15.1	25.89282
10	17	5	6	15.2	10.94873
11	17	5	7	15.15	13.0266
12	17	7	16	15.35	1.45734
13	17	7	22	15.25	2.20464
14	17	7	41	15.15	5.69139
15	17	7	26	15.3	2.74915
16	17	7	65	14.75	11.21007
17	17	5	44	13.8	91.37039
18	17	5	7	15.05	13.09311
19	17	5	40	14.7	81.38821
20	17	5	37	14.8	76.49599
21	17	5	82	14.65	145.52176
24	17	5	16	14.9	35.72062
25	17	5	14	15	30.06794
26	17	7	60	15.1	10.3754
27	17	4	47	14.6	209.70229
28	17	5	10	15.1	19.38071
29	17	5	13	13.85	29.19918
30	17	7	42	15.15	5.94441
31	17	7	18	15.4	1.68139
32	17	7	60	15.1	10.3754
33	17	7	26	15.3	2.74915
34	17	5	51	14.7	95.92674
35	17	5	30	14.75	66.38392
36	17	5	25	14.9	56.16972
37	17	7	25	15.3	2.61015
38	17	7	52	15.15	8.46722
39	17	5	20	14.9	46.85371
40	17	7	32	15.3	3.72054
41	17	5	16	14.8	35.92372
42	17	7	100	14.7	16.92993
42	17	5	3	15	5.09934
43	17	7	41	15.2	5.67622
44	17	5	21	14.75	49.13027
45	17	5	61	14.7	112.24361
46	17	5	5	15.1	8.9822
46	17	7	100	14.5	17.13288

Appendix B

Core Plug Permeability and Porosity Data

APPENDIX B

Core plug porosity and permeability table

Coordinates X	Coordinates Y	Porosity (ϕ)	Permeability (md)	Coordinates X	Coordinates Y	Porosity (ϕ)	Permeability (md)
25	4	3.6	0.12	1428	6	4.1	0.03
25	9	19.1	116.	1428	8	7.3	0.08
25	10	19.8	127.	1428	9	13.7	62.62
25	11	20.8	15.27	1428	10	19.5	567.
25	12	24.6	69.82	1428	14	18.4	129.
25	12	18.	58.28	1428	15	18.4	880.
25	18	8.4	5.5	1428	16	19.6	333.
25	19	9.5	5.26	1428	16	17.5	616.
25	21	4.6	0.28	1428	17	21.	774.
25	22	12.4	5.16	1428	18	18.	776.
240	2	13.	2.58	1428	19	12.	1.64
240	8	12.7	2.92	1428	20	9.	55.6
240	12	18.8	159.	1428	20	4.1	1.37
240	13	15.6	13.67	2125	5	1.3	0.03
240	15	11.9	26.41	2125	6	4.8	0.04
240	20	10.5	1.01	2125	8	11.4	40.7
240	21	13.4	6.36	2125	10	7.7	39.5
240	22	9.2	3.2	2125	11	12.2	8.22
455	2	9.5	13.51	2125	12	9.3	22.53
455	3	9.4	0.33	2125	13	11.1	150.
455	7	8.5	0.71	2125	14	12.3	71.01
455	9	7.8	5.27	2125	15	9.4	0.15
455	10	11.	3.98	2125	16	5.7	0.22
455	11	13.	11.99	2125	17	11.4	5.87
455	13	11.1	26.61	2125	18	8.3	8.5
455	14	13.7	18.18	2125	19	9.5	55.5
455	15	10.9	11.67	2633	4	7.9	1.83
455	16	14.3	10.57	2633	5	6.7	0.06
455	17	12.7	21.	2633	6	5.6	13.
455	18	10.2	16.42	2633	6	5.4	0.1
455	19	11.8	26.1	2633	7	7.5	0.61
455	20	11.8	30.84	2633	8	7.4	0.75
455	21	9.4	16.36	2633	9	11.9	4.51
455	21	10.2	43.59	2633	10	5.5	0.19
1428	2	5.8	0.01	2633	11	13.3	9.42
1428	3	6.5	0.47	2633	12	8.6	1.74
1428	4	6.4	0.03	2633	13	10.7	0.22
1428	5	4.4	0.01	2633	15	11.5	3.33

APPENDIX C

PERMEABILITY CALCULATION PROGRAM AND INPUT INSTRUCTIONS

Program NEWCALC (from BKCALC: Goggin, unpublished)

```
      PROGRAM BKCALC
C  ****************************************************************************************
C  VARIABLE DEFINITION:
C     ATMPR:    ATMOSPHERIC PRESSURE, PSIA
C     BPMMHG:   BAROMETRIC PRESSURE, MM HG
C     CORED:    CORE DIAMETER, CM
C     COREL:    CORE LENGTH, CM
C     CORER:    CORE RADIUS, CM
C     DELP:     PRESSURE DROP, ATM
C     FRC:      MATRIX OF FLOWMETER CALIBRATION VALUES
C     IMETER:   INDEX OF METER USED, 1-8
C     ITYPE:    1 = CONVENTIONAL 1-D CORE PLUG MEASUREMENT
C               2 = FIELD PERMEAMETER MEASUREMENT
C     ISYSPL:   0 = SYSTEM PRESSURE LOSS ASSUMED ZERO
C               1 = SYSTEM PRESSURE LOSS (PSIG) IS OBTAINED FROM THE MATRIX PL(IMETER,NCP)
C                  WHICH IS USED IN THE TABLE LOOKUP ROUTINE SYSPL. THE INTERPOLATED VALUES
C                  ARE DETERMINED AS A FUNCTION OF THE GIVEN ROTAMETER READING.
C     IMODE:    1 = FLOW RATE IN %FS FROM ROTAMETERS. FLOW RATE IN STANDARD (CC/SEC) IS
C                  OBTAINED FROM THE MANUFACTURER'S RATING FOR ROTAMETER #IM. A SIMPLE BOLYE'S
C                  LAW CORRECTION IS USED TO ACCOUNT FOR THE EFFECT OF SYSTEM PRESSURE ON RATE.
C               2 = FLOW RATE IN %FS FROM ROTAMETERS. FLOWRATE IN (CC/SEC) IS OBTAINED FROM
C                  THE RINTM AND RSLPM MATRICES USED IN THE ROUTINE FRCAL.
C               3 = FLOW RATE IN SCCM/SEC FROM BUBBLE METER. NO ADJUSTMENT FOR SYSTEM PRESSURE.
C     NDATA:    NUMBER OF DATA POINTS
C     NSETS:    NUMBER OF DATA SETS
C     PERMA:    CALCULATED VALUE OF AIR PERMEABILITY, MD
C     PL:       MATRIX OF PRESSURE LOSS VALUES
C     RMETER:   FLOWMETER CONVERSION CONSTANTS
C     VIS:      VISCOSITY OF NITROGEN AT 70F, CP
C     XCOORD:   COORDINATE ON X-AXIS
C     YCOORD:   COORDINATE ON Y-AXIS
C  ****************************************************************************************
      COMMON/CALIB/PLM(10,10),RINTM(10,10),RSLPM(10,10),RMETER(10)
      COMMON/CNTRL1/NSETS,ITYPE,IDIM,IKREL
      COMMON/CNTRL2/ISYSPL,ILEAK,IHVC,IMODE
      COMMON/CNTRL3/IHVPLT,IDSPL
      COMMON/CURVE/GRATIO(50),REYGA2(50),B(50),C(50),D(50),NCPTS
      COMMON/DATA1/IMETER(5000),RAWPR(5000),RAWFR(5000),IDATA,NDATA
      COMMON/DATA2/PINV(5000),PERMA(5000),XDATA(5000),YDATA(5000)
      COMMON/DATA3/ARAD,GEOM,AREA,BPMMHG,CORED,COREL
      COMMON/DATA4/ACONST,AEXP,BCONST,BEXP,ALPHA,BETA,STEMP
      COMMON/DATA5/XZEROP,YZEROP,ZZEROP,DELXP,DELYP,DELZP
      COMMON/DATA6/XPOSN(5000),YPOSN(5000),ZPOSN(5000)
      COMMON/GFACT/HSGEOM(50),BD(50),BGF(50),CGF(50),DGF(50),NHSG
      COMMON/TITLE/ILABEL(5)
      COMMON/PFUN2/FRMASS,PATM0,PATM1,PRPSI
      COMMON/INPUT/TUBE(5000),F(5000),P(5000)
C
      CALL START
      DO 100 I=1,NSETS
        CALL DATSET
        CALL REPORT
  100 CONTINUE
C
      STOP
      END
C
C  ****************************************************************************************
      SUBROUTINE START
C  ****************************************************************************************
      COMMON/CALIB/PLM(10,10),RINTM(10,10),RSLPM(10,10),RMETER(10)
      COMMON/CNTRL1/NSETS,ITYPE,IDIM,IKREL
      COMMON/CNTRL2/ISYSPL,ILEAK,IHVC,IMODE
      COMMON/CNTRL3/IHVPLT,IDSPL
      COMMON/CURVE/GRATIO(50),REYGA2(50),B(50),C(50),D(50),NCPTS
      COMMON/DATA1/IMETER(5000),RAWPR(5000),RAWFR(5000),IDATA,NDATA
      COMMON/DATA2/PINV(5000),PERMA(5000),XDATA(5000),YDATA(5000)
      COMMON/DATA3/ARAD,GEOM,AREA,BPMMHG,CORED,COREL
      COMMON/DATA4/ACONST,AEXP,BCONST,BEXP,ALPHA,BETA,STEMP
      COMMON/DATA5/XZEROP,YZEROP,ZZEROP,DELXP,DELYP,DELZP
```

```
      COMMON/DATA6/XPOSN(5000),YPOSN(5000),ZPOSN(5000)
      COMMON/GFACT/HSGEOM(50),BD(50),BGF(50),CGF(50),DGF(50),NHSG
      COMMON/TITLE/ILABEL(5)
      COMMON/PFUN2/FRMASS,PATM0,PATM1,PRPSI
      COMMON/INPUT/TUBE(5000),F(5000),P(5000)
C ++++++++++++++++++++++++++++++++++++++++++++++++++++++++++++++++++++++++++++++++++++++++++++
C     SET THE MANUFACTURER'S FULL SCALE RATING OF EACH ROTAMETER (CM3/SEC)
C ++++++++++++++++++++++++++++++++++++++++++++++++++++++++++++++++++++++++++++++++++++++++++++
      RMETER(1)=471.94744
      RMETER(2)=165.18161
      RMETER(3)=55.060535
      RMETER(4)=21.237635
      RMETER(5)=8.6523698
      RMETER(6)=130./60.
      RMETER(7)=80./60.
      RMETER(8)=315./60.
      RMETER(9)=1150./60.
      RMETER(10)=12000./60.
      STEMP=60.
C ++++++++++++++++++++++++++++++++++++++++++++++++++++++++++++++++++++++++++++++++++++++++++++
C     INPUT PROGRAM CONTROL PARAMETERS
C ++++++++++++++++++++++++++++++++++++++++++++++++++++++++++++++++++++++++++++++++++++++++++++
      OPEN(5,FILE='INPUT.DAT',STATUS='OLD')
      READ(5,*) NSETS
      WRITE(*,999) NSETS
 999  FORMAT(2X,'SUBROUTINE START   NSETS =',I4)
C ++++++++++++++++++++++++++++++++++++++++++++++++++++++++++++++++++++++++++++++++++++++++++++
C     INPUT PRESSURE LOSS AND FLOW RATE CALIBRATION MATRICES. NOTE: SUBROUTINES SYSPL AND FRCAL
C        EXPECT THE MATRIX DATA TO BE FIXED ACCORDING TO SUCCESSIVE 10% FS (FULL SCALE)
C        INCREMENTS OF THE ROTAMETER TUBE OR MASS FLOW CONTROLLER RESPONSE.  SYSTEM PRESSURE
C        LOSSES INCLUDE ALL LOSSES IN THE TUBING, VALVES OR TIP SEAL DOWNSTREAM OF THE PRESSURE
C        SENSOR AND UPSTREAM OF THE POINT OF INJECTION IN UNITS OF PSIG.  THE FLOW CALIBRATION
C        CONSISTS OF TWO MATRICES (RINTM AND RSLPM) WHICH STORE THE INTERCEPT AND SLOPES OF A
C        LINEAR-FIT OF FLOW RATE (SCCS) AGAINST SYSTEM OPERATING PRESSURE (PSIG) FOR A FIXED
C        %FS READING.  FOR EXAMPLE, A CALIBRATION EXPERIMENT WAS PERFORMED ON TUBE #10.  THE
C        ROTAMETER FLOAT WAS MAINTAINED AT 20% FS FOR A SERIES OF FLOW RATE VS. SYSTEM
C        OPERATING PRESSURE MEASUREMENTS.  A LINEAR-FIT OF THESE MEASUREMENTS GAVE AN INTERCEPT
C        OF 3 STD CC/SEC AND A SLOPE OF 0.15 CC/SEC-PSIG. THE MINT AND RSLPM MATRIX ENTRIES
C        ARE AS FOLLOWS:
C             RINTM(10,2) = 3.0
C             RSLPM(10,2) = 0.15
C        FLOW CALIBRATION IS EXPECTED IN SCCM/SEC (60 °F AND 14.696 PSIA)
C ++++++++++++++++++++++++++++++++++++++++++++++++++++++++++++++++++++++++++++++++++++++++++++
      OPEN(1,FILE='CALF.DAT',STATUS='OLD')
      DO 110 ICP=1,10
        READ(1,*) (PLM(IM,ICP),IM=1,10)
 110    CONTINUE
      DO 120 IM=1,10
       READ(1,*) (RINTM(IM,ICP),ICP=1,10)
 120    CONTINUE
      DO 130 IM=1,10
       READ(1,*) (RSLPM(IM,ICP),ICP=1,10)
 130  CONTINUE
      CLOSE(1)
C ++++++++++++++++++++++++++++++++++++++++++++++++++++++++++++++++++++++++++++++++++++++++++++
C     INPUT DATA FROM DIGITIZED (GAPP/G0) VERSUS (NRE/(PI*G0)**2) CURVE.  THEN, COMPUTE CUBIC
C        SPLINE KNOTS FOR EACH POINT ON CURVE.
C ++++++++++++++++++++++++++++++++++++++++++++++++++++++++++++++++++++++++++++++++++++++++++++
      OPEN(2,FILE='GAPP.DAT',STATUS='OLD')
      READ(2,*) NCPTS
      DO 140 I=1,NCPTS
        READ(2,*) REYGA2(I),GRATIO(I)
 140  CONTINUE
      CALL SPLINE(NCPTS,REYGA2,GRATIO,B,C,D)
C ++++++++++++++++++++++++++++++++++++++++++++++++++++++++++++++++++++++++++++++++++++++++++++
C     INPUT THE COEFFICIENTS AND EXPONENTS OF THE USER-DEFINED POWER-LAW RELATIONSHIPS BETWEEN
C       THE LIQUID PERMEABILITY (K0) AND ALPHA OR BETA.  THE GENERIC FORMS ARE TAKEN TO BE:
C             ALPHA=ACONST*(K0)**AEXP  -- (1/CM)
C             BETA =BCONST*(K0)**BEXP  -- (ATM)
C ++++++++++++++++++++++++++++++++++++++++++++++++++++++++++++++++++++++++++++++++++++++++++++
```

```
      READ(5,*) ACONST,AEXP
      READ(5,*) BCONST,BEXP
C
      RETURN
      END
C
C ***********************************************************************************
      SUBROUTINE DATSET
C ***********************************************************************************
      COMMON/CALIB/PLM(10,10),RINTM(10,10),RSLPM(10,10),RMETER(10)
      COMMON/CNTRL1/NSETS,ITYPE,IDIM,IKREL
      COMMON/CNTRL2/ISYSPL,ILEAK,IHVC,IMODE
      COMMON/CNTRL3/IHVPLT,IDSPL
      COMMON/CURVE/GRATIO(50),REYGA2(50),B(50),C(50),D(50),NCPTS
      COMMON/DATA1/IMETER(5000),RAWPR(5000),RAWFR(5000),IDATA,NDATA
      COMMON/DATA2/PINV(5000),PERMA(5000),XDATA(5000),YDATA(5000)
      COMMON/DATA3/ARAD,GEOM,AREA,BPMMHG,CORED,COREL
      COMMON/DATA4/ACONST,AEXP,BCONST,BEXP,ALPHA,BETA,STEMP
      COMMON/DATA5/XZEROP,YZEROP,ZZEROP,DELXP,DELYP,DELZP
      COMMON/DATA6/XPOSN(5000),YPOSN(5000),ZPOSN(5000)
      COMMON/GFACT/HSGEOM(50),BD(50),BGF(50),CGF(50),DGF(50),NHSG
      COMMON/TITLE/ILABEL(5)
      COMMON/PFUN2/FRMASS,PATM0,PATM1,PRPSI
      COMMON/INPUT/TUBE(5000),F(5000),P(5000)
C
      PI = 2.*ACOS(0.)
      VIS=0.0178
C ++++++++++++++++++++++++++++++++++++++++++++++++++++++++++++++++++++++++++++++++++
C READ CONTROL PARAMETERS  DETERMINE THE DIMENSION OF INPUT DATA:
C   IDIM=2:  2-D DATA FROM AN AREAL GRID PATTERN (X,Y)
C ++++++++++++++++++++++++++++++++++++++++++++++++++++++++++++++++++++++++++++++++++
      READ(5,*) ITYPE,IDIM,ISYSPL,ILEAK,IHVC,IHVPLT,IDSPL
      IF(IDIM.GE.1) READ(5,*) XZEROP,DELXP
      IF(IDIM.GE.2) READ(5,*) YZEROP,DELYP
      IF(IDIM.EQ.3) READ(5,*) ZZEROP,DELZP
C
      IF(ITYPE.EQ.2) GO TO 150
C ++++++++++++++++++++++++++++++++++++++++++++++++++++++++++++++++++++++++++++++++++
C ITYPE = 2  FIELD MFP MEASUREMENTS
C ++++++++++++++++++++++++++++++++++++++++++++++++++++++++++++++++++++++++++++++++++
  150 CONTINUE
      READ(5,5000) (ILABEL(J),J=1,5)
      READ(5,*) NDATA,ARAD,GEOM,BPMMHG,IMODE
      ATMPR=14.696*(BPMMHG/760.)
      AREA=PI*ARAD**2
      WRITE(*,990) NDATA
 990  FORMAT(2X,'SUBROUTINE DATASET   NDATA =',I4)
C
      DO 170 IDATA=1,NDATA
        IM=0
        CSYSPL=0.0
        FRM=0.0
        DP=0.0
       IM=0
        READ(5,*) XLOC,YLOC,IM,FRM,DP
       TUBE(IDATA)=IM
       F(IDATA)=FRM
       P(IDATA)=DP
        XPOSN(IDATA)=XZEROP+XLOC*DELXP
        YPOSN(IDATA)=YZEROP+YLOC*DELYP
C        IF(ISYSPL.EQ.1) CALL SYSPL(IM,FRM,CSYSPL)
        CALL FRCAL(IM,FRM,DP,CSYSPL,CFR)
C        IF(ILEAK.EQ.1) CALL SYSLEAK(IM,FRM,DP,CFR)
C
        P0=(BPMMHG/760.)
        P1=(DP-CSYSPL+ATMPR)/14.696
        DELP=P1**2-P0**2
        IMETER(IDATA)=IM
        RAWPR(IDATA)=P1
        RAWFR(IDATA)=CFR
```

```
        PINV(IDATA)=2./(P0+P1)
        PERMA(IDATA)=(2.*CFR*VIS)/(ARAD*GEOM*DELP)
       WRITE(*,*) PERMA(IDATA),IDATA
        XDATA(IDATA)=0.001183*(CFR/AREA)/VIS
       IF(PERMA(IDATA).EQ.0.0000)THEN
          YDATA(IDATA)=1./(0.00000000000000000001)
       ELSE
          YDATA(IDATA)=1./PERMA(IDATA)
       ENDIF
C
        IF(IHVC.EQ.1) CALL HVCORR
C
 170  CONTINUE
C
 5000 FORMAT(5A10)
C
      CLOSE(5)
C
      RETURN
      END
C
C  ******************************************************************************************
      SUBROUTINE REPORT
C  ******************************************************************************************
      COMMON/CALIB/PLM(10,10),RINTM(10,10),RSLPM(10,10),RMETER(10)
      COMMON/CNTRL1/NSETS,ITYPE,IDIM,IKREL
      COMMON/CNTRL2/ISYSPL,ILEAK,IHVC,IMODE
      COMMON/CNTRL3/IHVPLT,IDSPL
      COMMON/CURVE/GRATIO(50),REYGA2(50),B(50),C(50),D(50),NCPTS
      COMMON/DATA1/IMETER(5000),RAWPR(5000),RAWFR(5000),IDATA,NDATA
      COMMON/DATA2/PINV(5000),PERMA(5000),XDATA(5000),YDATA(5000)
      COMMON/DATA3/ARAD,GEOM,AREA,BPMMHG,CORED,COREL
      COMMON/DATA4/ACONST,AEXP,BCONST,BEXP,ALPHA,BETA,STEMP
      COMMON/DATA5/XZEROP,YZEROP,ZZEROP,DELXP,DELYP,DELZP
      COMMON/DATA6/XPOSN(5000),YPOSN(5000),ZPOSN(5000)
      COMMON/GFACT/HSGEOM(50),BD(50),BGF(50),CGF(50),DGF(50),NHSG
      COMMON/TITLE/ILABEL(5)
      COMMON/PFUN2/FRMASS,PATM0,PATM1,PRPSI
      COMMON/INPUT/TUBE(5000),F(5000),P(5000)
      REAL Z
C
      OPEN(6,FILE='OUTPUT.DAT',STATUS='NEW')
      OPEN(7,FILE='KOUT.DAT',STATUS='NEW')
C
C  ++++++++++++++++++++++++++++++++++++++++++++++++++++++++++++++++++++++++++++++++++++++++++
C  ITYPE = 2      MFP MEASUREMENT OF PERMEABILITY
C    IMODE = 1
C    IMODE = 2
C  FLOWRATE IN % FS FROM ROTAMETERS
C  ++++++++++++++++++++++++++++++++++++++++++++++++++++++++++++++++++++++++++++++++++++++++++
      Z=0.
      DO 200 J=1,NDATA
      Z=PERMA(J)*1000.
        WRITE(6,6600) J,IMETER(J),RAWFR(J),RAWPR(J),PINV(J),
     &               Z,XDATA(J),YDATA(J)
        WRITE(7,7000) XPOSN(J),YPOSN(J),TUBE(J),F(J),P(J),Z
      Z=0.
 200  CONTINUE
C  ******************************************************************************************
C  FORMAT STATEMENTS
C  ******************************************************************************************
 6600 FORMAT(3X,I3,6X,I3,4X,G12.5,1X,G12.5,1X,G12.5,1X,G12.5,
     +       2X,G12.5,10X,G12.5)
 7000 FORMAT(1X,2F12.5,2X,I4,2F8.2,2X,F12.5)
C  ******************************************************************************************
      CLOSE(6)
C
      RETURN
      END
C
```

```
C ******************************************************************************************
      SUBROUTINE FRCAL(IM,FRM,DP,CSYSPL,CFR)
C ******************************************************************************************
      COMMON/CALIB/PLM(10,10),RINTM(10,10),RSLPM(10,10),RMETER(10)
      COMMON/CNTRL1/NSETS,ITYPE,IDIM,IKREL
      COMMON/CNTRL2/ISYSPL,ILEAK,IHVC,IMODE
      COMMON/CNTRL3/IHVPLT,IDSPL
      COMMON/CURVE/GRATIO(50),REYGA2(50),B(50),C(50),D(50),NCPTS
      COMMON/DATA1/IMETER(5000),RAWPR(5000),RAWFR(5000),IDATA,NDATA
      COMMON/DATA2/PINV(5000),PERMA(5000),XDATA(5000),YDATA(5000)
      COMMON/DATA3/ARAD,GEOM,AREA,BPMMHG,CORED,COREL
      COMMON/DATA4/ACONST,AEXP,BCONST,BEXP,ALPHA,BETA,STEMP
      COMMON/DATA5/XZEROP,YZEROP,ZZEROP,DELXP,DELYP,DELZP
      COMMON/DATA6/XPOSN(5000),YPOSN(5000),ZPOSN(5000)
      COMMON/GFACT/HSGEOM(50),BD(50),BGF(50),CGF(50),DGF(50),NHSG
      COMMON/TITLE/ILABEL(5)
      COMMON/PFUN2/FRMASS,PATM0,PATM1,PRPSI
      COMMON/INPUT/TUBE(5000),F(5000),P(5000)
C
      IF(IMODE-2) 10,50,90
C
   10 CONTINUE
      IF(ITYPE.EQ.1) P1=(DP-CSYSPL/2.+14.696*(BPMMHG/760.))/14.696
      IF(ITYPE.EQ.2) P1=(DP-CSYSPL+14.696*(BPMMHG/760.))/14.696
      CFR=P1*FRM*RMETER(IM)/100.
      RETURN
C
   50 CONTINUE
      IF(FRM.LE.10.) GO TO 80
      IF(FRM.GE.100.) GO TO 85
      ITEST=INT(FRM/10.)
C
   60 CONTINUE
      FR1=10.*FLOAT(ITEST)
      FR2=10.*FLOAT(ITEST+1)
      IF(FRM.LT.FR1) GO TO 70
      IF(FRM.GE.FR2) GO TO 75
      FRAC=(RINTM(IM,ITEST+1)-RINTM(IM,ITEST))/(FR2-FR1)
      FINT=RINTM(IM,ITEST)+(FRM-FR1)*FRAC
      FRAC=(RSLPM(IM,ITEST+1)-RSLPM(IM,ITEST))/(FR2-FR1)
      FSLP=RSLPM(IM,ITEST)+(FRM-FR1)*FRAC
      CFR=FINT+FSLP*DP
      RETURN
C
   70 ITEST=ITEST-1
      IF(ITEST.EQ.0) GO TO 80
      GO TO 60
C
   75 ITEST=ITEST+1
      IF(ITEST.GE.10) GO TO 85
      GO TO 60
C
   80 CONTINUE
      FINT=FRM*RINTM(IM,1)/10.
      FSLP=FRM*RSLPM(IM,1)/10.
      CFR=FINT+FSLP*DP
      RETURN
C
   85 CONTINUE
      FRAC=(RINTM(IM,10)-RINTM(IM,9))/10.
      FINT=RINTM(IM,10)+(FRM-100.)*FRAC
      FRAC=(RSLPM(IM,10)-RSLPM(IM,9))/10.
      FSLP=RSLPM(IM,10)+(FRM-100.)*FRAC
      CFR=FINT+FSLP*DP
      RETURN
C
   90 CONTINUE
      CFR=FRM
      RETURN
      END
```

```
C
C **************************************************************************************
      SUBROUTINE HVCORR
C **************************************************************************************
      COMMON/CALIB/PLM(10,10),RINTM(10,10),RSLPM(10,10),RMETER(10)
      COMMON/CNTRL1/NSETS,ITYPE,IDIM,IKREL
      COMMON/CNTRL2/ISYSPL,ILEAK,IHVC,IMODE
      COMMON/CNTRL3/IHVPLT,IDSPL
      COMMON/CURVE/GRATIO(50),REYGA2(50),B(50),C(50),D(50),NCPTS
      COMMON/DATA1/IMETER(5000),RAWPR(5000),RAWFR(5000),IDATA,NDATA
      COMMON/DATA2/PINV(5000),PERMA(5000),XDATA(5000),YDATA(5000)
      COMMON/DATA3/ARAD,GEOM,AREA,BPMMHG,CORED,COREL
      COMMON/DATA4/ACONST,AEXP,BCONST,BEXP,ALPHA,BETA,STEMP
      COMMON/DATA5/XZEROP,YZEROP,ZZEROP,DELXP,DELYP,DELZP
      COMMON/DATA6/XPOSN(5000),YPOSN(5000),ZPOSN(5000)
      COMMON/GFACT/HSGEOM(50),BD(50),BGF(50),CGF(50),DGF(50),NHSG
      COMMON/TITLE/ILABEL(5)
      COMMON/PFUN2/FRMASS,PATM0,PATM1,PRPSI
      COMMON/INPUT/TUBE(5000),F(5000),P(5000)
C
      MAXIT=100
      PERMTOL=1.0E-6
C
      NITER=0
      TOL=1.E-6
      T=STEMP
      TCN2=227.
      PCN2=493.
C
      GFACT=GEOM
      FRMASS=0.001183*RAWFR(IDATA)
      PERM0=PERMA(IDATA)
C
      PATM0=BPMMHG/760.
      PATM1=RAWPR(IDATA)
      PRPSI=PATM1*14.696
C
 400  NITER=NITER+1
      ALPHA=ACONST
      BETA=BCONST
      IF(PERM0.LT.TOL) GO TO 410
      ALPHA=ACONST*PERM0**AEXP
      BETA=BCONST*PERM0**BEXP
 410  CONTINUE
      CALL PPHI(PATM0,PPHI0)
      CALL PPHI(PATM1,PPHI1)
      DMPHI=PPHI1-PPHI0
      CALL ZFACT(PRPSI,T,PCN2,TCN2,Z)
      CALL GASVIS(PRPSI,T,PCN2,TCN2,Z,GV)
C
      XDATA(IDATA)=1.E-7*(ALPHA*(1.+BETA/PATM1)*PERM0*PERM0*
     +                    DMPHI)/(ARAD*GV)
      IF(XDATA(IDATA).GE.TOL) GO TO 420
      YDATA(IDATA)=1.
      IF(XDATA(IDATA).GE.1.E-10) RETURN
      PERMA(IDATA)=FRMASS/(ARAD*GEOM*DMPHI)
      RETURN
C
 420  CONTINUE
      YDATA(IDATA)=SEVAL(NCPTS,XDATA(IDATA),REYGA2,GRATIO,B,C,D)
      GFACT=YDATA(IDATA)*GEOM
      PERM1=FRMASS/(ARAD*GFACT*DMPHI)
      PERMA(IDATA)=PERM1
      PRATIO=ABS((PERM1-PERM0)/PERM1)
      IF(PRATIO.LE.PERMTOL) RETURN
C      WRITE(3,3000) NITER,PERM1,PERMTOL
      IF(NITER.GE.MAXIT) RETURN
      PERM0=PERM1
      GO TO 400
C
```

```
      END
C
C ******************************************************************************
      SUBROUTINE SPLINE (N, X, Y, B, C, D)
C ******************************************************************************
      INTEGER N
      REAL X(N), Y(N), B(N), C(N), D(N)
C ++++++++++++++++++++++++++++++++++++++++++++++++++++++++++++++++++++++++++++++
C  THE COEFFICIENTS B(I), C(I), AND D(I), I=1,2,...,N ARE COMPUTED FOR A CUBIC INTERPOLATING
C    SPLINE  ---  S(X) = Y(I) + B(I)*(X-X(I)) + C(I)*(X-X(I))**2 + D(I)*(X-X(I))**3
C    FOR  X(I) .LE. X .LE. X(I+1)
C  INPUT...     N = THE NUMBER OF DATA POINTS OR KNOTS (N.GE.2)
C               X = THE ABSCISSAS OF THE KNOTS IN STRICTLY INCREASING ORDER
C               Y = THE ORDINATES OF THE KNOTS
C  OUTPUT..    B, C, D  = ARRAYS OF SPLINE COEFFICIENTS AS DEFINED ABOVE.
C  USING  P  TO DENOTE DIFFERENTIATION,
C      Y(I) = S(X(I))
C      B(I) = SP(X(I))
C      C(I) = SPP(X(I))/2
C      D(I) = SPPP(X(I))/6  (DERIVATIVE FROM THE RIGHT)
C  THE ACCOMPANYING FUNCTION SUBPROGRAM  SEVAL  CAN BE USED TO EVALUATE THE SPLINE.
C ++++++++++++++++++++++++++++++++++++++++++++++++++++++++++++++++++++++++++++++
      INTEGER NM1, IB, I
      REAL T
C
      NM1 = N-1
      IF ( N .LT. 2 ) RETURN
      IF ( N .LT. 3 ) GO TO 550
C ++++++++++++++++++++++++++++++++++++++++++++++++++++++++++++++++++++++++++++++
C  SET UP TRIDIAGONAL SYSTEM  B = DIAGONAL, D = OFFDIAGONAL, C = RIGHT HAND SIDE.
C ++++++++++++++++++++++++++++++++++++++++++++++++++++++++++++++++++++++++++++++
      D(1) = X(2) - X(1)
      C(2) = (Y(2) - Y(1))/D(1)
      DO 500 I = 2, NM1
         D(I) = X(I+1) - X(I)
         B(I) = 2.*(D(I-1) + D(I))
         C(I+1) = (Y(I+1) - Y(I))/D(I)
         C(I) = C(I+1) - C(I)
  500 CONTINUE
C ++++++++++++++++++++++++++++++++++++++++++++++++++++++++++++++++++++++++++++++
C  END CONDITIONS. THIRD DERIVATIVES AT X(1) AND X(N) OBTAINED FROM DIVIDED DIFFERENCES.
C ++++++++++++++++++++++++++++++++++++++++++++++++++++++++++++++++++++++++++++++
      B(1) = -D(1)
      B(N) = -D(N-1)
      C(1) = 0.
      C(N) = 0.
      IF ( N .EQ. 3 ) GO TO 510
      C(1) = C(3)/(X(4)-X(2)) - C(2)/(X(3)-X(1))
      C(N) = C(N-1)/(X(N)-X(N-2)) - C(N-2)/(X(N-1)-X(N-3))
      C(1) = C(1)*D(1)**2/(X(4)-X(1))
      C(N) = -C(N)*D(N-1)**2/(X(N)-X(N-3))
C ++++++++++++++++++++++++++++++++++++++++++++++++++++++++++++++++++++++++++++++
C  FORWARD ELIMINATION
C ++++++++++++++++++++++++++++++++++++++++++++++++++++++++++++++++++++++++++++++
  510 DO 520 I = 2, N
         T = D(I-1)/B(I-1)
         B(I) = B(I) - T*D(I-1)
         C(I) = C(I) - T*C(I-1)
  520 CONTINUE
C ++++++++++++++++++++++++++++++++++++++++++++++++++++++++++++++++++++++++++++++
C  BACK SUBSTITUTION
C ++++++++++++++++++++++++++++++++++++++++++++++++++++++++++++++++++++++++++++++
      C(N) = C(N)/B(N)
      DO 530 IB = 1, NM1
         I = N-IB
         C(I) = (C(I) - D(I)*C(I+1))/B(I)
  530 CONTINUE
C ++++++++++++++++++++++++++++++++++++++++++++++++++++++++++++++++++++++++++++++
C  C(I) IS NOW THE SIGMA(I) OF THE TEXT COMPUTE POLYNOMIAL COEFFICIENTS
C ++++++++++++++++++++++++++++++++++++++++++++++++++++++++++++++++++++++++++++++
```

```
      B(N) = (Y(N) - Y(NM1))/D(NM1) + D(NM1)*(C(NM1) + 2.*C(N))
      DO 540 I = 1, NM1
         B(I) = (Y(I+1) - Y(I))/D(I) - D(I)*(C(I+1) + 2.*C(I))
         D(I) = (C(I+1) - C(I))/D(I)
         C(I) = 3.*C(I)
 540  CONTINUE
      C(N) = 3.*C(N)
      D(N) = D(N-1)
      RETURN
C
 550  B(1) = (Y(2)-Y(1))/(X(2)-X(1))
      C(1) = 0.
      D(1) = 0.
      B(2) = B(1)
      C(2) = 0.
      D(2) = 0.
C
      RETURN
      END
C
C ***************************************************************************************
      FUNCTION SEVAL(N, U, X, Y, B, C, D)
C ***************************************************************************************
C  THIS SUBROUTINE EVALUATES THE CUBIC SPLINE FUNCTION
C    SEVAL = Y(I) + B(I)*(U-X(I)) + C(I)*(U-X(I))**2 + D(I)*(U-X(I))**3
C        WHERE  X(I) .LT. U .LT. X(I+1), USING HORNER@S RULE
C  IF  U .LT. X(1) THEN  I = 1  IS USED.
C  IF  U .GE. X(N) THEN  I = N  IS USED.
C  INPUT..
C     N = THE NUMBER OF DATA POINTS
C     U = THE ABSCISSA AT WHICH THE SPLINE IS TO BE EVALUATED
C     X,Y = THE ARRAYS OF DATA ABSCISSAS AND ORDINATES
C     B,C,D = ARRAYS OF SPLINE COEFFICIENTS COMPUTED BY SPLINE
C  IF  U  IS NOT IN THE SAME INTERVAL AS THE PREVIOUS CALL, THEN A BINARY SEARCH IS
C  PERFORMED TO DETERMINE THE PROPER INTERVAL.
C ***************************************************************************************
      INTEGER N, I, J, K
      REAL  DX, U, X(N), Y(N), B(N), C(N), D(N)
C
      DATA I/1/
      IF ( I .GE. N ) I = 1
      IF ( U .LT. X(I) ) GO TO 600
      IF ( U .LE. X(I+1) ) GO TO 620
C +++++++++++++++++++++++++++++++++++++++++++++++++++++++++++++++++++++++++++++++++++++++
C  BINARY SEARCH
C +++++++++++++++++++++++++++++++++++++++++++++++++++++++++++++++++++++++++++++++++++++++
 600  I = 1
      J = N+1
 610  K = (I+J)/2
      IF ( U .LT. X(K) ) J = K
      IF ( U .GE. X(K) ) I = K
      IF ( J .GT. I+1 ) GO TO 610
C +++++++++++++++++++++++++++++++++++++++++++++++++++++++++++++++++++++++++++++++++++++++
C  EVALUATE SPLINE
C +++++++++++++++++++++++++++++++++++++++++++++++++++++++++++++++++++++++++++++++++++++++
 620  DX = U - X(I)
      SEVAL = Y(I) + DX*(B(I) + DX*(C(I) + DX*D(I)))
C
      RETURN
      END
C
C ***************************************************************************************
      SUBROUTINE PPHI(PRESS,FPPHI)
C ***************************************************************************************
C     PPHI EVALUATES THE PSEUDO-POTENTIAL FUNCTION INTEGRAL
C        USING THE AUTOMATIC QUADRATURE ROUTINE QUANC8.
C ***************************************************************************************
      EXTERNAL FUN
C
      COMMON/DATA4/ACONST,AEXP,BCONST,BEXP,ALPHA,BETA,STEMP
```

```
C  +++++++++++++++++++++++++++++++++++++++++++++++++++++++++++++++++++++++++++++++++++++++++
C   COMPUTE THE PSEUDO-POTENTIAL FUNCTION INTEGRAL, (FPPHI) FROM THE REFERENCE POTENTIAL (ALIM)
C   TO THE 'PRESS' POTENTIAL (BLIM) IN UNITS OF (GM-ATM/CM3-CP).
C  +++++++++++++++++++++++++++++++++++++++++++++++++++++++++++++++++++++++++++++++++++++++++
      PREF=0.5
      PHIREF=PREF*PREF/2.+BETA*PREF
      ALIM=PHIREF
      BLIM=PRESS*PRESS/2.+BETA*PRESS
C
      IF(BETA.LT.0.2) GO TO 700
C
      AERR=1.E-6
      RERR=1.E-6
C
      CALL QUANC8(FUN,ALIM,BLIM,AERR,RERR,FPPHI,ERR,NIT,FLAG)
      IF(FLAG.NE.0.0) WRITE(6,6700) ALIM,BLIM,PRESS,NIT,FLAG
      RETURN
C  +++++++++++++++++++++++++++++++++++++++++++++++++++++++++++++++++++++++++++++++++++++++++
C     THIS SECTION WAS ADDED TO SPEED-UP THE PPHI CALCULATION FOR PRACTICAL CASES WHERE BETA IS
C     SMALL AND THE MEASURED DIFFERENTIAL PRESSURE IS SMALL. THE SPEED-UP MAY BE REMOVED BY
C     DELETING THE IF-STATEMENT ABOVE.
C  +++++++++++++++++++++++++++++++++++++++++++++++++++++++++++++++++++++++++++++++++++++++++
 700  CONTINUE
      PCN2=493.
      TCN2=227.
      GMW=28.013
      R=82.06
      PRPSI=14.696
      T=STEMP
      TKELV=5.*(T-32.)/9.+273.
      CALL ZFACT(PRPSI,T,PCN2,TCN2,Z)
      CALL GASVIS(PRPSI,T,PCN2,TCN2,Z,GV)
C
      FPPHI=(BLIM-ALIM)*GMW/(R*TKELV*GV*Z)
      RETURN
C
 6700 FORMAT(2X,'WARNING -- PHI CALCULATION MAY BE UNRELIABLE --',
     &        //5X,'ALIM  =',G10.3,10X,'BLIM  =',G10.3,
     &        /5X,'PRESS =',G10.3,/5X,'NIT   =',I5,
     &        /5X,'FLAG  =',G10.3)
C
      END
C
C  *****************************************************************************************
      REAL FUNCTION FUN(X)
C  *****************************************************************************************
C     FUN(X) EVALUATES THE INTEGRAND OF THE PSEUDO-POTENTIAL INTEGRAL AND IS CALLED BY QUANC8
C  -- SET THE CRITICAL PROPERTIES FOR NITROGEN
C          PC  IN UNITS OF PSIA
C          TC  IN UNITS OF DEGREES RANKINE
C          GMW IN UNITS OF LBM/LB-MOLE
C          R   UNIVERSAL GAS CONSTANT (CM**3 ATM / GM-MOLE DEG-K)
C  -- NOTE:  1 ATM = 14.696 PSIA = 760. MMHG
C  *****************************************************************************************
      COMMON/CALIB/PLM(10,10),RINTM(10,10),RSLPM(10,10),RMETER(10)
      COMMON/CNTRL1/NSETS,ITYPE,IDIM,IKREL
      COMMON/CNTRL2/ISYSPL,ILEAK,IHVC,IMODE
      COMMON/CNTRL3/IHVPLT,IDSPL
      COMMON/CURVE/GRATIO(50),REYGA2(50),B(50),C(50),D(50),NCPTS
      COMMON/DATA1/IMETER(5000),RAWPR(5000),RAWFR(5000),IDATA,NDATA
      COMMON/DATA2/PINV(5000),PERMA(5000),XDATA(5000),YDATA(5000)
      COMMON/DATA3/ARAD,GEOM,AREA,BPMMHG,CORED,COREL
      COMMON/DATA4/ACONST,AEXP,BCONST,BEXP,ALPHA,BETA,STEMP
      COMMON/DATA5/XZEROP,YZEROP,ZZEROP,DELXP,DELYP,DELZP
      COMMON/DATA6/XPOSN(5000),YPOSN(5000),ZPOSN(5000)
      COMMON/GFACT/HSGEOM(50),BD(50),BGF(50),CGF(50),DGF(50),NHSG
      COMMON/TITLE/ILABEL(5)
      COMMON/PFUN2/FRMASS,PATM0,PATM1,PRPSI
      COMMON/INPUT/TUBE(5000),F(5000),P(5000)
C
```

```
      PCN2=493.
      TCN2=227.
      GMW=28.013
      R=82.06
C ++++++++++++++++++++++++++++++++++++++++++++++++++++++++++++++++++++++++++++++++++++++
C -- COMPUTE THE PRESSURE ASSOCIATED WITH A GIVEN X-POTENTIAL
C ++++++++++++++++++++++++++++++++++++++++++++++++++++++++++++++++++++++++++++++++++++++
      PRATM=-BETA+SQRT(BETA*BETA+2.*X)
      PRPSI=14.696*PRATM
      T=STEMP
      TKELV=5.*(T-32.)/9.+273.
C ++++++++++++++++++++++++++++++++++++++++++++++++++++++++++++++++++++++++++++++++++++++
C -- COMPUTE THE Z-FACTOR AND VISCOSITY OF THE GAS FOR THE SPECIFIED TEMPERATURE AND PRESSURE.
C ++++++++++++++++++++++++++++++++++++++++++++++++++++++++++++++++++++++++++++++++++++++
      CALL ZFACT(PRPSI,T,PCN2,TCN2,Z)
      CALL GASVIS(PRPSI,T,PCN2,TCN2,Z,GV)
C
      FUN=GMW/(R*TKELV*GV*Z)
C
      RETURN
      END
C
C **************************************************************************************
      SUBROUTINE QUANC8(FUN,A,B,ABSE,RELE,RESULT,ERREST,NOFUN,FLAG)
C **************************************************************************************
C  ESTIMATE THE INTEGRAL OF FUN(X) FROM A TO B TO A USER PROVIDED TOLERANCE. AN AUTOMATIC
C          ADAPTIVE ROUTINE BASED ON THE 8-PANEL NEWTON-COTES RULE.
C  INPUT ..
C     FUN     THE NAME OF THE INTEGRAND FUNCTION SUBPROGRAM FUN(X).
C     A       THE LOWER LIMIT OF INTEGRATION.
C     B       THE UPPER LIMIT OF INTEGRATION.(B MAY BE LESS THAN A.)
C     RELE    A RELATIVE ERROR TOLERANCE. (SHOULD BE NON-NEGATIVE)
C     ABSE    AN ABSOLUTE ERROR TOLERANCE. (SHOULD BE NON-NEGATIVE)
C  OUTPUT ..
C     RESULT  AN APPROXIMATION TO THE INTEGRAL HOPEFULLY SATISFYING THE LEAST STRINGENT OF THE
C             TWO ERROR TOLERANCES.
C     ERREST  AN ESTIMATE OF THE MAGNITUDE OF THE ACTUAL ERROR.
C     NOFUN   THE NUMBER OF FUNCTION VALUES USED IN CALCULATION OF RESULT.
C     FLAG    A RELIABILITY INDICATOR.  IF FLAG IS ZERO, THEN RESULT PROBABLY SATISFIES THE
C             ERROR TOLERANCE. IF FLAG IS XXX.YYY, THEN XXX = THE NUMBER OF INTERVALS WHICH
C             HAVE NOT CONVERGED AND 0.YYY = THE FRACTION OF THE INTERVAL LEFT TO DO WHEN THE
C             LIMIT ON NOFUN  WAS APPROACHED
C **************************************************************************************
      REAL FUN, A, B, ABSE, RELE, RESULT, ERREST, FLAG
      REAL W0,W1,W2,W3,W4,AREA,X0,F0,STONE,STEP,COR11,TEMP
      REAL QPREV,QNOW,QDIFF,QLEFT,ESTERR,TOLERR
      REAL QRIGHT(31),F(16),X(16),FSAVE(8,30),XSAVE(8,30)
      INTEGER LEVMIN,LEVMAX,LEVOUT,NOMAX,NOFIN,LEV,NIM,I,J
      INTEGER NOFUN
C ++++++++++++++++++++++++++++++++++++++++++++++++++++++++++++++++++++++++++++++++++++++
C  ***   STAGE 1 ***   GENERAL INITIALIZATION  --  SET CONSTANTS.
C ++++++++++++++++++++++++++++++++++++++++++++++++++++++++++++++++++++++++++++++++++++++
      LEVMIN = 1
      LEVMAX = 30
      LEVOUT = 6
      NOMAX = 5000
      NOFIN = NOMAX - 8*(LEVMAX-LEVOUT+2**(LEVOUT+1))
C ++++++++++++++++++++++++++++++++++++++++++++++++++++++++++++++++++++++++++++++++++++++
C  TROUBLE WHEN NOFUN REACHES NOFIN
C ++++++++++++++++++++++++++++++++++++++++++++++++++++++++++++++++++++++++++++++++++++++
      W0 =   3956.0 / 14175.0
      W1 =  23552.0 / 14175.0
      W2 =  -3712.0 / 14175.0
      W3 =  41984.0 / 14175.0
      W4 = -18160.0 / 14175.0
C ++++++++++++++++++++++++++++++++++++++++++++++++++++++++++++++++++++++++++++++++++++++
C  INITIALIZE RUNNING SUMS TO ZERO.
C ++++++++++++++++++++++++++++++++++++++++++++++++++++++++++++++++++++++++++++++++++++++
      FLAG = 0.0
      RESULT = 0.0
```

```
      COR11  = 0.0
      ERREST = 0.0
      AREA   = 0.0
      NOFUN = 0
      IF (A .EQ. B) RETURN
C ++++++++++++++++++++++++++++++++++++++++++++++++++++++++++++++++++++++++++++++++++++++++
C   *** STAGE 2 ***   INITIALIZATION FOR FIRST INTERVAL
C ++++++++++++++++++++++++++++++++++++++++++++++++++++++++++++++++++++++++++++++++++++++++
      LEV = 0
      NIM = 1
      X0 = A
      X(16) = B
      QPREV  = 0.0
      F0 = FUN(X0)
      STONE = (B - A) / 16.0
      X(8)  =  (X0  + X(16)) / 2.0
      X(4)  =  (X0  + X(8))  / 2.0
      X(12) =  (X(8)  + X(16)) / 2.0
      X(2)  =  (X0  + X(4))  / 2.0
      X(6)  =  (X(4)  + X(8))  / 2.0
      X(10) =  (X(8)  + X(12)) / 2.0
      X(14) =  (X(12) + X(16)) / 2.0
      DO 800 J = 2, 16, 2
         F(J) = FUN(X(J))
  800 CONTINUE
      NOFUN = 9
C ++++++++++++++++++++++++++++++++++++++++++++++++++++++++++++++++++++++++++++++++++++++++
C *** STAGE 3 *** CALCULATION REQUIRES QPREV,X0,X2,X4,...,X16,F0,F2,F4,...,F16.
C   CALCULATES X1,X3,...X15, F1,F3,...F15,QLEFT,QRIGHT,QNOW,QDIFF,AREA.
C ++++++++++++++++++++++++++++++++++++++++++++++++++++++++++++++++++++++++++++++++++++++++
  810 X(1) = (X0 + X(2)) / 2.0
      F(1) = FUN(X(1))
      DO 820 J = 3, 15, 2
         X(J) = (X(J-1) + X(J+1)) / 2.0
         F(J) = FUN(X(J))
  820 CONTINUE
      NOFUN = NOFUN + 8
      STEP = (X(16) - X0) / 16.0
      QLEFT  =  (W0*(F0 + F(8))  + W1*(F(1)+F(7))  + W2*(F(2)+F(6))
     1  + W3*(F(3)+F(5))  +  W4*F(4)) * STEP
      QRIGHT(LEV+1)=(W0*(F(8)+F(16))+W1*(F(9)+F(15))+W2*(F(10)+F(14))
     1  + W3*(F(11)+F(13)) + W4*F(12)) * STEP
      QNOW = QLEFT + QRIGHT(LEV+1)
      QDIFF = QNOW - QPREV
      AREA = AREA + QDIFF
C ++++++++++++++++++++++++++++++++++++++++++++++++++++++++++++++++++++++++++++++++++++++++
C   *** STAGE 4 *** INTERVAL CONVERGENCE TEST
C ++++++++++++++++++++++++++++++++++++++++++++++++++++++++++++++++++++++++++++++++++++++++
      ESTERR = ABS(QDIFF) / 1023.0
      TOLERR = AMAX1(ABSE,RELE*ABS(AREA)) * (STEP/STONE)
      IF (LEV .LT. LEVMIN) GO TO 830
      IF (LEV .GE. LEVMAX) GO TO 870
      IF (NOFUN .GT. NOFIN) GO TO 860
      IF (ESTERR .LE. TOLERR) GO TO 880
C ++++++++++++++++++++++++++++++++++++++++++++++++++++++++++++++++++++++++++++++++++++++++
C   *** STAGE 5   ***    NO CONVERGENCE  --  LOCATE NEXT INTERVAL.
C ++++++++++++++++++++++++++++++++++++++++++++++++++++++++++++++++++++++++++++++++++++++++
  830 NIM = 2*NIM
      LEV = LEV+1
C ++++++++++++++++++++++++++++++++++++++++++++++++++++++++++++++++++++++++++++++++++++++++
C   STORE RIGHT HAND ELEMENTS FOR FUTURE USE.
C ++++++++++++++++++++++++++++++++++++++++++++++++++++++++++++++++++++++++++++++++++++++++
      DO 840 I = 1, 8
         FSAVE(I,LEV) = F(I+8)
         XSAVE(I,LEV) = X(I+8)
  840 CONTINUE
C ++++++++++++++++++++++++++++++++++++++++++++++++++++++++++++++++++++++++++++++++++++++++
C   ASSEMBLE LEFT HAND ELEMENTS FOR IMMEDIATE USE.
C ++++++++++++++++++++++++++++++++++++++++++++++++++++++++++++++++++++++++++++++++++++++++
      QPREV = QLEFT
```

```
      DO 850 I = 1, 8
         J = -I
         F(2*J+18) = F(J+9)
         X(2*J+18) = X(J+9)
 850  CONTINUE
      GO TO 810
C ++++++++++++++++++++++++++++++++++++++++++++++++++++++++++++++++++++++++++++++++++++++++++
C  *** STAGE 6 ***  NUMBER OF FUNCTION VALUES IS ABOUT TO EXCEED LIMIT.
C ++++++++++++++++++++++++++++++++++++++++++++++++++++++++++++++++++++++++++++++++++++++++++
 860  NOFIN = 2*NOFIN
      LEVMAX = LEVOUT
      FLAG = FLAG + (B - X0) / (B - A)
      GO TO 880
C ++++++++++++++++++++++++++++++++++++++++++++++++++++++++++++++++++++++++++++++++++++++++++
C   CURRENT LEVEL IS LEVMAX.
C ++++++++++++++++++++++++++++++++++++++++++++++++++++++++++++++++++++++++++++++++++++++++++
 870  FLAG = FLAG + 1.0
C ++++++++++++++++++++++++++++++++++++++++++++++++++++++++++++++++++++++++++++++++++++++++++
C   ***   STAGE 7   ***   INTERVAL CONVERGED ADD CONTRIBUTIONS INTO RUNNING SUMS.
C ++++++++++++++++++++++++++++++++++++++++++++++++++++++++++++++++++++++++++++++++++++++++++
 880  RESULT = RESULT + QNOW
      ERREST = ERREST + ESTERR
      COR11  = COR11  + QDIFF / 1023.0
C ++++++++++++++++++++++++++++++++++++++++++++++++++++++++++++++++++++++++++++++++++++++++++
C   LOCATE NEXT INTERVAL.
C ++++++++++++++++++++++++++++++++++++++++++++++++++++++++++++++++++++++++++++++++++++++++++
 890  IF (NIM .EQ. 2*(NIM/2)) GO TO 900
      NIM = NIM/2
      LEV = LEV-1
      GO TO 890
 900  NIM = NIM + 1
      IF (LEV .LE. 0) GO TO 920
C ++++++++++++++++++++++++++++++++++++++++++++++++++++++++++++++++++++++++++++++++++++++++++
C   ASSEMBLE ELEMENTS REQUIRED FOR THE NEXT INTERVAL.
C ++++++++++++++++++++++++++++++++++++++++++++++++++++++++++++++++++++++++++++++++++++++++++
      QPREV = QRIGHT(LEV)
      X0 = X(16)
      F0 = F(16)
      DO 910 I = 1, 8
         F(2*I) = FSAVE(I,LEV)
         X(2*I) = XSAVE(I,LEV)
 910  CONTINUE
      GO TO 810
C ++++++++++++++++++++++++++++++++++++++++++++++++++++++++++++++++++++++++++++++++++++++++++
C   ***   STAGE 8   ***   FINALIZE AND RETURN
C ++++++++++++++++++++++++++++++++++++++++++++++++++++++++++++++++++++++++++++++++++++++++++
 920  RESULT = RESULT + COR11
C ++++++++++++++++++++++++++++++++++++++++++++++++++++++++++++++++++++++++++++++++++++++++++
C   MAKE SURE ERREST NOT LESS THAN ROUNDOFF LEVEL.
C ++++++++++++++++++++++++++++++++++++++++++++++++++++++++++++++++++++++++++++++++++++++++++
      IF (ERREST .EQ. 0.0) RETURN
 930  TEMP = ABS(RESULT) + ERREST
      IF (TEMP .NE. ABS(RESULT)) RETURN
      ERREST = 2.0*ERREST
      GO TO 930
      END
C
C ******************************************************************************************
      SUBROUTINE ZFACT(P,TF,PC,TC,ZF)
C ******************************************************************************************
C  ZFACT COMPUTES THE GAS DEVIATION FACTOR FOR A PURE COMPONENT WITH A GIVEN PC AND TC FOR A
C    USER-SPECIFIED PRESSURE AND TEMPERATURE USING THE HALL-YARBOROUGH METHOD (1973) AS
C    DEVELOPED FROM THE STARLING-CARNAHAN EQUATION OF STATE.
C ******************************************************************************************
      EPS=1.E-10
      TOL=1.E-6
      TRANK=TF+460.
      T=TC/TRANK
      PR=P/PC
      IF(ABS(PR).LT.EPS) GO TO 1030
```

```
      Y=0.5
C
 1000 F=-0.06125*PR*T*EXP(-1.2*(1.-T)*(1.-T))
     &  +(Y+Y*Y+Y*Y*Y-Y*Y*Y*Y)/(1.-Y)**3
     &  -(14.7*T-9.76*T*T+4.58*T*T*T)*Y*Y
     &  +(90.7*T-242.2*T*T+42.4*T*T*T)*Y**(2.18+2.82*T)
      FPRIME=3.*(Y+Y*Y+Y*Y*Y-Y*Y*Y*Y)*(1.-Y)**(-4)
     &  +(1.+2.*Y+3.*Y*Y-4.*Y*Y*Y)/(1.-Y)**3
     &  -2.*Y*(14.7*T-9.76*T*T+4.58*T*T*T)
     &  +(2.18+2.82*T)*(90.7*T-242.2*T*T+42.4*T*T*T)*Y**(1.18+2.82*T)
C
      YNEW=Y-F/FPRIME
      YFRAC=ABS(1.-YNEW/Y)
      IF(YFRAC.LT.TOL) GO TO 1010
      IF((ABS(YNEW-1.0).LT.EPS).OR.ABS(YNEW).LT.EPS) GO TO 1020
      Y=YNEW
      GO TO 1000
C
 1010 ZF=0.06125*PR*T*EXP(-1.2*(1.-T)*(1.-T))/YNEW
      RETURN
C
 1020 WRITE(ITTY,*) YNEW,'CONVERGENCE PROBLEM IN ZFACT ROUTINE'
      STOP
C
 1030 ZF=1.0
C
      RETURN
      END
C
C  *****************************************************************************************
      SUBROUTINE GASVIS(P,T,PC,TC,ZFACT,GV)
C  *****************************************************************************************
C  -- GASVIS COMPUTES THE GAS VISCOSITY FOR A MIXTURE OF HYDROCARBON GASES GIVEN THE CRITICAL
C        PROPERTIES OF THE GAS, PRESSURE, TEMPERATURE AND GAS GRAVITY USING THE CARR, KOBAYASHI
C        AND BURROWS (1954) CORRELATION.
C    IF THE IFORM OPTION IS SET TO ZERO, A PURE COMPONENT VISCOSITY IS COMPUTED USING A
C        CORRECTION FACTOR IF A NON-HYDROCARBON IS USED (ITYPE = 0). THE USER-INPUT PC AND TC
C        ARE USED TO GAS COMPUTE REDUCED PROPERTIES DIRECTLY.
C    IF THE IFORM OPTION IS SET TO ONE, THE PSEUDOCRITICAL PRESSURE AND TEMPERATURE IS ESTIMATED
C        FROM THE THOMAS, HANKINSON ANDPHILLIPS (1970) CORRELATIONS. THE REDUCED PROPERTIES ARE
C        THEN COMPUTED IN THE USUAL MANNER.
C    IF THE IFORM OPTION IS SET TO TWO, THE LEE, GONZALES AND EAKIN CORRELATION IS USED.
C    UNITS:
C       T          -- INPUT TEMPERATURE IN DEGREES F
C       TC         -- INPUT/COMPUTED CRITICAL TEMPERATURE IN DEGREES R
C       TK         -- SYSTEM TEMPERATURE IN DEGREES K
C       TS         -- SYSTEM TEMPERATURE IN DEGREES R
C       P          -- INPUT PRESSURE IN PSIA
C       PC         -- INPUT/COMPUTED CRITICAL PRESSURE IN PSIA
C       GGRAV      -- GAS GRAVITY = MW(GAS) / MW(AIR)
C       GMW        -- MOLECULAR WEIGHT OF GAS
C       GVC        -- GAS VISCOSITY CORRECTION FACTOR FOR PURE NON-HYDROCARBON GASES AT 1 ATM
C       GV1        -- COMPUTED GAS VISCOSITY AT 1 ATM
C       GV         -- OUTPUT GAS VISCOSITY AT SPECIFIED T AND P IN CP
C       RG         -- COMPUTED GAS DENSITY IN GM/CC
C       ZFACT      -- GAS DEVIATION FACTOR OR Z-FACTOR
C  *****************************************************************************************
      DATA  GMW/28.013/
      DATA  GVC/0.0086/
      DATA  A0/-2.46211820/,     A1/2.97054714/,      A2/-0.286264054/,     A3/8.05420522E-03/,
     &        A4/2.80860949/,      A5/-3.49803305/,     A6/0.36037302/,       A7/-0.0104432413/,
     &        A8/-0.793385684/,    A9/1.39643306/,      A10/-0.149144925/,    A11/0.00441015512/,
     &        A12/0.0839387178/,   A13/-0.186408848/,   A14/0.0203367881/,    A15/-0.000609579263/
C
      DATA  B0/1.11231913E-02/,  B1/1.67726604E-05/,  B2/2.11360496E-09/,  B3/-1.0948505E-04/,
     &        B4/-6.40316395E-08/, B5/-8.99374533E-11/, B6/4.57735189E-07/,  B7/2.1290339E-10/,
     &        B8/3.97732249E-13/
C
      IFORM=0
      GGRAV=GMW/28.97
```

```
      TS=T+460
      IF(IFORM.GT.0) GO TO 1200
C
      PR=P/PC
      TR=TS/TC
C
 1100 GV1=GVC+B0+B1*T+B2*T*T+B3*GMW+B4*T*GMW+B5*T*T*GMW+B6*GMW*GMW+B7*T*GMW*GMW+B8*T*T*GMW
C
      ARG0=A0+A1*PR+A2*PR*PR+A3*PR*PR*PR
      ARG1=A4+A5*PR+A6*PR*PR+A7*PR*PR*PR
      ARG2=A8+A9*PR+A10*PR*PR+A11*PR*PR*PR
      ARG3=A12+A13*PR+A14*PR*PR+A15*PR*PR*PR
      ARG=ARG0+ARG1*TR+ARG2*TR*TR+ARG3*TR*TR*TR
      VRATIO=EXP(ARG)/TR
      GV=GV1*VRATIO
      RETURN
C
 1200 IF(IFORM.GT.1) GOTO 1300
C
      PPC=709.604-58.718*GGRAV
      TPC=170.491+307.344*GGRAV
      GO TO 1100
C
 1300 X=3.5+986/TS+0.01*GMW
      Y=2.4-0.2*X
      TK=5.*(T-32.)/9.+273.
      RG=(P*GMW/14.69)/(82.057477*ZFACT*TK)
      CONST=(9.4+0.02*GMW)*TS**1.5/(209+19*GMW+TS)
      GV=1.E-4*CONST*EXP(X*RG**Y)
C
      RETURN
      END
```

APPENDIX D

FORTRAN CODE OF VARIOGRAM COMPUTATION ROUTINE

(Adapted from David, 1977).

Program VGCODE4

```
          PROGRAM VGCODE4
C   *****************************************************************
C   PROGRAM VGCODE4
C   VERSION AUTHOR: MALCOLM A. FERRIS  (ADAPTED FROM DAVIS, 1977)
C   DATE: 11/8/90
C
C   PURPOSE:  TO CREATE A 2-D VARIOGRAM FROM DATA.  TAKEN FROM
C          DAVID (1977), THIS PROGRAM SEARCHES THE DATA SET FOR
C          PAIRS BASED UPON THE DIRECTION AND WINDOW PARAMETERS.
C   VARIABLES:  TITLE(80) - PRIMARY TITLE OF DATA SET
C               X(2000) - INPUT COORDINATE (HORIZONTAL)
C               Y(2000) - INPUT COORDINATE (VERTICAL)
C               Z(2000) - COMPUTATIONAL VALUE OF DATA
C               ZL(2000) - LOG10 TRANSFORMED DATA VALUES
C               PHI(10) - SEARCH DIRECTION OF PROGRAM RUN
C               PSI(10) - WINDOW ANGLE OF PROGRAM RUN
C               ILOG - INDICATOR FOR COMPUTATION OF LOG VALUES
C               NDIR - NUMBER OF SEARCH DIRECTIONS TO RUN
C               STEP - STEP INTERVAL USED TO GROUP DATA SEPARATION
C*******************************************************************
          COMMON /DATA1/ X(2000),Y(2000),Z(2000),ZL(2000)
          COMMON /DATA2/ STEP(10),PHI(10),PSI(10)
          COMMON /DATA3/ NDIR,NUM,J,ID,L
          COMMON /VARGR/ PAIRS(400),DIST(400),S1(400),S2(400)
          CHARACTER*80 TITLE,TEMPLATE
          INTEGER N2,ID,ND,ILOG
C
        READ(15,'(A)') TITLE
        WRITE(3,1000) TITLE
        READ(15,*) NDIR,ILOG
        DO 100 ND=1,NDIR
           READ(15,*) STEP(ND),PHI(ND),PSI(ND)
 100    CONTINUE
        READ(15,'(A)') TEMPLATE
          READ(15,TEMPLATE,END=110) (X(N),Y(N),Z(N),N=1,2000)
 110    NUM = N - 1
        DO 120 N2=1,NUM
          IF(ILOG.EQ.1) THEN
             IF(Z(N2).LE.0.0) THEN
               ZL(N2)=-1.301
             ELSE
               ZL(N2) = LOG10(Z(N2))
             ENDIF
          ENDIF
          IF(ILOG.EQ.2) THEN
             IF(Z(N2).LE.0.0) THEN
               ZL(N2)=-2.9957
             ELSE
               ZL(N2) = LOG(Z(N2))
             ENDIF
          ENDIF
          IF(ILOG.EQ.0) THEN
             ZL(N2) = Z(N2)
          ENDIF
 120    CONTINUE
C*******************************************************************
C
```

```
C     DESCRIPTION OF INPUT CARDS
C     **************************
C
C   COL   FORMAT    NAME      DESCRIPTION
C  ***** ********  ******    *************
C
C  CARD ONE
C  ********
C   1-80    A80     TITLE    TITLE OF RUN
C
C  CARD TWO
C  ********
C    *   INTEGER    NDIR     NUMBER OF SEARCH DIRECTIONS IN RUN
C                              (10 MAXIMUM)
C    *   INTEGER    ILOG     TRANSFORM INDICATOR
C                                1 = DATA TO BE TRANFORMED TO LOG10
C                                2 = DATA TO BE TRANFORMED TO LOG-N
C                                0 = DATA NOT TO BE TRANFORMED
C
C  CARD THREE     PARAMETERS OF VARIOGRAM SEARCH ROUTINE
C  **********      ONE CARD REQUIRED PER "NDIR".
C    *      REAL     PHI(I)   SEARCH DIRECTION OF VARIOGRAM RUN
C                                HORIZONTAL-RIGHT = 0°
C                                COUNTER-CLOCKWISE INCREASING ANGLES
C    *      REAL     PSI(I)   SEARCH WINDOW ANGLE OF PROGRAM
C
C  CARD FOUR
C  *********
C    *      A80     TEMPLATE  FORMAT OF INPUT DATA (X, Y, "VARIABLE")
C
C  DATA CARDS      X,Y COORDINATES AND VARIABLE VALUES MUST BR IN THE
C                  FORMAT SUPPLIE ABOVE
C*******************************************************************
        NUM=N2-1
        WRITE(*,*) X(1),Y(1),Z(1),ZL(1)
        WRITE(*,*) X(NUM),Y(NUM),Z(NUM),ZL(NUM)
        WRITE(3,1300) NUM
C*******************************************************************
C   HAVING WRITTEN TO SCREEN THE FIRST AND LAST DATA AND LOG-TRANS-
C   FORMS, THE OUTPUT FILES ARE HEADED WITH THE STATISTICAL
C   PARAMETERS FROM THE SUBROUTINE 'MOMENT'.
C*******************************************************************
        DO 130 ID=1,NDIR
         WRITE(3,'(A)') ' POPULATION STATISTICS FROM NUMERICAL '
     &        'RECIPES '
        CALL MOMENT(Z,NUM,AVE,ADEV,SDEV,VAR,SKEW,CURT)
         WRITE(3,'(A)') ' POPULATION STATISTICS ON UNALTERED DATA '
         WRITE(3,3100) AVE,ADEV,SDEV,VAR,SKEW,CURT
        IF (ILOG.GT.0) THEN
        CALL MOMENT(ZL,NUM,AVE,ADEV,SDEV,VAR,SKEW,CURT)
         WRITE(3,'(A)') ' POPULATION STATISTICS ON ALTERED DATA '
          IF(ILOG.EQ.0) WRITE(3,1100)
          IF(ILOG.EQ.1) WRITE(3,1101)
          IF(ILOG.EQ.2) WRITE(3,1102)
         WRITE(3,3100) AVE,ADEV,SDEV,VAR,SKEW,CURT
        ENDIF
C******************************************************************
```

```
C   SUBROUTINE 'DATASET' SEARCHES THE INPUT DATA FOR PAIRS BASED
C  UPON THE 'PHI(I)' AND 'PSI(I)' [DIRECTION AND WINDOW] PARAMETERS.
C*******************************************************************
          CALL DATASET
          CALL OUTPUT
 130      CONTINUE
C  **  FORMAT STATEMENTS  **
 1000    FORMAT(16X,'STARTING PROGRAM VGCODE4 - RUN TITLED:',/,A80,
     &          /,22X,'EQUAL DISTANCE SEARCH ROUTINE')
 1100    FORMAT(2X,'DATA UNCONVERTED FROM INPUT')
 1101    FORMAT(2X,'DATA CONVERTED TO LOG BASE 10')
 1102    FORMAT(2X,'DATA CONVERTED TO NATURAL LOG')
 1300    FORMAT(2X,I5,2X,'DATA SETS READ FROM FILE INPUT')
 3100    FORMAT(2X,'AVERAGE',F9.3,', ADEV',F9.3,', SDEV',F9.3,
     &          ', VARIANCE',F9.3,/,5X'SKEW',F9.3,', CURTOSIS',F9.3)
          STOP
          END
C
      SUBROUTINE MOMENT(DATA,N,AVE,ADEV,SDEV,VAR,SKEW,CURT)
C*******************************************************************
C   THIS SUBROUTINE IS TRANSLATED DIRECTLY FROM "NUMERICAL RECIPES",
C   PRESS AND OTHERS, 1986.
C*******************************************************************
      DIMENSION DATA(N)
      IF(N.LE.1)PAUSE 'N must be at least 2'
      S=0.
      DO 11 J=1,N
        S=S+DATA(J)
11    CONTINUE
      AVE=S/N
      ADEV=0.
      VAR=0.
      SKEW=0.
      CURT=0.
      DO 12 J=1,N
        S=DATA(J)-AVE
        ADEV=ADEV+ABS(S)
        P=S*S
        VAR=VAR+P
        P=P*S
        SKEW=SKEW+P
        P=P*S
        CURT=CURT+P
12    CONTINUE
      ADEV=ADEV/N
      VAR=VAR/(N-1)
      SDEV=SQRT(VAR)
      IF(VAR.NE.0.)THEN
        SKEW=SKEW/(N*SDEV**3)
        CURT=CURT/(N*VAR**2)-3.
      ELSE
        PAUSE 'no skew or kurtosis when zero variance'
      ENDIF
      RETURN
      END
C
          SUBROUTINE DATASET
```

```
C*********************************************************************
C   THIS FORM OF THE PROGRAM SEARCHES FOR [CC1.EQ.T1], THE SEARCH
C   WINDOW PARAMETERS, THE AVERAGE DISTANCES ARE ASSUMED EQUAL STEP
C   INCREMENTS OF THE SEPARATION/LAG DISTANCE.
C*********************************************************************
          COMMON /DATA1/ X(2000),Y(2000),Z(2000),ZL(2000)
          COMMON /DATA2/ STEP(10),PHI(10),PSI(10)
          COMMON /DATA3/ NDIR,NUM,J,ID,L
          COMMON /VARGR/ PAIRS(400),DIST(400),S1(400),S2(400)
          INTEGER IK,IP,ICOUNT
          REAL SUM,D2,DELTZ,D1
C
           APSI=3.141592*PSI(ID)/180.
           T1=COS(APSI)
           APHI=3.141592*PHI(ID)/180.
           CA=COS(APHI)
           SA=SIN(APHI)
C*********************************************************************
C   DIRECTION (PHI) IS SET FOR SINE AND COSINE WINDOW (PSI) IS SET
C   TO T1 AS THE COSINE VALUE OF THE ANGLE.
C*********************************************************************
           DO 210 IP=1,40
              PAIRS(IP)=0.
              DIST(IP)=0.
              S1(IP)=0.
              S2(IP)=0.
 210       CONTINUE
C*********************************************************************
C   PAIRS(IP) THE COUNTER-ARRAY OF DISTANCES WHERE PAIRS EXIST
C   DIST(IP) THE SUMS OF THE DISTANCES SEPARATED BY THE MULTIPLE
C            OF THE CLASS SIZE (MULTIPLE VALUE IS IP
C   S1(IP) VARIANCE - THE SUMS OF THE DIFERENCES IN VARIABLES
C   S2(IP) ST. DEV. - THE SUMS OF THE SQUARED DIFERENCES IN VALUES
C*********************************************************************
          D1=0.
          J=40
          DELTZ=0.
          IK=0
          L=0
          WRITE(3,998) NUM
          ICOUNT=0
          DO 240 L1=1,NUM
              I2=L1+1
              IF(I2.GT.NUM) GO TO 260
              DO 250 L2=I2,NUM
              ICOUNT=ICOUNT+1
              D2=((X(L1)-X(L2))*(X(L1)-X(L2)))+
     &             ((Y(L1)-Y(L2))*(Y(L1)-Y(L2)))
               IF(D2.LT.0.00000001) GO TO 250
                 D1=SQRT(D2)
                 CC=((X(L1)-X(L2))*CA/D1)+((Y(L1)-Y(L2))*SA/D1)
                 CC1=ABS(CC)
                 IK=1+(D1/STEP(ID))
C
                 IF(IK.GT.41) GO TO 250
C
                 IF(CC1.EQ.T1)THEN
```

```
                  IF(L.LT.IK) L=IK
                  IF(J.GT.IK) J=IK
                 DELTZ=ZL(L1)-ZL(L2)
                 PAIRS(IK)=PAIRS(IK)+1.
                 S1(IK)=S1(IK)+DELTZ
                 S2(IK)=S2(IK)+DELTZ*DELTZ
                 DIST(IK)=DIST(IK)+D1
                 DELTZ=0.
                 D1=0.
                 IK=0
                ENDIF
 250        CONTINUE
 240      CONTINUE
 260     CONTINUE
 998     FORMAT(1X,'NUM CARRIED FROM MAIN PROGRAM. CHECK NUM =',I6)
           RETURN
           END
C
           SUBROUTINE OUTPUT
C*******************************************************************
C   WRITES TO FILE 3 AND FILE 13 (VGCODE4.OUT AND GRAPH.DAT)
C   OUTPUT IS FORMATED FOR STANDARD DISPLAY OF THE STATISTICS FOR
C   THE SAMPLE SET AND THE GRAPH-READY DATA (NUMBER OF PAIRS,
C   AVERAGE DISTANCE IN THE SET AND VALUE OF SEMIVARIANCE).
C*******************************************************************
           COMMON /DATA1/ X(2000),Y(2000),Z(2000),ZL(2000)
           COMMON /DATA2/ STEP(10),PHI(10),PSI(10)
           COMMON /DATA3/ NDIR,NUM,J,ID,L
           COMMON /VARGR/ PAIRS(400),DIST(400),S1(400),S2(400)
           REAL BINF,BSUP,M1,M2,DISMOY
           INTEGER I
           WRITE(3,3000) ID,PHI(ID),PSI(ID),STEP(ID)
           WRITE(3,3200)
           DO 300 I=J,L
              IF(I.GT.40) GO TO 300
              IF(PAIRS(I).LE.0) GO TO 300
              M1=S1(I)/PAIRS(I)
              M2=0.5*S2(I)/PAIRS(I)
              DISMOY=DIST(I)/PAIRS(I)
              BINF=(STEP(ID)*I)-STEP(ID)
              BSUP=STEP(ID)*I
              WRITE(3,3300) BINF,BSUP,PAIRS(I),M1,M2,DISMOY
              WRITE(13,3400) PAIRS(I),DISMOY,M2
 300       CONTINUE
C
C  **  FORMAT STATEMENTS  **
 3000    FORMAT(2X,'RUN NUMBER',I3,', DIRECTION',F5.1,', '
     &          'WINDOW',F5.1,', STEP',F5.1)
 3200    FORMAT(6X,'DISTANCE',4X,'# PAIRS',5X,'DRIFT',7X,'GAMMA',5X,
     &           'AVER DIST')
 3300    FORMAT(1X,F6.1,' - ',F6.1,F7.0,2X,2E12.3,F12.2)
 3400    FORMAT(1X,2F12.2,E12.4)
           RETURN
           END
```

APPENDIX E

VARIOGRAM OUTPUT DATA

STARTING PROGRAM VGCODE4 - RUN TITLED:
GRID A/ final variogram runs/ BEG:VGCODE4/ MAF - 6/25/91

320 DATA SETS READ FROM FILE INPUT

RUN NUMBER 1, DIRECTION 0.0, WINDOW 0.0, STEP100.0

DISTANCE	# PAIRS	DRIFT	GAMMA	AVER DIST
0.0 - 100.0	155.	0.842E-01	0.238E+00	57.34
100.0 - 200.0	198.	-0.433E-01	0.283E+00	137.92
200.0 - 300.0	227.	0.488E-01	0.305E+00	253.54
300.0 - 400.0	181.	0.916E-01	0.298E+00	355.05
400.0 - 500.0	125.	0.545E-01	0.396E+00	436.31
500.0 - 600.0	115.	0.792E-01	0.460E+00	540.72
600.0 - 700.0	162.	0.109E+00	0.488E+00	651.68
700.0 - 800.0	84.	0.438E-01	0.497E+00	748.29
800.0 - 900.0	66.	-0.372E+00	0.437E+00	867.59
900.0 - 1000.0	98.	0.474E-01	0.476E+00	952.97
1000.0 - 1100.0	98.	0.361E-01	0.682E+00	1047.46
1100.0 - 1200.0	38.	-0.259E+00	0.439E+00	1162.34
1200.0 - 1300.0	84.	0.255E+00	0.655E+00	1256.98
1300.0 - 1400.0	70.	-0.696E-01	0.477E+00	1346.34
1400.0 - 1500.0	73.	0.154E+00	0.481E+00	1449.78
1500.0 - 1600.0	52.	0.225E+00	0.638E+00	1565.85
1600.0 - 1700.0	62.	0.275E+00	0.669E+00	1654.33
1700.0 - 1800.0	41.	0.552E+00	0.839E+00	1744.10
1800.0 - 1900.0	36.	0.272E+00	0.451E+00	1855.97
1900.0 - 2000.0	66.	0.706E+00	0.780E+00	1954.30

RUN NUMBER 2, DIRECTION 0.0, WINDOW 0.0, STEP 50.0

DISTANCE	# PAIRS	DRIFT	GAMMA	AVER DIST
0.0 - 50.0	32.	0.159E+00	0.258E+00	37.23
50.0 - 100.0	123.	0.648E-01	0.233E+00	62.57
100.0 - 150.0	126.	-0.458E-01	0.315E+00	119.36
150.0 - 200.0	72.	-0.388E-01	0.227E+00	170.40
200.0 - 250.0	98.	0.180E-01	0.270E+00	220.69
250.0 - 300.0	129.	0.722E-01	0.332E+00	278.48
300.0 - 350.0	89.	0.478E-01	0.246E+00	331.70
350.0 - 400.0	92.	0.134E+00	0.348E+00	377.64
400.0 - 450.0	74.	0.160E+00	0.400E+00	414.90
450.0 - 500.0	51.	-0.980E-01	0.391E+00	467.38
500.0 - 550.0	59.	0.130E+00	0.506E+00	515.27
550.0 - 600.0	56.	0.259E-01	0.412E+00	567.53
600.0 - 650.0	72.	0.192E+00	0.422E+00	624.52
650.0 - 700.0	90.	0.424E-01	0.541E+00	673.41
700.0 - 750.0	50.	0.572E-01	0.306E+00	724.44
750.0 - 800.0	34.	0.242E-01	0.777E+00	783.35
800.0 - 850.0	23.	-0.205E+00	0.346E+00	831.91
850.0 - 900.0	43.	-0.462E+00	0.486E+00	886.67
900.0 - 950.0	40.	-0.630E-01	0.358E+00	927.05
950.0 - 1000.0	58.	0.124E+00	0.557E+00	970.84
1000.0 - 1050.0	57.	0.508E-01	0.674E+00	1026.11

RUN NUMBER 3, DIRECTION 0.0, WINDOW 0.0, STEP 45.0

DISTANCE	# PAIRS	DRIFT	GAMMA	AVER DIST
0.0 - 45.0	31.	0.145E+00	0.262E+00	36.92
45.0 - 90.0	110.	0.100E+00	0.225E+00	58.40
90.0 - 135.0	105.	-0.768E-01	0.271E+00	108.32
135.0 - 180.0	79.	-0.679E-01	0.320E+00	153.25
180.0 - 225.0	94.	0.498E-01	0.234E+00	203.64
225.0 - 270.0	67.	0.548E-01	0.335E+00	249.96
270.0 - 315.0	100.	0.477E-01	0.323E+00	286.61
315.0 - 360.0	95.	0.486E-01	0.307E+00	336.25
360.0 - 405.0	113.	0.205E+00	0.389E+00	386.62
405.0 - 450.0	41.	0.238E-01	0.227E+00	426.45
450.0 - 495.0	44.	0.290E-01	0.335E+00	462.51
495.0 - 540.0	59.	0.557E-01	0.566E+00	510.29
540.0 - 585.0	63.	-0.711E-02	0.393E+00	564.47
585.0 - 630.0	45.	-0.384E-01	0.272E+00	615.57

```
630.0 -  675.0    77.      0.229E+00   0.505E+00       655.16
675.0 -  720.0    51.     -0.777E-02   0.576E+00       691.29
720.0 -  765.0    39.      0.128E+00   0.358E+00       727.95
765.0 -  810.0    34.      0.242E-01   0.777E+00       783.35
810.0 -  855.0    23.     -0.205E+00   0.346E+00       831.91
855.0 -  900.0    43.     -0.462E+00   0.486E+00       886.67
900.0 -  945.0    40.     -0.630E-01   0.358E+00       927.05
945.0 -  990.0    51.      0.754E-01   0.606E+00       967.28
990.0 - 1035.0    48.     -0.878E-01   0.533E+00      1014.74

RUN NUMBER  4, DIRECTION 90.0, WINDOW  0.0, STEP  1.0
    DISTANCE     # PAIRS     DRIFT       GAMMA     AVER DIST
  0.0 -    1.0     6.      0.865E-01   0.263E+00         0.50
  1.0 -    2.0   268.     -0.410E-01   0.236E+00         1.01
  2.0 -    3.0   238.     -0.101E+00   0.319E+00         2.01
  3.0 -    4.0   213.     -0.158E+00   0.342E+00         3.02
  4.0 -    5.0   187.     -0.221E+00   0.367E+00         4.01
  5.0 -    6.0   170.     -0.356E+00   0.454E+00         5.01
  6.0 -    7.0   153.     -0.433E+00   0.485E+00         6.02
  7.0 -    8.0   134.     -0.465E+00   0.541E+00         7.01
  8.0 -    9.0   122.     -0.594E+00   0.659E+00         8.02
  9.0 -   10.0   105.     -0.550E+00   0.646E+00         9.02
 10.0 -   11.0    93.     -0.623E+00   0.771E+00        10.03
 11.0 -   12.0    82.     -0.756E+00   0.796E+00        11.03
 12.0 -   13.0    69.     -0.838E+00   0.868E+00        12.04
 13.0 -   14.0    57.     -0.788E+00   0.956E+00        13.04
 14.0 -   15.0    41.     -0.701E+00   0.742E+00        14.05
 15.0 -   16.0    30.     -0.652E+00   0.588E+00        15.05
 16.0 -   17.0    20.     -0.591E+00   0.552E+00        16.08
 17.0 -   18.0    13.     -0.405E+00   0.270E+00        17.08
 18.0 -   19.0     9.     -0.487E+00   0.363E+00        18.11
 19.0 -   20.0     5.     -0.248E+00   0.225E+00        19.00
 20.0 -   21.0     4.     -0.346E+00   0.228E+00        20.00
 21.0 -   22.0     2.     -0.141E+00   0.127E+00        21.00
 22.0 -   23.0     1.      0.416E+00   0.864E-01        22.00


              STARTING PROGRAM VGCODE4 - RUN TITLED:
GRID B/ final variogram runs/ BEG:VGCODE4/ MAF - 6/25/91

  221  DATA SETS READ FROM FILE INPUT

RUN NUMBER  1, DIRECTION  0.0, WINDOW  0.0, STEP 35.0
    DISTANCE     # PAIRS     DRIFT       GAMMA     AVER DIST
  0.0 -   35.0   339.     -0.111E+00   0.453E+00        14.47
 35.0 -   70.0   227.     -0.771E-01   0.490E+00        45.26
 70.0 -  105.0   186.      0.370E-01   0.476E+00        80.19
105.0 -  140.0   132.      0.449E+00   0.672E+00       113.90
140.0 -  175.0   131.      0.171E+00   0.299E+00       151.37
175.0 -  210.0    38.      0.294E-01   0.305E+00       175.00
210.0 -  245.0    24.     -0.215E+00   0.640E+00       210.00
245.0 -  280.0     9.     -0.132E+00   0.372E+00       245.00

RUN NUMBER  2, DIRECTION  0.0, WINDOW  0.0, STEP 10.0
    DISTANCE     # PAIRS     DRIFT       GAMMA     AVER DIST
  0.0 -   10.0    86.     -0.426E-01   0.378E+00         5.00
 10.0 -   20.0   136.     -0.923E-01   0.455E+00        12.24
 20.0 -   30.0    89.     -0.136E+00   0.571E+00        22.13
 30.0 -   40.0   121.     -0.111E+00   0.409E+00        33.84
 40.0 -   50.0    45.     -0.843E-01   0.561E+00        42.33
 50.0 -   60.0    45.     -0.133E+00   0.570E+00        52.44
 60.0 -   70.0    44.     -0.843E-01   0.436E+00        62.61
 70.0 -   80.0    96.      0.166E-02   0.428E+00        70.83
 80.0 -   90.0    34.      0.950E-01   0.502E+00        82.50
 90.0 -  100.0    38.      0.218E-01   0.575E+00        92.37
100.0 -  110.0    85.      0.123E+00   0.537E+00       103.94
110.0 -  120.0    20.      0.777E+00   0.675E+00       112.75
120.0 -  130.0    23.      0.763E+00   0.725E+00       122.83
```

130.0 - 140.0	22.	0.832E+00	0.974E+00	132.73
140.0 - 150.0	61.	0.259E+00	0.379E+00	140.98
150.0 - 160.0	26.	0.100E+00	0.186E+00	152.50
160.0 - 170.0	28.	0.202E+00	0.245E+00	162.32
170.0 - 180.0	54.	-0.921E-02	0.296E+00	173.52
210.0 - 220.0	24.	-0.215E+00	0.640E+00	210.00
240.0 - 250.0	9.	-0.132E+00	0.372E+00	245.00

RUN NUMBER 3, DIRECTION 90.0, WINDOW 0.0, STEP 1.0

DISTANCE	# PAIRS	DRIFT	GAMMA	AVER DIST
1.0 - 2.0	190.	-0.388E-01	0.313E+00	1.00
2.0 - 3.0	175.	-0.418E-01	0.411E+00	2.00
3.0 - 4.0	165.	-0.619E-01	0.446E+00	3.00
4.0 - 5.0	152.	-0.875E-01	0.446E+00	4.00
5.0 - 6.0	139.	-0.164E+00	0.508E+00	5.00
6.0 - 7.0	128.	-0.197E+00	0.427E+00	6.00
7.0 - 8.0	117.	-0.246E+00	0.486E+00	7.00
8.0 - 9.0	105.	-0.339E+00	0.549E+00	8.00
9.0 - 10.0	94.	-0.427E+00	0.695E+00	9.00
10.0 - 11.0	84.	-0.510E+00	0.805E+00	10.00
11.0 - 12.0	72.	-0.570E+00	0.711E+00	11.00
12.0 - 13.0	61.	-0.671E+00	0.721E+00	12.00
13.0 - 14.0	52.	-0.685E+00	0.705E+00	13.00
14.0 - 15.0	45.	-0.679E+00	0.721E+00	14.00
15.0 - 16.0	36.	-0.908E+00	0.845E+00	15.00
16.0 - 17.0	26.	-0.105E+01	0.899E+00	16.00
17.0 - 18.0	23.	-0.104E+01	0.799E+00	17.00
18.0 - 19.0	19.	-0.970E+00	0.641E+00	18.00
19.0 - 20.0	14.	-0.113E+01	0.857E+00	19.00
20.0 - 21.0	10.	-0.113E+01	0.850E+00	20.00
21.0 - 22.0	7.	-0.107E+01	0.752E+00	21.00
22.0 - 23.0	3.	-0.789E+00	0.819E+00	22.00
23.0 - 24.0	1.	-0.839E+00	0.352E+00	23.00
24.0 - 25.0	1.	-0.568E+00	0.161E+00	24.00

STARTING PROGRAM VGCODE4 - RUN TITLED:

GRID C/ final variogram run/ BEG:VGCODE4/ MAF - 6/25/91

235 DATA SETS READ FROM FILE INPUT

RUN NUMBER 1, DIRECTION 0.0, WINDOW 0.0, STEP 1.0

DISTANCE	# PAIRS	DRIFT	GAMMA	AVER DIST
0.0 - 1.0	40.	0.825E-01	0.171E+00	0.50
1.0 - 2.0	226.	0.164E-01	0.191E+00	1.08
2.0 - 3.0	206.	-0.355E-01	0.218E+00	2.07
3.0 - 4.0	181.	-0.264E-01	0.218E+00	3.07
4.0 - 5.0	155.	-0.374E-01	0.269E+00	4.05
5.0 - 6.0	139.	-0.123E+00	0.263E+00	5.06
6.0 - 7.0	127.	-0.941E-01	0.256E+00	6.06
7.0 - 8.0	114.	-0.850E-01	0.244E+00	7.06
8.0 - 9.0	104.	-0.842E-01	0.203E+00	8.06
9.0 - 10.0	94.	-0.681E-01	0.204E+00	9.05
10.0 - 11.0	84.	-0.937E-01	0.231E+00	10.05
11.0 - 12.0	76.	-0.143E+00	0.222E+00	11.04
12.0 - 13.0	62.	-0.104E+00	0.212E+00	12.02
13.0 - 14.0	53.	-0.190E+00	0.252E+00	13.02
14.0 - 15.0	45.	-0.207E+00	0.258E+00	14.00
15.0 - 16.0	39.	-0.219E+00	0.334E+00	15.00
16.0 - 17.0	29.	-0.358E+00	0.318E+00	16.00
17.0 - 18.0	23.	-0.376E+00	0.208E+00	17.00
18.0 - 19.0	12.	-0.429E+00	0.400E+00	18.00
19.0 - 20.0	9.	-0.624E+00	0.451E+00	19.00
20.0 - 21.0	5.	-0.484E+00	0.153E+00	20.00
21.0 - 22.0	2.	-0.585E+00	0.187E+00	21.00

RUN NUMBER 2, DIRECTION 90.0, WINDOW 0.0, STEP 1.0

DISTANCE	# PAIRS	DRIFT	GAMMA	AVER DIST

0.0 - 1.0	62.	-0.127E+00	0.196E+00	0.53
1.0 - 2.0	215.	-0.346E-01	0.281E+00	1.10
2.0 - 3.0	176.	-0.141E+00	0.339E+00	2.07
3.0 - 4.0	143.	-0.222E+00	0.308E+00	3.06
4.0 - 5.0	127.	-0.226E+00	0.354E+00	4.06
5.0 - 6.0	104.	-0.265E+00	0.354E+00	5.07
6.0 - 7.0	89.	-0.342E+00	0.340E+00	6.06
7.0 - 8.0	65.	-0.335E+00	0.288E+00	7.02
8.0 - 9.0	47.	-0.338E+00	0.309E+00	8.01
9.0 - 10.0	30.	-0.391E+00	0.479E+00	9.02
10.0 - 11.0	17.	-0.178E+00	0.354E+00	10.03
11.0 - 12.0	4.	-0.728E+00	0.432E+00	11.00

STARTING PROGRAM VGCODE4 - RUN TITLED:

GRID D/ final variogram run/ BEG:VGCODE4/ MAF - 6/25/91

191 DATA SETS READ FROM FILE INPUT

RUN NUMBER 1, DIRECTION 0.0, WINDOW 0.0, STEP 1.0

DISTANCE	# PAIRS	DRIFT	GAMMA	AVER DIST
1.0 - 2.0	105.	0.154E-01	0.500E+00	1.00
2.0 - 3.0	102.	-0.197E-01	0.516E+00	2.00
3.0 - 4.0	100.	-0.503E-02	0.604E+00	3.00
4.0 - 5.0	98.	0.436E-01	0.602E+00	4.00
5.0 - 6.0	94.	0.615E-01	0.504E+00	5.00
6.0 - 7.0	90.	0.406E-01	0.637E+00	6.00
7.0 - 8.0	87.	0.122E+00	0.616E+00	7.00
8.0 - 9.0	85.	0.158E+00	0.710E+00	8.00
9.0 - 10.0	84.	0.114E+00	0.557E+00	9.00
10.0 - 11.0	82.	0.172E+00	0.688E+00	10.00
11.0 - 12.0	103.	0.208E+00	0.601E+00	11.00
12.0 - 13.0	102.	0.157E+00	0.678E+00	12.00
13.0 - 14.0	99.	0.265E+00	0.705E+00	13.00
14.0 - 15.0	74.	0.965E-01	0.516E+00	14.00
15.0 - 16.0	72.	0.121E+00	0.587E+00	15.00
16.0 - 17.0	69.	0.193E+00	0.613E+00	16.00
17.0 - 18.0	64.	0.238E+00	0.574E+00	17.00
18.0 - 19.0	63.	0.124E+00	0.491E+00	18.00
19.0 - 20.0	59.	0.177E+00	0.518E+00	19.00
20.0 - 21.0	57.	0.240E+00	0.572E+00	20.00

RUN NUMBER 2, DIRECTION 90.0, WINDOW 0.0, STEP 1.0

DISTANCE	# PAIRS	DRIFT	GAMMA	AVER DIST
1.0 - 2.0	110.	-0.199E-02	0.571E+00	1.00
2.0 - 3.0	106.	0.646E-01	0.759E+00	2.00
3.0 - 4.0	102.	0.103E+00	0.793E+00	3.00
4.0 - 5.0	99.	0.108E+00	0.878E+00	4.00
5.0 - 6.0	95.	0.112E+00	0.654E+00	5.00
6.0 - 7.0	87.	0.543E-01	0.802E+00	6.00
7.0 - 8.0	83.	0.421E-01	0.665E+00	7.00
8.0 - 9.0	76.	0.111E+00	0.637E+00	8.00
9.0 - 10.0	72.	0.179E+00	0.890E+00	9.00
10.0 - 11.0	68.	0.232E+00	0.917E+00	10.00
11.0 - 12.0	108.	-0.319E+00	0.968E+00	11.00
12.0 - 13.0	59.	0.382E+00	0.670E+00	12.00
13.0 - 14.0	55.	0.442E+00	0.702E+00	13.00
14.0 - 15.0	50.	0.457E+00	0.745E+00	14.00
15.0 - 16.0	47.	0.354E+00	0.733E+00	15.00
16.0 - 17.0	43.	0.302E+00	0.660E+00	16.00
17.0 - 18.0	35.	0.340E+00	0.866E+00	17.00
18.0 - 19.0	31.	0.178E+00	0.838E+00	18.00
19.0 - 20.0	24.	0.242E+00	0.427E+00	19.00
20.0 - 21.0	20.	0.313E+00	0.417E+00	20.00

The vita has been removed from the digitized version of this document.

THESIS PLATE

DISTRIBUTION OF PERMEABILITY PATTERNS - UPPER SAN ANDRES FORMATION OUTCROP, GUADALUPE MOUNTAINS, NEW MEXICO

Malcolm A. Ferris
M.A., May 1993

Plate 1. Contoured map of log-transformed permeability measurements collected on Lawyer Canyon outcrop of uSA1, first parasequence; GRID A sample data. Vertical and horizontal heterogeneities are observed in areas of concentrated sample points. Continuous patterns of high permeabilities are observed, but are contoured around relatively few data points.